TABLE OF CONTENTS

TABLE OF CONTENTS i
LIST OF FIGURES v
LIST OF TABLES xii
LIST OF TABLES xii
NOTATIONS xiii
ACKNOWLEDGEMENTS xvi
DISCLAIMER xvii
ABSTRACT xviii

1. INTRODUCTION–SUPERSTRUCTURE TO SUBSTRUCTURE CONNECTION 1
   1.1 Current Bridge Design Practice 1
   1.2 Seismic Design Issues 9
   1.3 Past Research 10
   1.4 Research Objective and Experimental Program 12
   1.5 Outline of the Report 13

2. PROTOTYPE DESIGN AND CONNECTION DETAILS 15
   2.1 Overview 15
   2.2 Prototype Design 15
   2.3 Prototype Column Design 16
   2.4 Prototype Steel Plate Girder Design 20
      2.4.1 Prototype Gravity Loads 20
      2.4.2 Prototype Seismic Loads 21
   2.5 Prototype Composite Deck Design 24
   2.6 Prototype Bent Cap Design 26
      2.6.1 Prototype Gravity Loads 26
      2.6.2 Prototype Seismic Loads 28
         2.6.2.1 History of Torsion Analysis 29
         2.6.2.2 Torsion Design 32
      2.6.3 Post-Tensioned Design 40
   2.7 Bent Cap-Girder Interface 42
      2.7.1 Shear Studs on Girder Web 42
      2.7.2 Shear Studs on Girder Flanges 45
      2.7.3 Bearing Stiffeners on Girder Web 45
      2.7.4 Details for Testing 49

3. DEVELOPMENT OF COMPONENT TESTS 51

3.1 Overview....51
3.2 Design of Component Test Specimen 51
3.2.1 Boundary Conditions of Component Test Specimen.... 56
3.3 Construction of Component Test Specimens 61
3.3.1 Construction of Concrete Column and Support Block for Component Test Specimen 61
3.3.2 Construction of Bent Cap for Component Test Specimen.... 62
3.3.3 Construction of Deck for Component Test Specimen 63
3.4 Properties of Component Test Specimen Materials 66
3.4.1 Steel Plate Girder Material Properties, Component Tests 66
3.4.2 Steel Reinforcement Material Properties, Component Tests 66
3.4.3 Concrete Material Properties, Component Tests 66
3.5 Instrumentation of Component Test Specimen 69
3.5.1 Strain Gage Locations in Component Tests.... 69
3.5.2 External Displacement Measurement Devices in Component Tests 75
3.6 Loading Protocol for Component Tests....77

4. EXPERIMENTAL RESULTS OF COMPONENT TESTS.... 79
4.1 Overview....79
4.2 Presentation of Component Test Results....79
4.3 Specimen 1-Conventionally Reinforced, No Stiffeners (CR-NS)....81
4.3.1 Observed Performance, CR-NS 81
4.3.2 Measured Response, CR-NS.... 87
4.4 Specimen 2–Conventionally Reinforced, Stiffeners (CR-S)....97
4.4.1 Observed Performance, CR-S 97
4.4.2 Measured Response, CR-S.... 104
4.5 Specimen 3–Post-Tensioned, No Stiffeners (PT-NS) 115
4.5.1 Observed Performance, PT-NS.... 115
4.5.2 Measured Response, PT-NS 119
4.6 Specimen 4–Post-Tensioned, Stiffeners (PT-S) 130
4.6.1 Observed Performance, PT-S.... 130
4.6.2 Measured Response, PT-S 137
4.7 Comparison of Component Test Results 149
4.7.1 Correlation of Specimen 1 (CR-NS) and Specimen 2 (CR-S)..... 153
4.7.2 Correlation of Specimen 1 (CR-NS) and Specimen 3 (PT-NS) 162
4.7.3 Correlation of Specimen 2 (CR-S) and Specimen 4 (PT-S) 171
4.7.4 Correlation of Specimen 3 (PT-NS) and Specimen 4 (PT-S) 180
4.8 Summary....188

5. DEVELOPMENT OF SYSTEM TEST.... 189
5.1 Overview....189
5.2 Design of Connection Detail 189
5.3 Design of System Test Specimen 190

5.3.1 Boundary Conditions 194
5.4 Construction of System Test Specimen 198
5.4.1 Construction of Deck, Girders and End Stub for System Test Specimen 199
5.4.2 Construction of Column and Bent Cap for System Test Specimen 199
5.5 Properties of System Test Specimen Material Properties 201
5.5.1 Steel Reinforcement Material Properties, System Test 201
5.5.2 Concrete Material Properties, System Test 202
5.6 Instrumentation of System Test Specimen 202
5.6.1 Strain Gage Locations in System Test 203
5.6.2 External Displacement Measurement Devices in System Test 203
5.7 Loading Protocol for System Test 211

6. EXPERIMENTAL RESULTS OF SYSTEM TEST 213
6.1 Overview 213
6.2 Observed Performance, System Test 213
6.3 Measured Response, System Test 229

7. DEVELOPMENT OF DESIGN MODEL 251
7.1 Overview 251
7.2 Recommended Bent Cap Design Procedure 251
7.2.1 Bent Cap Torsional Moment Demand 253
7.2.2 Bent Cap Torsional Moment Capacity 257
7.3 Bent Cap Design Specifications 260
7.3.1 Joint Shear Reinforcement 260
7.3.2 Post-Tensioning Stress Levels 261
7.3.3 Continuous Reinforcement 261
7.3.4 Holes in Girder Webs 261
7.3.5 Stiffener Design 262
7.3.6 Shear Studs 262
7.4 Considerations For Design of Alternative Bent Configurations 262
7.5 Construction and Maintenance Considerations 263
7.6 Summary 265

8. CONCLUSIONS AND RECOMMENDATIONS 267
8.1 Overview 267
8.2 Summary 267
8.3 Design Recommendations 268
8.4 Recommendations for Future Work 268

Appendix A Supporting Data for design of Prototype Bent cap 270
A.1 Prototype Curve from Collins and Mitchell Procedure 270

A.1.1 Cracking 270
A.1.2 Post – Cracking..... 270
A.2 Prototype Curve from Hsu Procedure 272
A.2.1 Cracking 272
A.2.2 Post - Cracking 272

Appendix B Construction Details..... 274

B.1 Component Tests One and Two 274
B.2 Component Tests Three and Four 279
B.3 System Test 280

REFERENCES 290

LIST OF FIGURES

FIGURE 1-1 TYPICAL FREEWAY OVERCROSSING 1
FIGURE 1-2 BRIDGE SUPERSTRUCTURE CONFIGURATIONS 2
FIGURE 1-3 BRIDGE SUBSTRUCTURE CONFIGURATIONS 3
FIGURE 1-4 CONCRETE MULTI-CELL BOX GIRDER SUPERSTRUCTURE 4
FIGURE 1-5 MONOLITHIC CONCRETE MULTI-CELL BOX SUPERSTRUCTURE..... 4
FIGURE 1-6 STEEL SUPERSTRUCTURE ON CONCRETE HAMMERHEAD BENT CAP (4)..... 6
FIGURE 1-7 INTEGRAL STEEL SUPERSTRUCTURE CONCRETE SUBSTRUCTURE BRIDGE (5)..... 6
FIGURE 1-8 INTEGRAL CONNECTION DETAILS 7
FIGURE 1-9 POTENTIAL HINGE LOCATIONS 9
FIGURE 1-10 PRECAST SUPERSTRUCTURE CONFIGURATIONS (9) 11
FIGURE 1-11 PRECAST BATHTUB GIRDER TEST (9) 12

FIGURE 2-1 PROTOTYPE BRIDGE DIMENSIONS..... 16
FIGURE 2-2 PROTOTYPE MOMENT CURVATURE CHARACTERISTICS 17
FIGURE 2-3 DEFORMED SHAPE 18
FIGURE 2-4 PROTOTYPE COLUMN REINFORCEMENT DETAIL 20
FIGURE 2-5 PROTOTYPE SUPERSTRUCTURE MOMENT AND DEFLECTED SHAPE DUE TO SELF-WEIGHT 21
FIGURE 2-6 SUBSTRUCTURE SEISMIC MOMENT 22
FIGURE 2-7 SUPERSTRUCTURE SEISMIC MOMENT 22
FIGURE 2-8 DISTRIBUTION OF TORSIONAL MOMENT ALONG THE BENT CAP (9)..... 23
FIGURE 2-9 PROTOTYPE PLATE GIRDER PROPERTIES..... 24
FIGURE 2-10 PROTOTYPE SHEAR STUD DESIGN..... 25
FIGURE 2-11 PROTOTYPE DECK REINFORCEMENT DETAIL 25
FIGURE 2-12 PROTOTYPE BENT CAP GEOMETRY..... 26
FIGURE 2-13 PROTOTYPE BENT CAP REINFORCEMENT..... 28
FIGURE 2-14 PROTOTYPE BENT CAP JOINT REGION 29
FIGURE 2-15 THIN TUBE ANALOGY (ADAPTED FROM (27)) 30
FIGURE 2-16 BEAM SHEAR REPRESENTED AS A PLANE TRUSS 31
FIGURE 2-17 DEVELOPMENT OF SPACE TRUSS ANALOGY (ADAPTED FROM (27))..... 32
FIGURE 2-18 SPACE TRUSS ANALOGY (ADAPTED FROM 27) 34
FIGURE 2-19 PROTOTYPE TORQUE – TWIST PREDICTION..... 38
FIGURE 2-20 TORSION SHEAR FRICTION THEORY (FIGURE FROM HOLOMBO, 9) 39
FIGURE 2-21 POST TENSIONING LAYOUT 41
FIGURE 2-22 POTENTIAL FAILURE MECHANISMS LOCATIONS 42
FIGURE 2-23 PURE MOMENT CONNECTION (40)..... 43
FIGURE 2-24 SHEAR STUD FORCE DEFORMATION CHARACTERISTICS (FROM (2-24))..... 44
FIGURE 2-25 STUD GROUP ON GIRDER WEB 45
FIGURE 2-26 YIELD LINE THEORY FOR CONCRETE SLABS (ADAPTED FROM 45)..... 46
FIGURE 2-27 YIELD LINE THEORY..... 48
FIGURE 2-28 TORSIONAL CAPACITY OF CONCRETE COMPRESSION STRUTS 49
FIGURE 2-29 DESIGNATION OF THE FOUR COMPONENT TEST SPECIMENS 50

FIGURE 3-1 COMPONENT TEST REGION OF INVESTIGATION 51
FIGURE 3-2 COMPONENT TEST SPECIMEN PROTOTYPE AND MODEL 52
FIGURE 3-3 COMPONENT TEST SPECIMEN GEOMETRY 53
FIGURE 3-4 COMPONENT TEST SPECIMEN 54
FIGURE 3-5 COMPONENT TEST SPECIMEN BEFORE TESTING 55
FIGURE 3-6 COMPONENT TEST SPECIMEN LOADING 57
FIGURE 3-7 DEMAND PROFILES ALONG LONGITUDINAL BRIDGE AXIS 58
FIGURE 3-8 DEMAND PROFILES ALONG TRANSVERSE BRIDGE AXIS 59
FIGURE 3-9 COMPONENT TEST SPECIMEN WITH LOADING FIXTURES IN PLACE 60
FIGURE 3-10 BENT CAP JOINT REGION 64
FIGURE 3-11 BENT CAP REINFORCEMENT THROUGH GIRDER WEB 64
FIGURE 3-12 POST-TENSIONING ANCHORING IN SUPPORT BLOCK 65
FIGURE 3-13 POST-TENSIONING DUCTS 65
FIGURE 3-14 STIRRUP STRAIN GAGE LOCATIONS AND DESIGNATIONS 71
FIGURE 3-15 FLEXURAL REINFORCEMENT STRAIN GAGE LOCATIONS AND DESIGNATIONS 72
FIGURE 3-16 DECK REINFORCEMENT STRAIN GAGE LOCATIONS AND DESIGNATIONS 73
FIGURE 3-17 GIRDER STRAIN GAGE LOCATIONS AND DESIGNATIONS 74
FIGURE 3-18 VERTICAL DISPLACEMENT MEASUREMENT LOCATIONS AND DESIGNATIONS 76
FIGURE 3-19 HORIZONTAL DISPLACEMENT MEASUREMENT LOCATIONS AND DESIGNATIONS 77
FIGURE 3-20 COMPONENT TEST LOADING SEQUENCE 78

FIGURE 4-1 BENT CAP FACE ORIENTATION 80
FIGURE 4-2 TORSIONAL MOMENT DIRECTIONS IN COMPONENT TESTS 80
FIGURE 4-3 SPECIMEN CR-NS: FIRST TORSIONAL CRACK ON LEAD FACE 82
FIGURE 4-4 SPECIMEN CR-NS: LEAD FACE OF BENT CAP AT 0.01 RADIANS 83
FIGURE 4-5 SPECIMEN CR-NS: BOTTOM FACE AT 0.01 RADIANS 83
FIGURE 4-6 SPECIMEN CR-NS: LEAD FACE AT MAXIMUM TORSIONAL MOMENT 84
FIGURE 4-7 SPECIMEN CR-NS: BOTTOM FACE AT MAXIMUM TORSIONAL MOMENT 84
FIGURE 4-8 SPECIMEN CR-NS: GIRDER/CAP INTERFACE AT $\theta = 0.02$ RADIANS 85
FIGURE 4-9 SPECIMEN CR-NS: LEAD FACE AT MAXIMUM TORSIONAL ROTATION, $\theta = 0.03$ RADIANS 85
FIGURE 4-10 SPECIMEN CR-NS: BOTTOM FACE AT MAXIMUM TORSIONAL ROTATION 86
FIGURE 4-11 SPECIMEN CR-NS: DECK DAMAGE AT MAXIMUM TORSIONAL ROTATION 86
FIGURE 4-12 SPECIMEN CR-NS: TORSIONAL MOMENT-ROTATION RESPONSE 88
FIGURE 4-13 SPECIMEN CR-NS: MEASURED BENT CAP DILATION 89
FIGURE 4-14 SPECIMEN CR-NS: STRAIN GAGE LOCATION WITH RESPECT TO ACTUATORS 90
FIGURE 4-15 SPECIMEN CR-NS: MEASURED STRAIN IN FLEXURAL REINFORCEMENT 90
FIGURE 4-16 SPECIMEN CR-NS: MEASURED STRAIN IN BENT CAP STIRRUPS 92

FIGURE 4-17 SPECIMEN CR-NS: MEASURED STRAIN IN LONGITUDINAL DECK REINFORCEMENT 95
FIGURE 4-18 SPECIMEN CR-NS: MEASURED STRAIN IN GIRDER FLANGES 96
FIGURE 4-19 SPECIMEN CR-S: FIRST TORSIONAL CRACK ON BENT CAP LEAD FACE 99
FIGURE 4-20 SPECIMEN CR-S: BENT CAP LEAD FACE AT 0.005 RADIANS 99
FIGURE 4-21 SPECIMEN CR-S: BENT CAP UNDERSIDE AT 0.005 RADIANS 100
FIGURE 4-22 SPECIMEN CR-S: BENT CAP LEAD FACE AT 0.02 RADIANS 100
FIGURE 4-23 SPECIMEN CR-S: BENT CAP/GIRDER INTERFACE AT 0.02 RADIANS 101
FIGURE 4-24 SPECIMEN CR-S: BENT CAP UNDERSIDE AT 0.02 RADIANS 101
FIGURE 4-25 SPECIMEN CR-S: DECK AT 0.02 RADIANS 102
FIGURE 4-26 SPECIMEN CR-S: BENT CAP LEAD FACE AT ULTIMATE ROTATION, θ=0.03 RADIANS 102
FIGURE 4-27 SPECIMEN CR-S: BENT CAP UNDERSIDE AT ULTIMATE ROTATION 103
FIGURE 4-28 SPECIMEN CR-S: DECK AT ULTIMATE ROTATION 103
FIGURE 4-29 SPECIMEN CR-S: TORSIONAL MOMENT ROTATION RESPONSE 105
FIGURE 4-30 SPECIMEN CR-S: MEASURED BENT CAP DILATION 106
FIGURE 4-31 SPECIMEN CR-S: GAGE LOCATION WITH RESPECT TO ACTUATORS 107
FIGURE 4-32 SPECIMEN CR-S: MEASURED STRAIN IN FLEXURAL REINFORCEMENT 107
FIGURE 4-33 SPECIMEN CR-S: MEASURED STRAIN IN BENT CAP STIRRUPS 109
FIGURE 4-34 SPECIMEN CR-S: MEASURED STRAIN IN LONGITUDINAL DECK REINFORCEMENT 112
FIGURE 4-35 SPECIMEN CR-S: MEASURED STRAIN IN GIRDER FLANGES 113
FIGURE 4-36 SPECIMEN CR-S: MEASURED STRAIN IN GIRDER STIFFENERS 114
FIGURE 4-37 SPECIMEN PT-NS: FIRST TORSIONAL CRACK ON BENT CAP LEAD FACE 116
FIGURE 4-38 SPECIMEN PT-NS: BENT CAP LEAD FACE AT MAXIMUM TORSIONAL MOMENT 116
FIGURE 4-39 SPECIMEN PT-NS: BENT CAP UNDERSIDE AT MAXIMUM TORSIONAL MOMENT 117
FIGURE 4-40 SPECIMEN PT-NS: BENT CAP LEAD FACE AT ULTIMATE ROTATION, θ=0.03 RADIANS 117
FIGURE 4-41 SPECIMEN PT-NS: BENT CAP UNDERSIDE AT ULTIMATE ROTATION (θ=0.03 RADIANS) 118
FIGURE 4-42 SPECIMEN PT-NS: BENT CAP/GIRDER INTERFACE AT ULTIMATE ROTATION (θ=0.03 RADIANS) 118
FIGURE 4-43 SPECIMEN PT-NS: TORSIONAL MOMENT ROTATION RESPONSE 120
FIGURE 4-44 SPECIMEN PT-NS: MEASURED BENT CAP DILATION 121
FIGURE 4-45 SPECIMEN PT-NS: GAGE LOCATION WITH RESPECT TO ACTUATORS 122
FIGURE 4-46 SPECIMEN PT-NS: MEASURED STRAIN IN FLEXURAL REINFORCEMENT 122
FIGURE 4-47 SPECIMEN PT-NS: MEASURED STRAIN IN BENT CAP STIRRUPS 124
FIGURE 4-48 SPECIMEN PT-NS: MEASURED STRAIN IN LONGITUDINAL DECK REINFORCEMENT 128
FIGURE 4-49 SPECIMEN PT-NS: MEASURED STRAIN IN GIRDER FLANGES 129
FIGURE 4-50 SPECIMEN PT-S: FIRST TORSIONAL CRACK ON BENT CAP LEAD FACE 131
FIGURE 4-51 SPECIMEN PT-S: BENT CAP LEAD FACE AT θ=0.005 RADIANS 132
FIGURE 4-52 SPECIMEN PT-S: BENT CAP AT MAXIMUM TORSIONAL MOMENT 132

FIGURE 4-53 SPECIMEN PT-S: BENT CAP UNDERSIDE AT MAXIMUM TORSIONAL MOMENT 133
FIGURE 4-54 SPECIMEN PT-S: DECK AT MAXIMUM TORSIONAL MOMENT 133
FIGURE 4-55 SPECIMEN PT-S: BENT CAP LEAD FACE AT θ = 0.02 RADIANS 134
FIGURE 4-56 SPECIMEN PT-S: BENT CAP UNDERSIDE AT θ = 0.02 RADIANS 134
FIGURE 4-57 SPECIMEN PT-S: BENT CAP LEAD FACE AT MAXIMUM ROTATION (θ=0.03 RADIANS) 135
FIGURE 4-58 SPECIMEN PT-S: BENT CAP UNDERSIDE AT MAXIMUM ROTATION 135
FIGURE 4-59 SPECIMEN PT-S: DECK AT MAXIMUM ROTATION 136
FIGURE 4-60 SPECIMEN PT-S: TORSIONAL MOMENT - ROTATION RESPONSE 138
FIGURE 4-61 SPECIMEN PT-S: MEASURED BENT CAP DILATION 139
FIGURE 4-62 SPECIMEN PT-S: GAGE LOCATION WITH RESPECT TO ACTUATORS 140
FIGURE 4-63 SPECIMEN PT-S: MEASURED STRAIN IN FLEXURAL REINFORCEMENT 140
FIGURE 4-64 SPECIMEN PT-S: MEASURED STRAIN IN BENT CAP STIRRUPS 142
FIGURE 4-65 SPECIMEN PT-S: MEASURED STRAIN IN LONGITUDINAL DECK REINFORCEMENT 146
FIGURE 4-66 SPECIMEN PT-S: MEASURED STRAIN IN GIRDER FLANGES 147
FIGURE 4-67 SPECIMEN PT-S: MEASURED STRAIN IN GIRDER STIFFENERS 148
FIGURE 4-68 COMPARISON OF TORSIONAL MOMENT-ROTATION ENVELOPES 151
FIGURE 4-69 TORQUE-TWIST RELATIONS 151
FIGURE 4-70 COMPARISON OF BENT CAP DILATION ENVELOPES 152
FIGURE 4-71 DAMAGE COMPARISON AT BENT CAP ROTATION=0.01 RADIANS 154
FIGURE 4-72 DAMAGE COMPARISON AT BENT CAP ROTATION=0.02 RADIANS 155
FIGURE 4-73 DAMAGE COMPARISON AT BENT CAP ROTATION=0.03 RADIANS (FAILURE) 156
FIGURE 4-74 GLOBAL RESPONSE CORRELATION 158
FIGURE 4-75 LATERAL BENT CAP DILATION, LEAD FACE, BOTTOM 158
FIGURE 4-76 MEASURED STRAIN IN FLEXURAL REINFORCEMENT AT BOTTOM CORNERS OF BENT CAP 159
FIGURE 4-77 MEASURED STRAIN IN BENT CAP STIRRUPS AT THE BOTTOM CORNERS OF BENT CAP 160
FIGURE 4-78 MEASURED STRAIN IN GIRDER FLANGE 161
FIGURE 4-79 DAMAGE COMPARISON AT BENT CAP ROTATION=0.01 RADIANS 163
FIGURE 4-80 DAMAGE COMPARISON AT BENT CAP ROTATION=0.02RADIANS 164
FIGURE 4-81 DAMAGE COMPARISON AT BENT CAP ROTATION=0.03 RADIANS (FAILURE) 165
FIGURE 4-82 GLOBAL RESPONSE CORRELATION 167
FIGURE 4-83 LATERAL BENT CAP DILATION, LEAD FACE, BOTTOM 167
FIGURE 4-84 MEASURED STRAIN IN FLEXURAL REINFORCEMENT AT BOTTOM CORNERS OF BENT CAP 168
FIGURE 4-85 MEASURED STRAIN IN BENT CAP STIRRUPS AT THE BOTTOM CORNERS OF BENT CAP 169
FIGURE 4-86 MEASURED STRAIN IN GIRDER FLANGE 170
FIGURE 4-87 DAMAGE COMPARISON AT BENT CAP ROTATION=0.01 RADIANS 172
FIGURE 4-88 DAMAGE COMPARISON AT BENT CAP ROTATION=0.02 RADIANS 173

FIGURE 4-89 DAMAGE COMPARISON AT BENT CAP ROTATION=0.03 RADIANS (FAILURE) 174
FIGURE 4-90 GLOBAL RESPONSE CORRELATION 176
FIGURE 4-91 TRANSVERSE BENT CAP DILATION 176
FIGURE 4-92 MEASURED STRAIN IN FLEXURAL REINFORCEMENT AT BOTTOM CORNERS OF BENT CAP 177
FIGURE 4-93 MEASURED STRAIN IN GIRDER FLANGES 178
FIGURE 4-94 STIFFENER BEHAVIOR 179
FIGURE 4-95 DAMAGE COMPARISON AT BENT CAP ROTATION=0.01 RADIANS 181
FIGURE 4-96 DAMAGE COMPARISON AT BENT CAP ROTATION=0.02RADIANS 182
FIGURE 4-97 DAMAGE COMPARISON AT BENT CAP ROTATION=0.03 RADIANS (FAILURE) 183
FIGURE 4-98 GLOBAL RESPONSE CORRELATION 185
FIGURE 4-99 TRANSVERSE BENT CAP DILATION 185
FIGURE 4-100 MEASURED STRAIN IN FLEXURAL REINFORCEMENT AT BOTTOM CORNERS OF BENT CAP 186
FIGURE 4-101 MEASURED STRAIN IN GIRDER FLANGES 187

FIGURE 5-1 RECOMMENDED CONNECTION DETAIL 190
FIGURE 5-2 SYSTEM TEST SPECIMEN 192
FIGURE 5-3 SYSTEM TEST SPECIMEN GEOMETRY 193
FIGURE 5-4 SYSTEM TEST SETUP 195
FIGURE 5-5 MOMENT AND DEFLECTED SHAPE DUE TO GRAVITY LOADS 196
FIGURE 5-6 PROTOTYPE MOMENT AND DEFLECTED SHAPE DUE TO SEISMIC LOADS 197
FIGURE 5-7 SEISMIC LOAD MODELING 198
FIGURE 5-8 BENT CAP REINFORCEMENT 200
FIGURE 5-9 JOINT REGION 201
FIGURE 5-10 LOCATION OF STRAIN GAGES ON COLUMN REINFORCEMENT 205
FIGURE 5-11 LOCATION OF STRAIN GAGES ON BENT CAP STIRRUPS 206
FIGURE 5-12 LOCATION OF STRAIN GAGES ON FLEXURAL REINFORCEMENT 207
FIGURE 5-13 LOCATION OF STRAIN GAGES ON DECK REINFORCEMENT 208
FIGURE 5-14 DISPLACEMENT MEASUREMENT LOCATIONS 209
FIGURE 5-15 BENT CAP FACE INSTRUMENTATION 210
FIGURE 5-16 SYSTEM TEST LOADING SEQUENCE 211

FIGURE 6-1 FIRST COLUMN CRACK 215
FIGURE 6-2 FIRST FLEXURAL CRACKS ON NEGATIVE LOADING 216
FIGURE 6-3 $\mu_\Delta = 1$ 217
FIGURE 6-4 COLUMN AT FIRST COLUMN LONGITUDINAL YIELD 217
FIGURE 6-5 FIRST BENT CAP TORSIONAL CRACK, $\mu_\Delta = 1$, CYCLE ONE 218
FIGURE 6-6 TORSIONAL CRACK DEVELOPMENT, $\mu_\Delta = 1$, CYCLE THREE 218
FIGURE 6-7 EAST SIDE OF BENT CAP AT $\mu_\Delta = 1.5$, CYCLE ONE 219
FIGURE 6-8 WEST SIDE OF BENT CAP AT $\mu_\Delta = 1.5$, CYCLE ONE 219
FIGURE 6-9 NORTH BENT CAP FACE, $\mu_\Delta = 2$, CYCLE 1 220
FIGURE 6-10 CRACKS IN NORTH BENT CAP FACE AT $\mu_\Delta = 2$, CYCLE 1 220

FIGURE 6-11 EAST SIDE, BOTTOM OF BENT CAP AT μ_Δ = 2, CYCLE THREE 221
FIGURE 6-12 GIRDER-CAP INTERFACE AT μ_Δ = 2, CYCLE THREE 221
FIGURE 6-13 SOUTH FACE OF COLUMN/BENT μ_Δ = 3, CYCLE ONE 222
FIGURE 6-14 SOUTH BENT CAP FACE μ_Δ = 3, CYCLE ONE 222
FIGURE 6-15 NORTH BENT CAP FACE AT μ_Δ = 4, CYCLE ONE 223
FIGURE 6-16 SOUTH BENT CAP FACE AT μ_Δ = 3, CYCLE ONE 223
FIGURE 6-17 μ_Δ = 6, CYCLE ONE 224
FIGURE 6-18 μ_Δ = 4, CYCLE ONE 224
FIGURE 6-19 μ_Δ = 10, CYCLE ONE 225
FIGURE 6-20 μ_Δ = 8, CYCLE ONE 225
FIGURE 6-21 μ_Δ = 10, NORTH BENT CAP FACE 226
FIGURE 6-22 μ_Δ = 10, FINAL DISPLACEMENT CYCLE 226
FIGURE 6-23 EAST BENT CAP BOTTOM FACE μ_Δ = 10 227
FIGURE 6-24 WEST BENT CAP BOTTOM FACE μ_Δ = 10 227
FIGURE 6-25 EAST BENT CAP BOTTOM FACE AT μ_Δ = 10 228
FIGURE 6-26 END OF TEST 228
FIGURE 6-27 COLUMN FORCE VERSUS DISPLACEMENT RESPONSE 232
FIGURE 6-28 COMPONENTS OF COLUMN DISPLACEMENT 232
FIGURE 6-29 BENT CAP TORSIONAL MOMENT VERSUS ROTATION 233
FIGURE 6-30 COLUMN MOMENT VERSUS DISPLACEMENT 234
FIGURE 6-31 TORSIONAL MOMENT AT SUPERSTRUCTURE CENTROID 234
FIGURE 6-32 DEAD LOAD MOMENT AND AXIAL LOAD PERFORMANCE 235
FIGURE 6-33 COLUMN CURVATURES 235
FIGURE 6-34 MEASURED LONGITUDINAL DECK DEFORMATION 236
FIGURE 6-35 MEASURED TRANSVERSE DECK DEFORMATION 238
FIGURE 6-36 MEASURED STRAIN IN COLUMN LONGITUDINAL BARS PRIOR TO FIRST YIELD 240
FIGURE 6-37 MEASURED STRAIN IN COLUMN LONGITUDINAL BARS POST-YIELD 241
FIGURE 6-38 MEASURED STRAIN IN FLEXURAL REINFORCEMENT 242
FIGURE 6-39 MEASURED STRAIN IN BENT CAP STIRRUPS 243
FIGURE 6-40 MEASURED STRAIN IN LONGITUDINAL DECK REINFORCEMENT 244
FIGURE 6-41 MEASURED STRAIN IN TRANSVERSE DECK REINFORCEMENT 247
FIGURE 6-42 MEASURED STRAIN IN FLANGES GIRDER TWO, JOINT REGION 249
FIGURE 6-43 MEASURED STRAINS IN FLANGES GIRDER THREE, JOINT REGION 250

FIGURE 7-1 DESIGN EXAMPLE BRIDGE 252
FIGURE 7-2 SUPERSTRUCTURE DESIGN MOMENT 254
FIGURE 7-3 DISTRIBUTION OF DESIGN MOMENT ALONG BENT CAP 254
FIGURE 7-4 GIRDER MOMENT PROFILES 256
FIGURE 7-5 CHECK OF BENT CAP STRESS 260
FIGURE 7-6 LIMITS OF JOINT REINFORCEMENT 261
FIGURE 7-7 STIFFENER THICKNESS 262
FIGURE 7-8 ALTERNATIVE BENT CONFIGURATIONS 263
FIGURE 7-9 CLOSE-UP OF BRIDGE 17, FORT WASHINGTON WAY, CINCINNATI, OHIO (COURTESY PARSONS BRINKERHOFF, OHIO (50)) 264

FIGURE 7-10 CONSTRUCTION OF BRIDGE 17, FORT WASHINGTON WAY, CINCINNATI, OHIO (COURTESY PARSONS BRINKERHOFF, OHIO (50)) 265

FIGURE B. 1 COMPONENT TEST SETUP SPECIMENS CR-NS AND CR-S 274
FIGURE B. 2 BENT CAP BEFORE GIRDER PLACEMENT 275
FIGURE B. 3 STEEL GIRDERS 275
FIGURE B. 4 BENT CAP STIRRUPS 276
FIGURE B. 5 BENT CAP REINFORCEMENT THROUGH GIRDER WEB 276
FIGURE B. 6 BENT CAP REINFORCEMENT 277
FIGURE B. 7 BENT CAP CAST 277
FIGURE B. 8 DECK STEEL 278
FIGURE B. 9 POST-TENSIONING DUCTS 279
FIGURE B. 10 POST-TENSIONING ANCHORING IN SUPPORT BLOCK 279
FIGURE B. 11 GIRDERS IN PLACE 280
FIGURE B. 12 GIRDER IN BENT CAP REGION 280
FIGURE B. 13 END STUBS TIED 281
FIGURE B. 14 COLUMN CAGE IN PLACE 281
FIGURE B. 15 COLUMN CAGE 282
FIGURE B. 16 END STUB REINFORCEMENT 282
FIGURE B. 17 STIRRUPS AND J-HOOKS IN JOINT REGION 283
FIGURE B. 18 REINFORCEMENT COMPLETE 283
FIGURE B. 19 DECK CONCRETE AND JOINT REINFORCEMENT 284
FIGURE B. 20 GIRDER AT DECK CONCRETE 284
FIGURE B. 21 DECK HAUNCH CONSTRUCTION 285
FIGURE B. 22 FORMWORK FOR BENT CAP AND END STUBS 285
FIGURE B. 23 COLUMN AND LOAD STUB FORMWORK 286
FIGURE B. 24 ROLLER AT ENDS 286
FIGURE B. 25 LOAD FRAME REACTION 287
FIGURE B. 26 AXIAL LOAD CONFIGURATION 288
FIGURE B. 27 LOAD CELL REACTION 288
FIGURE B. 28 JACK AT REACTION FRAME 289
FIGURE B. 29 ACTUATOR CONNECTED 289

LIST OF TABLES

TABLE 2.1 PROTOTYPE COLUMN DISPLACEMENT CAPACITIES AND DEMANDS 19

TABLE 3.1 STEEL GIRDER COUPONS 66
TABLE 3.2 MEASURED REINFORCEMENT PROPERTIES 67
TABLE 3.3 MEASURED REINFORCEMENT PROPERTIES 67
TABLE 3.4 CONCRETE MIX DESIGN WEIGHTS AND VOLUMES 68
TABLE 3.5 CONCRETE COMPRESSIVE STRENGTH 68

TABLE 5.1 MEASURED REINFORCEMENT PROPERTIES 202
TABLE 5.2 CONCRETE COMPRESSIVE STRENGTH 202

NOTATIONS

———	Tension Ties
--------	Compression Struts
●	Node
A_1	Area of concrete bound by centerline of stirrup
A_c	Area of cross section, including cover
A_f	Area of face shear acts over
A_i	Cross-sectional area of ith quadrant in torsion-shear friction analysis
A_o	Area of concrete enclosed by shear path
A^{jv}_s	20% of area of column longitudinal reinforcement anchored in joint
A_{st}	Area of column longitudinal reinforcement anchored in joint
A_t	Area of transverse
A_v	Cross sectional area of stirrup
b_f	Flange width
b_w	Bent cap width
C	St. Venant's Torsional Constant ($\beta x^3 y$)
C_{cr}	Post cracking torsional constant $\left(4A_1^2 h/u\right)$
d	Depth of Bent Cap
d_b	Bar diameter
D	Depth of Girder Web
D_c	Column diameter
D_2	Compression strut axial force
e_i	Eccentricity of post-tensioning
E_c	Concrete Modulus of elasticity, $57{,}000\sqrt{f_c^{'}}$, psi
E_m	Modified modulus of elasticity for composite sections $\left(E_s + C_3 E_c \left(A_c / A_s\right)\right)$
E_s	Modulus of elasticity of steel (29,000 ksi)
f'_c	Concrete compressive strength, ksi
f_{cr}	Cracking strength of concrete
f_{pc}	Post-tensioning stress (P/A_c)
f_{ty}	Yield strength of transverse steel
f_u	Ultimate steel strength

f_y	Yield strength of steel
F_i	Shear resistance in ith quadrant of shear friction plane
G_c	Shear Modulus, $E_c/2(1+\upsilon)$
G_{cr}	Post cracking shear modulus $\left(E_s/\{4n+(uh/A_c\rho_l)+(uh/A_c\rho_h)\}\right)$
G_m	Modified Shear Modulus, $E_m/2(1+\upsilon)$
l_a	Length of column reinforcement extending into bent cap
L_c	Clear length
L_p	Plastic hinge length
M	Material overstrength moment
M_i	Ideal moment
M_{max}	Maximum column moment
M'_{max}	Maximum moment at superstructure centerline
M_N	Design moment
M^o	Overstrength moment, capacity protected
M_T	Superstructure demand moment
M_u	Ultimate moment
n	E_s/E_c
p_c	Perimeter of concrete section, in.
p_o	Perimeter of A_o
P	Post tensioning force
s	Center to center spacing of steel reinforcement
t_d	Wall thickness of equivalent tube ($3A_c/4p_c$ – Collins & Mitchell)
t_f	Flange thickness
t_w	Web thickness
T	Torsion, k-ft
T_c	Torsion resisted by concrete, $\left(x^2y/3\right)\left(2.4\sqrt{f_c'}\right)$
T_{cr}	Cracking torque, k-ft $A_c t\left(5\sqrt{f_c'}\right)$ - Hsu
u	Perimeter of area bounded by center line of stirrup bar

V_s	Shear demand on stirrups less that resisted by concrete
V_u	Factored shear
β	Torsional coefficient tabulated in Hsu [19]
Δ_D	Demand displacement
Δ_u	Ultimate displacement
Δ_y	Yield displacement
ε_s	Steel strain
η	Coefficient, $= 0.57 + 2.86(h/x) = 2$ for a solid section
θ	Crack angle measured from horizontal (strut angle)
θ_{xy}	Strut angle in the x-y plane
θ_z	Strut angle with the x-y plane
μ	Coefficient of friction
ρ_h	Stirrup reinforcement ratio
ρ_l	Longitudinal reinforcement ratio
υ	Shear stress
ϕ_u	Ultimate curvature
ϕ_y	Yield curvature
μ	Coefficient of friction

ACKNOWLEDGEMENTS

Funding for this research was provided by the California Department of Transportation (Caltrans). Steve Altman, Lian Duan and Mark Reno served as the Caltrans project monitors. Assistance during construction, test setup and testing from the technical staff and undergraduate students of the UCSD Charles Lee Powell Structural Research Laboratories was greatly appreciated.

DISCLAIMER

The contents of this report reflect the views of the authors who are responsible for the facts and the accuracy of the data presented herein. The contents do not necessarily reflect the views or policies of the STATE OF CALIFORNIA or the FEDERAL HIGHWAY ADMINISTRATION. This report does not constitute a standard, specification or regulation.

ABSTRACT

A research program consisting of both experimental testing and force transfer modeling was conducted at the University of California in San Diego (UCSD) to characterize the behavior of a bridge design detail that integrates a steel superstructure with a concrete substructure using a concrete bent cap. When an integral bridge is subjected to a longitudinal seismic event, a moment is imposed on the girders that must be transferred to the column. This moment is transferred through torsional action in the bent cap. Because the bent cap is a designated capacity protected component, it must remain essentially elastic during the force transfer. Therefore, the research objective was to establish a behavior profile of the bent cap connection to define limit states. Clear definition of the entire behavior was needed to ensure that the proposed design recommendations placed the bent cap performance in the elastic range for a given seismic event.

The effect of two design parameters on the bent cap torsional behavior and moment capacity was investigated in a series of four component tests, with the most promising detail to be validated in a final system test. The two parameters investigated were (1) bent cap reinforcement (post-tensioned versus conventionally reinforced), and (2) girder web configuration inside the bent cap (with or without bearing stiffeners). The specimens with post-tensioned bent caps exhibited less crack dilation during the initial loading stages than the specimens with conventionally reinforced bent caps. The specimens with girder web bearing stiffeners reached maximum capacities approximately 25% higher than the specimens without girder web stiffeners.

The component test results lead to the recommended design for the system test of stiffened steel girders integrated with a post-tensioned bent cap. The system test demonstrated that the bent cap could be designed to perform essentially elastically while the column developed an inelastic mechanism.

Based on the experimental findings and force transfer models, design guidelines for an integral bridge were developed. The procedure for determining the bent cap torsional strength for a given earthquake, as well as recommended limits, is outlined in a design example.

Chapter 1

Introduction–Superstructure to Substructure Connection

1.1 Current Bridge Design Practice

For short distances (<50 feet [<15 m]), a bridge can consist solely of a deck that spans abutment to abutment. As the span increases, girders are typically used to support the deck and live loads, and to distribute these loads to the bents and abutments (Figure 1-1). Girders can be constructed of steel sections, reinforced cast-in-place (CIP) concrete, prestressed concrete sections, or recently even fiber reinforced polymers (1). A deck slab alone or in conjunction with longitudinal girders comprises the bridge superstructure.

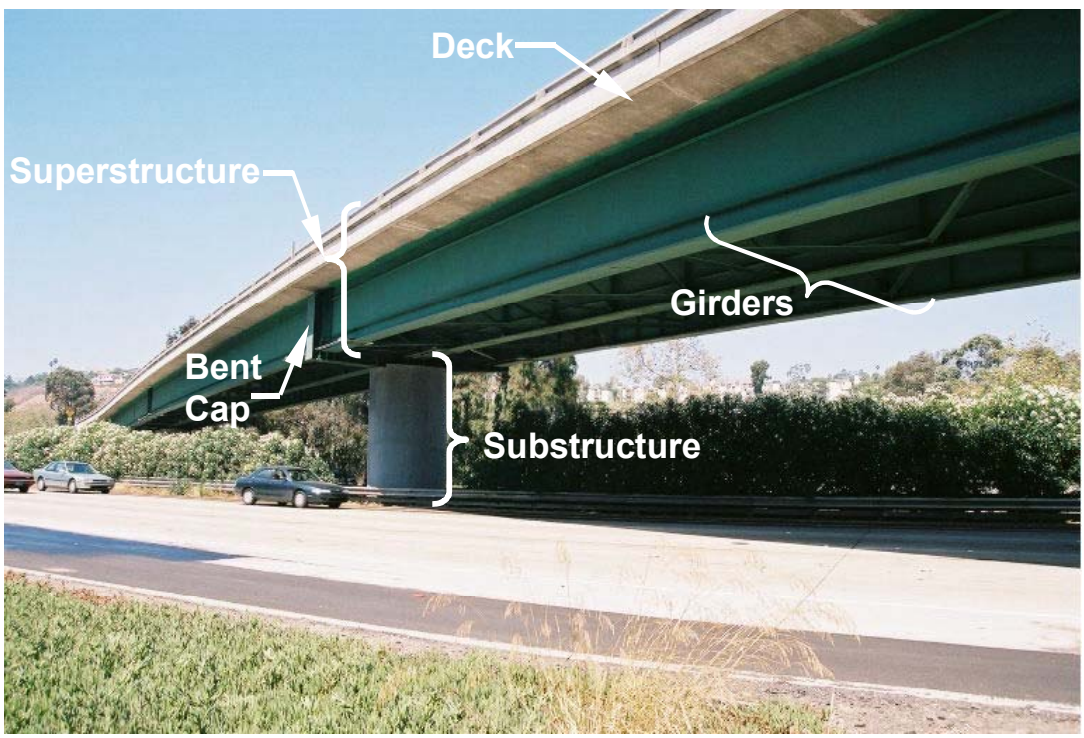

Figure 1-1 Typical Freeway Overcrossing

Common superstructure configurations consist of longitudinal girders composite with a reinforced concrete deck (Figure 1-2). Reinforced concrete is typically used for

the deck because it is durable and requires low maintenance over the life of the bridge. Longitudinal RC (reinforced concrete) or PC (prestressed concrete) girders can be precast bathtub sections, bulb tee sections or cast-in-place (CIP) single or multi-cell box girders (Figure 1-2a). In addition to its durability, concrete can be formed and constructed to match the bridge alignment as needed.

Steel plate girders or box sections (Figure 1-2b) can also function as longitudinal girders of the superstructure and can be made composite with a concrete deck with shear studs. The high strength-to-weight ratio of steel reduces the superstructure weight and increases the distance that can be spanned. Because steel girder fabrication is done at a mill, the girders are delivered to the site already constructed and ready to be set in place, eliminating the need for formwork and associated construction hazards that may necessitate road closures or traffic interruptions.

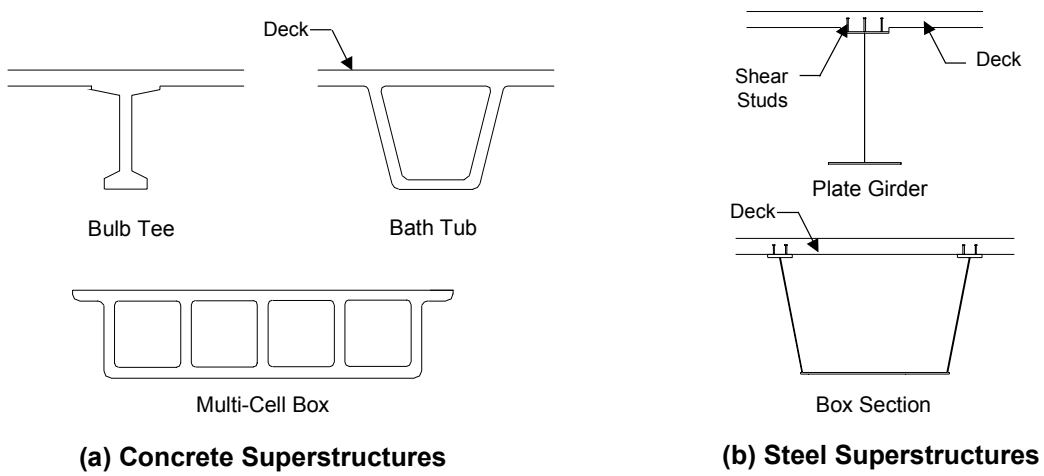

Figure 1-2 Bridge Superstructure Configurations

As the span increases, the superstructure requires intermediate supports. Depending on span and geometric constraints, this support can be provided either above or below the superstructure by such means as cables, arches, trusses or columns. Support with cables is only cost effective for long spans (>660 ft [>200 m]). More commonly, long bridges or viaducts (>200 ft [>60 m]) are intermediately supported from below by bridge bents. A bridge bent typically consists of a bent cap with the width of the bridge superstructure, which is supported by one or more columns (Figure 1-3). This superstructure-supporting assembly of columns and bent caps is termed the substructure.

As with the deck of the superstructure, reinforced concrete is favored over steel for the substructure components because of its durability and low maintenance requirements.

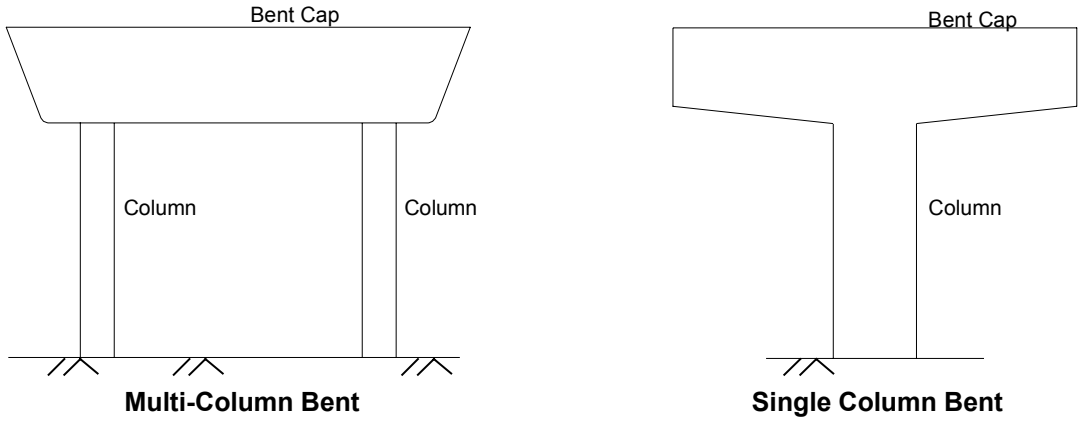

Figure 1-3 Bridge Substructure Configurations

The State of California and its local agencies own and operate over 24,000 bridges in the State. Of the 12,000 state highway bridges, only 7% (approximately 800) are constructed of steel (2). The majority of California's bridges are concrete multi-cell box girder bridges monolithically connected to a concrete column (Figure 1-4 and Figure 1-5) because they provide a clean, durable bridge design that requires low maintenance over its life span. The multi-cell box girder superstructure can be integrally connected to the concrete column without a bent cap (Figure 1-4) or with an outrigger concrete bent cap that can be used as alignment constraints require (Figure 1-5).

Figure 1-4 Concrete Multi-Cell Box Girder Superstructure

Figure 1-5 Monolithic Concrete Multi-Cell Box Superstructure

When a steel superstructure bridge with a concrete substructure is constructed in California (Figure 1-1 and Figure 1-6), the superstructure is typically connected to the substructure by a pin or rocker bearing, a connection which requires high maintenance to protect the pin component against rust. Unlike the monolithic concrete super-to-substructure connections, this steel superstructure to concrete substructure pin connection detail allows relative rotation between the superstructure and substructure.

The Tennessee Department of Transportation in 1978 constructed the first known application of the integral bridge with steel girders continuous through a concrete bent cap (3). Between 1978 and 1982, three integral bridges had been built in Knoxville, Tennessee. As of 1997, all three bridges had proved serviceable with no cracking. In 2001, designers from the Ohio Department of Transportation (ODOT), a low seismic region, constructed a similar steel superstructure bridge integral with a concrete bent cap and column (4) (Figure 1-7). The design is constructable, efficient and increases overhead clearance by eliminating the drop hammer head bent cap that typically supports steel superstructures on concrete substructures (as seen in Figure 1-6). Additionally, by integrating the superstructure to substructure, the structure redundancy is increased.

Designers in seismic regions such as California, however, are reluctant to embrace this integral super-to-substructure connection due to the lack of knowledge of its seismic performance. Of specific concern is its performance under a longitudinal seismic event, which would test the connection ability to prevent relative rotation between the superstructure and substructure.

Figure 1-6 Steel Superstructure on Concrete Hammerhead Bent Cap (4)

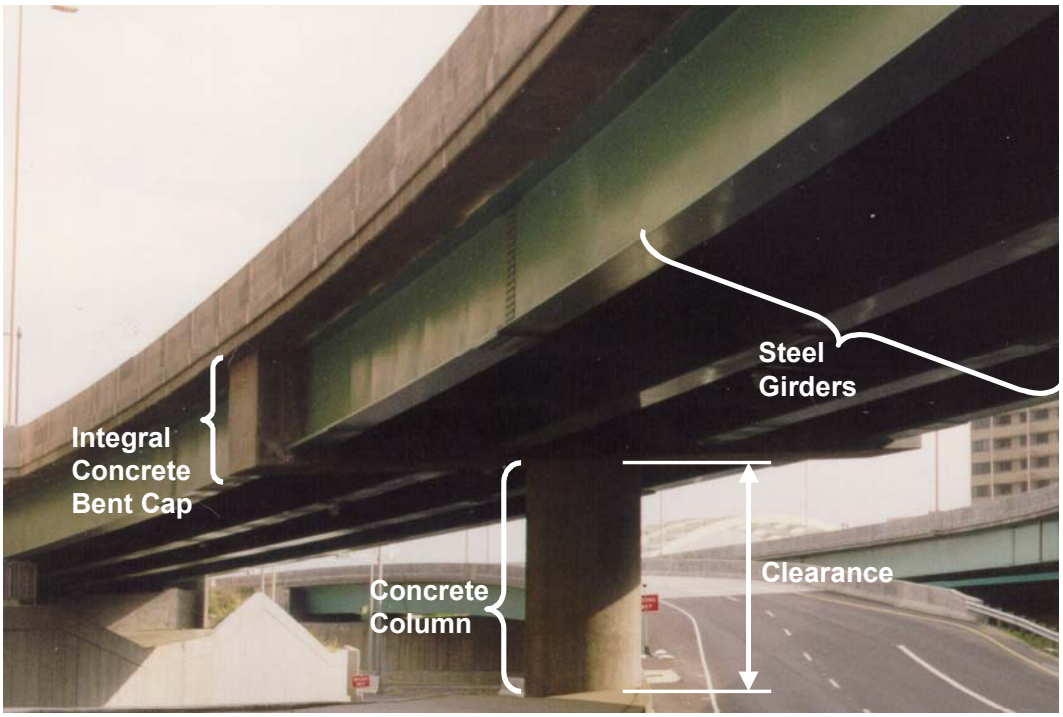

Figure 1-7 Integral Steel Superstructure Concrete Substructure Bridge (5)

A pier detail from Fort Washington Way in Ohio (6) is shown in

Figure 1-8a, and consists of five girders (instead of four as seen in Figure 1-7) continuous through a concrete bent cap supported on a single column. The bent cap is post-tensioned with a draped tendon and one girder is located directly over the column. In seismic regions, it is not desirable to place a single girder over the column, as the majority of the demand from a longitudinal seismic event is transferred to the abutments by this single girder rather than distributed evenly between two girders. This force transfer will be discussed in further detail in Section 1.2.

Details of integral bridges designed by the Nevada Department of Transportation (7, 8) are similar to the Ohio detail, however more adaptable to seismic regions because of the girder spacing. The two details presented here (

Figure 1-8b & c) have four girders evenly spaced on either side of the column. All details have draped post-tensioning in the bent cap. The girders in the Fort Washington Way Bridge and the I-15/Tropicana interchange have shear studs welded on the girder webs inside the bent cap region.

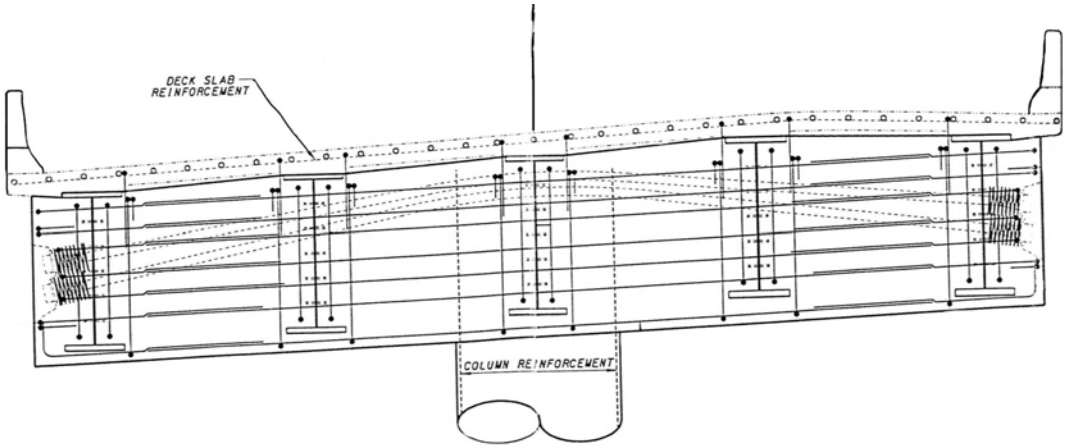

(a) Fort Washington Way, Cincinnati, Ohio (6)

Figure 1-8 Integral Connection Details[1]

[1] Some drawing text omitted for clarity. Intended for illustrative purposes only.

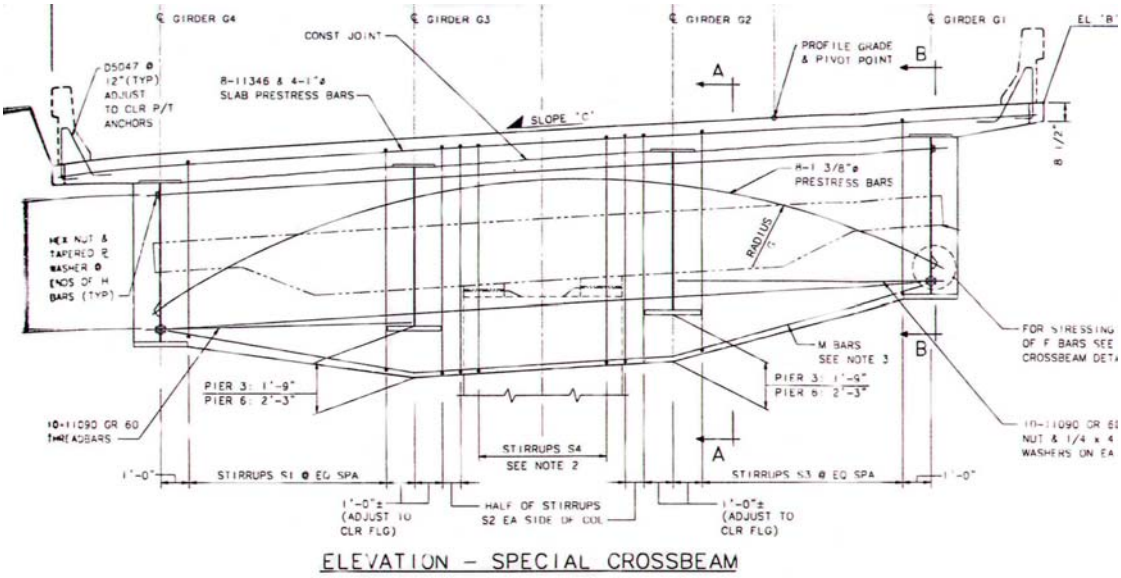

(b) Sahara Avenue Interchange, Nevada (7)

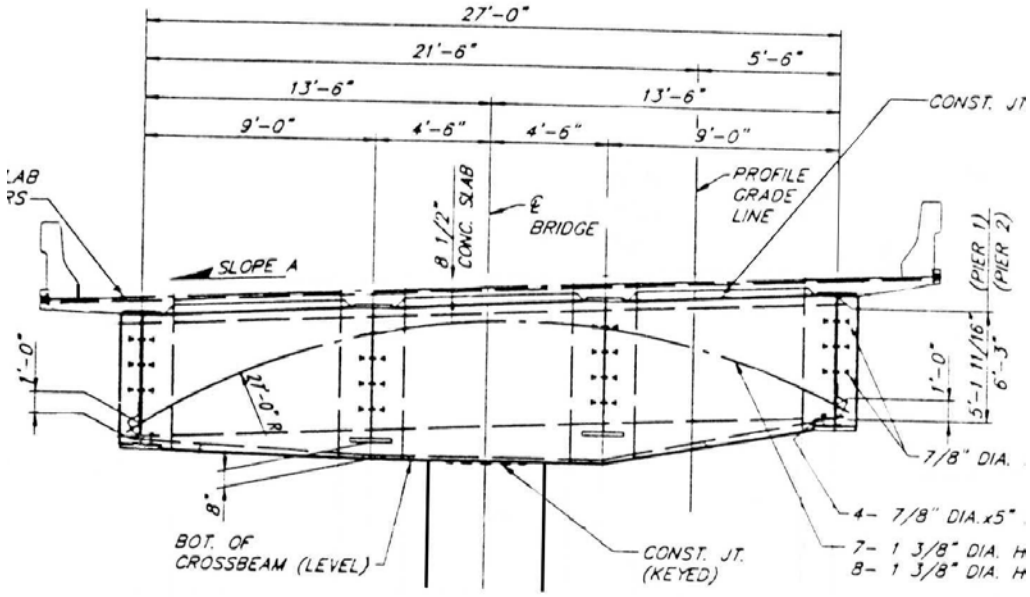

(c) I-15/Tropicana Interchange, Nevada (8)

Figure 1-8 Integral Connection Details (continued)

1.2 SEISMIC DESIGN ISSUES

Current seismic design philosophy, particularly in California, relies on structural redundancy, ductility, and capacity design concepts. Since seismic input is largely unknown, bridges are designed such that redundancy (or static indeterminacy) allows the formation of local mechanisms at selected locations in which design detailing provides for large inelastic ductile deformations. Seismic bridge design places these inelastic mechanisms, or plastic hinges, in the columns where damage can be inspected and repaired without bridge closure. In addition to being durable, concrete has high axial load capacity and, with appropriate spiral or hoop reinforcement, large flexural capacities with large ductile deformations, making it an ideal material for bridge columns to provide the required plastic hinge deformation response to seismic input.

To ensure that the inelastic mechanism occurs in the desired location (the column), adjacent members, where inelastic actions are not desired, must be designed to ensure elastic response. All locations susceptible to inelastic action are identified in Figure 1-9, on the deformed shape of a bridge model subjected to a longitudinal seismic motion. The desired failure mechanism locations are highlighted by dashed ovals at the top and bottom of each column. At these locations, the column is detailed to ensure flexural ductility. At each pier, the bent cap, the girders, and the interface between the bent cap and girders must perform elastically. These members are considered capacity protected components and need to be designed using the full column overstrength moment based on capacity design principles.

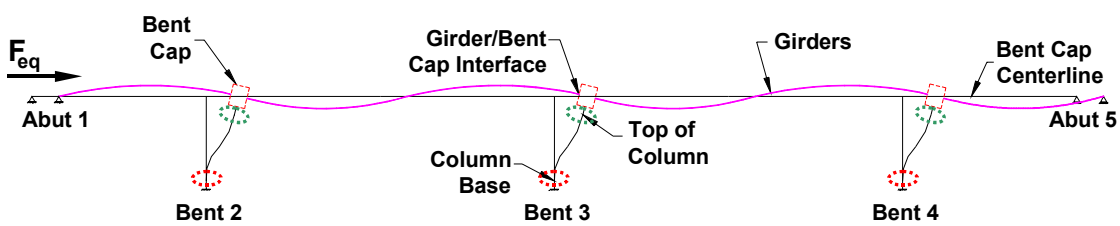

Figure 1-9 Potential Hinge Locations

In order for a flexural hinge to form in the column, the column must be subjected to moments greater than yield. This moment must be transferred at the base to the footing and at the top to the bent cap. If the superstructure is simply supported on the bent cap, no moment is transferred to the bent cap and therefore no plastic hinge can form at the

top of the column. Therefore, to increase the bridge's redundancy and to force hinging in the column, an integral connection between the superstructure and the substructure is required to transfer the moments between the super and substructure.

For a connection to be integral, relative deformations between the connected components need to be prevented. In order to prevent this deformation, integrally connected components need to elastically transfer the forces that would cause this deformation. Subjected to a longitudinal seismic event, the bent caps need to transfer the seismic moment from the superstructure/girders through torsion in the bent cap to the supporting columns. Bent cap failure would be difficult to inspect, costly to repair, and almost certainly require bridge closure following a major seismic event.

Once the bent cap has elastically transferred the seismic moment, the girders are required to carry this moment in addition to the pre-existing gravity loads. Girder failure would be difficult to inspect following a seismic event. Additionally, repair of longitudinal bridge girders would almost certainly cause bridge closure and consequently be quite costly. Finally, any degradation of bent cap concrete around the steel girder would limit the force transfer capacity of the connection and consequently not develop the desired column failure mechanism.

Therefore, seismic bridge design in California requires the superstructure and the connection of the superstructure to the substructure to carry loads (seismic and gravity loads) elastically while the columns deform plastically. Subjected to a longitudinal seismic event, an integral bent cap, like the one shown in Figure 1-7, would have to transfer a seismic moment between girders and column through torsion. Because a steel superstructure bridge is typically more flexible than a concrete superstructure bridge, uncertainty exists in the ability of a steel superstructure bridge to elastically transfer the seismic forces to a concrete substructure. It is this uncertainty that prevents this otherwise desirable detail from being constructed in seismic regions, indicating a need for research to establish the abilities of such connections.

1.3 PAST RESEARCH

Research into the behavior of integral connections between steel/concrete composite superstructures and reinforced concrete substructures is needed to demonstrate

the viability of such connections under a longitudinal seismic event. A similar issue arises with precast girder/concrete composite superstructures integral with concrete substructures. Holombo, et al. (9, 10) investigated the use of precast concrete girders integrally connected to a CIP concrete substructure through a research program that included two large-scale tests (Figure 1-10a). The girders of the first test were precast bulb tee girders that ran continuously through the bent cap, integrating the cap into the superstructure (Figure 1-10b). The second test had precast bathtub girders, which terminated a distance inside the bent cap (Figure 1-10c). In both tests, the girders were supported while the bent cap was cast around them.

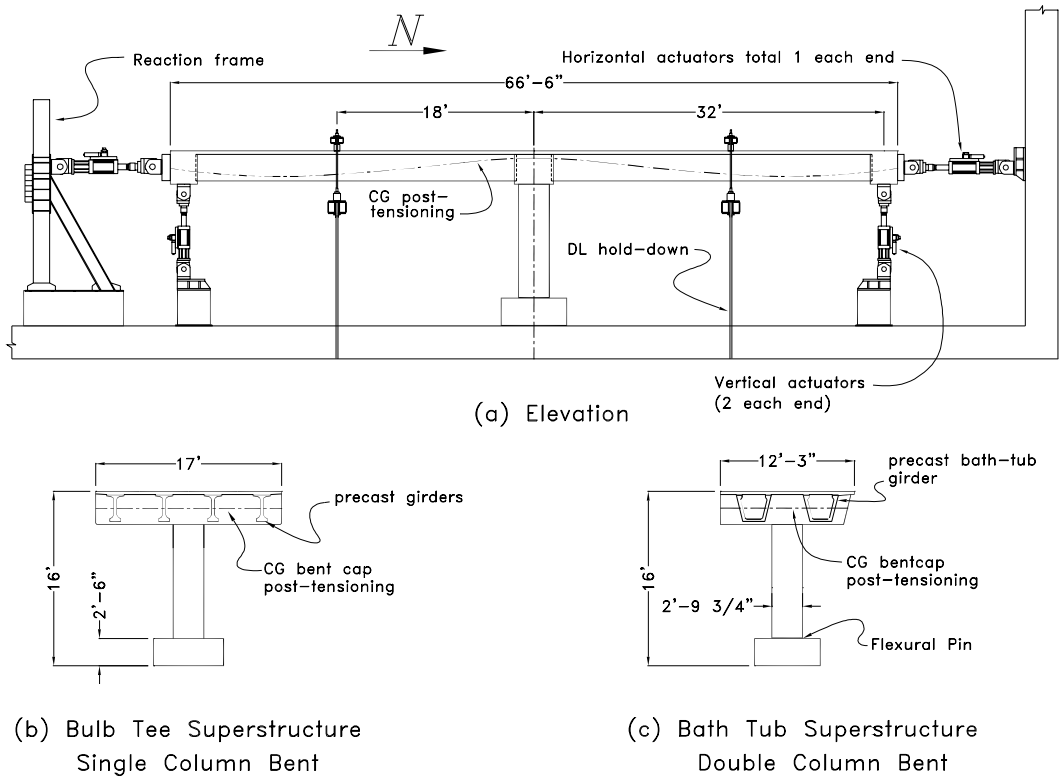

Figure 1-10 Precast Superstructure Configurations (9)

The two tests, constructed at 40% scale were subjected to a simulated longitudinal seismic event (Figure 1-11). Both tests performed well and demonstrated that a reliable connection could be developed between precast superstructure girders and the cast-in-place concrete bent cap, forcing hinging into the column with minimal superstructure damage.

Figure 1-11 Precast Bathtub Girder Test (9)

Alternative integral connection configurations have been proposed (11, 12) including superstructure variations of steel bent caps and box girders. Researchers at Iowa State University are investigating concrete column/steel bent cap/steel girder integral bridge systems (13). For any proposed design to be suitable in regions of high seismicity, the detail must ensure elastic performance when subjected to the full column overstrength moment.

1.4 RESEARCH OBJECTIVE AND EXPERIMENTAL PROGRAM

The objective of this research is to develop design procedures for a steel superstructure bridge that is integrally connected to a concrete substructure. Developing a reliable integral connection between a steel superstructure and a concrete substructure will produce a bridge with a lightweight superstructure, a low maintenance connection, and a desirable, ductile damage mechanism in a seismic event. It is the goal of this research to clearly characterize and define the behavior of such connections, and to develop reliable design procedures for bridge design engineers.

In order to develop design procedures, it is imperative to first understand the complete behavior of the composite integral bridge system. Then, it is necessary to

predict and specify design limit states with reference to a complete force-displacement response of the system, including all possible local mechanisms. One of these local mechanisms, as previously described, is bent cap torsion between the column and the interior girder.

Initial experiments were performed on a setup that ensured torsional failure in the bent cap to characterize the complete bent cap behavior. Four component tests with different design details were tested to failure in the bent cap in order to develop four behavior curves. One parameter was varied at a time for the four tests so that the contribution of each parameter to the force transfer mechanism was evident and quantifiable.

After testing and analysis of the four component test specimens, the expected performance of the recommended detail was validated through a system test. The system test specimen included a column with four girders in the full superstructure width. The purpose of the system test was to demonstrate that an integral connection bridge could be designed to successfully designate the column as the location of the inelastic failure mechanism while the bent cap and superstructure experience minimal damage under a longitudinal seismic event. Force transfer mechanisms were investigated using simplified force transfer strut and tie models for the critical cap region.

1.5 OUTLINE OF THE REPORT

The beginning portion of Chapter 2 presents the design of the prototype bridge and bridge components that form the basis for this research, including the column, bent cap, and steel girders. Also presented is a summary of existing research on the behavior of beams in torsion.

Chapter 3 covers the design, construction, instrumentation and testing of the component test specimens. Strain gage and instrumentation locations are presented as well as the test loading sequence.

Chapter 4 presents experimental results from the four component tests. The observed and measured performance of each test specimen is presented. The chapter concludes with comparisons of test specimen performance.

Chapter 5 presents the detail recommended based on the component tests and design of the system test specimen. A detailed explanation of the system test boundary conditions is presented as well as the loading sequence and strain gage and instrumentation locations.

Chapter 6 presents experimental results from the system test through photographs and measured response.

Chapter 7 presents recommendations on design approach with reference to a design example. Design specifications as well as suggestions for design of alternative configurations are included.

Chapter 8 summarizes the report, highlights the contribution to the state-of-the-art and engineering practice and provides recommendations for areas of further work.

Chapter 2

Prototype Design and Connection Details

2.1 OVERVIEW

This chapter presents the design of the prototype bridge and development of the girder-cap connection detail. Sections 2.2 through 2.6 discuss the design of all components of the prototype bridge including the column, girder, and bent cap design. Section 2.6 includes a history of the development of torsion analysis. Section 2.7 focuses on the integration of the steel girder to the concrete bent cap by assessing design configurations at the cap/girder interface.

2.2 PROTOTYPE DESIGN

The prototype bridge provided by Caltrans for this project represented a typical Caltrans four-span, two-lane freeway over-crossing supported on a single column bent, shown in Figure 2-1. Preliminary sizing by Caltrans outlined the column diameter (5.5 ft [1.7 m]), span lengths (132.5 ft – 160 ft [40.4 m – 48.8 m]), and approximate superstructure depth (6 ft [1.8 m]). The bridge was detailed in accordance with Caltrans Bridge Design Specifications and AASHTO Standards (14, 15).

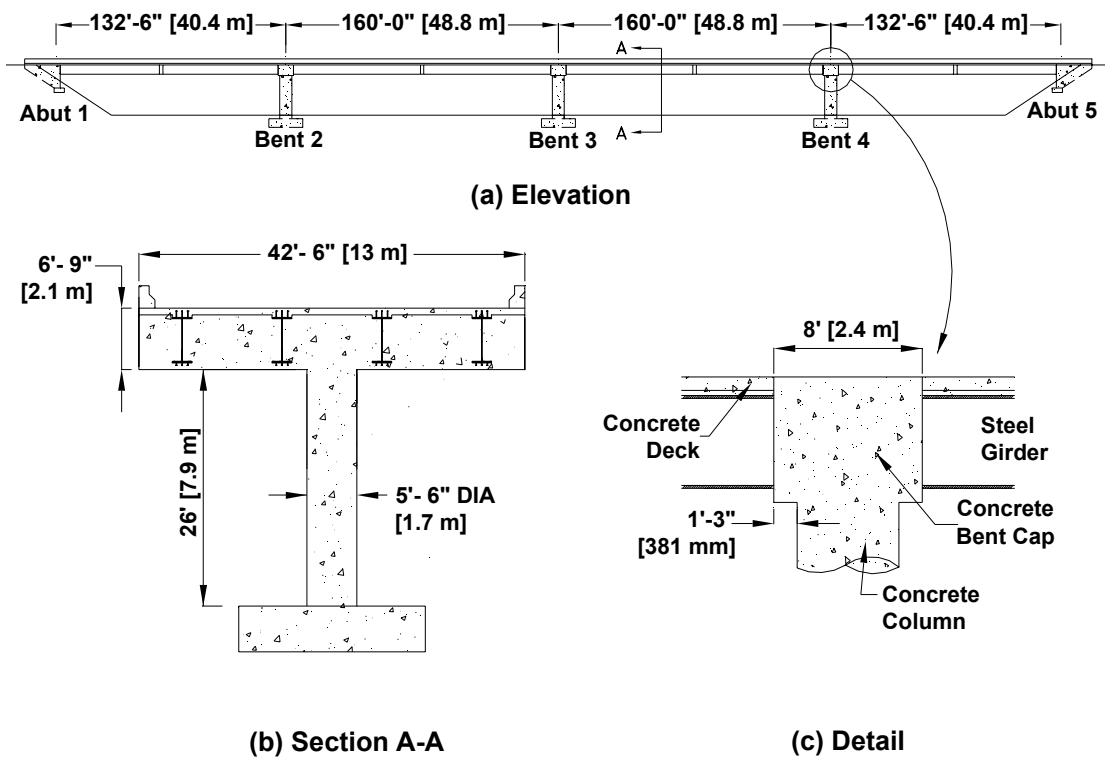

Figure 2-1 Prototype Bridge Dimensions

2.3 PROTOTYPE COLUMN DESIGN

In the prototype composite bridge, the columns were fixed-fixed in the longitudinal direction and cantilevered in the transverse direction. Therefore, under longitudinal seismic input, the columns deform in double curvature bending. To impose the maximum possible seismic demands on the capacity protected components, the column was designed with a 2% longitudinal reinforcement ratio, achieved by 44 No. 11 [36 mm] reinforcing bars.

With a displacement response spectrum (16) for soil profile type D with a magnitude of 7.25±0.25 and peak ground acceleration of 0.6g, the seismic displacement demands were determined using force based design. Two moment curvature analyses of the column were performed using the SEQAD Moment Curvature Program (SEQMC) (17) to determine column design strength and column overstrength. The design strength was determined using the specified material properties (f_c'=4 ksi [28 MPa] for concrete and f_y=60 ksi [414 MPa] for reinforcing steel) in the program. The design moment is the minimum column capacity. In reality, the column will perform above design levels

because materials typically reach strength levels higher than their specified minimum values. This characterization of increased material strengths is referred to as material overstrength properties. The maximum expected strengths of the constituent materials was obtained by multiplying the specified material strengths by 1.3 (18) (f_c'=5.2 ksi [36 MPa] for concrete and f_y=78 ksi [538 MPa] for reinforcing steel). Figure 2-2 compares the moment-curvature results for the design strength, the overstrength and a line representing the maximum overstrength value multiplied by a protected component overstrength factor of 1.2. The increased maximum overstrength value, M_o, is used for the elastic design of the superstructure and is discussed further in Section 2.4.2.

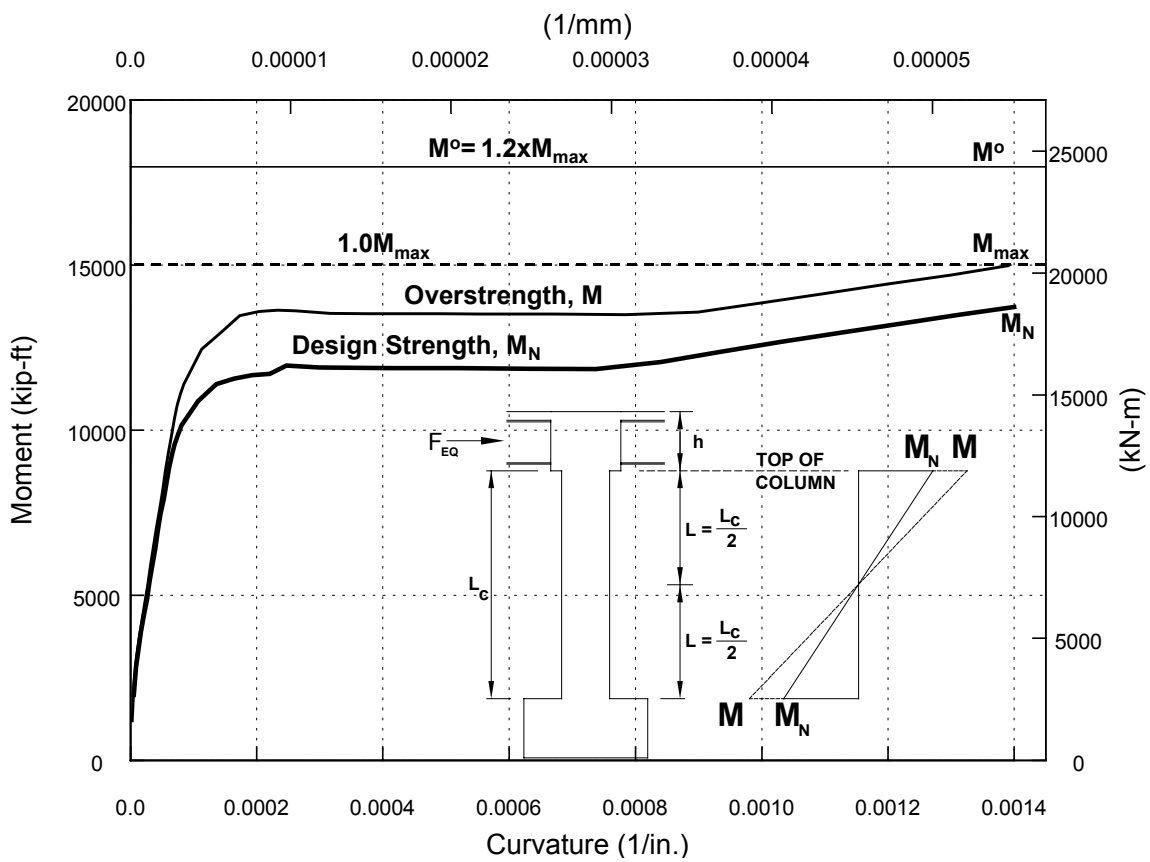

Figure 2-2 Prototype Moment Curvature Characteristics

To determine the structural yield displacement, the yield curvature from the moment curvature analysis was used in the equation presented in Priestley et al. (19):

$$\Delta_y = \phi_y L^2 / 3 \qquad \textbf{(2-1)}$$

where ϕ_y is the yield curvature and L is the length of column generating the displacement. For displacements in the longitudinal bridge direction, the displacements are calculated by treating the column with clear column height L_c as two cantilevered sections of length L (Figure 2-3a). The yield displacement of each cantilevered section is calculated using Equation 2-1 with a length of half the clear column height, L_c. Therefore, total column displacement in the longitudinal direction is the sum of the displacement of two cantilevered sections of the same length ($L_c/2$). In the transverse direction, the column deforms in single bending and the length of column generating the displacement extends from the footing to the centerline of the superstructure. Hence the length $L_c + h/2$ is used to calculate the yield displacement in the transverse direction.

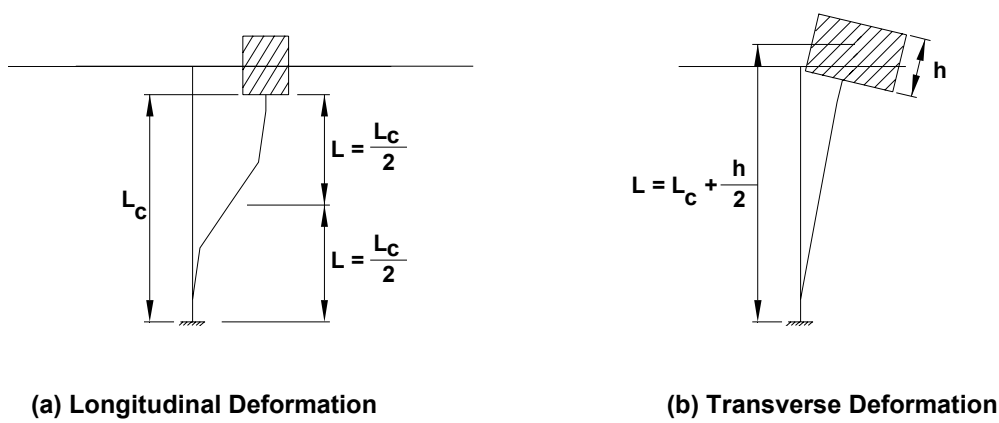

Figure 2-3 Deformed Shape

Once the column reaches its yield displacement, further displacement is concentrated in the plastic hinge region. Therefore, the ultimate displacement is comprised of the yield displacement occurring over the lengths explained above and any plastic deformation occurring over the plastic hinge(s) at the member end(s). The plastic hinge length, L_p, is the nominal length at the end of the column that is expected to deform plastically and is approximated by an empirically established value of 8% of the column shear span, L, plus a value for plastic strain penetration. Strain penetration is the amount of plastic deformation that extends into the adjacent member. It is a function of the column longitudinal reinforcement yield strength, f_y, and the column longitudinal bar diameter, d_b (19),

$$L_p = \begin{cases} 0.08L + 0.15 f_y d_b & \left(f_y \text{ in ksi}\right) \\ 0.08L + 0.022 f_y d_b & \left(f_y \text{ in MPa}\right) \end{cases} \quad \textbf{(2-2)}$$

The yield and ultimate curvatures, ϕ_y and ϕ_u, and the ideal and ultimate moments, M_i and M_u are obtained from the moment-curvature analysis. Yield displacement and plastic hinge length in each direction are calculated from the methods previously discussed. With these values, the ultimate displacement in each direction is calculated from (19):

$$\Delta_u = \Delta_y \left(\frac{M_u}{M_i} \right) + \left(\phi_u - \phi_y \left(\frac{M_u}{M_i} \right) \right) L_p L \quad \textbf{(2-3)}$$

where the same procedure in the yield displacement calculations regarding column length is used for the length, L. The displacement capacities and demands for the prototype bridge column in Figure 2-4 are tabulated in Table 2.1.

Table 2.1 Prototype Column Displacement Capacities and Demands

	Transverse Direction	**Longitudinal Direction**
Yield, Δ_y, in. [mm]	3.4 [86]	1.4 [36]
Ultimate Capacity, Δ_u, in. [mm]	22 [559]	11.7 [297]
Demand, Δ_D, in. [mm]	18 [457]	7 [178]

The No. 11 [36 mm] longitudinal reinforcement was bundled in 22 pairs to meet Caltrans spacing requirements and extended into the cap 11-1/4 inches [286 mm] below the top of the deck. Shear demands required No. 8 [25 mm] reinforcing hoops at 6 inches [152 mm] center to center in the plastic end region and No. 8 [25 mm] reinforcing spirals at 16 inches [406 mm] in the non-confined regions all with two inches [51 mm] of cover. The final column design is shown in Figure 2-4.

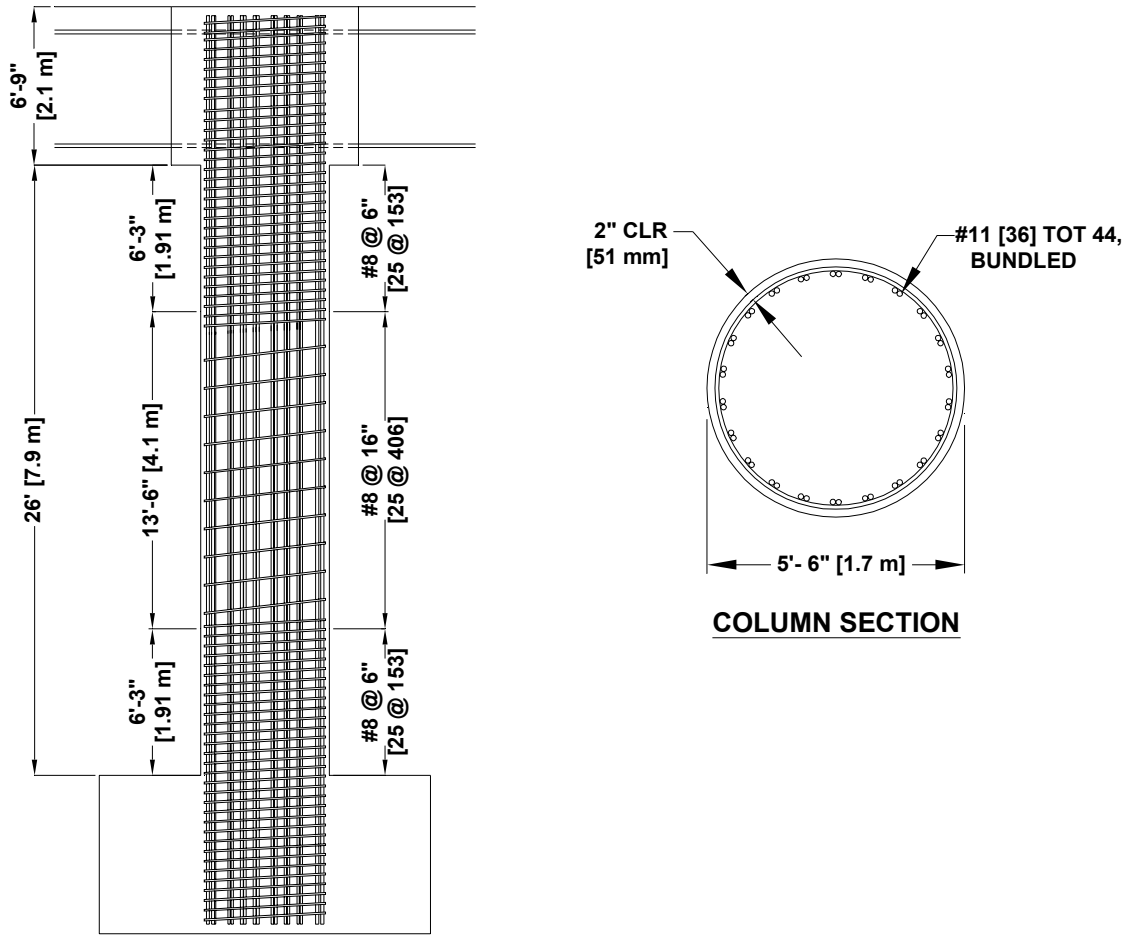

Figure 2-4 Prototype Column Reinforcement Detail

2.4 PROTOTYPE STEEL PLATE GIRDER DESIGN

2.4.1 Prototype Gravity Loads

Since the superstructure was continuous, it was in positive bending at midspan and negative bending over the piers (Figure 2-5). Therefore, the section over the supports where the concrete deck can be assumed cracked was designed considering only the girders and the deck reinforcing steel contributed to the flexural capacity while flexural capacity of the midspan section included the contribution from the deck concrete. Using influence lines, the maximum live load demands on the girder were determined and the section was designed for the load cases specified in Caltrans Bridge Design Specifications (BDS) (14).

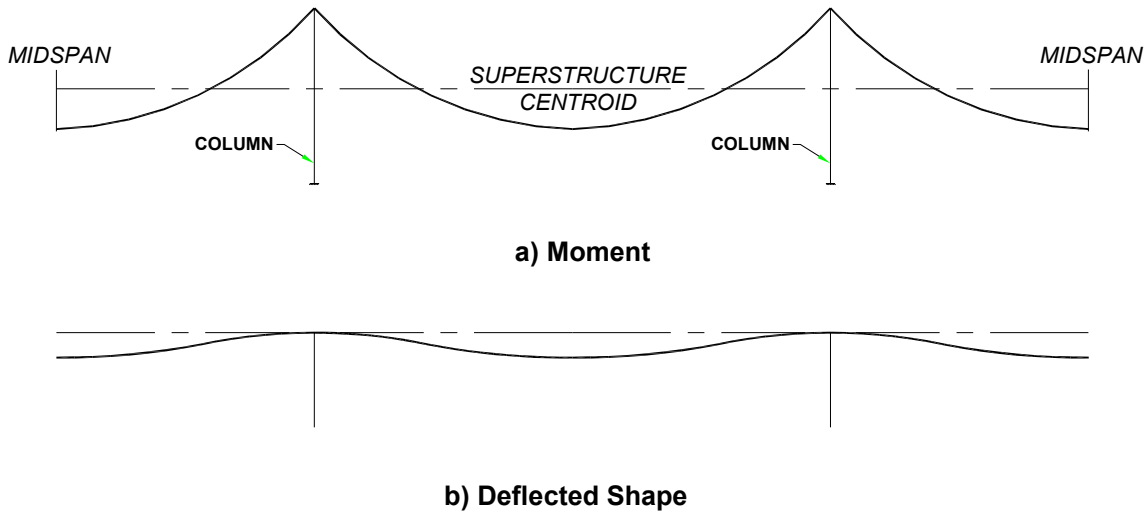

Figure 2-5 Prototype Superstructure Moment and Deflected Shape Due to Self-Weight

2.4.2 Prototype Seismic Loads

Under a longitudinal seismic event, a large moment occurs at the top of the column in an integral connection. To satisfy equilibrium, this moment must be transferred to the girders through the bent cap. In order to protect these superstructure components from damage, they are designed for a demand moment corresponding to the full possible column overstrength moment.

The moment at the top of the column due to full material overstrengths, M_{max}, (Figure 2-2) was extrapolated to the center of the girder section (Figure 2-6). This extrapolated moment, M'_{max}, is the moment expected to be transferred through the bent cap to the girders via equilibrium torsion. To ensure the superstructure elastically transfers the moment M'_{max}, it is multiplied by an overstrength factor of 1.2, a component overstrength factor designated in the Caltrans Seismic Design Criteria (20). This results in a column overstrength moment at bent cap centerline M_T.

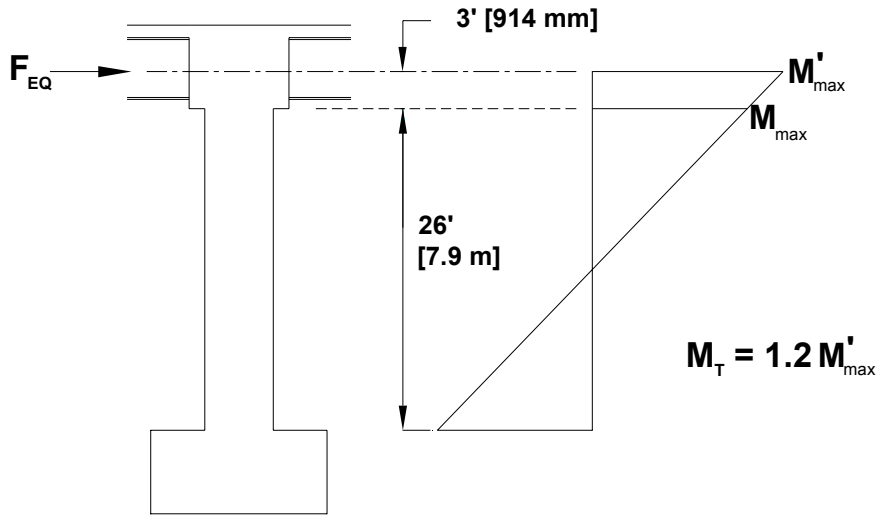

Figure 2-6 Substructure Seismic Moment

The superstructure design moment, M_T, is assumed to be equally resisted on either side of the column (Figure 2-7). Because the torsional moment enters the bent cap between the interior girders, the interior girders carry the larger amount of the seismic moment and the remainder is distributed again through cap torsion to the exterior girders. The distribution of this moment was investigated in the tests of Holombo et al. (9) where strain gage readings on longitudinal deck bars indicated approximately 2/3 of the moment was carried by the interior girders while the remaining 1/3 of the moment was transferred to the exterior girders (Figure 2-8), a distribution adopted for the present prototype design. The seismic design moment for the girders is obtained by adding the seismic moment to the dead load moment, as specified by design load cases of AASHTO (15).

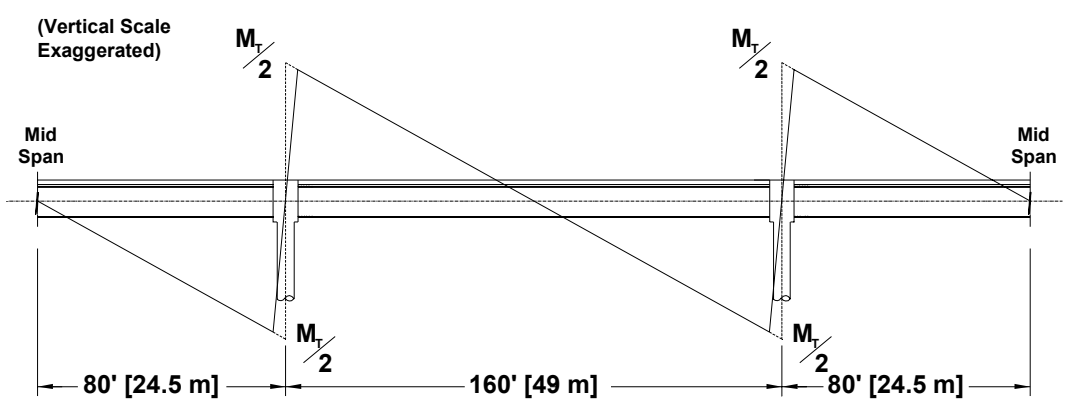

Figure 2-7 Superstructure Seismic Moment

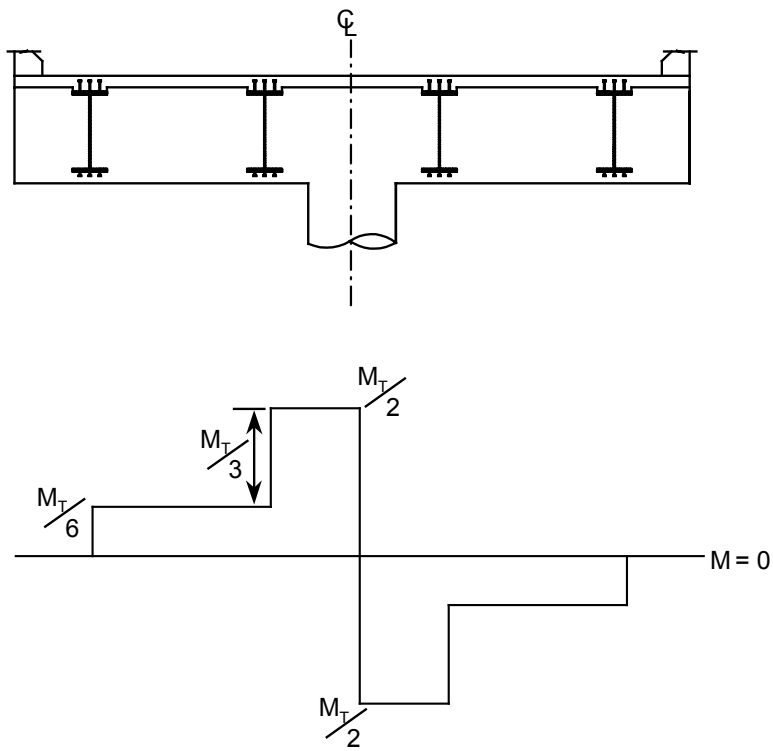

Figure 2-8 Distribution of Torsional Moment along the Bent Cap (9)

Built-up sections, as opposed to rolled sections, are typically preferred for girders of steel superstructure bridges. Because the majority of rolled sections are compact, they satisfy the limit states for local buckling (21). Therefore, in order to use a rolled beam section that is satisfactory in flexure, the web is typically very thick and overly conservative for the shear requirements common on bridges. This additional web thickness can significantly add to the superstructure weight with no benefit to the overall bridge performance. By using a built up section, a web is specified with a thickness that satisfies the shear demands and a depth that provides sufficient moment arm to satisfy the flexure demands. The ratio of the web depth, D, to web thickness, t_w, is called the slenderness ratio which determines if a section is compact or noncompact. The compactness of a section is also a property of the flange slenderness ratio. While the prototype flange slenderness ratio was satisfactory to qualify for a compact section, the high web slenderness ratio made the section noncompact.

All structural steel was specified to be ASTM A709 Grade 50 (AASHTO M270 Grade 50) (22) and welding to comply with ANSI/AASHTO/AWS D1.5-95 (23). In the negative moment region, shear stiffeners on the girder web outside the cap region were

welded every 4'-6" [1.4 m]. In the positive moment region, shear stiffeners were spaced at 10 ft [3 m]. Shear stiffeners were specified to be a tight fit between flanges but welded only to the web and the bottom flange. Lateral bracing along the span was specified at every 20 ft [6.1 m]. The final steel plate girder design is shown in Figure 2-9.

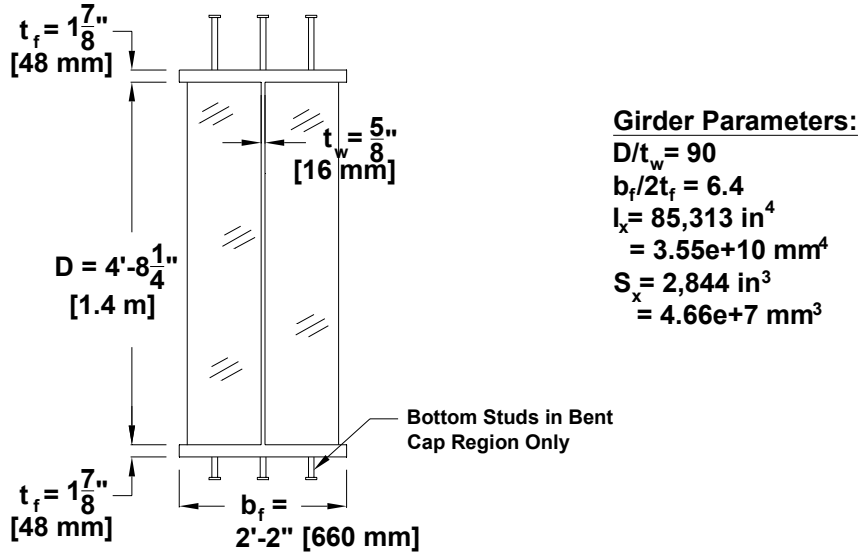

Figure 2-9 Prototype Plate Girder Properties

2.5 PROTOTYPE COMPOSITE DECK DESIGN

Headed studs welded to the top of the steel girders provide the connection to the RC deck in a composite steel girder/concrete deck. The shear stud design was controlled by fatigue loading. Studs on the top flange were 8 1/8 in. [206 mm] long and spaced in rows of three at 24 in. [610 mm] on center, between the bent and a distance of 0.2*L* on either side of the bent, and continued through the bent cap (Figure 2-9). Three rows of studs were also placed on the bottom flange of the girder, in the cap region only, at the same spacing as the top studs but were only 3 ½ in. [89 mm] long due to the reduced cover concrete at the bottom. All studs were 7/8 in. [22 mm] diameter and the final stud design is shown in Figure 2-10.

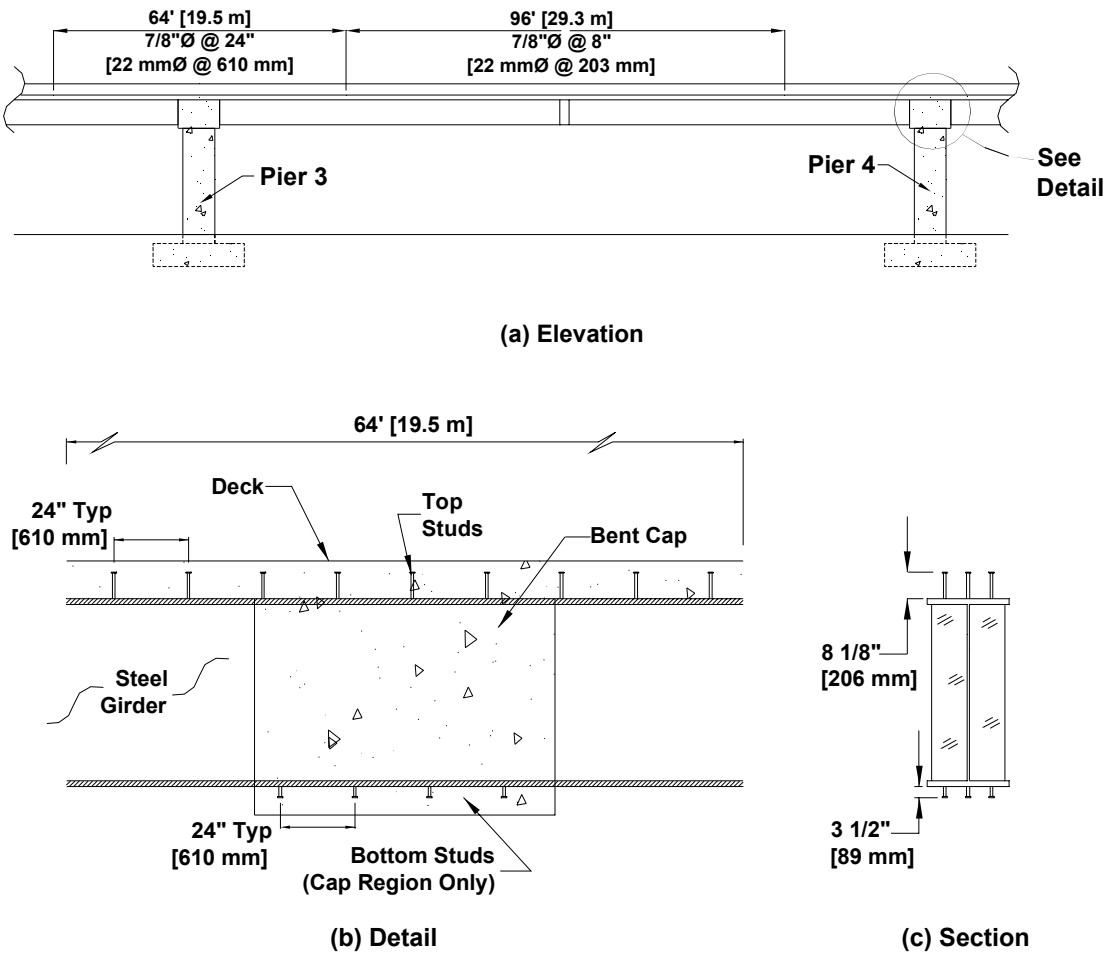

Figure 2-10 Prototype Shear Stud Design

The deck was designed in accordance with Caltrans Bridge Design Details (BDD) (20). The effective span of the 8 5/8 in. [219 mm] thick deck slab was 10 ft [3 m], and haunches over the girders were 3 3/8 in. [86 mm]. Reinforcement spacing requirements were obtained from "Deck Slab Reinforcement" in Caltrans BDD (24), page 8-30. The final deck design including reinforcement details is shown in Figure 2-11.

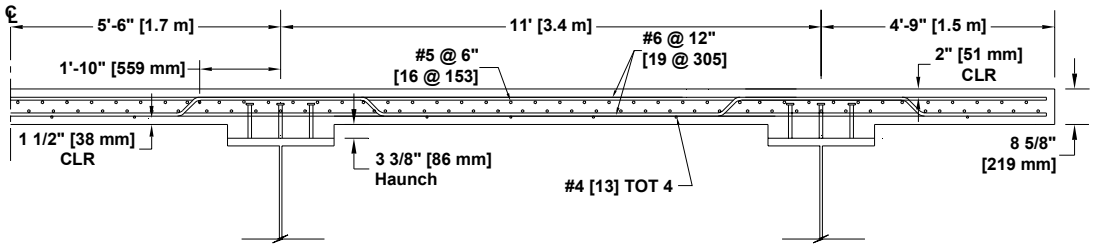

Figure 2-11 Prototype Deck Reinforcement Detail

2.6 PROTOTYPE BENT CAP DESIGN

2.6.1 Prototype Gravity Loads

The bent cap flexural design followed typical Caltrans practice for a continuous concrete bridge as presented in Bridge Design Specifications (BDS) and Bridge Design Practice (BDP) (14, 25). The original bent cap was 6 ft [1.8 m] deep to accommodate the five-foot [1.5 m] deep girders, the 3 3/8 in. [89 mm] haunch and the 8 5/8 in. [216 mm] deck. To allow the bottom cap steel to pass under the girders, the original cap depth was increased by 9 in. [229 mm] resulting in the prototype bent cap depth of 6' – 9" [2,057 mm]. The bent cap width, 8 feet [2.4 m] was controlled by seismic detailing and is discussed in Section 2.6.2.

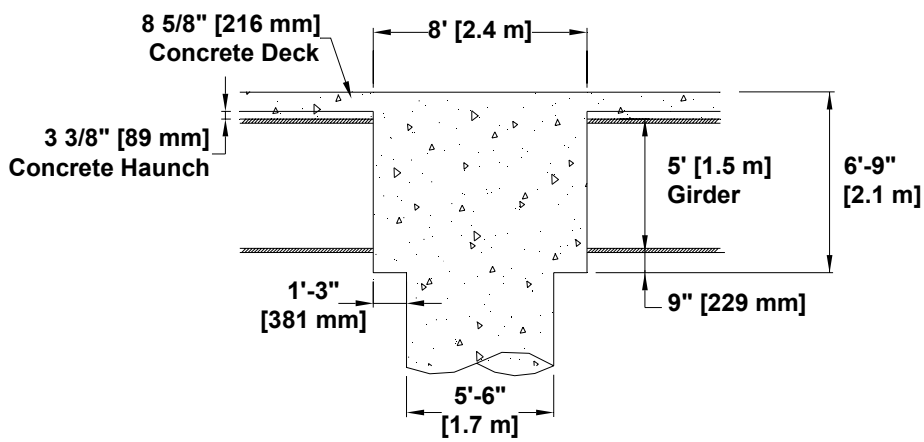

Figure 2-12 Prototype Bent Cap Geometry

The bent cap was designed to carry its self-weight, the superstructure weight and live loads. Using influence lines and load factors defined in Caltrans BDS (14), the maximum moment in the bent cap at the column face due to self-weight and live load was determined. With this factored moment, M_u, bent cap depth, d, the section material properties, and an assumed rectangular concrete compression block across the section face as in Caltrans BDP (25), the required area of main flexural reinforcement was determined. The required area of main flexural reinforcement was 51 in.^{2} [329 cm^2] and was located at the top of the bent cap in the form of 32-No. 11 [36 mm] bars (Figure 2-13), passing over the top flange of the steel girders.

Construction reinforcement is required to provide enough strength to the bridge during construction to carry its own self-weight. The moment demand due to bent cap self-weight dictated the area of steel required for construction reinforcement and was determined assuming a rectangular compression block stress distribution across the section. This construction reinforcement, namely eight No. 11 [36 mm] bars, was located below the top girder flange, just below the construction joint between the bent cap and the deck. For the construction reinforcement to be continuous through the bent cap, holes were predrilled in the girder web. While these holes reduced the girder's shear capacity by 9%, this portion of girder is cast in concrete and therefore effectively continuously supported, causing no concern for this decrease in shear capacity. Crack control reinforcement was included at the side and bottom faces of the bent cap, also continuous through predrilled holes in the girder web.

With the factored shear, V_u, determined from influence lines as in Section 2.2.4.1 and pre-selecting a reinforcing bar size No. 7 [25 mm], the required spacing for shear reinforcement was determined from:

$$s = \frac{A_v f_y d}{V_s} \tag{2-4}$$

with A_v equal to the cross-sectional area of stirrup, d the depth of the bent cap, and V_s denoting the total shear demand less that resisted by concrete. The shear capacity of the concrete is determined from $2\sqrt{f_c'}b_w d$, where f_c' is the compressive strength of the concrete and b_w and d are the width and depth of the section, respectively. The maximum spacing for a pair of No. 7 [25 mm] stirrups was 10 in. [254 mm] center to center. The stirrups at the cap/girder interface were butted up to the girder flanges. The only reinforcement integrating the girder with the cap was the cap flexural reinforcement that passed above, below and through the girder. The final bent cap reinforcement details are shown in Figure 2-13.

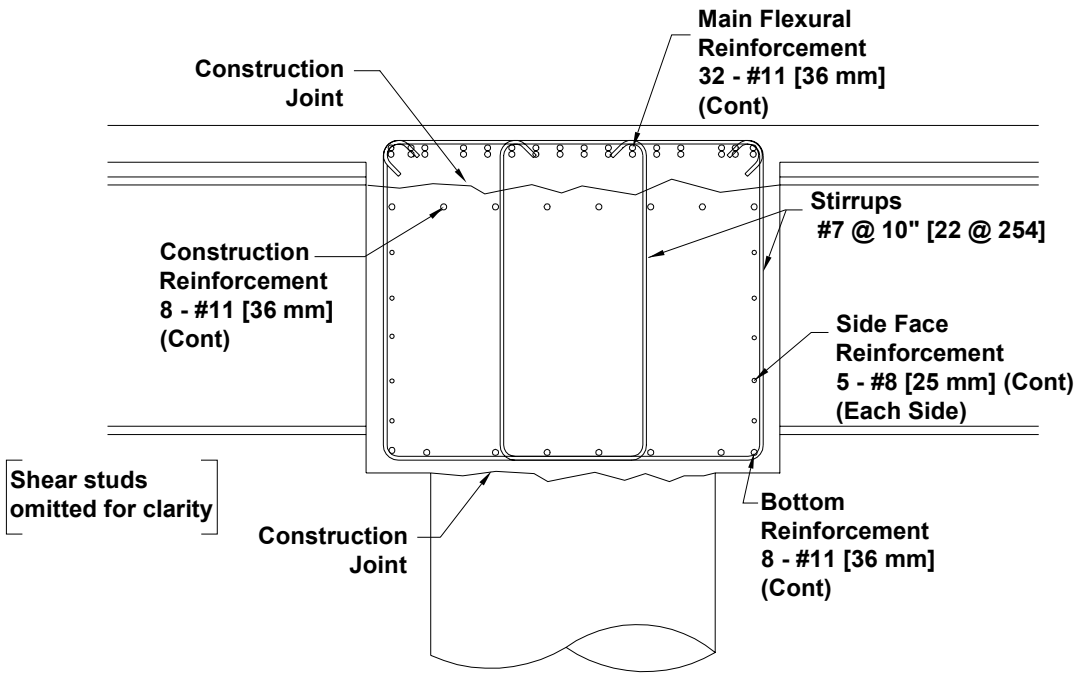

Figure 2-13 Prototype Bent Cap Reinforcement

2.6.2 Prototype Seismic Loads

To design the bent cap for seismic loading, two requirements need to be met. First, the bent cap needed to be detailed according to Caltrans Seismic Design Criteria (SDC) (20). The SDC specifies minimum reinforcing details for all bridges constructed in California. The second was to ensure that the bent cap transfer the torsional moment due to longitudinal seismic forces as determined in Section 2.4.2. First the minimum requirements were met, and then a torsion analysis of the detailed cap was performed.

The minimum bent cap width specified in the SDC is the column diameter plus a minimum one-foot [305 mm] width on either side of the column in the longitudinal direction for reliable joint shear force transfer (20). Thus, the prototype bent cap was detailed with 1'-3" [381 mm] on either side of the column (Figure 2-14). This dimension allowed for shear reinforcement to be located outside the column. The joint region (the location of column and bent cap integration) is defined in the SDC as the area extending a distance of half the column diameter, D_c, from either face of the column in the transverse direction, which in this case also corresponded to the center to center girder spacing.

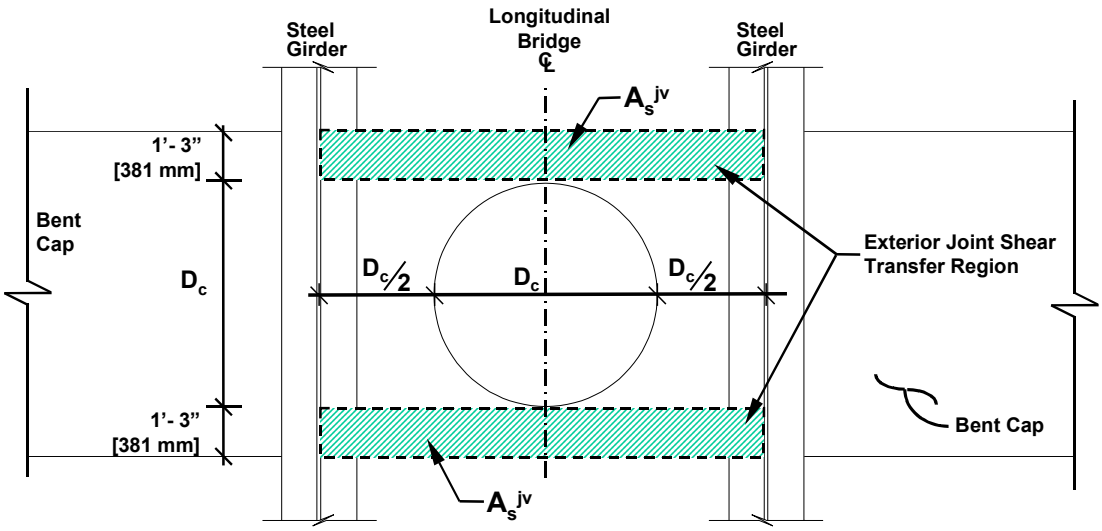

Figure 2-14 Prototype Bent Cap Joint Region

The SDC defines the area of external or vertical joint shear reinforcement to be placed in each exterior joint shear transfer region, A_s^{jv}, as 20% of the area of column longitudinal reinforcement anchored in the joint, A_{st}. This external joint shear reinforcement is located in the joint shear transfer region on either side of the column in the form of No. 7 [25 mm] stirrups tied in pairs spaced at 5 ½ in. [140 mm] on center.

The second part of the seismic design for the bent cap involves ensuring that the bent cap torsion capacity exceeds the torsional moment demand from the column overstrength moment during a longitudinal seismic event. Before presenting the design of the section for torsion, a summary of the development of torsion theory[2] and explanation of the methods used is presented in the next section.

2.6.2.1 History of Torsion Analysis

Prior to 1855, equations for explaining torsion only existed for circular sections. Not until 1855, when Saint Venant (28) applied his torsional constant for noncircular sections to existing equations for circular sections was a method for solving noncircular sections in torsion developed. The development of Saint Venant's torsional constant was based on the premise that a member subjected to torsion transfers the torsion through

[2] The historical torsion review of Section 2.6.2.1 was written with reference to Hsu's "Torsion of Reinforced Concrete" (26) and Collins and Mitchell's "Prestressed Concrete Structures" (27).

circulating shear stresses around the perimeter of the section. Saint Venant's theory proved to accurately predict the elastic torsional strength of noncircular sections.

Extrapolating Saint Venant's description of torsion being resisted by shear stresses circulating around the perimeter of the section, Bredt (29) developed a thin-tube analogy (Figure 2-15) in 1896 to describe the elastic torsional behavior of a concrete section. In Bredt's thin-tube, the circulating shear stresses are located in the walls of the tube.

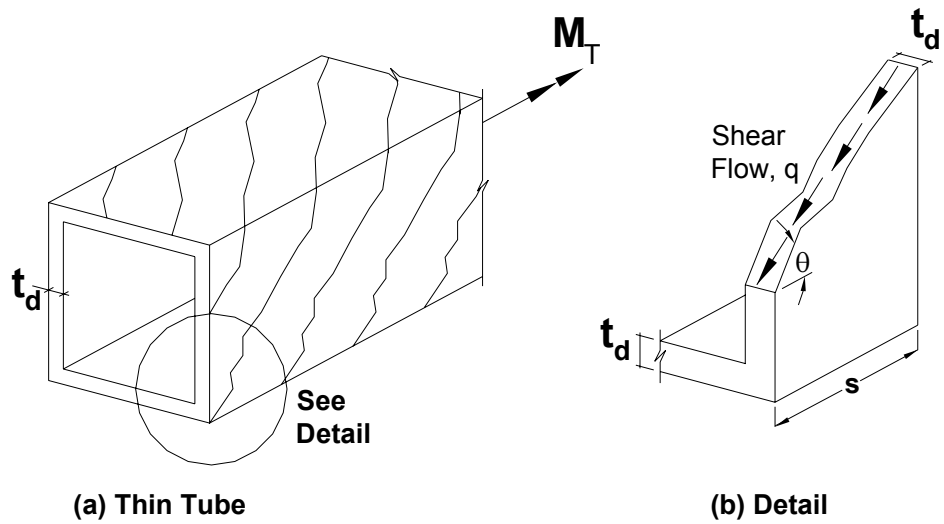

Figure 2-15 Thin Tube Analogy (adapted from (27))

Truss Modeling

Around the same time, Ritter, in 1899 (30) introduced the concept of using a truss model to explain load paths in cracked reinforced concrete members (Figure 2-16). He explained the transfer of shear in a beam as a series of diagonal compression forces balanced by horizontal and vertical tension forces. In his model, the concrete compression stresses were assumed to act at 45° angles while the stirrups and flexural reinforcement made up the vertical and horizontal members of the truss. The inclination of compression members corresponds to the inclination of crack patterns. Mörsch (31) in 1902 expanded on Ritter's truss analogy by suggesting the compression force was more akin to a continuous compression field rather than discrete struts. In both Ritter and Mörsch's models, the contribution of tensile stress in the concrete is neglected as is the dowel action of reinforcement.

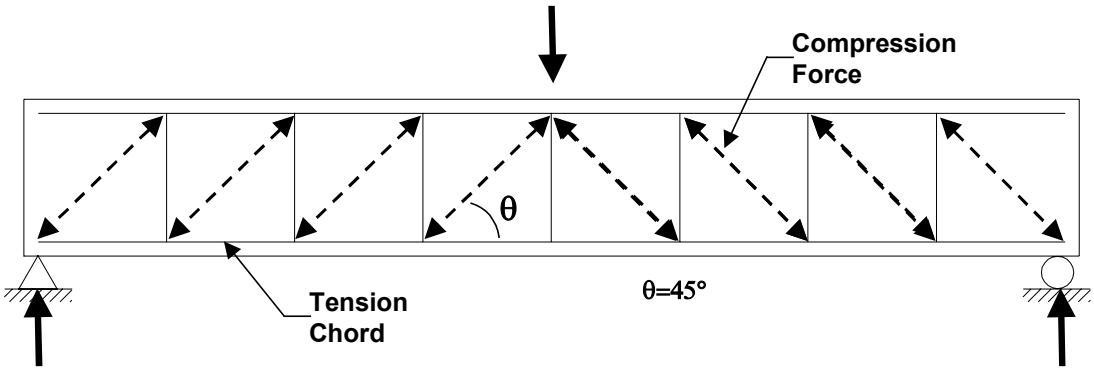

Figure 2-16 Beam Shear Represented as a Plane Truss

Development of a model in which angles other than 45º occurred followed in the appropriately titled "variable angle truss model" (26). In 1982, Collins and Vecchio (32, 33) conducted tests that determined the principal compressive strength was a function of both the tensile and compressive strains. Consequently, the tensile strength of concrete is accounted for in their model, which is termed the modified compression field theory.

All the previously described scientific developments before 1929 were combined in Rausch's Ph.D. thesis (34) to develop a space truss model to describe a section in torsion. The space truss uses Saint Venant's circulating shear stresses and Bredt's thin tube. Rausch then uses four plane trusses as described by Morsch to make up the walls of the tube. This leads to a three-dimensional explanation of the post-cracking behavior of a section in torsion.

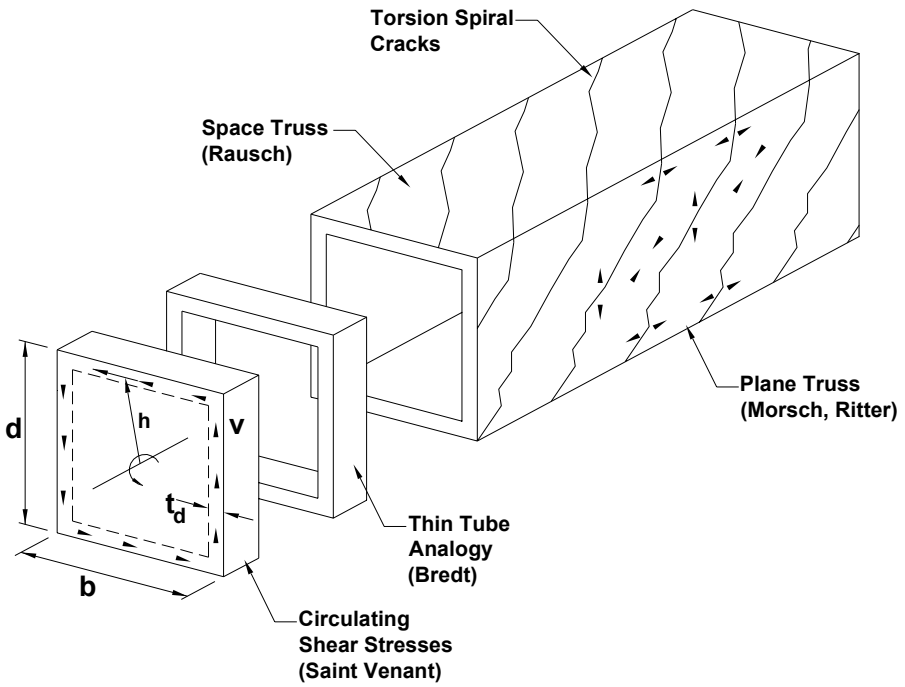

Figure 2-17 Development of Space Truss Analogy (adapted from (27))

A variation of the space truss model is presented by Holombo (35). The deviation exists at the column where the struts are inclined toward the center of the section beyond the equivalent tube thickness. In his models, Holombo examined the clamping mechanism of the column in the joint region when the bent cap is subjected to torsion. Plane truss models for concrete bridge joints subjected to shear were presented in doctoral dissertations of Sritharam (36) and Ingham (37). The truss method of modeling is applied in Chapter 5, where strut and tie models are developed for the component tests. Due to the rigorous nature of strut and tie modeling, the prototype design is done using existing equations that are based on the theories just described.

2.6.2.2 Torsion Design

Torque-Twist Relationships

Two procedures were used to construct a torque-twist curve for the prototype bridge. This section will first outline the method described by Collins and Mitchell (27). The second part of this section will present the method described by Hsu (26). Both procedures are rooted in the fundamentals previously explained, but each has particular features that warrant presentation. It should be recognized that both methods are for pure

torsion. While the bent cap of the prototype is subjected to shear as well as torsion, it was decided that too many unknowns in the behavior did not warrant complicating the procedure and that the pure torsion case would provide a reasonable basis for comparison.

Prior to cracking, a reinforced concrete section behaves essentially as a homogeneous material resisting torsion in the concrete. If the reinforcement contribution is neglected, the cracking torque for a conventionally reinforced concrete section can be obtained from the section properties:

$$T_{cr} = \frac{A_c^2}{p_c} f_{cr} \tag{2-5}$$

where A_c and p_c are the area and perimeter, respectively, of the concrete section and f_{cr} is the cracking strength of the concrete ($4\sqrt{f'_c}$ psi [$0.33\sqrt{f'_c}$ MPa]) (27).

The twist of a section is equal to the applied torsion divided by the torsional stiffness of the section. Collins and Mitchell use the principle of virtual work to determine the torsional stiffness. The external work is a function of the applied torque, T_n, and resulting rotation, θ. As previously stated, the torsional resistance of the section comes from to shear stresses acting over the thickness of the equivalent tube t_d (Figure 2-18). The tube thickness is approximated as 75% of the ratio of cross sectional area to perimeter $(3A_c/4p_c)$. Therefore, the internal work is found by integrating the shear stresses, ($\upsilon = T/2A_o t_d$ where A_o is the area enclosed by the shear stress), and shear strains, $(\gamma = \upsilon/G = T/2GA_o t_d)$, over the volume of the equivalent tube. This results in the equation

$$T\theta = \int_V \upsilon\gamma\, dV = L\int_p \frac{T}{2A_o t_d}\gamma t_d\, dp \tag{2-6}$$

where L is the length of twist in the section. Assuming a constant tube thickness and substituting the expression for shear strains, the twist, or amount of rotation per unit length, is determined as

$$\psi = \frac{\theta}{L} = \frac{\gamma p_o}{2A_o} = \frac{Tp_o}{4A_o^2 t_d G} \tag{2-7}$$

This cracking torque and twist according to Collins and Mitchell is plotted with a circle in Figure 2-19.

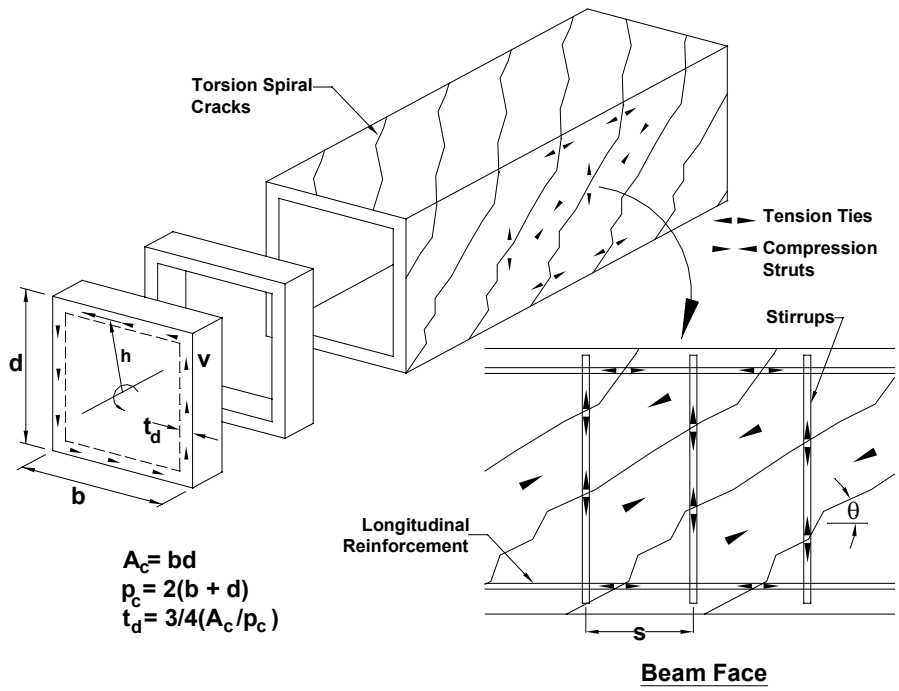

Figure 2-18 Space Truss Analogy (adapted from 27)

Once the section has cracked, compression struts of thickness t_d are balanced by horizontal forces in the longitudinal reinforcement and by vertical forces in the stirrups. Consequently, the ultimate capacity is dependent on the capacity of three distinct mechanisms, namely, the crushing strength of the concrete struts, the yielding of the stirrups and yielding of the longitudinal reinforcement. Therefore, because determination of the ultimate torsional capacity requires assuming one mechanism has reached its capacity, then checking to see that the other mechanisms haven't already reached their capacities, expressions are needed to assess the level of demand at each mechanism location.

The total shear, or shear flow, is simply the shear stress multiplied by the wall thickness, giving a force per unit length, q (Figure 2-15b). Each transverse reinforcement leg carries a vertical component of the compression strut. To determine the vertical

component of the strut, the shear flow is resolved into a single force, or compression force that acts at an angle θ, where θ, is the angle of cracking. The length of the strut is equal to $s/cos\theta$ (Figure 2-15b) where s is the stirrup spacing. Therefore, the force in the transverse ties is equal to $qstan\theta$. The total force in the longitudinal reinforcement, N_v, is determined from the amount of shear flow that is distributed over the total length required for the strut to complete one spiral around the beam ($qp_o cot\theta$). This total force is divided by the amount of reinforcement to determine the force per bar. The allowable tie forces are limited to the yield strength of the reinforcement.

For the compression struts, Collins and Mitchell (27) limit the crushing strength of concrete to:

$$f_{2\max} = \frac{f_c^{'}}{0.8 + 170\varepsilon_l} \tag{2-8}$$

where ε_l is equal to the principal tensile strain. The ultimate torsional capacity of the section is determined by assuming one of the three torsional resisting mechanisms has reached capacity and then checking the demand on the other two. For example, a crack angle is assumed and the stress in the transverse reinforcement is assumed to have reached yield. The torsion is solved for as is the stress in the longitudinal reinforcement and the concrete struts. If either stress component is beyond its defined limit state, it reached its limit before the transverse reinforcement and an iterative analysis procedure is repeated. Because this assessment is iterative in nature, the calculations are not shown here but are presented in Appendix A.

With the corresponding shear strain, the twist is determined from $\gamma p_o / 2A_o$. With the cracking and ultimate torque and twist values determined, the bilinear dashed curve in Figure 2-19 can be established.

Tests conducted by Hsu suggested that the cracking torque is also a function of the reinforcement (26). Therefore, in his equations for cracking, he has included the ratio of total reinforcement in his cracking strength equation:

$$T_{cr} = (1 + 4\rho_t)T_{np} \tag{2-9}$$

$$T_{np} = 6\left(x^2 + 10\right)y \cdot \sqrt[3]{f_c^{'}} \tag{2-10}$$

where T_{np} is the torque based on the skew bending theory, ρ_t is the total steel percentage and x and y are the shortest and longest dimensions of the section, respectively. While the cracking torque from Hsu's (26) method is higher than that of Collins and Mitchell (27), the difference is attributed to the T_{np} term and not from including contribution to reinforcement (Figure 2-19).

The initial slope (or the torsional rigidity) of Hsu's curve (26) is nearly identical Collins and Mitchell (27) because both are determined from the section geometry. While Collins & Mitchell (27) use the principle of virtual work to determine the torsional rigidity, Hsu (26) uses St. Venant's torsional rigidity which is the product of the shear modulus of the material, G_c, and St. Venant's torsional constant, C.

$$\psi = \frac{T}{G_c C} \tag{2-11}$$

The shear modulus is $E_c/2(1+\upsilon)$ where E_c is the modulus of elasticity and υ is Poisson's ratio of said material. The torsional constant is equal to $\beta x^3 y$ where x and y are the smallest and largest cross-sectional dimensions, respectively, and the coefficient β is a function of x/y and is tabulated in Hsu's "Torsion of Reinforced Concrete" (26).

The second portion of the torque-twist curve is determined using the procedure outlined in Hsu (26). While the fundamental concept is that the torsion is resisted through a series of strut and ties, various differences distinguish Hsu's model (26) from Collins & Mitchell (27). The remainder of this section will describe only the major topics that are different and the reader is directed to Appendix A for the complete derivation of each curve.

The tube thickness as defined by Hsu is

$$t_d = \frac{A_c}{p_c}\left(0.082 + 3.405\frac{v}{f_c^{'}}\right)\frac{1}{\sin 2\theta} \tag{2-12}$$

where:

$$v = \frac{T_n p_c}{A_c^2} \tag{2-13}$$

where A_c and p_c are the area and perimeter, respectively, of the outer concrete boundaries (Figure 2-18). The angle of the compression struts is denoted by θ and f'_c is the concrete compression strength. The torsional stress of the section, v, is a function of the applied torque, T_n, perimeter of the entire section, p_c, and the cross sectional area, A_c. Hsu simplified Equation 2-12 for design practicality (38) by neglecting the first term in parenthesis and substituting Equation 2-13 for the torsional stress. Recognizing that the angle of cracking is often close to 45°, $sin2\theta$ is taken as unity, resulting in the simplified expression

$$t_d = \frac{4T_n}{A_c f'_c} \tag{2-14}$$

In determining the maximum allowable stress in the concrete struts, Hsu includes an empirical coefficient to account for the "softening effect" in the concrete struts due to the diagonal shear cracking of concrete. Determination of Hsu's curve, plotted with a continuous line in Figure 2-19, is also an iterative process where a strain is assumed in the steel ties and the concrete stress is calculated to ensure it has not already reached its crushing strength. All calculations are presented in Appendix A.

This section presented two procedures for developing torque-twist curves for the prototype bridge. The procedures are based on the assumption that the section is of sufficient length for a full helical failure surface to develop. The torsion shear friction analysis presented in the next section predicts ultimate force capacity for short sections that fail in a vertical shear friction plane.

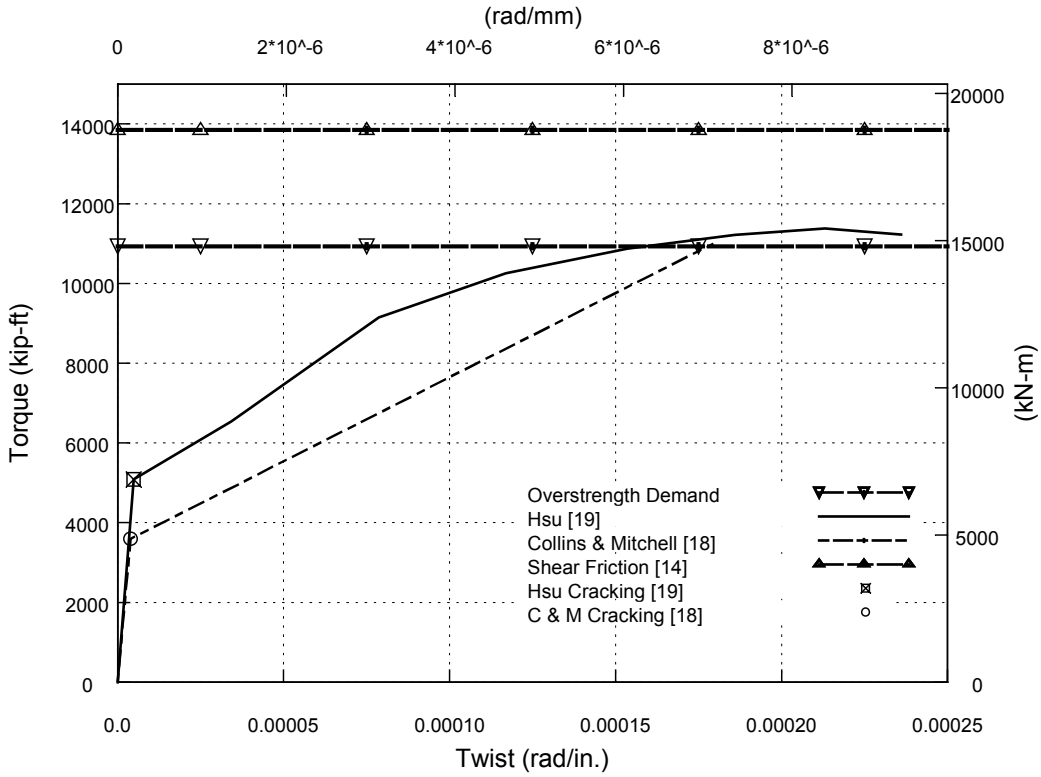

Figure 2-19 Prototype Torque – Twist Prediction

Torsion Shear Friction Analysis

A torsion shear friction failure mechanism was observed in testing of the San Francisco viaduct bridges (39). In a torsion shear friction mechanism (19), the area of the failure plane can be divided into four unequal quadrants as shown in Figure 2-20. Each quadrant contributes a shear resistance, F_i, proportional to its cross-sectional area, A_i, and the applied axial force, P. Each shear resistance is multiplied by its moment arm, x_i or y_i, from the center of rotation of the section to determine the torsional strength.

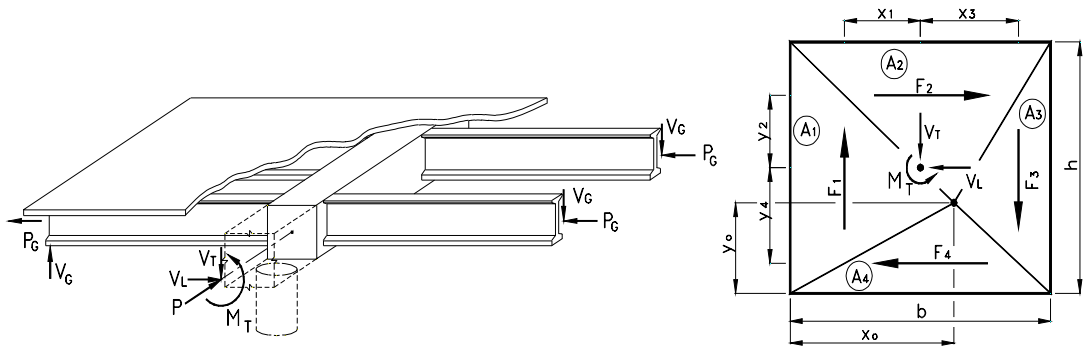

(a) Torsion Shear-Friction in Bent **(b) Torsion Shear-Friction Plane**

Figure 2-20 Torsion Shear Friction Theory (Figure from Holombo, 9)

$$F_i = \frac{\mu P A_i}{A} \tag{2-15}$$

$$P = \varepsilon_s E_s A_{st} + F \tag{2-16}$$

$$V_T = F_1 - F_3 \tag{2-17}$$

$$V_L = F_2 - F_4 \tag{2-18}$$

$$M_T = F_1 x_1 + F_2 y_2 + F_3 x_3 + F_4 y_4 \tag{2-19}$$

The steel girder flanges were expected to prevent a shear friction failure mechanism from developing at the bent cap-girder web interface, however a failure plane could develop in the bent cap between the column face and the first girder. Using a friction coefficient μ = 1.4 for monolithically cast concrete, the shear force in each quadrant was determined. The clamping force, P, is a function of the longitudinal rebar strain ($\varepsilon_s E_s A_{st}$) and the amount of post-tensioning, F, in the section. Experimentally, significant strength degradation loss was observed when the strain in the flexural reinforcement reached 0.0012 (39). As crack dilation increases, aggregate interlock decreases. Therefore, as ε_s increases, the value of μ should decrease. Rather than iterating both values, Priestley, et al. (19), recommends limiting the strain in convention reinforcement to 0.006 for a section with post-tensioning. For simplicity, the predicted

torsion shear-friction capacity of the experimental specimens was calculated using $\varepsilon_s = \varepsilon_y = 0.002$.

The location of the center of rotation of the section was determined by iterating the coordinates, x_o and y_0, and checking that the resulting shear capacities, V_T and V_L, meet the torsion demands. Once the location of the center of rotation is found, the torsional capacity of the section can be determined by multiplying each quadrant force by the distance from its centroid to the center of rotation. The shear friction prediction based on Priestley, et al. (19) for the prototype design is plotted in Figure 2-19. It should be noted that the above shear friction assessment results only in an ultimate capacity and does not determine the rotation at which it occurs.

2.6.3 Post-Tensioned Design

As Henry J. Cowan is quoted in Collins and Mitchell (27) "If torsion is a dominant design factor in a large concrete member, it is wise to resort to prestressing", a post-tensioned bent cap warranted consideration from in the research program. Both the torque-twist mechanism and the torsion shear friction mechanism can be improved by bent cap post-tensioning. A further benefit of a post-tensioned bent cap is reduced reinforcement congestion, resulting in a more constructable bent cap.

The post-tensioning layout and stress distributions are shown in Figure 2-21. The post-tensioning was continuous, passing through precut holes in the girders. Again, the shear capacity decrease due to the holes is not an issue as the girder in that region was essentially continually braced as a result of being cast in the cap. The required post-tensioning value is determined by imposing the moments due to live loads and dead loads as determined in Section 2.6.1 and limiting the concrete tensile stress to 0.57 ksi [4 MPa] and the compressive strength to 4 ksi [28 MPa]. The post-tensioning force, F, is the same in all five rods, e_1 and e_2 are the post-tension eccentricity from the section centroid of the top and bottom post-tensioning, respectively, and S is the bent cap section modulus.

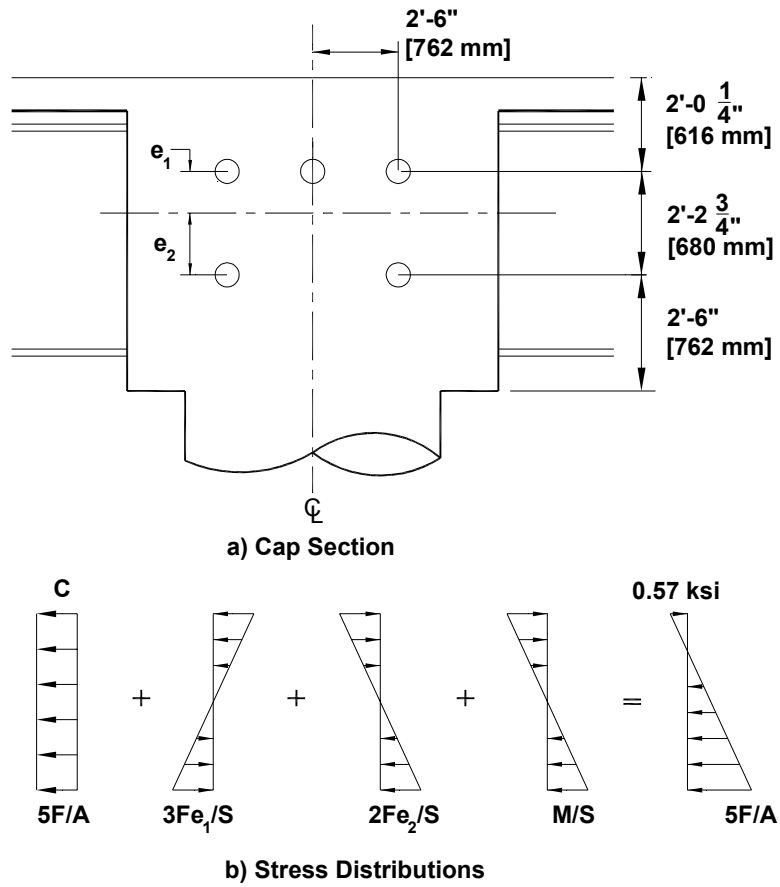

Figure 2-21 Post Tensioning Layout

To minimize variables, the post-tensioned bent caps are designed to have the same torsional moment capacity as the conventionally reinforced bent caps. The equation for the cracking torque of the post-tensioned section is the same as for the conventionally reinforced section with an additional term to account for the contribution of the post-tensioning. This equation, from Collins and Mitchell (27), is

$$T_{cr} = \frac{A_c^2}{p_c} f_{cr} \sqrt{1 + \frac{f_{pc}}{4\sqrt{f_c^{'}}}} \qquad \text{(in psi)} \qquad (2\text{-}20)$$

where the additional term includes f_{pc}, the stress in the concrete due to post-tensioning. The angle of twist at cracking is found from (27)

$$\psi = \frac{T_{cr} p_o}{4 A_o^2 t G} \qquad (2\text{-}21)$$

where G is the shear modulus and the twist ψ is in terms of radians per unit length.

2.7 BENT CAP-GIRDER INTERFACE

As stated in Section 1.2, all undesirable inelastic actions need to be prevented to ensure the desired failure mechanism occurs in the column. Section 2.6.2 outlined how the bent cap is designed to prevent a torsion failure. The girders are designed to prevent a flexural failure by accounting for the additional moment demand imposed from a seismic event. The final component to be designed using capacity protection principles is the interface of the steel girder and the bent cap (Figure 2-22).

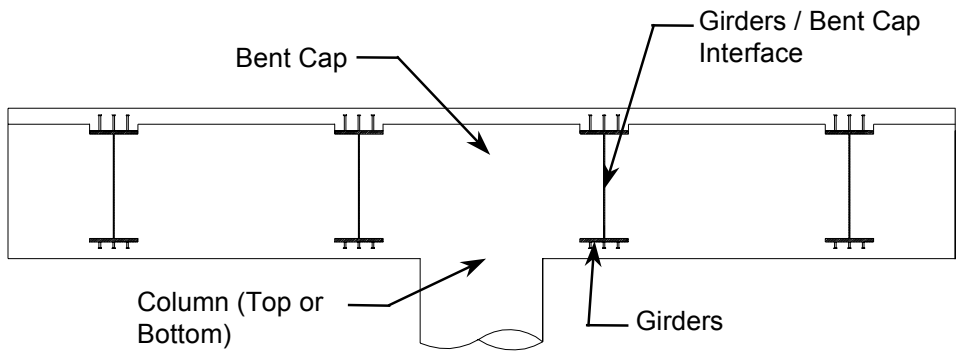

Figure 2-22 Potential Failure Mechanisms Locations

Because of the large stiffness differential between the steel and the concrete, the behavior at the interface warrants special investigation. Potential force transfer mechanisms investigated include: (1) shear studs on the girder web, (2) studs on the girder flanges, and (3) compression of concrete bound by bearing stiffeners on the web inside the concrete bent cap. The remainder of this section discusses the merits of these alternatives.

2.7.1 Shear Studs on Girder Web

The torsional capacity of a connection with shear studs on the girder web inside the bent cap is determined by simulating the stud group as an eccentrically loaded bolt group. In Figure 2-23a, a bolt group joining a plate to a beam is subjected to a pure moment. The moment creates a rotation of the plate about an instantaneous center of rotation causing the plate to bear on the bolts, causing forces in the fasteners.

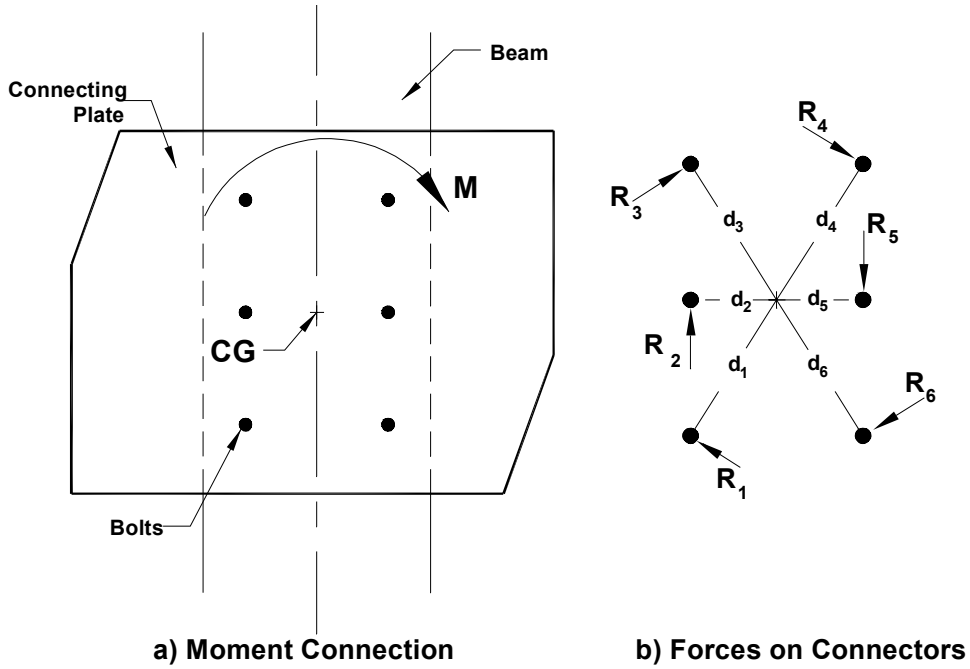

Figure 2-23 Pure Moment Connection (40**)**

The amount of force each fastener can carry is its ultimate capacity reduced by a function of its deformation. Assuming the plate remains rigid, the fasteners at the outer edges experience the maximum deformation. The reaction that each fastener provides is a function of this deformation and is calculated from (40)

$$R_i = R_{ult}\left(1 - e^{-10\Delta}\right)^{0.55} \qquad \textbf{(2-22)}$$

where R_{ult} equals the ultimate fastener strength which is equivalent to the fastener cross sectional area multiplied by the ultimate shear strength (approximately 70% of the tensile strength), e is the logarithmic e, and Δ is the fastener deformation. Each fastener reaction is then multiplied by its distance from the centroid of the section to obtain the moment capacity of the connection. For instance, in Figure 2-23, the moment capacity is determined by summing the moments:

$$M = \Sigma R_i d_i \qquad \textbf{(2-23)}$$

To use this theory on a stud group, the stud shear capacity Q_n, was used in Equation 2-22 in place of ultimate fastener strength, R_{ult}. The stud shear capacity was determined just as in a composite girder section from

$$Q_n = 0.5 A_{sc} \sqrt{f_c^{'} E_c} \leq A_{sc} F_u^b = Q_u \qquad \textbf{(2-24)}$$

where A_{sc} is the cross sectional area of an individual shear stud and f'_c and E_c are the concrete compressive strength and modulus of elasticity, respectively. The force deformation characteristics, based on Equation 2-22, of a 7/8 in. [22 mm] diameter shear stud with an ultimate tensile strength of 55 ksi [380 MPa] is plotted in Figure 2-24.

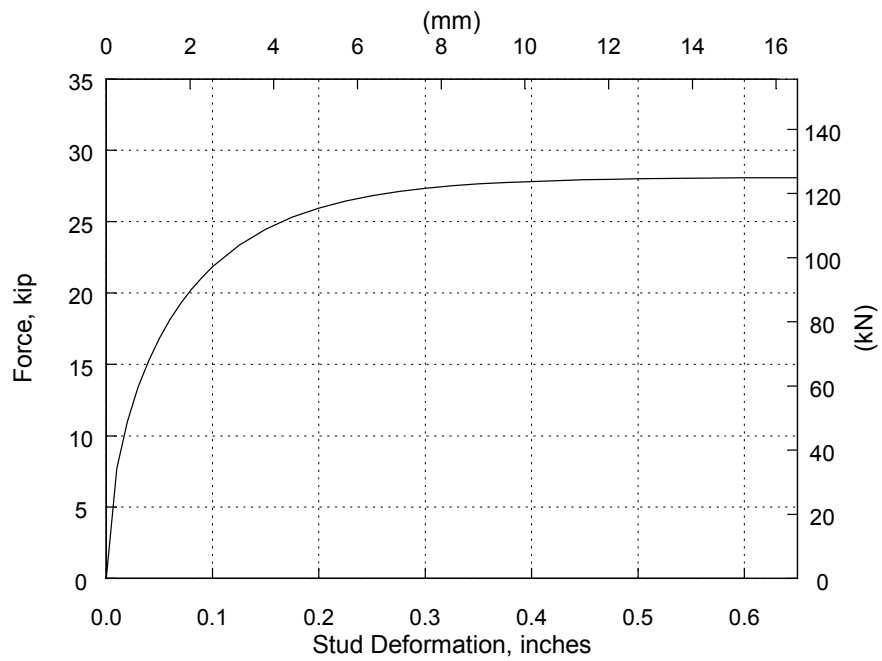

Figure 2-24 Shear Stud Force Deformation Characteristics (from (2-24))

Limiting the maximum stud deformation at the edge to 0.17 in. [4 mm] and linearly relating all other deformations to the maximum deformation at the edge by

$$\Delta_i = \frac{d_i}{d_{\max}} \Delta_{\max} \qquad \textbf{(2-25)}$$

the reaction force on each shear stud is determined. A total of 90 studs were distributed on the girder web as shown in Figure 2-25a. Applying the concept of eccentrically loaded connections to this shear stud distribution on the girder web, the stud group was expected to carry 6,000 k-ft [8,130 kN-m] of the 9,000 k-ft [12,195 kN-m] demand.

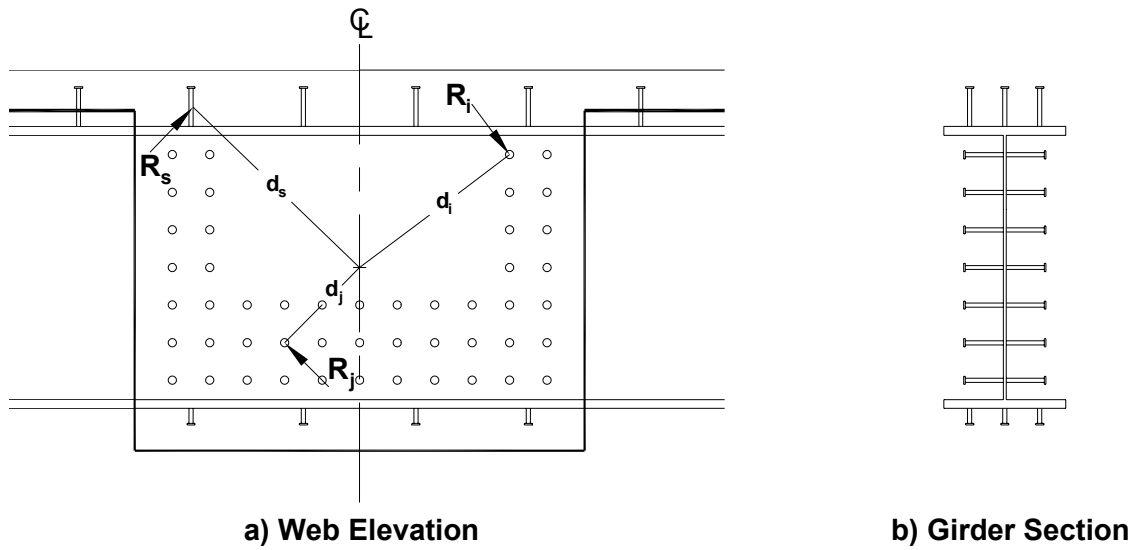

Figure 2-25 Stud Group on Girder Web

This evaluation quantifies an assumed contribution to torsional capacity due to girder web shear studs based on a slip between concrete and the steel web. However, examination of the cross section (Figure 2-25b) suggests that the contribution of shear studs may be inconsequential and slip prohibited because the flanges would tend to force the failure plane away from the girder web. The shear studs could be extended beyond the flanges, however, due to requiring an excessively high deformation in the studs, as well as a large number of studs, this option is deemed unfeasible, as well as impractical for construction.

2.7.2 Shear Studs on Girder Flanges

Using the same principles as in Section 2.7.1, the contribution of studs on the top and bottom girder flanges is approximated. The shear capacity of each stud, R_s, is determined from Equations 2-22 and 2-23 and multiplied by its distance from an assumed center of rotation, shown in Figure 2-25. With 27 studs on the top and bottom each, and assuming that all studs act at full capacity, the contribution is estimated as 4,800 k-ft [6,504 kN-m], still less than the demand moment of 9,000 k-ft [12,195 kN-m].

2.7.3 Bearing Stiffeners on Girder Web

As explained in Section 2.6.2.2, torsional moment in a reinforced concrete section is resisted through concrete compression struts and steel reinforcement ties. In an

integral connection, the concrete strut extends from the steel girder to the joint region. Full height bearing stiffeners can increase the concrete strut compression capacity by providing additional confinement (41). Using stiffeners to mobilize concrete has been examined in composite concrete-steel building frames, where steel girders are integrated with concrete columns (42, 43, 44)

The preliminary stiffener spacing is determined using yield line theory (45). Yield line theory is a limit analysis that is typically used to predict the ultimate load in reinforced concrete slabs. This theory assumes that all plastic deformation occurs through slab sections rotating about the yield lines that divide them. Because it is an upper bound approach which gives either the correct answer or an answer that is too high, iteration of yield line locations is required to ensure the correct failure mechanism, and hence lowest capacity, is found. The rationale behind using yield line theory here is that it will optimize stiffener spacing to prevent flange yielding from occurring before concrete crushing, essentially maximizing the concrete strut capacity.

In Figure 2-26a, yield lines are assumed for a uniformly loaded concrete slab fixed on three edges and free on one edge. The five yield lines (two diagonals across the section and one along each fixed edge) serve as axes of rotation for the three sections they divide the slab into. The ultimate load this slab can carry is determined using the yield lines and the principle of virtual work. The principle of virtual work states that the sum of all work done on a system in equilibrium is zero. Therefore, the work due to the external force to apply the displacement γ is equal to the work due to internal actions along the yield lines that resist it.

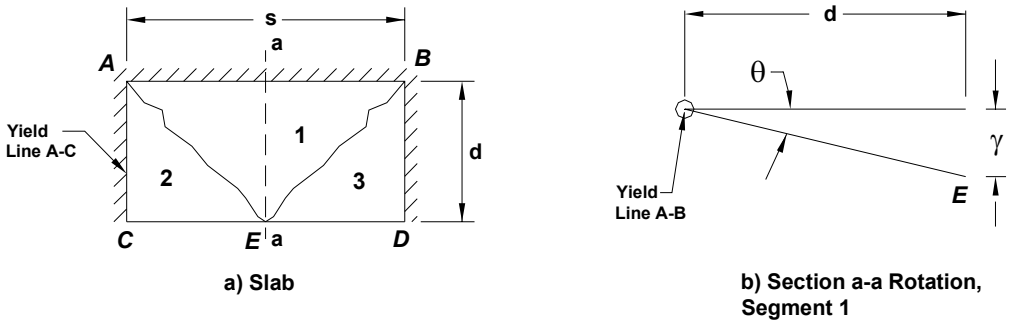

Figure 2-26 Yield Line Theory for Concrete Slabs (adapted from 45)

An arbitrary displacement is applied at point E and is denoted as γ. The rotation of section one about the yield line A-B due to the applied displacement at E is denoted as θ (Figure 2-26b). The external work of each section due to the application of γ is equal to the total load on a section multiplied by the displacement of the section's centroid

$$\Sigma W_u \Delta = w_u A_i \Delta_i \qquad \textbf{(2-26)}$$

where the distributed load w_u on a section is multiplied by the section's area A_i. The displacement of each section's centroid can be solved for in terms of γ. The internal work is due to the moments at the yield lines

$$-\Sigma m_{un} \theta_n l_o \qquad \textbf{(2-27)}$$

where the work is negative because the moment resisting the rotation is in the opposite direction of the applied force. The rotation θ_n between sections occurs over the length of the yield line, l_o and is solved for in terms of γ. The equations are set equal, the γ terms cancel out and the distributed load w_u is solved for in terms of m_u.

This concept was used to optimize the spacing of stiffeners on the steel girder web in the bent cap region. The intent was to maximize the compressive strength of the concrete struts in the bent cap due to torsion by confining them at the girder web with stiffeners Figure 2-27 (a). The slab geometry corresponds to the steel flanges bound by stiffeners and the web with s equal to the stiffener spacing and the depth of the slab is equal to half of the quantity of the flange width minus the web thickness. The slab can be thought of as fixed at the web and the two stiffeners, and free on the side opposite the web Figure 2-27 (c).

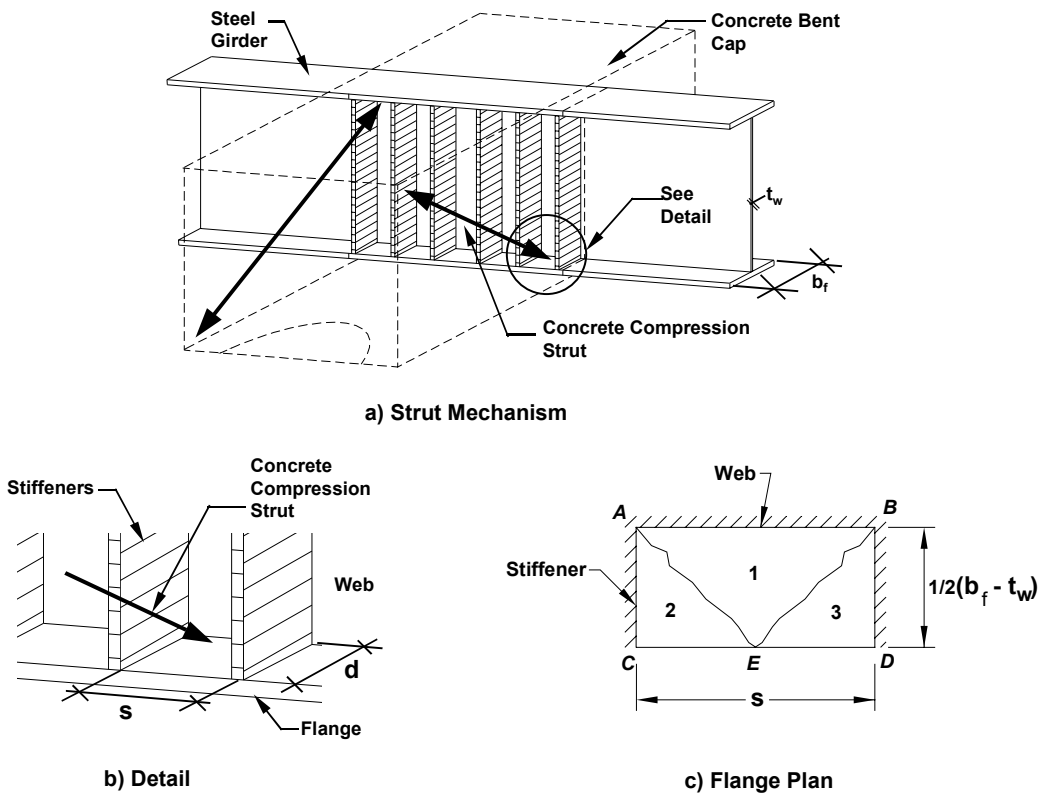

Figure 2-27 Yield Line Theory

An assumed pattern along which the flange will yield is depicted in the plan view shown in Figure 2-27c. For the external work, the concrete stress is limited to a crushing strength of 5 ksi [34 MPa] and it is assumed that the compression of the concrete acts uniformly over the flange bound by the stiffeners. For the internal work, M_{un} is the moment resistance per unit length, $m_{un} = {zf_y}/{b}$, where z is the plastic section modulus of the flange $z = bd/4$. The spacing of the stiffeners is iterated until w_u=5 ksi [34 MPa].

Once the stiffener spacing is found to maximize the compression strut, the force from the strut is found by multiplying the concrete compressive strength by the area of flange the strut acts over. This gives a resultant force oriented as shown in Figure 2-28, which is multiplied by the moment arm to obtain an approximation for the moment transferred by the concrete struts. With the spacing determined from this analysis, the resultant moment transferred in the two outermost struts is 5,040 k-ft [6,829 kN-m] of the 9,000 k-ft [12,195 kN-m] moment demand.

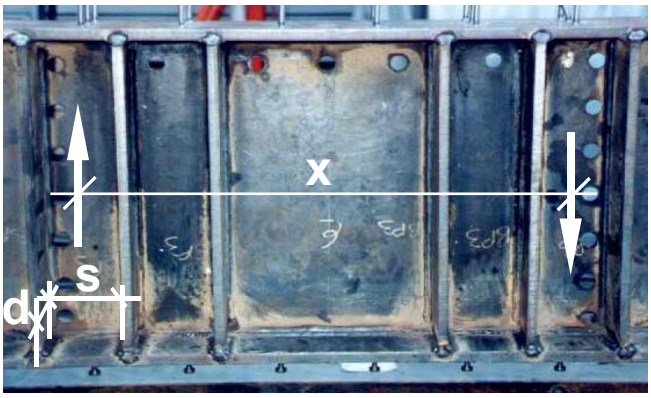

Figure 2-28 Torsional Capacity of Concrete Compression Struts

2.7.4 Details for Testing

Based on the above deliberations, four details of the girder in the bent cap region are shown in Figure 2-29. The first test (Figure 2-29a) was a conventionally reinforced (CR) bent cap. The section of girder web that passed through the bent cap did not have any stiffening elements (NS). This test would provide the base line of comparison for subsequent tests. The second test also had a conventionally reinforced bent cap, but full height bearing stiffeners were included on the girder web in the bent cap region (Figure 2-29b). There were three pairs of bearing stiffeners on either side of the girder in the bent cap region. The third test was similar to the first test in that there were no stiffening elements on the girder web (Figure 2-29c) however the bent cap was post-tensioned (PT). The fourth and final component test was a combination of stiffeners and post-tensioning (Figure 2-29d). Detailed development of all four component tests depicted in Figure 2-29 is presented in the following chapter.

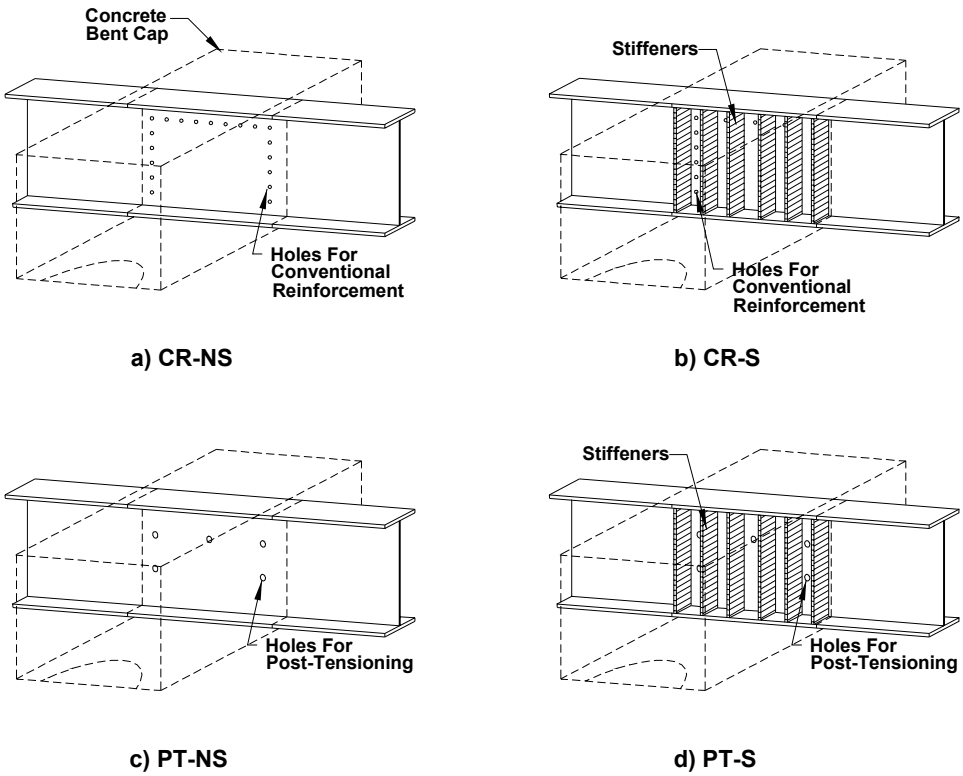

Figure 2-29 Designation of the Four Component Test Specimens

Chapter 3

Development of Component Tests

3.1 OVERVIEW

This chapter presents the design, construction, testing procedures, and instrumentation layouts of the component tests. Section 3.2 presents the design of the component tests including validation of the boundary conditions. Section 3.3 details the construction process for the test specimens. Properties of the constituent materials are presented in Section 3.4. Instrumentation layouts are presented in Section 3.5 and Section 3.6 outlines the loading protocol used for all four component tests.

3.2 DESIGN OF COMPONENT TEST SPECIMEN

Due to symmetry of the prototype structure about Pier 3 (see Figure 2-1), all tests are designed for Pier 3. As shown in Figure 2-8, the maximum bent cap torsional moment occurs at the column centerline and is equally distributed to the superstructure on either side of the column. Hence, the portion of superstructure between the column centerline and the interior girders is the critical location (Figure 3-1). In order to capture the highest torsional moment demand on the bent cap, it is only necessary to model the superstructure between the column centerline and either interior girder.

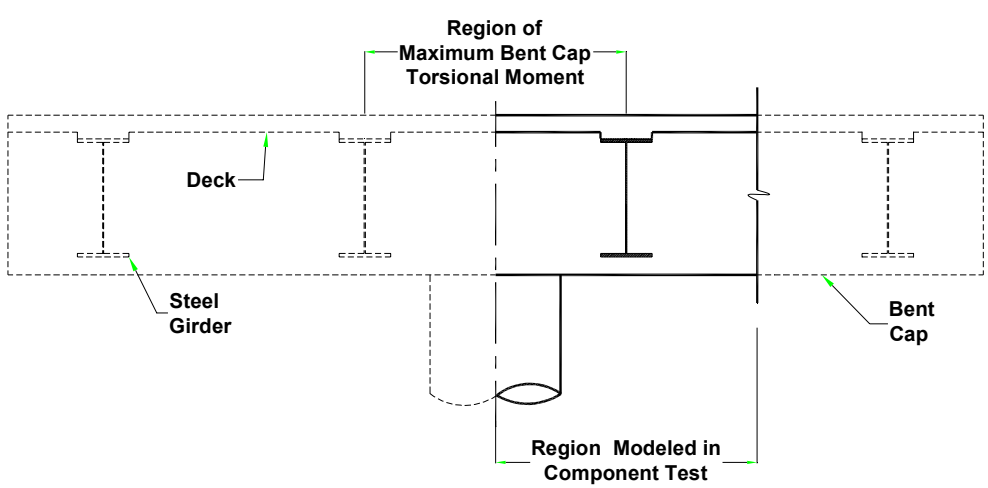

Figure 3-1 Component Test Region of Investigation

Capacity protection of the bent cap in torsion requires that the torsional behavior of the bent cap, including the progressive damage patterns and failure modes, is fully understood. The prototype bridge is designed for the inelastic failure mechanism to occur in the column. In order to develop complete torsional behavior profiles of the bridge section shown in Figure 3-2a, the component test setup needs to ensure failure will occur in the bent cap while protecting against inelastic column behavior.

To protect against premature column failure, the bridge section shown in Figure 3-2a is supported by a rigid concrete block (Figure 3-2b). The block is post-tensioned to the laboratory floor with 1-⅜" [35 mm] diameter Grade 150 [1,034 MPa] high strength rods. A partial column with vertical and spiral reinforcement was designed to protrude from the support block.

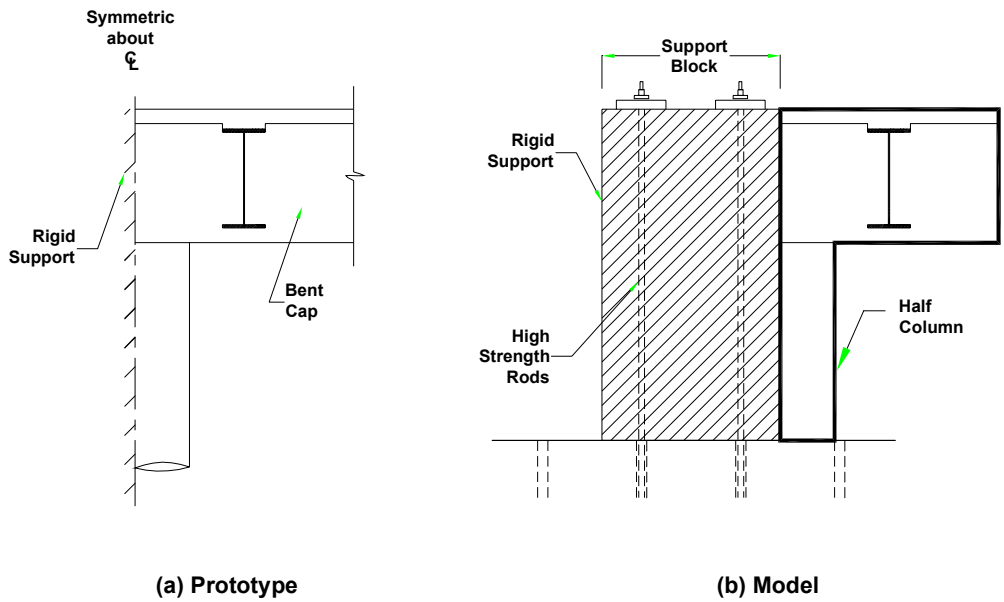

Figure 3-2 Component Test Specimen Prototype and Model

Because the support block is required to remain elastic while the bent cap is tested to failure, it is essentially undamaged following bent cap failure. Therefore, it is feasible and advantageous to cantilever one cap beam off either side of the support block. The resulting test setup is shown in Figure 3-3. All component tests were designed and constructed at 40% scale of the prototype. The model is scaled to maintain a stress equivalent to the prototype stress. When the stress of the scaled model is not correct, as in dead load where scaling distorts the moments, additional loading is applied to produce

the correct stresses. A three-dimensional rendering of the setup is presented in Figure 3-4 and the setup as it was prior to instrumentation and testing is shown in Figure 3-5.

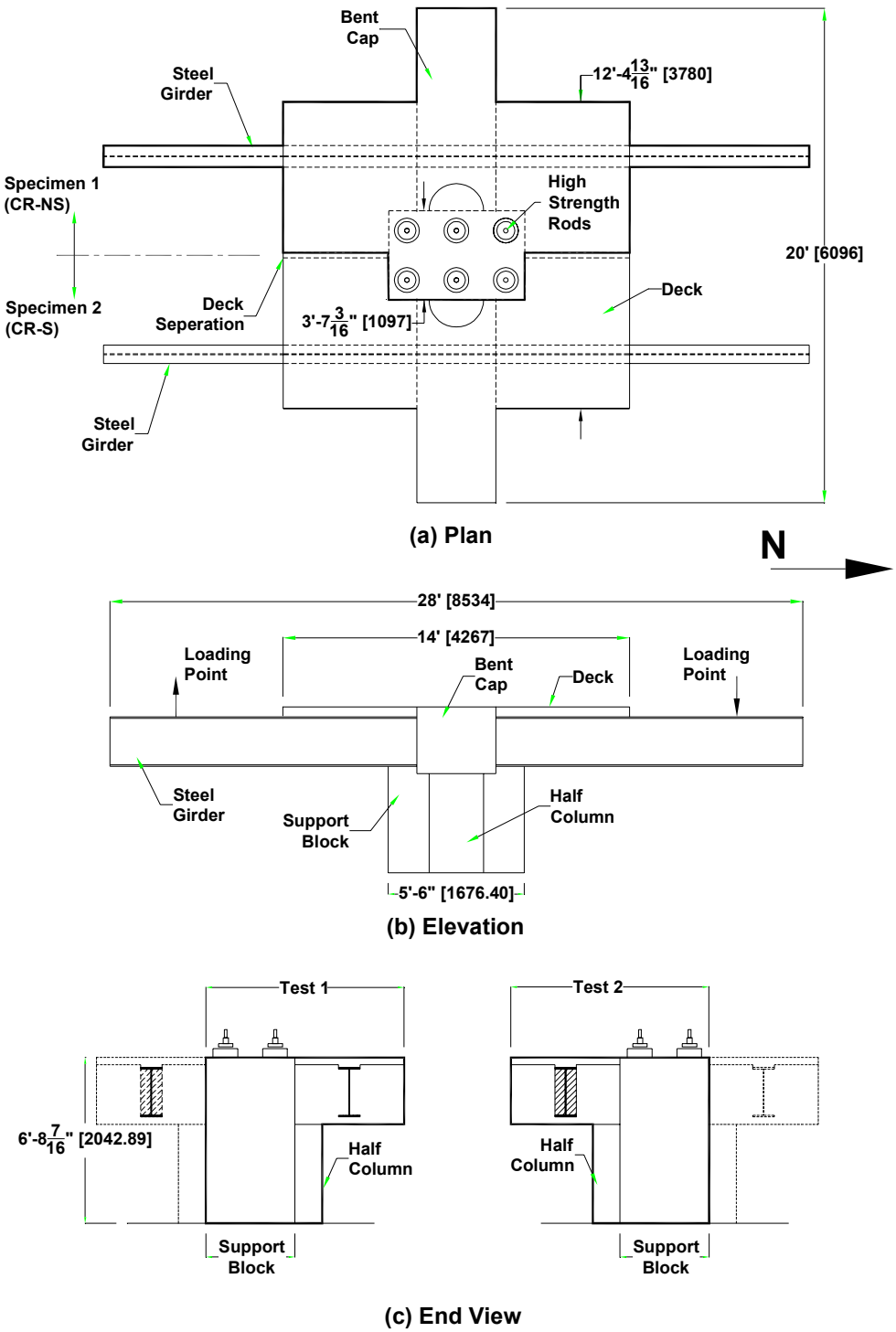

Figure 3-3 Component Test Specimen Geometry

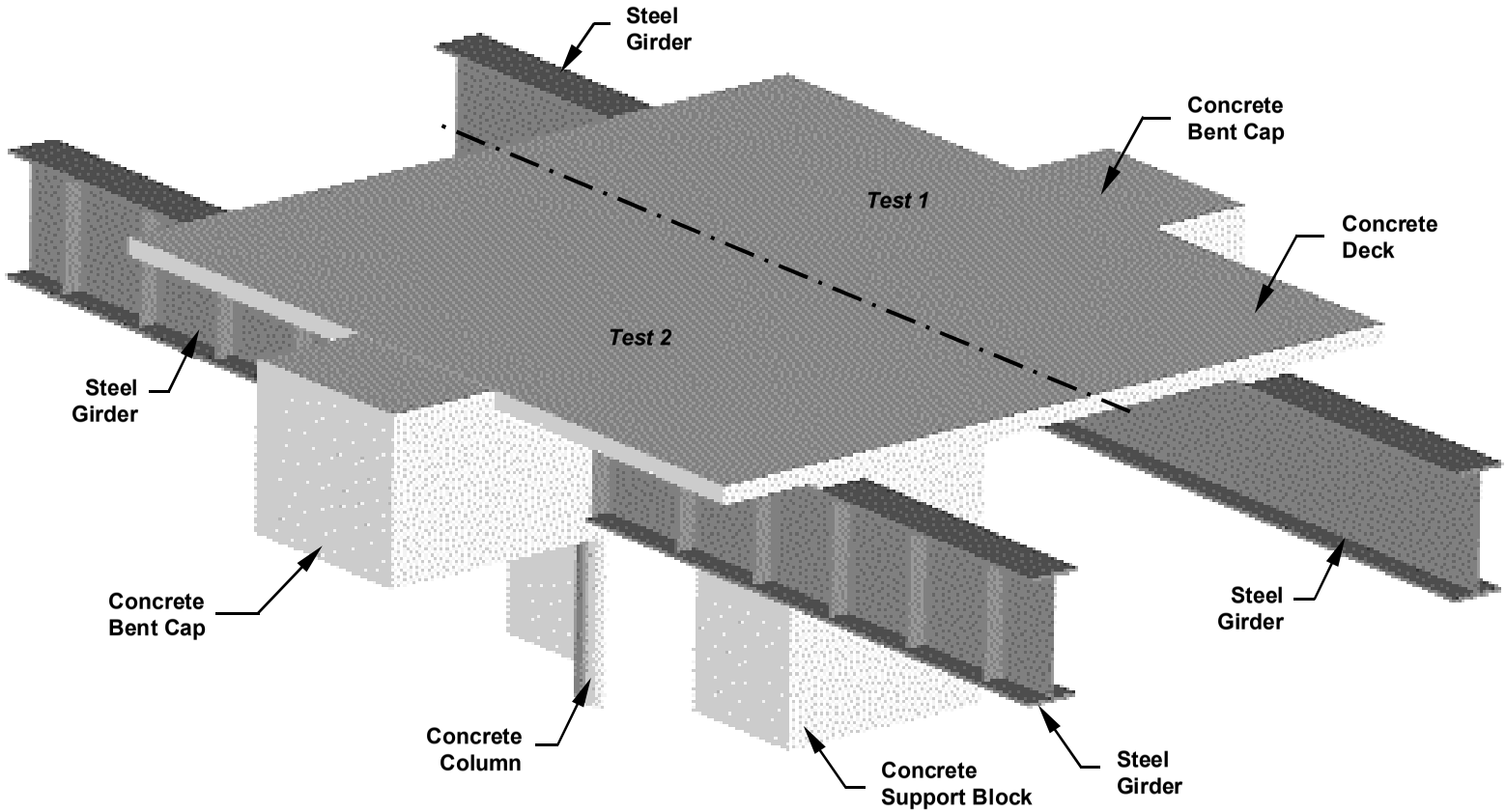

Figure 3-4 Component Test Specimen

Figure 3-5 Component Test Specimen Before Testing

3.2.1 Boundary Conditions of Component Test Specimen

In the longitudinal bridge direction, the correct shear and moment demand due to superstructure self-weight is created by applying the appropriate vertical downward force at girder dead load inflection points (Figure 3-6). In the transverse bridge direction, hydraulic jacks on the bent cap created the correct shear and moment demand due to the superstructure self-weight. To guard against overturning of the component test specimen during testing of Specimen 1, hydraulic jacks on the bent cap of Specimen 2 were set to the same pressure as those on Specimen 1.

In the prototype bridge, the superstructure moment induced by a longitudinal seismic event is transferred to the substructure proportionally over the entire superstructure width. In the component tests, the interior girder transfers the entire seismic moment into the bent cap by applying equal and opposite forces at the interior girder dead load inflection points. While this produces the correct bent cap torsional moment between the interior girder and the column, the seismic moment demand on the girder at the cap/girder interface is greater than the seismic moment demand of the girder in the prototype. However, since the prototype girder design was controlled by live load, it was more than adequate for the simulated seismic demands.

The seismic loads applied to the test specimens were determined by appropriately scaling the prototype loads based on the 40% geometrical scaling of the model. Figure 3-7 shows the moment and shear demand profiles along the longitudinal bridge axis. The "Target" moment and shear are the demands that would appear in an appropriately scaled prototype. The "Dead Load" demands include the actual self-weight of the component test plus dead load correction imposed by the actuators. Curves designated "Seismic" represent the seismic demands created by imposing equal and opposite forces with the actuators. The "Total" demand is the sum of the dead load and seismic demands created in the component test and should correlate with the "Target".

Figure 3-8 shows the moment and shear demand profiles along the transverse bridge axis. The demands designated by "Self Weight" represent the forces created by actual self-weight of the bent cap and girder in the test setup. The "Dead Load Follower" designates the moment and shear demand from the portion of the superstructure that was not modeled and is created with hydraulic jacks. The "Total" of these two compares very

well with the "Target". The resulting test set up is shown in Figure 3-9 with all loading fixtures connected.

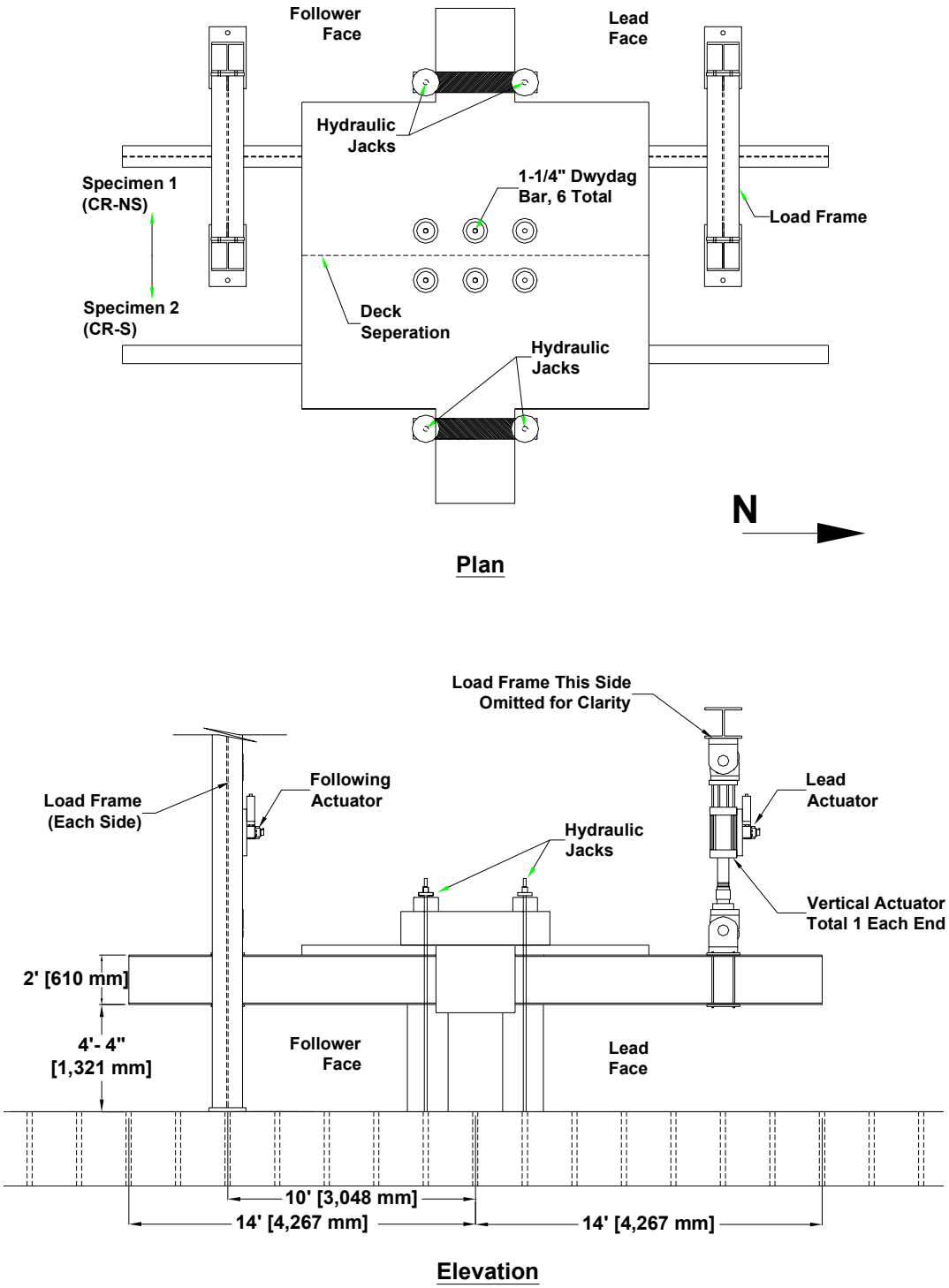

Figure 3-6 Component Test Specimen Loading

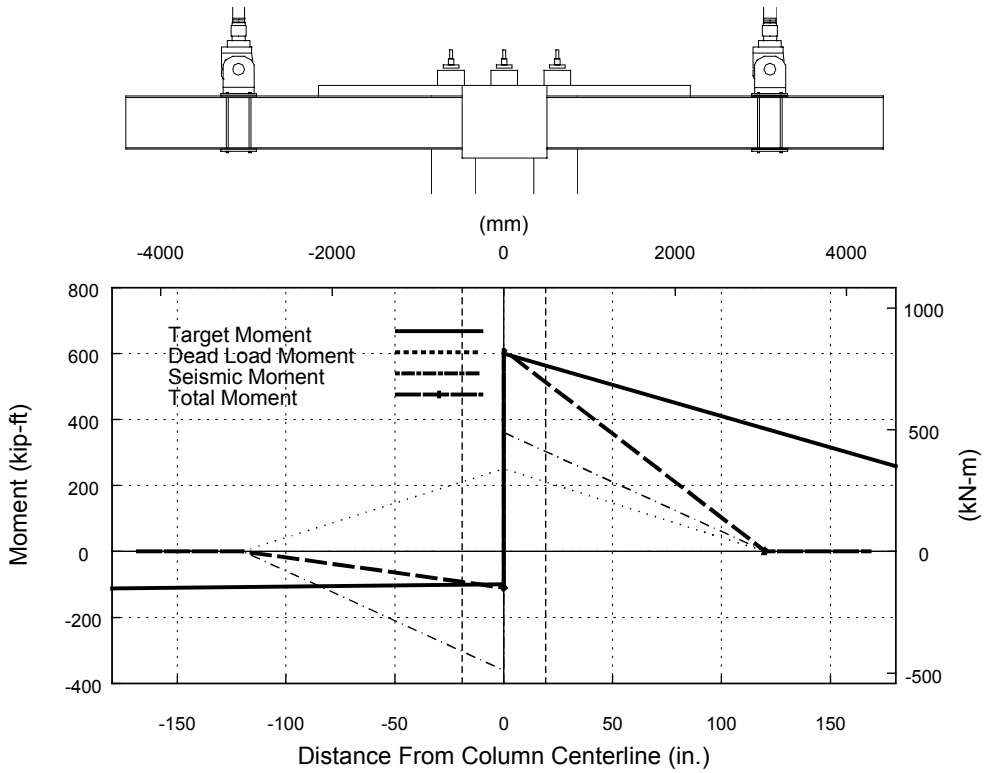

a) Moment Profile

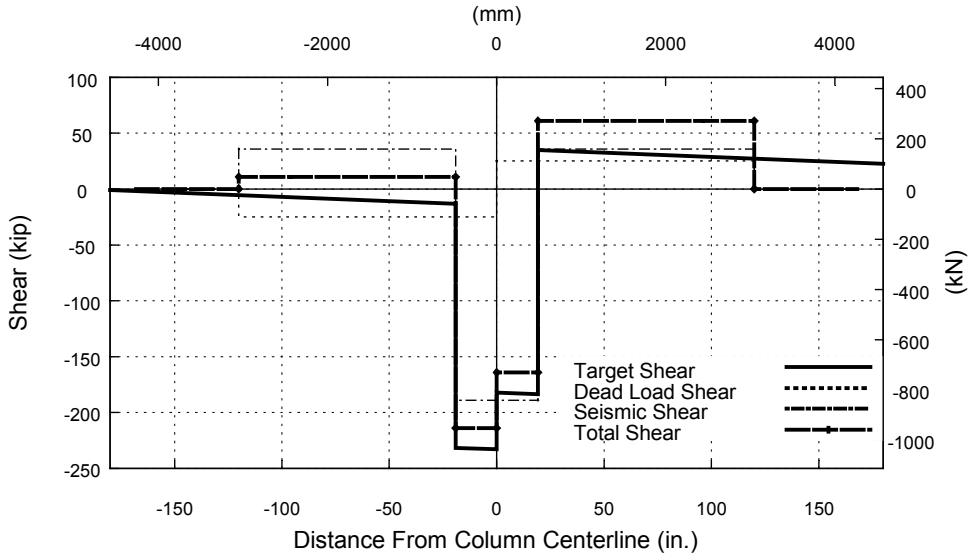

b) Shear Profile

Figure 3-7 Demand Profiles along Longitudinal Bridge Axis

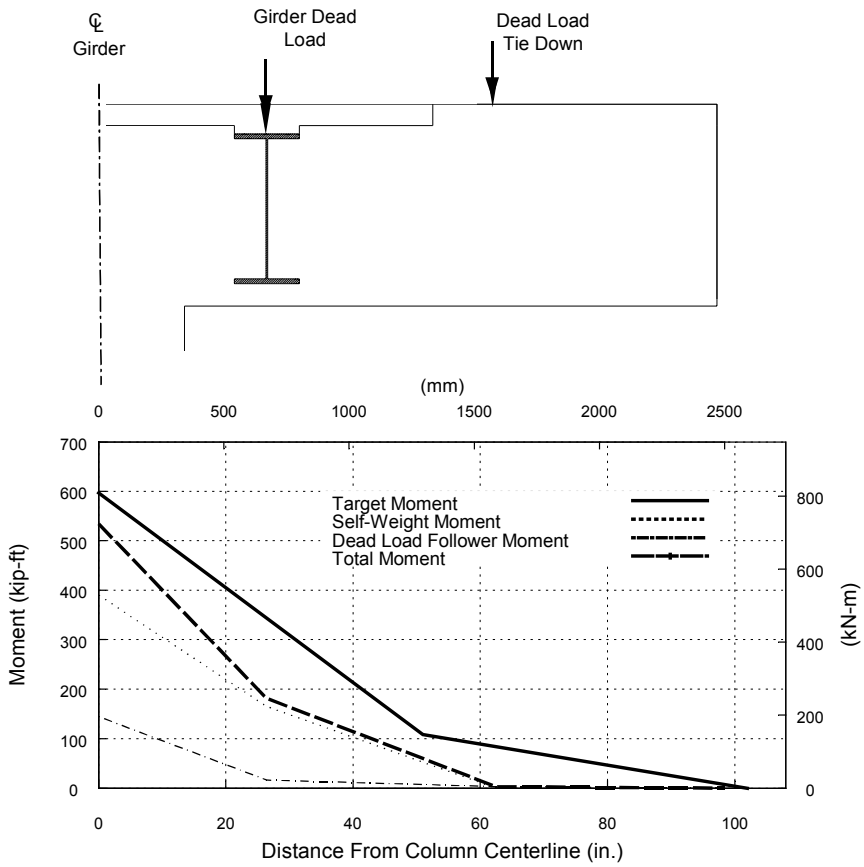

a) Moment Profile

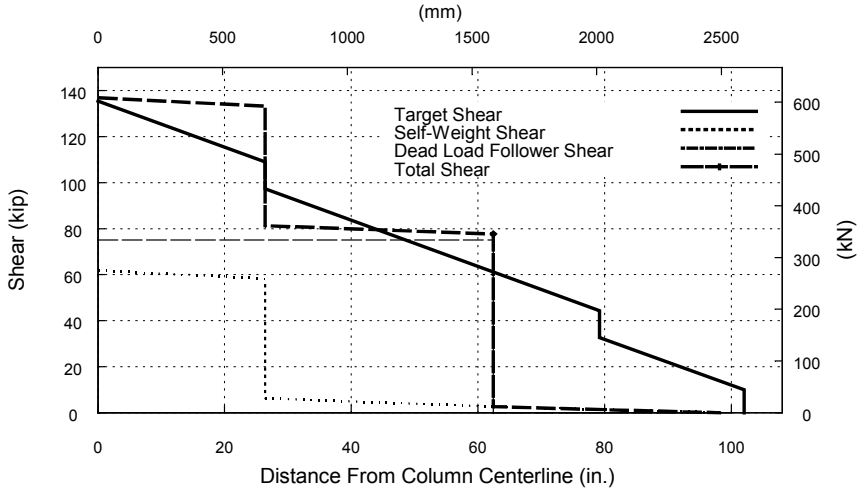

b) Shear Profile

Figure 3-8 Demand Profiles along Transverse Bridge Axis

Figure 3-9 Component Test Specimen with Loading Fixtures in Place

3.3 CONSTRUCTION OF COMPONENT TEST SPECIMENS

All construction and testing was performed at the Charles Lee Powell Structural Research Laboratories on the University of California, San Diego campus. All steel reinforcement was cut and bent off site. Strain gages were applied to the reinforcement and steel girders on site in the Powell Laboratories. Construction of test specimens, including building the formwork, tying the steel reinforcement and casting of concrete also was executed at the Powell Laboratories.

The steel plate girders for all four specimens were fabricated by a local steel fabricator. The girders were built-up steel sections with shear studs on the top and bottom flanges, holes in the girder web, shear stiffeners along the full length of the girder and full height bearing stiffeners in the bent cap region. The fabricator was required to provide mill reports and welding certification to ensure compliance with ANSI/AASHTO/AWS D1.5-95

Web warping of the girders during welding was a concern because at test scale the girder web was only ¼" [6 mm] thick. The fabricator was informed of this concern and monitored the web during welding to ensure warping did not occur. The girder for Specimen 3, however, did exhibit minor warping. Adverse affects from this warping were prevented during testing by applying lateral bracing at the beam ends.

Two site visits were made to the steel fabricator during construction of the girders for the first two test specimens. On the first site visit, the shear studs on the bottom of the girder in the cap region were incorrectly installed in two rows instead of three. Because the bottom studs were expected to be of minimal consequence, the girder was accepted as fabricated and the stud detail for the girders of specimens three and four were modified to match the stud spacing used for the first two girders.

3.3.1 Construction of Concrete Column and Support Block for Component Test Specimen

While prototype column details called for hoops in the confined region, spirals were used along the full column height for ease of test unit construction. The prototype column diameter of 5'-6" [1,676 mm] scaled to 2'-2 3/8" [670 mm] in the model component tests. In scaling the column longitudinal and the transverse reinforcement, the

ratio of steel to concrete was maintained from prototype to test. To maintain the longitudinal reinforcement ratio in the prototype of ρ_l=0.02, thirty-six No. 5 [16 mm] bars were used. For shear reinforcement, No. 3 [10 mm] spirals spaced at 2" [51 mm] center to center with ¾" [19 mm] clear cover achieved a transverse reinforcement ratio of ρ_s=0.009.

Two column rebar cages were assembled in a horizontal orientation by supporting the ends of the cage and allowing the assembly to rotate. Once both cages were tied, they were placed on the casting bed so that half of each column cage protruded out of the rectangular support block footprint. Over the bottom four feet [1,219 mm], four levels of U-shaped No. 6 [19 mm] bars were slid into the column cages and overlapped. One hook in the longitudinal direction and two in the transverse direction were placed at every U-bar level.

The support block was cast in one pour to the bottom of the future bent cap. The column reinforcement, vertical hooks and tie down hollows extended to or near the future deck surface. The completed support block was moved to a position in the lab where remaining construction and eventual testing occurred.

3.3.2 Construction of Bent Cap for Component Test Specimen

The test specimen width was only one foot [305 mm] clear of the laboratory walls on either side. Due to this space limitation, the 20 ft [6,096 mm] flexural reinforcement in the bent cap had to be set in place prior to girder placement. Therefore, the cap/column joint region stirrups were placed first, followed by the bottom flexural reinforcement bars. The formwork was constructed to the bottom elevation of the bent cap and extended beyond the length of the future deck. The extended formwork was to serve as deck falsework.

With their locations marked on the formwork, the girders were lowered into place using the laboratory overhead crane. Once the girders were in place, the outside stirrups were threaded under the bottom flexural reinforcement and the cap face steel was guided through predrilled holes in the girder web (Figure 3-10, Figure 3-11). Again due to laboratory space constraints, the bent cap construction reinforcement and side face reinforcement were discontinuous and overlapped in the support block.

Horizontal J-hooks were tied across each stirrup at two levels: one at the level of the third side face reinforcement and one at the level of the construction reinforcement. All main flexural reinforcement was placed across the top of the two girders. The outer flexural reinforcement was tied to the hooks in the stirrup corners. The open stirrups were closed by tying hooks over the top flexural reinforcement, across the cap width. The remaining flexural reinforcement was tied up to the level of the J-hooks, straddling the shear studs on the top of the girders. Once rebar for the bent cap was tied, the cap was cast to the bottom of the future deck.

For the post-tensioned bent caps, the post-tension rods were anchored in the support block by means of large steel plates cast in the support block (Figure 3-12). The post-tensioned rods were continuous the length of the bent cap through predrilled holes in the girder web (Figure 3-13).

3.3.3 Construction of Deck for Component Test Specimen

The bottom deck formwork was constructed and the deck steel was tied in place. To separate the deck of Test 1 from the deck of Test 2, an aluminum sheet was placed at the centerline of the component test specimen. The deck steel consisted of bottom and top longitudinal bars and bottom and top transverse bars staggered between truss bars. The transverse deck steel of each test terminated at the centerline of the test specimen. Once all deck steel was tied, the sides of the deck formwork were built. Next, the deck was cast and the concrete was finished. After the deck concrete cured for three days, the deck formwork and all construction false work were removed.

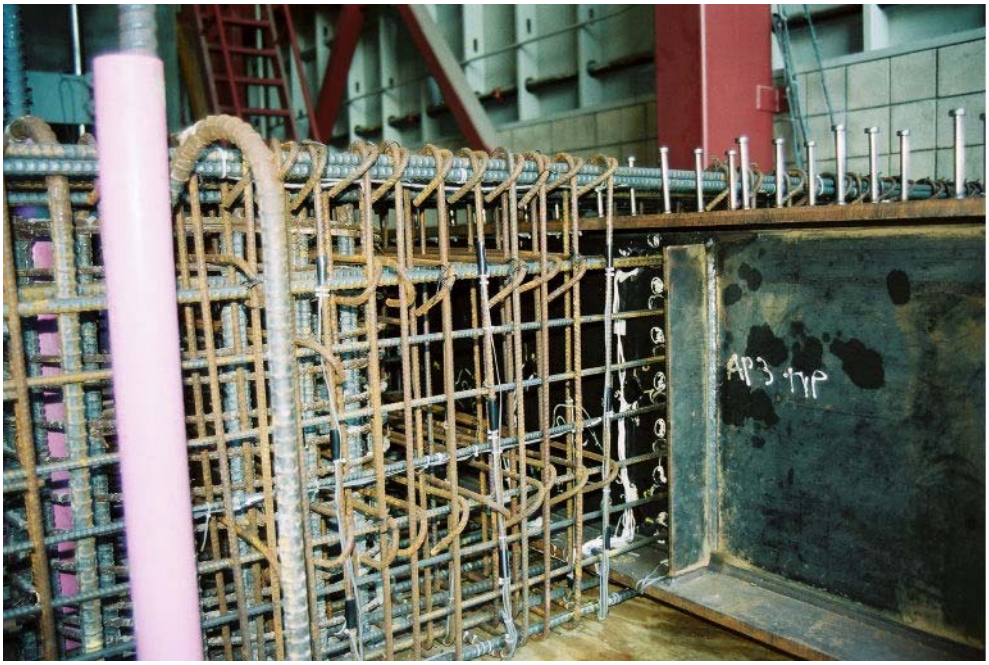

Figure 3-10 Bent Cap Joint Region

Figure 3-11 Bent Cap Reinforcement Through Girder Web

Figure 3-12 Post-Tensioning Anchoring in Support Block

Figure 3-13 Post-Tensioning Ducts

3.4 PROPERTIES OF COMPONENT TEST SPECIMEN MATERIALS

3.4.1 Steel Plate Girder Material Properties, Component Tests

One 16-in. [406 mm] long standard ASTM tensile coupon was machined from the girder web and one flange for each phase of testing. Results from the tensile tests are tabulated in Table 3.1.

Table 3.1 Steel Girder Coupons

Coupon		Yield Stress, f_y ksi [MPa]	Ultimate Stress f_{ult} ksi [MPa]	Elongation* ε_{su} %
Specimens 1 & 2	Flange	62 [428]	83 [572]	27
(CR-NS, CR-S)	Web	52.2 [360]	75.6 [521]	19.2
Specimens 3 & 4	Flange	52.8 [364]	77.6 [535]	25
(PT-NS, PT-S)	Web	54.7 [377]	77.8 [536]	30.5

* based on 8 in. (203 mm) gage length

3.4.2 Steel Reinforcement Material Properties, Component Tests

The steel reinforcement bar properties derived from tensile tests are tabulated in Table 3.2 and Table 3.3. The stirrup bars used in the bent cap and the deck truss bars did not exhibit any yielding plateaus. The reinforcement specified was A706, Grade 60 [414 MPa]. The reinforcement supplier was unable to deliver A706 in No. 3 [10 mm] size rebar, so Grade 60 [414 MPa] was used.

3.4.3 Concrete Material Properties, Component Tests

The concrete was specified to have a compressive strength of 4 ksi [27.6 MPa], ½" [13 mm] aggregate and a design slump of 4" [102 mm]. The mix design for the concrete is summarized in Table 3.4. Due to the highly congested reinforcement in the bent cap, a plasticizer was added to the concrete to increase its viscosity. This helped to ensure that the concrete would flow around the flexural reinforcement and through the holes in the web of the steel girder. The measured concrete compressive strengths at 7-day, 28-day and day of test were determined from standard cylinder compression tests and are presented in Table 3.5.

Table 3.2 Measured Reinforcement Properties (Conventionally Reinforced Specimens)

Item		Yield Stress, f_y ksi [MPa]	Ultimate Stress f_{ult} ksi [MPa]	Elongation* ε_{su} %
Bentcap:	Flexural #3 [10 mm]	62.4 [430]	99.3 [685]	13.2
	Stirrup #3 [10 mm]	75.3 [519]	114.4 [789]	12.9
	Flexural #5 [16 mm]	68.1 [470]	98.6 [680]	14.2
Deck:	Truss #3 [10 mm]	74.7 [515]	114.0 [786]	14.8
	Transverse #3 [10 mm]	62.5 [431]	99.8 [688]	14.3

* based on 8 in. (203 mm) gage length

Table 3.3 Measured Reinforcement Properties (Post-Tensioned Specimens)

Item		Yield Stress, f_y ksi [MPa]	Ultimate Stress f_{ult} ksi [MPa]	Elongation* ε_{su} %
Bentcap	Stirrup #3 [10 mm]	78.3 [540]	105.8 [730]	6.6
	Flexural #3 [10 mm]	66.3 [457]	104.0 [723]	10.7

* based on 8 in. (203 mm) gage length

Table 3.4 Concrete Mix Design Weights and Volumes

Material	Batch Quantity	% of Aggregate	Specific Gravity	Absolute Volume
Cement	600.00		3.15	3.05
Flyash	108.00		2.05	0.84
½" CG	1235.00	44.28	2.61	7.58
3/8" CG	345.00	12.44	2.60	2.13
WCS	1235.00	43.28	2.67	7.41
Water, gal. (Lbs.)	40.80 (339.86)			5.45
Admixtures				
WRDA-64	21.00			0.00
DARAVAIR 1000	1.50			0.00
Air Percentage	2.00			0.54
				27.00
W/(C+F) Ratio	0.48			

Table 3.5 Concrete Compressive Strength

Location	7 Days ksi [MPa]	28 Days ksi [MPa]	Day of Test ksi [MPa]	Age Days
Conventionally Reinforced				
Column	3.39 [23]	4.51 [31]	*NS* 5.71 [39] *S* 5.86 [40]	180 191
Bent Cap	2.66 [18]	3.97 [27]	*NS* 5.00 [34] *S* 5.18 [36]	82 93
Deck	2.56 [18]	4.01 [28]	*NS* 4.11 [28] *S* 4.36 [31]	33 44
Post-Tensioned				
Column	3.56 [25]	5.01 [35]	*NS* 6.36 [44] *S* 6.70 [46]	105 121
Bent Cap	3.74 [26]	4.87 [34]	*NS* 5.42 [37] *S* 5.64 [39]	48 64
Deck	2.97 [20]	4.42 [31]	*NS* 4.13 [28] *S* 4.4 [30]	22 38

NS = No Stiffeners
S = Stiffeners

3.5 INSTRUMENTATION OF COMPONENT TEST SPECIMEN

On each test specimen, the girder flanges, webs, and where applicable, interior stiffeners were instrumented with post-yield strain gages. While post-yield strain gages are used primarily for measurements of large post-yield strains (46) they also record strain measurements before yield. The webs of the plate girder were instrumented with strain rosettes. Selected reinforcing bars in the column, bent cap and deck were instrumented with strain gages. Externally, the specimen's response was recorded by linear displacement transducers, inclinometers and actuator readings.

3.5.1 Strain Gage Locations in Component Tests

Figure 3-14 shows strain gage locations on the bent cap stirrups. Strain gages were applied to three stirrups in vertical planes in the joint region, labeled 1, 2, and 3. These stirrups were located at the column centerline, the column face and the face of the girder. Strain gages were also applied to the joint region stirrups at all four corners and midpoints. The internal midpoint gages (B and J) were included for redundancy.

Strain gages were placed at the midpoints of two stirrup locations outside the joint region (labeled 4 and 5 in Figure 3-14). A total of thirty-six strain gages monitored stirrup behavior in the joint region and twelve strain gages monitored stirrup behavior outside the joint region.

The locations of strain gages on the flexural reinforcement are shown in Figure 3-15. The strain gage locations along the flexural reinforcement corresponded to the location where gaged stirrups were placed. In the joint region (locations 1, 2, and 3), strain gages were placed in locations on the bars that are indicated in the section view shown in Figure 3-15. Outside the joint region (locations 4 and 5), strain gages were only placed on the top and bottom flexural reinforcement, thus eliminating gages C and G. A total of twenty-four strain gages monitored the behavior of flexural reinforcement inside the joint region and twelve strain gages monitored the behavior outside the joint region.

Strain gages on the deck reinforcement were concentrated on the longitudinal reinforcement (Figure 3-16). The locations of strain gages on the deck bars corresponded to the locations of the gaged stirrups. An additional gaged bar was located above the girder centerline. Strain gages were placed on the deck bars two feet [610 mm] outward

from the face of the bent cap. No strain gages were located on deck bars in the bent cap. Strain gages were applied to one transverse bar at either face of the bent cap. Strain gages were not applied to the truss bars.

The girder behavior was monitored by post-yield strain gages placed on both flanges and the stiffeners as well as strain rosettes placed on the girder web (Figure 3-17). The elevation in Figure 3-17 shows the locations of the strain rosettes as well as enlarged views of the post-yield strain gages for location reference. Gages on the stiffeners were placed near the bottom and the top of the stiffeners (Section A-A). Section B-B of Figure 3-17 shows the locations of the post-yield strain gages on the flanges. The strain gages on the flange were located on the inside of the girder. All strain gages were located on the joint region side of the girder. There were a total of nine strain rosettes per girder, twelve post-yield strain gages on the stiffeners and seven strain gages per flange.

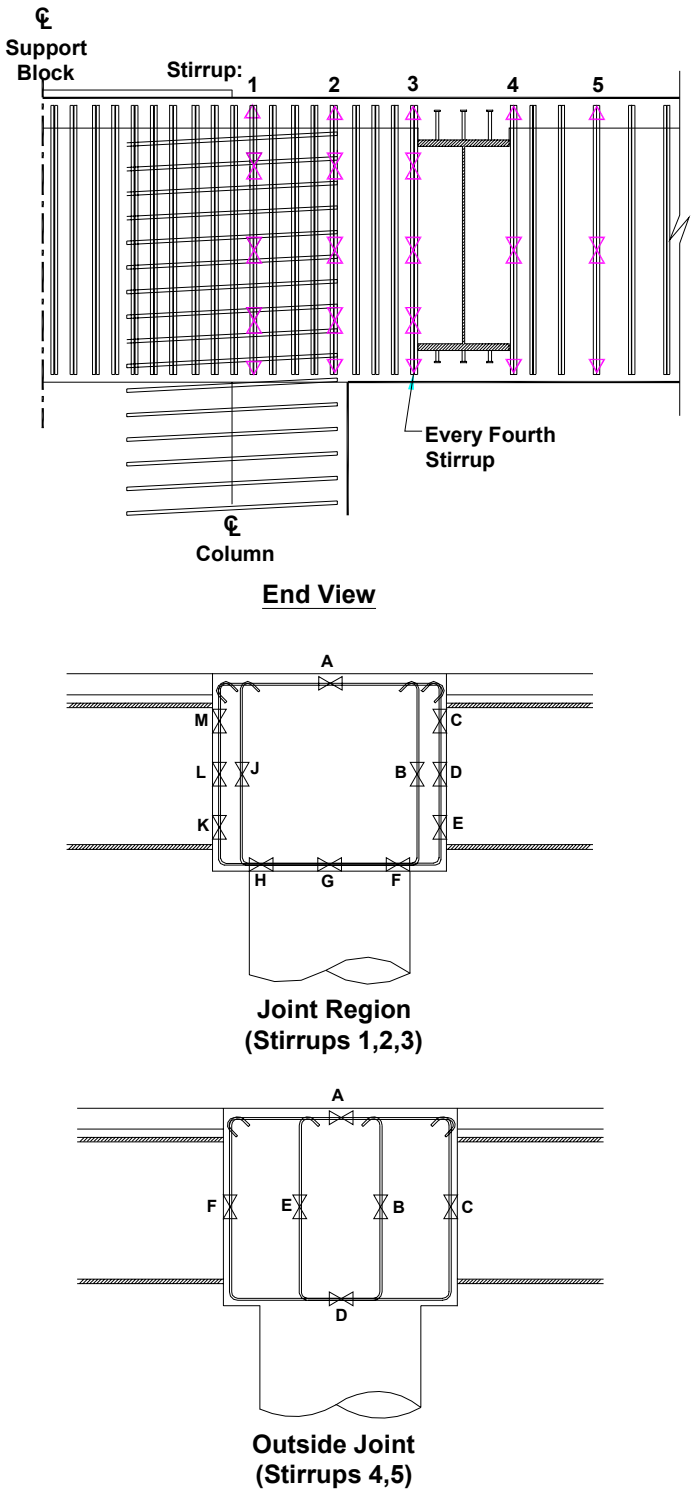

Figure 3-14 Stirrup Strain Gage Locations and Designations

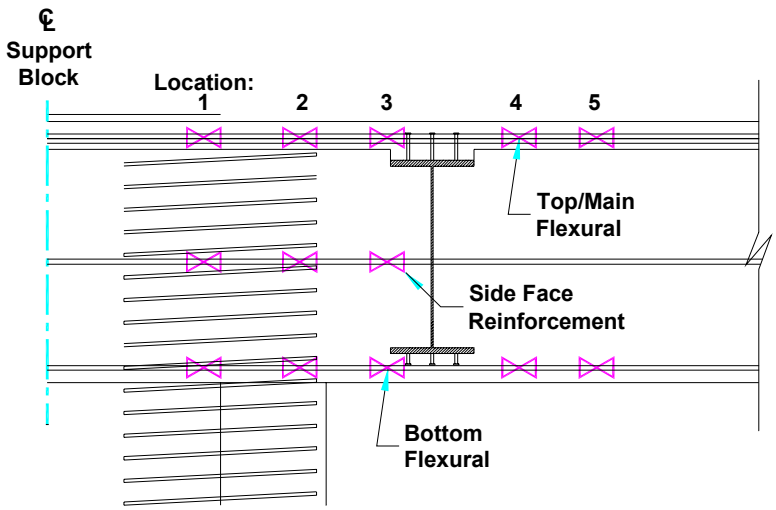

End View

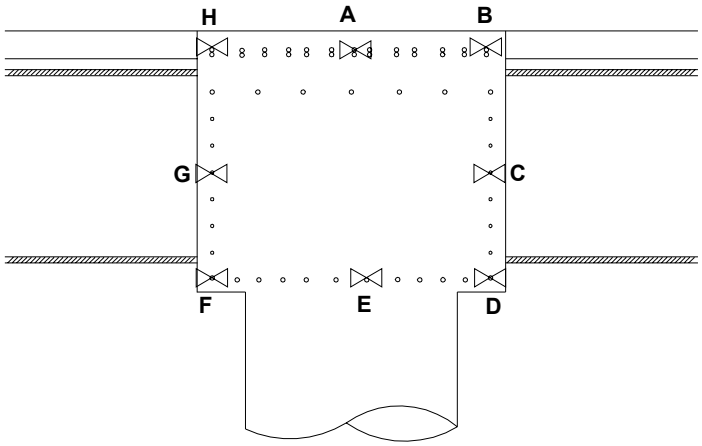

Section

Figure 3-15 Flexural Reinforcement Strain Gage Locations and Designations

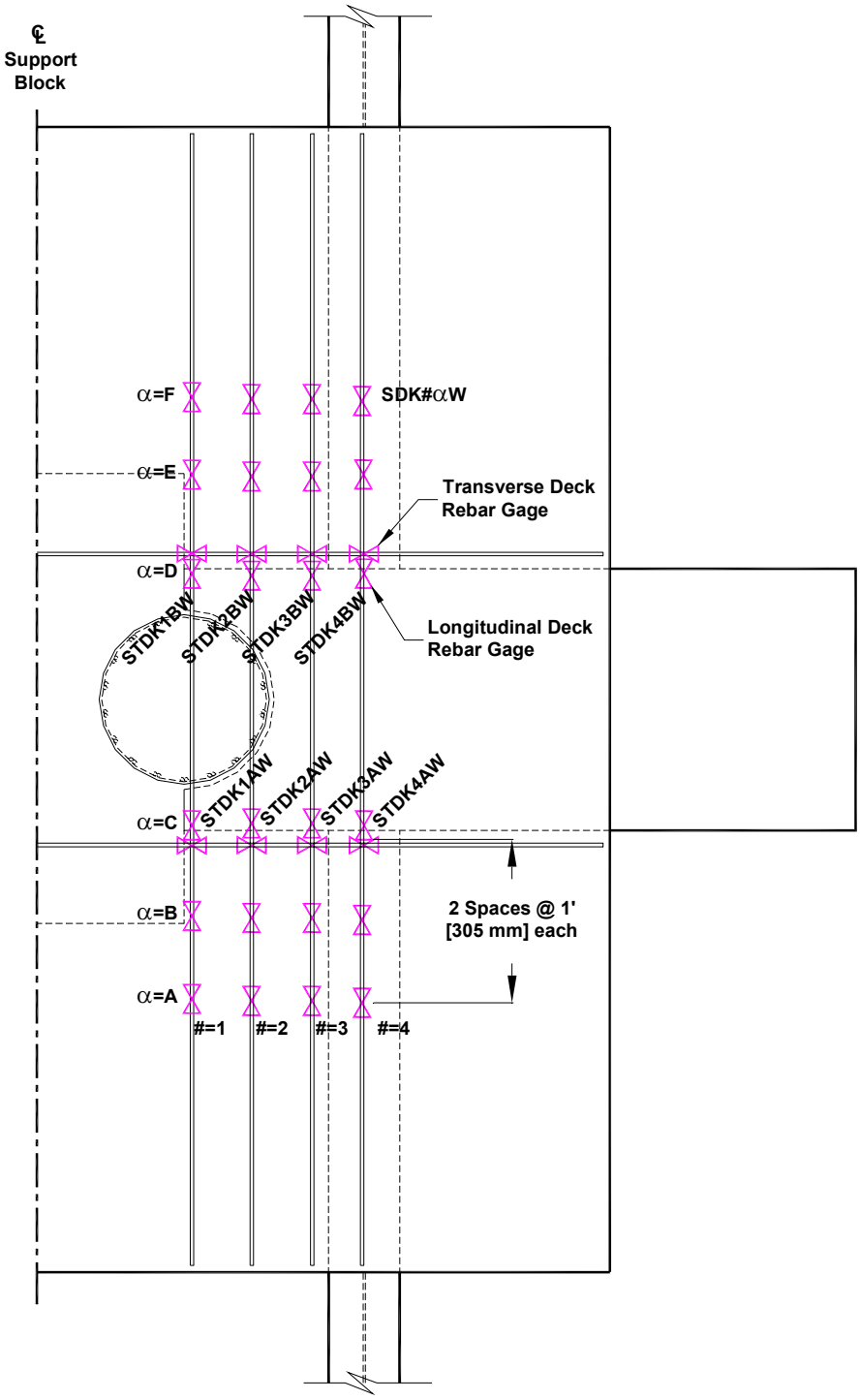

Plan View

Figure 3-16 Deck Reinforcement Strain Gage Locations and Designations

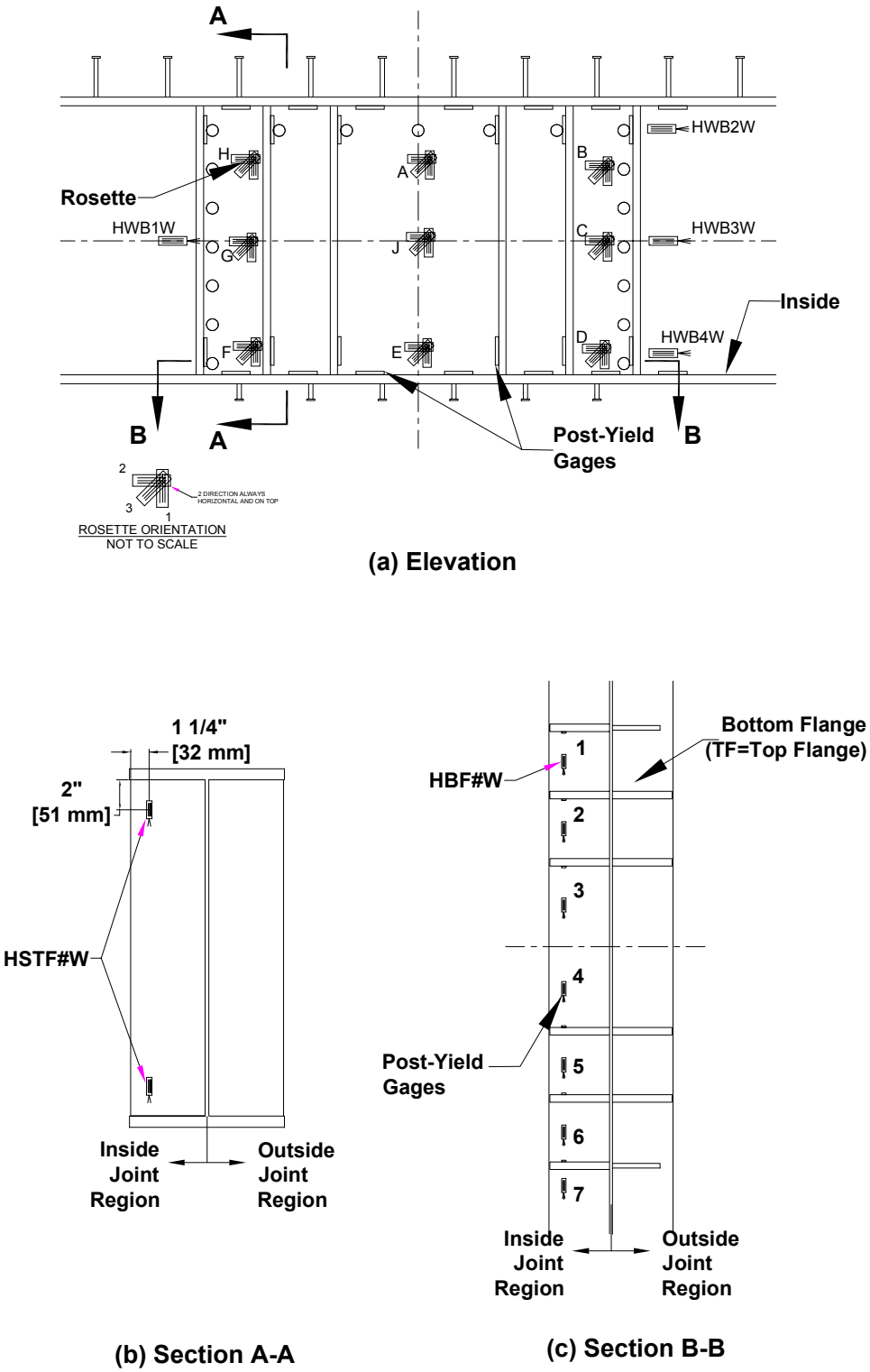

Figure 3-17 Girder Strain Gage Locations and Designations

3.5.2 External Displacement Measurement Devices in Component Tests

Figure 3-18 shows the location of the external measuring devices. Girder deformation profiles were obtained from vertical measurements taken along the length of the girder. Girder displacements at four locations on either side of the bent cap were recorded by linear potentiometers.

Bent cap rotation was measured three ways: (1) a rotational device at the end of the bent cap, (2) two vertical measurements a specified distance apart under the bent cap, and (3) two horizontal measurements at the face of the bent cap. In addition to providing multiple rotational measurements, the different means by which to measure rotation described characteristics such as rigid body rotations or twist along the beam length.

Horizontal displacement measurements were taken by linear displacement transducers that were mounted horizontally and used the bent cap as the target (Figure 3-19). One pair of transducers was mounted to the girder to measure relative rotation between the girder and bent cap and another pair was mounted to the floor to measure global rotation. Both pairs of horizontal potentiometers produced valuable data during the initial stages of testing but were rendered inaccurate once significant bent cap spalling had occurred.

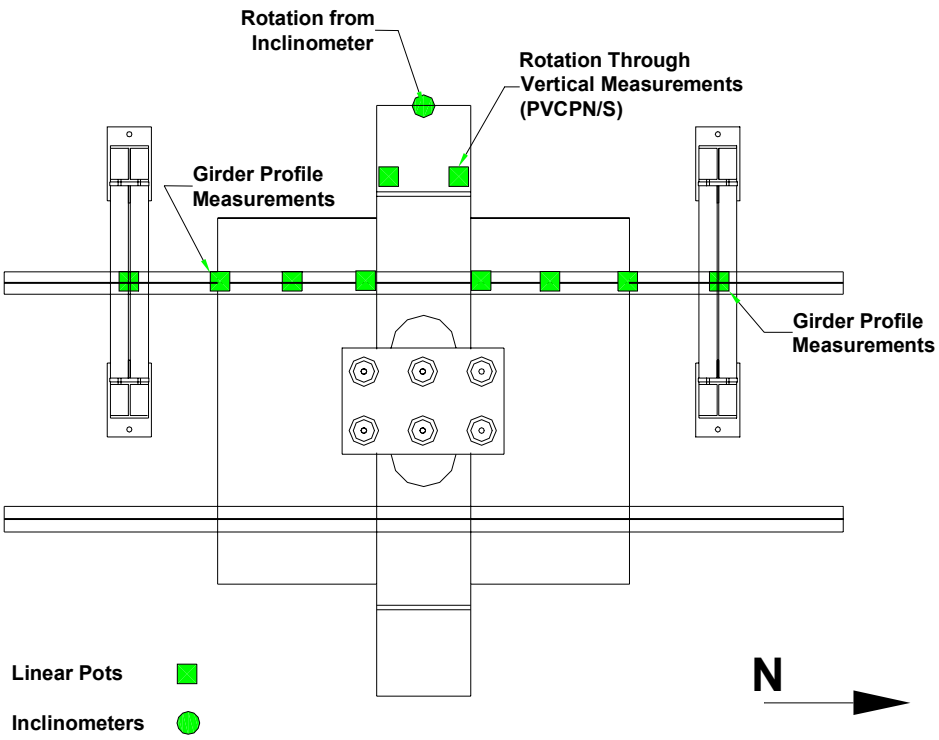

(a) Plan View

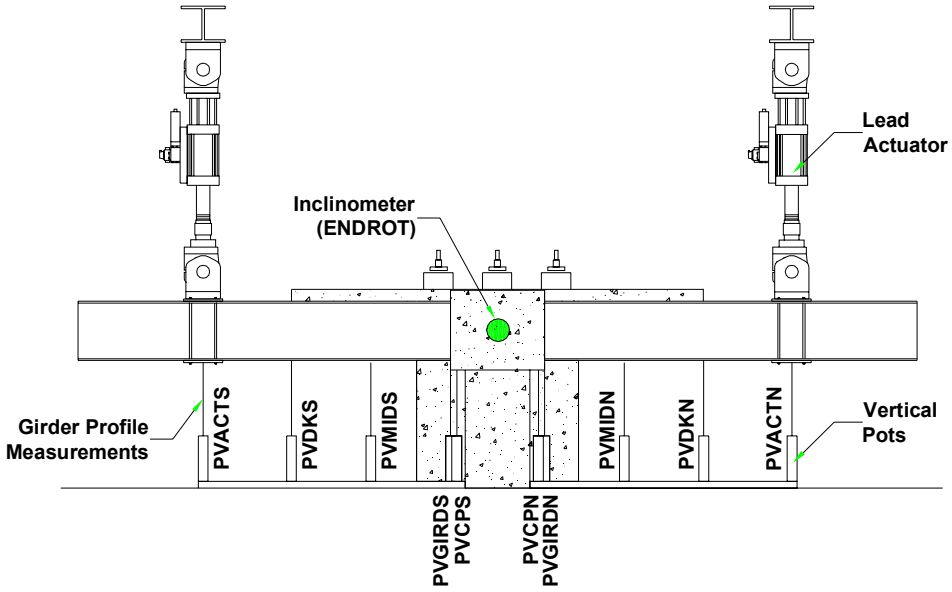

(b) Elevation

Figure 3-18 Vertical Displacement Measurement Locations and Designations

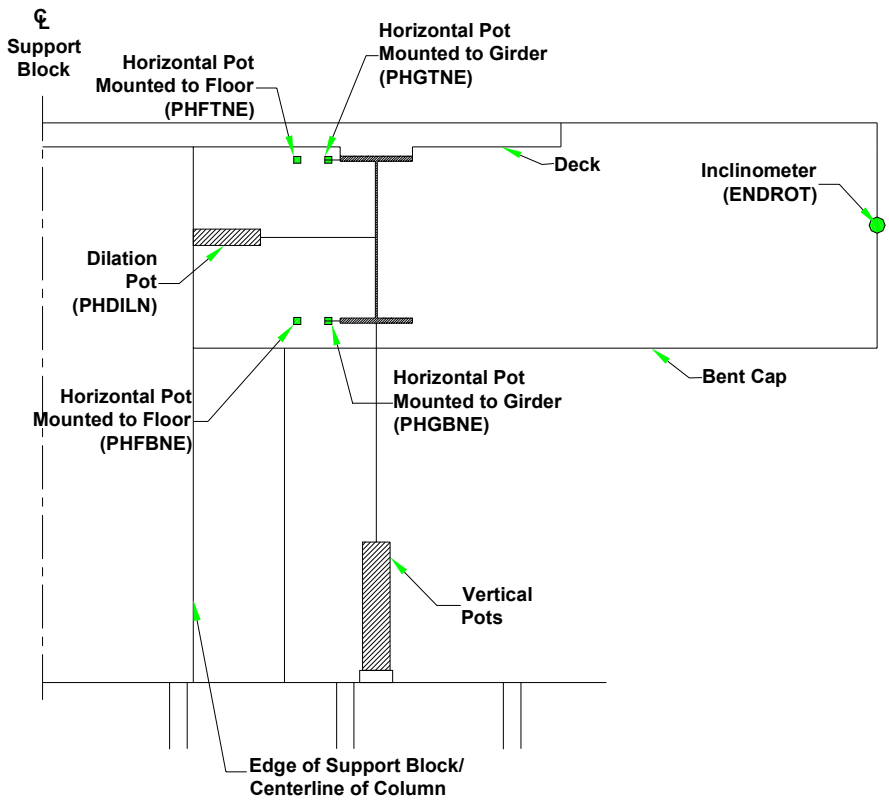

End View (Lead Face)

Figure 3-19 Horizontal Displacement Measurement Locations and Designations

3.6 LOADING PROTOCOL FOR COMPONENT TESTS

The seismic load is introduced into the bent cap by controlling one actuator (hereafter referred to as the "lead actuator") while the second actuator (hereafter referred to as the "follower actuator") was designated to apply equal and opposite displacements of the lead actuator. All loading is in reference to the lead actuator. When the lead actuator applied a downward displacement, it was referred to as "push".

Each component test specimen was subjected to a quasi-static, fully reversed cyclic testing protocol. Equal and opposite vertical displacements were applied via servo-controlled hydraulic actuators located at both dead load inflection points on the girder (Figure 3-6). Testing began by loading each hydraulic jack to 37.5 kip [167 kN]. The load level in the jacks was maintained and monitored throughout the test. Each actuator then applied a downward force on the girders of 25 kip [111 kN]. With all dead loads

applied, the seismic loading protocol began. Seismic loading began in pseudo force control (displacement control while monitoring the force) in single cycles of 5 kip [22 kN] increments to first torsional cracking. After the first crack, the specimen was loaded in single cycle displacement increments of 0.25 in. [6 mm] to 1 in. [25.4 mm]. The specimen was then subjected to three cycles of 0.5 in. [12.7 mm] displacement increments up to 2 in. [51 mm]. After 2 in. [51 mm] displacement was reached, three cycles of 1 in. [25.4 mm] increments were imposed until failure. The loading sequence is detailed in Figure 3-20.

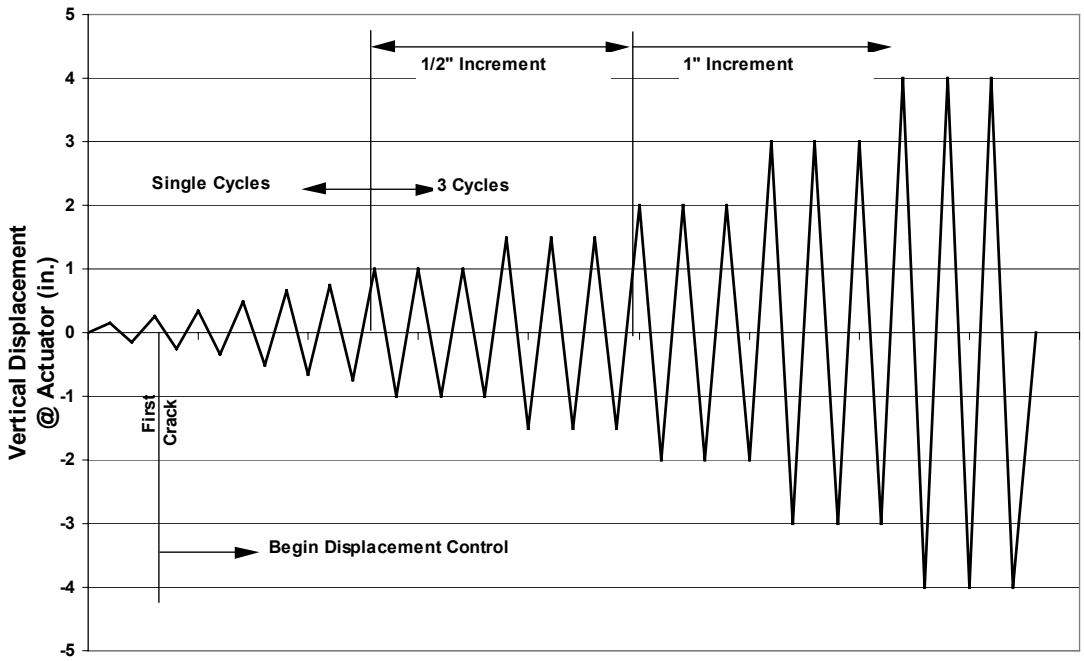

Figure 3-20 Component Test Loading Sequence

Chapter 4

Experimental Results of Component Tests

4.1 Overview

This chapter presents photographic documentation and measured response of all four component test specimens. Section 4.2 explains the manner in which the experimental results are presented in this chapter. Sections 4.3, 4.4, 4.5, and 4.6 present the test results of Specimen 1 (CR-NS), Specimen 2 (CR-S), Specimen 3 (PT-NS) and Specimen 4 (PT-S), respectively. Each section starts with a description of observed specimen performance supported by photos taken during testing. Following the photo documentation of each specimen, the measured response of the specimen is presented, including, but not limited to, measurements recorded from strain gages on steel reinforcement bars and measured moment rotation response. Section 4.7 concludes the chapter by comparing the observed and measured performance of the four specimens, including comparison of moment rotation envelopes.

4.2 Presentation of Component Test Results

The component test results are presented with reference to the actuator loading and locations. The bent cap faces are named to indicate their relationship to the actuators. The joint region of the component test specimen is shown in Figure 4-1, with the support block and a portion of the deck removed for clarity. The figure indicates the location of the lead actuator with reference to the joint region. The bent cap face designated "Lead Bent Cap Face" is the vertical bent cap face nearest the lead actuator. The "Bottom Bent Cap Face" is the horizontal face that intersects the column. The "Following Bent Cap Face" is the vertical bent cap face nearest the follower actuator. The "Top Bent Cap Face" is the horizontal face with the deck.

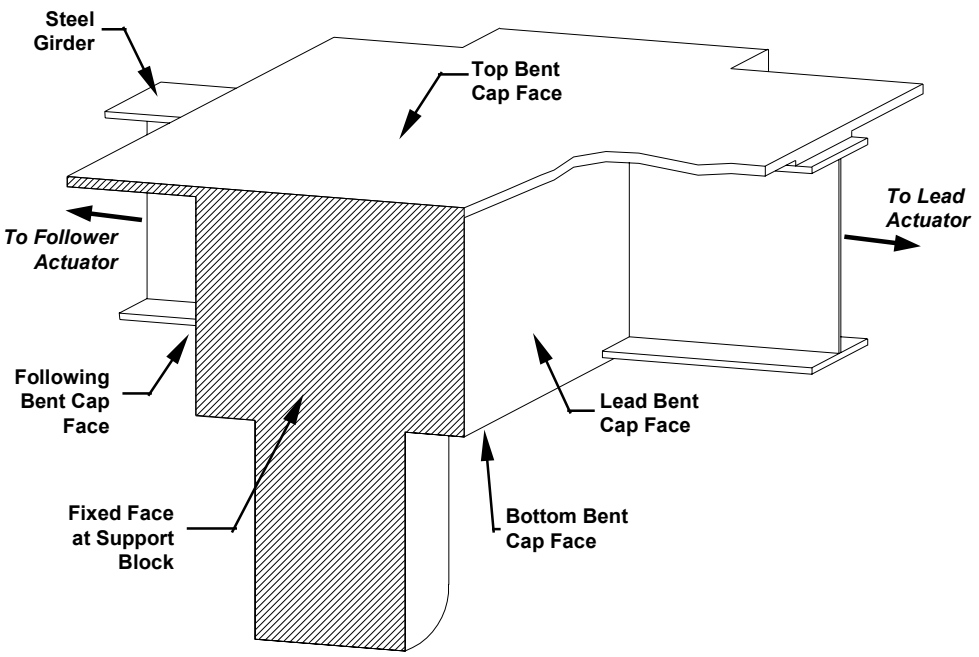

Figure 4-1 Bent Cap Face Orientation

When the lead actuator is in push, it creates a positive moment about the transverse bridge axis (Figure 4-2a), resulting in the bent cap torsion indicated. This torsional moment in the bent cap is reacted by an opposing moment at the support block. The same equilibrium requirements apply to the lead actuator in pull (Figure 4-2b).

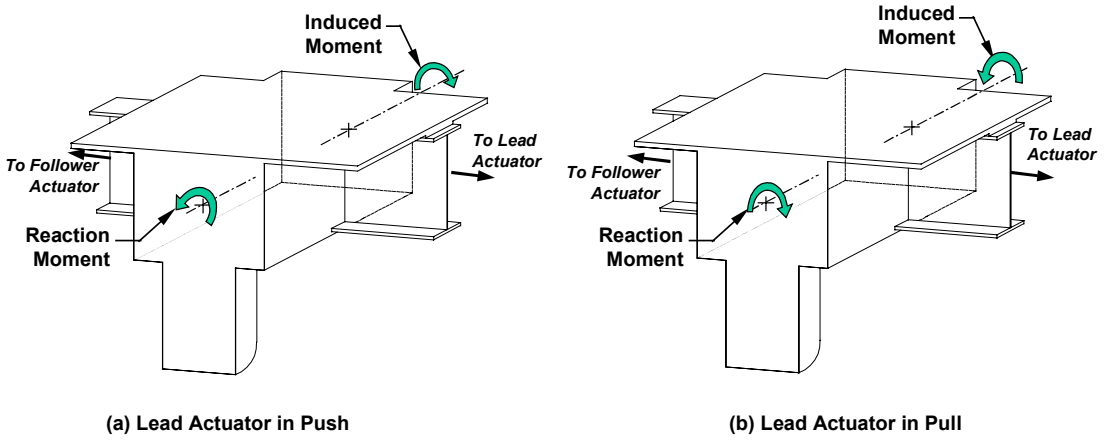

Figure 4-2 Torsional Moment Directions in Component Tests

The majority of the bent cap damage photographs presented in this chapter are of the lead face because it experienced the first cycle of every new loading increment. The

name of each bent cap face remains the same throughout the presentation of the experimental results. The only variable in describing experimental results is the direction of loading (push down, pull up) with reference to the lead actuator. The remainder of the chapter uses the designations described in this section to present the experimental results of the four component test specimens.

The torsional moment reported is the absolute sum of the two actuator forces multiplied by the distance from the centerline of the bent cap to the point of load application. The torsional rotation is a measure of the total bent cap rotation due to torsion, not the twist of the section (twist being a measurement of rotation per length). For ease of comparison, this chapter presents the total torsional rotation. The rotation is measured from the inclinometer at the end of the bent cap (Figure 3.18). A discussion of the twist angle definition is presented in Chapter 5.

4.3 SPECIMEN 1-CONVENTIONALLY REINFORCED, NO STIFFENERS (CR-NS)

4.3.1 Observed Performance, CR-NS

The first torsional crack appeared on the lead bent cap face and occurred at a torsional moment of 368 k-ft [499 kN-m] and a corresponding bent cap torsional rotation of 0.001 radians (Figure 4-3). The crack initiated at the edge of the top flange of the girder and extended down toward the column at an angle of approximately sixty-five degrees from the horizontal. The crack ended approximately six inches [152 mm] above the bottom of the bent cap. At a torsional moment of 992 k-ft [1,344 kN-m] and torsional rotation of 0.0128 radians, numerous spiral cracks developed on the bent cap face, including one that developed from the bottom flange of the girder and spiraled down and around the bottom of the bent cap (Figure 4-4). Incipient spalling of a crack located closest to the girder was observed. On the underside of the bent cap, incipient spalling was observed near the column (Figure 4-5).

At the maximum torsional moment (1,125 k-ft [1,524 kN-m], 0.022rad), multiple minor spiral cracks developed on the bent cap face. A crack that initiated at the girder web and extended to the bottom of the cap at an angle of approximately eighty degrees began to spall significantly (Figure 4-6). Damage on the underside of the bent cap was concentrated between the girder and the column, where cracks initiated at the girder and

extended toward the column (Figure 4-7). The bent cap concrete under the girder had spalled, exposing a portion of the girder flange and a single bent cap flexural reinforcement bar. At this load level, deck cracks were mostly superficial. Upon further loading, the bent cap concrete under the girder was significantly damaged, exposing two bottom bent cap flexural reinforcement bars as well as two shear studs (Figure 4-8).

At the maximum bent cap torsional rotation of 0.031 radians, the torsional moment was 952 k-ft [1,290 kN-m]. A torsional shear friction plane at the first crack location (Figure 4-9) was the failure mechanism. The underside of the bent cap between the girder and column spalled significantly, exposing bent cap flexural reinforcement and transverse reinforcement near the column face (Figure 4-10). Under the girder, the bent cap concrete had spalled to expose multiple shear studs as well as portions of all the bottom flexural reinforcement bars. The deck only experienced cracking and exhibited no significant damage (Figure 4-11). The column concrete remained undamaged.

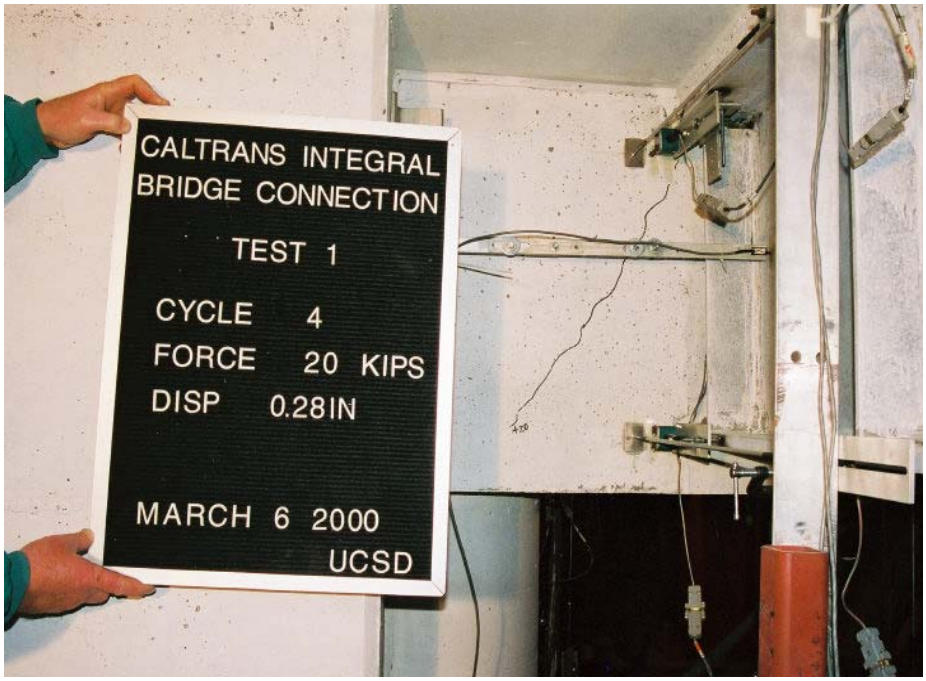

Figure 4-3 Specimen CR-NS: First Torsional Crack on Lead Face

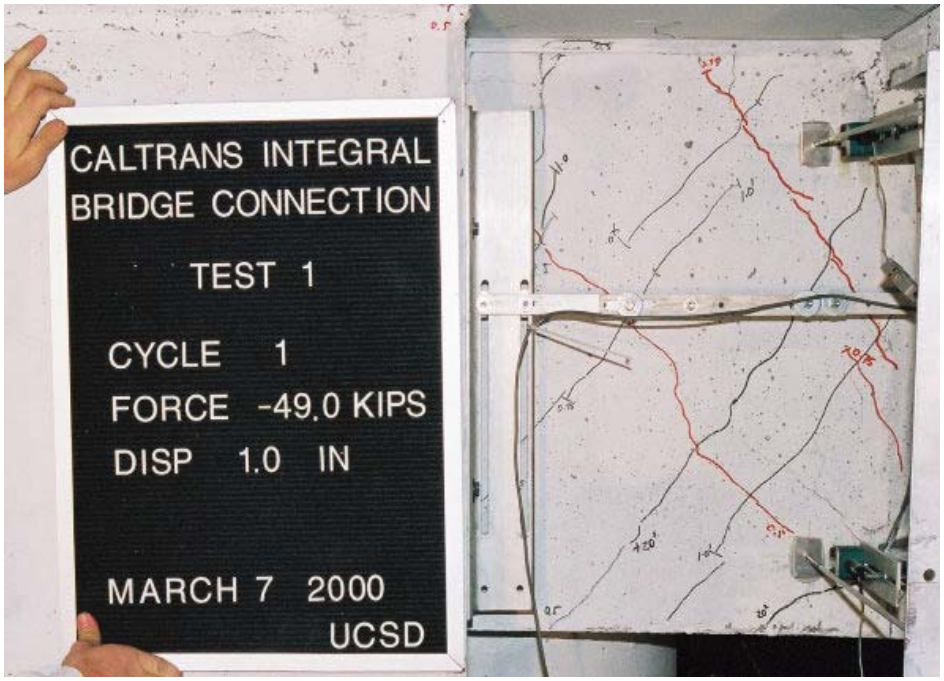

Figure 4-4 Specimen CR-NS: Lead Face of Bent Cap at 0.01 radians

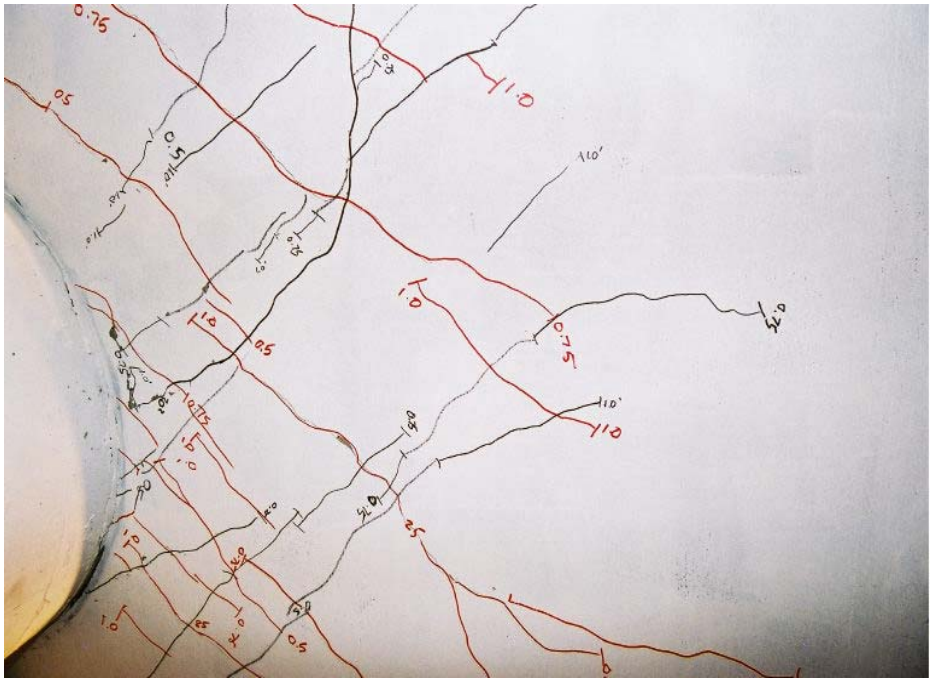

Figure 4-5 Specimen CR-NS: Bottom Face at 0.01 radians

Figure 4-6 Specimen CR-NS: Lead Face at Maximum Torsional Moment

Figure 4-7 Specimen CR-NS: Bottom Face at Maximum Torsional Moment

Figure 4-8 Specimen CR-NS: Girder/Cap Interface at θ = 0.02 radians

Figure 4-9 Specimen CR-NS: Lead Face at Maximum Torsional Rotation, θ = 0.03 radians

Figure 4-10 Specimen CR-NS: Bottom Face at Maximum Torsional Rotation

Figure 4-11 Specimen CR-NS: Deck Damage at Maximum Torsional Rotation

4.3.2 Measured Response, CR-NS

The torsional moment versus torsional rotation response of the bent cap is shown in Figure 4-12. The maximum torsional moment of 1,125 k-ft [1,524 kN-m] exceeded the moment corresponding to bent cap design moment of 700 k-ft [948 kN-m] by 38 percent. The bent cap exhibited minimal cracking and performed nearly elastically at the column overstrength moment. The bent cap dilation shown in Figure 4-13 represents the total bent cap crack dilation along the transverse bridge axis. This bent cap dilation was measured by potentiometers mounted horizontally on the support block with the target at the girder. This measured the amount the bent cap elongated due to crack dilation. On both faces, cap dilation was less than 0.05 in. [1.3 mm] at 700 k-ft [948 kN-m].

Figure 4-14 shows selected strain gage locations with respect to the lead actuator. All plots refer to strains as they correspond to whether the lead actuator is pushing down (designated "Push") or pulling up (designated "Pull") on the specimen. Zero on the horizontal axis indicates the column centerline. The joint region is between this zero designation and the centerline of the girder. The highest strains in the bent cap flexural reinforcement where recorded in bars located at the bent cap corners near the girders. Bent cap flexural reinforcement behavior is documented in Figure 4-15. The highest stirrup strains also occurred at the bent cap corners near the girder and are plotted in Figure 4-16.

In all flexural reinforcement, the highest strains occur in the joint region, with the highest values of strain occurring at the location nearest the girder. Bar D yielded during the push portion of a cycle and bar F yielded during the pull portion of the same cycle. Bar H, located at the top of the bent cap, did not yield.

All of the strain gages on the stirrups recorded yielding. The first gages to record bar yielding were located on the vertical legs of the stirrups and on one horizontal stirrup leg at the bottom of the bent. The remaining selected strain gage on the horizontal leg of the stirrup at the bottom of the bent recorded yield next. The last stirrup locations to record yield were the horizontal legs at the top of the bent. As with the flexural reinforcement, the highest strain readings were from gages located on the stirrups near the girder. Gages E and F recorded the highest tensile strains during the push portion of the cycle and Gages H and K recorded the highest tensile strains during the pull cycle.

Strain gages were also placed on longitudinal deck bars located between the column and the girder. Recordings from strain gages located on reinforcement in the deck are shown in Figure 4-17. The deck bars first yielded at the bent cap face (Locations C and D). The location on the bar farthest from the bent cap performed elastically.

Strains recorded from the top and bottom flange of the girder are plotted in Figure 4-18. The top flange inside the cap experienced only minor strain deformation. The strain gage located just outside the bent cap recorded strains approaching yield. The bottom flange yielded toward the bent cap follower face during the push portion of the 0.75 in. [19 mm] displacement cycle and toward the lead actuator face on the pull portion of the same cycle.

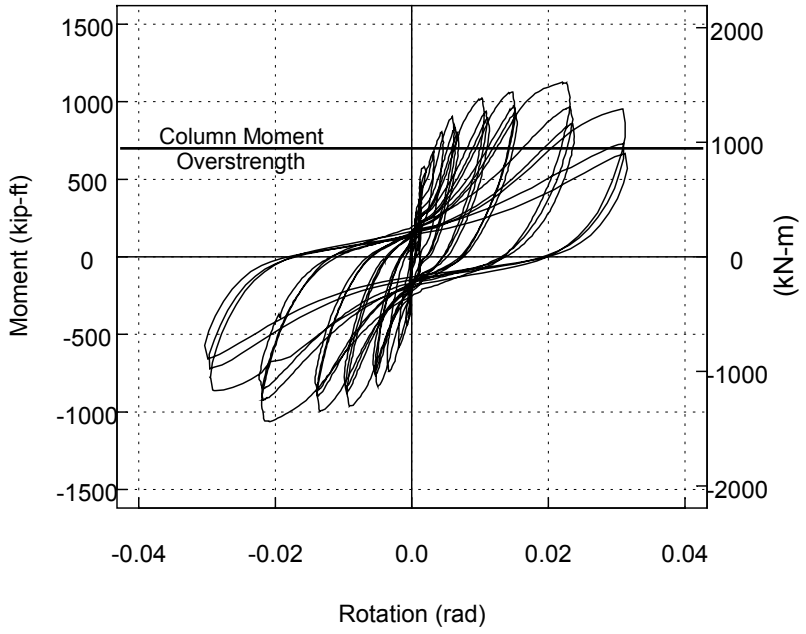

Figure 4-12 Specimen CR-NS: Torsional Moment-Rotation Response

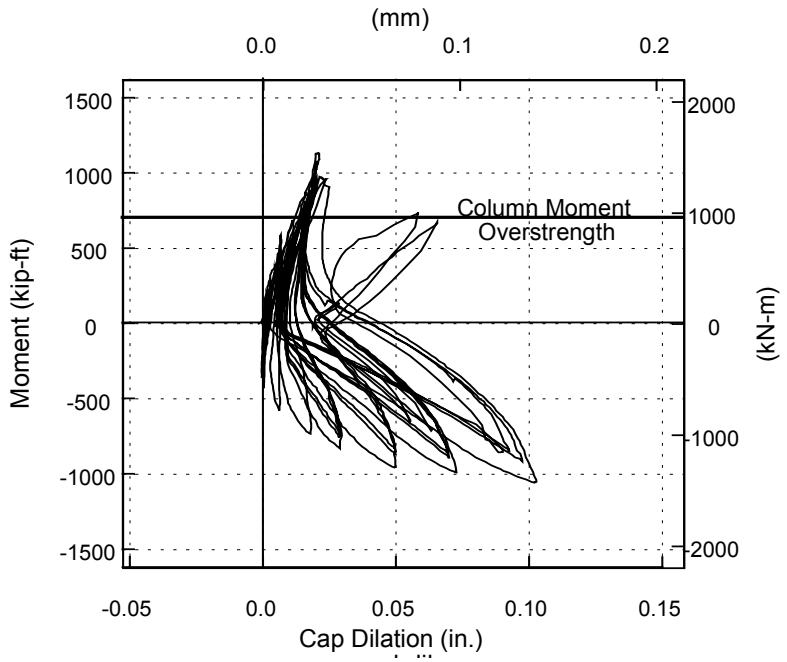

(a) Lead Face

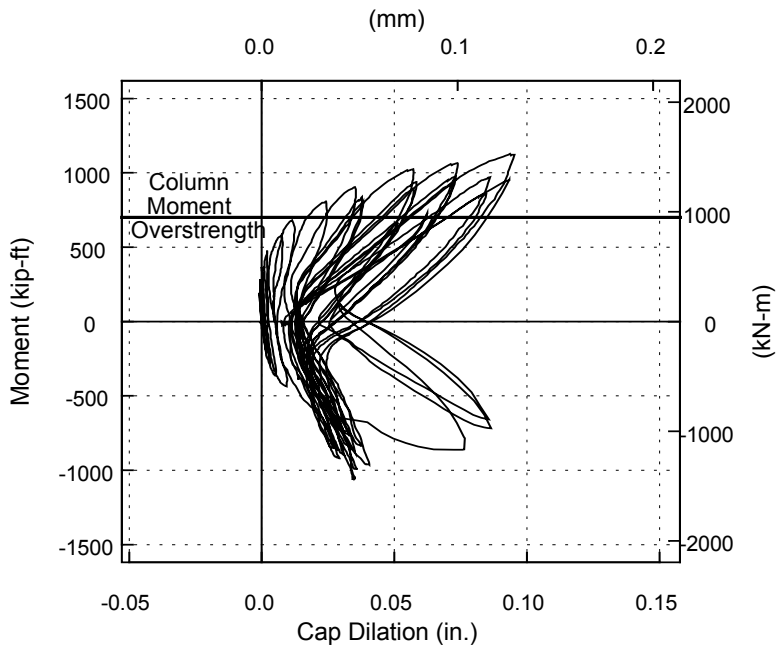

(b) Follower Face

Figure 4-13 Specimen CR-NS: Measured Bent Cap Dilation

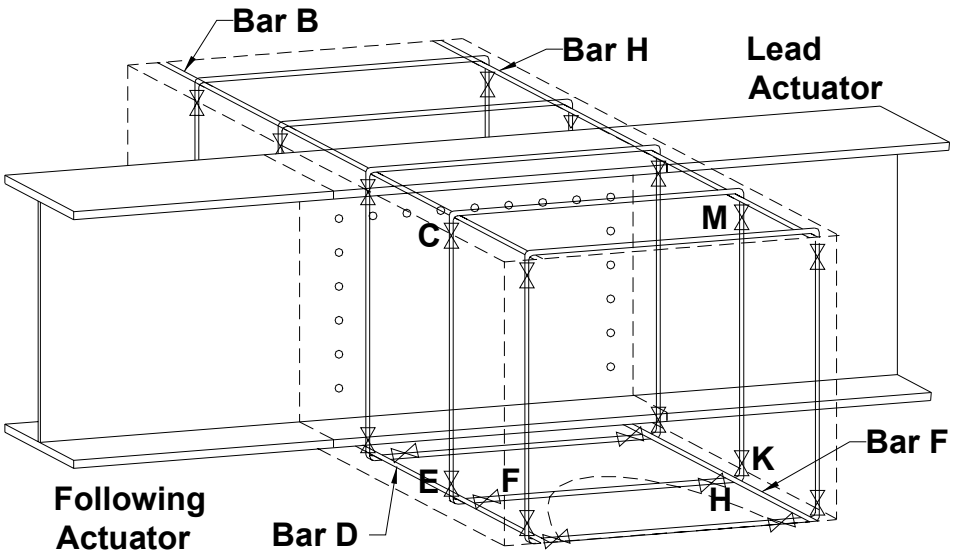

Figure 4-14 Specimen CR-NS: Strain Gage Location with Respect to Actuators

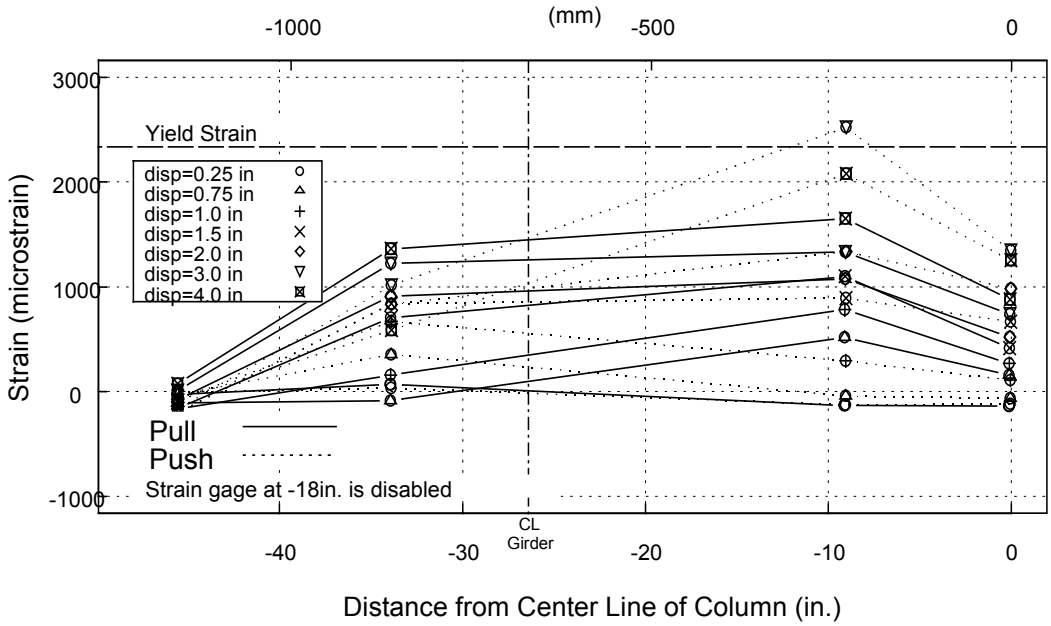

(a) Bar D

Figure 4-15 Specimen CR-NS: Measured Strain in Flexural Reinforcement

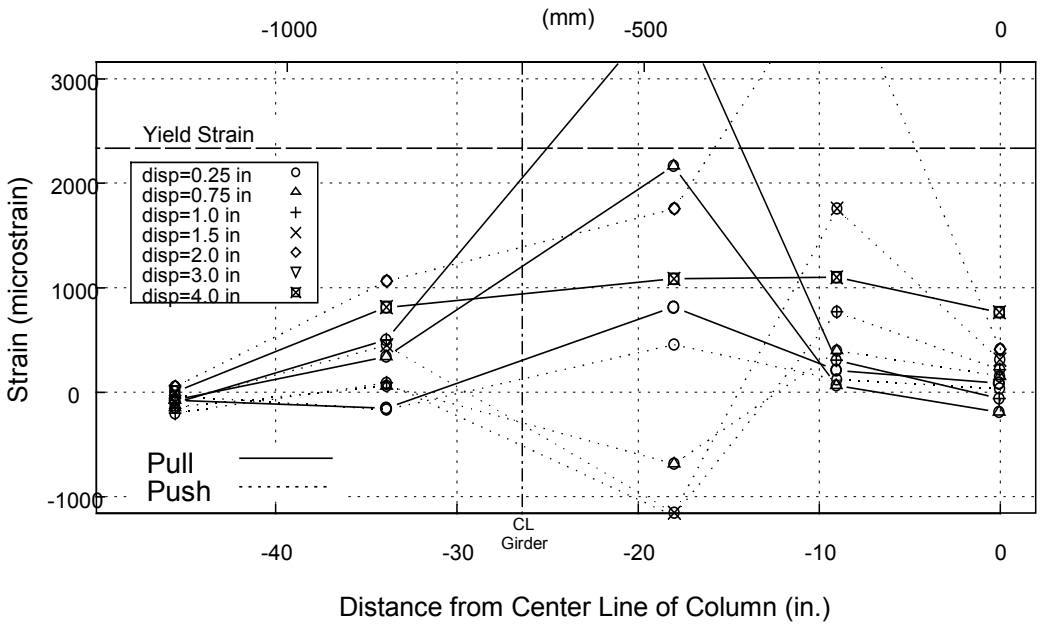

(b) Bar F

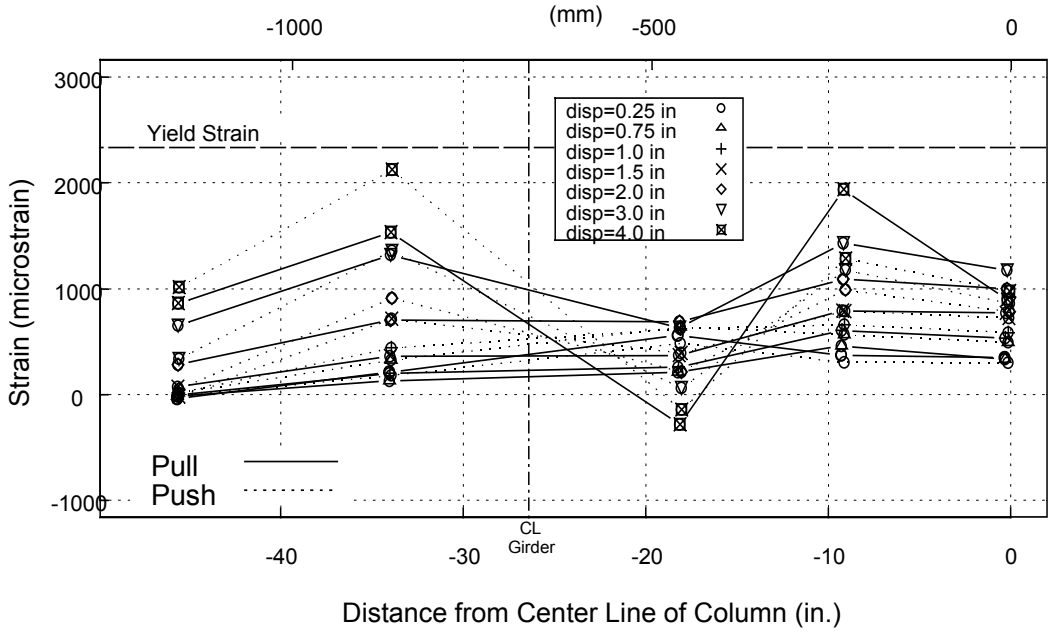

(c) Bar H

Figure 4-15 Specimen CR-NS: Measured Strain in Flexural Reinforcement (cont.)

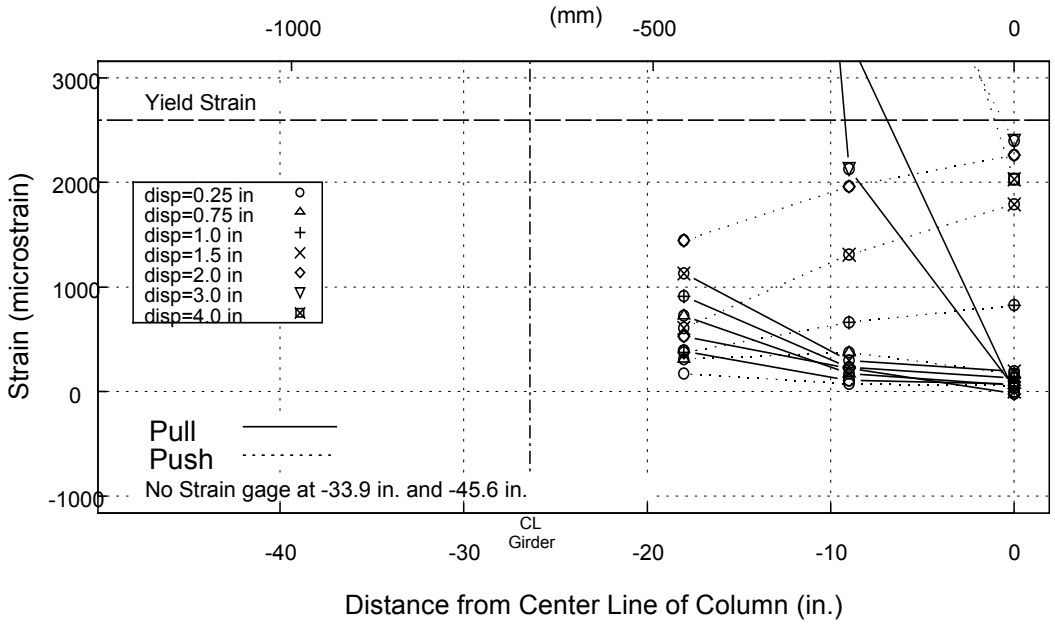

(a) Gage C

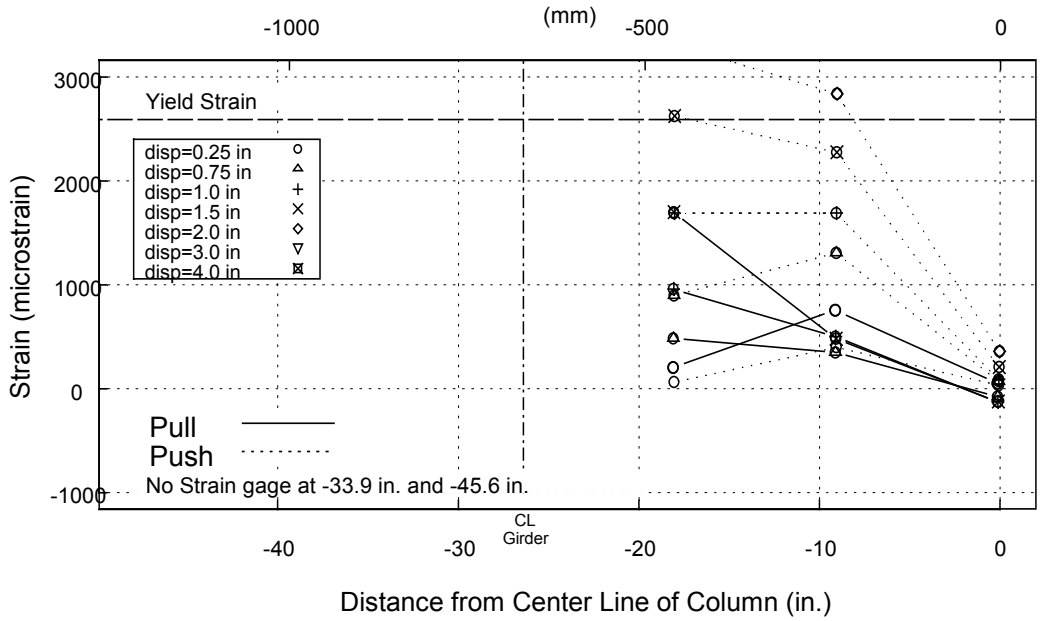

(b) Gage E

Figure 4-16 Specimen CR-NS: Measured Strain in Bent Cap Stirrups

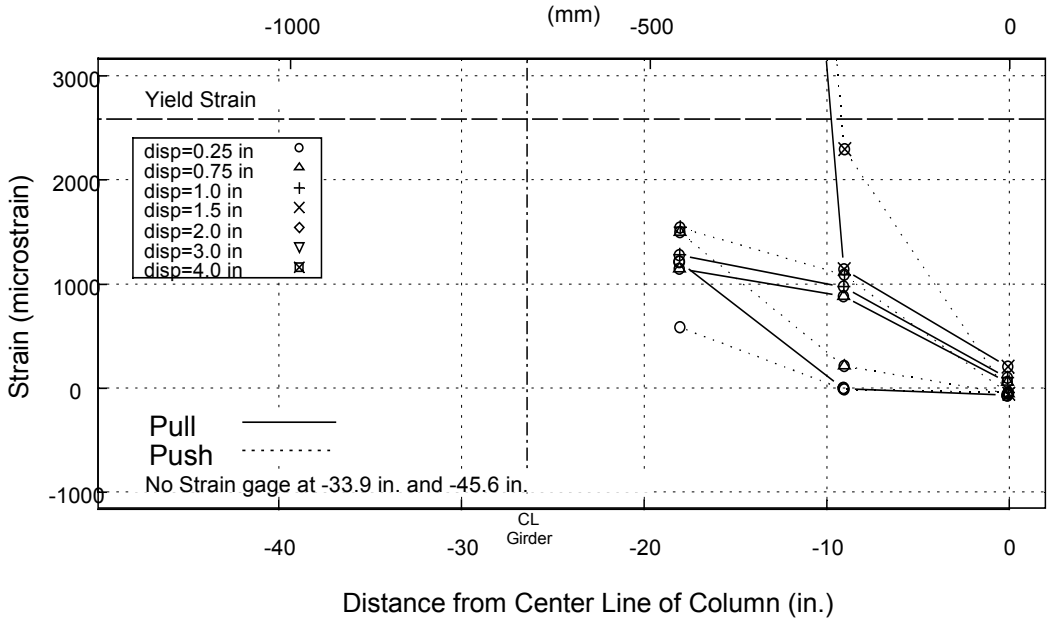

(c) Gage F

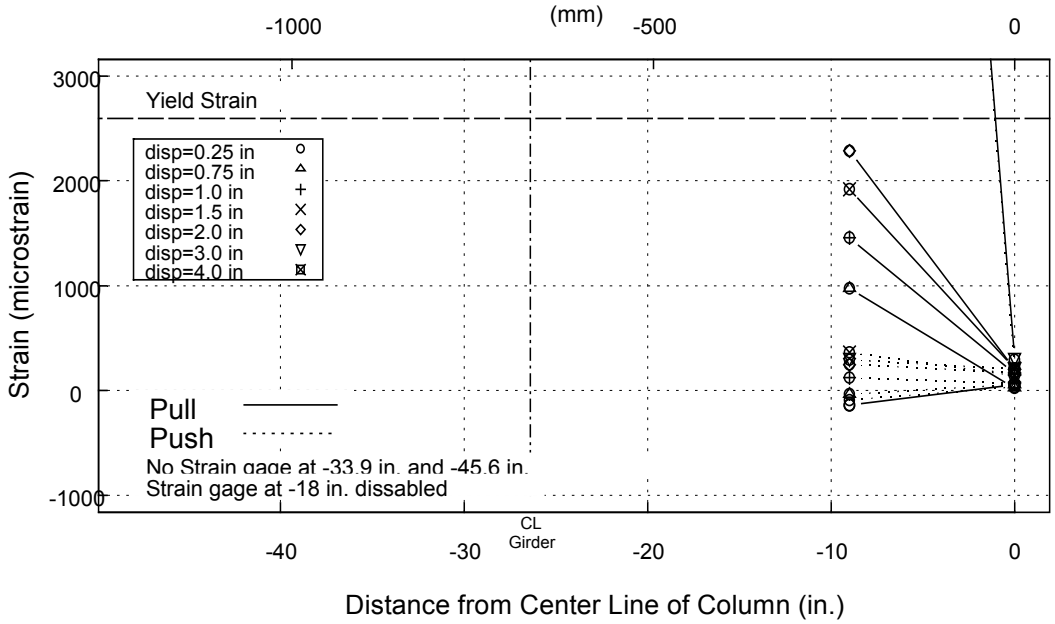

(d) Gage H

Figure 4-16 Specimen CR-NS: Measured Strain in Bent Cap Stirrups (cont.)

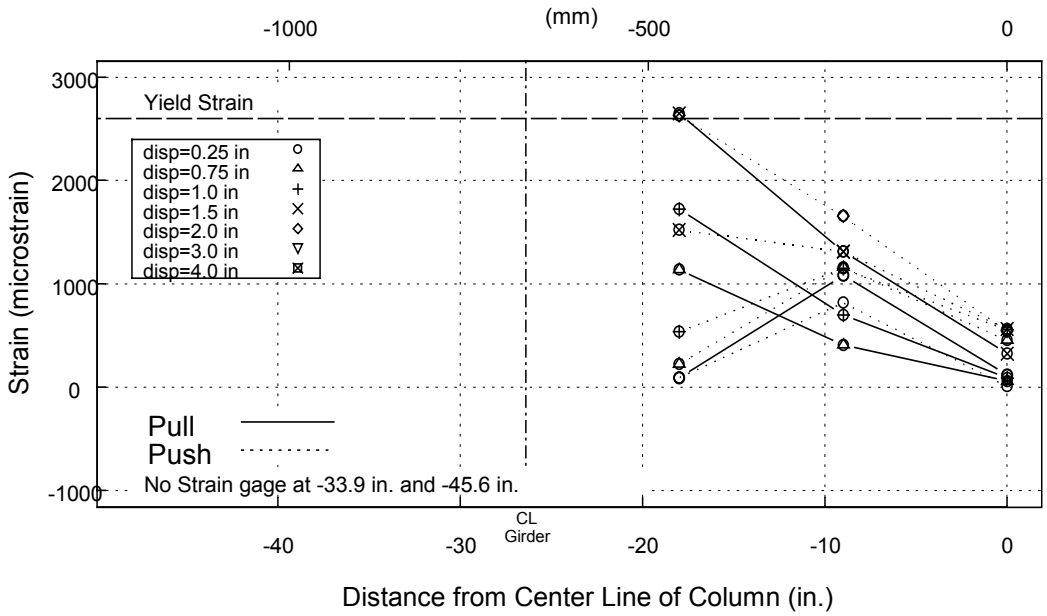

(e) Gage K

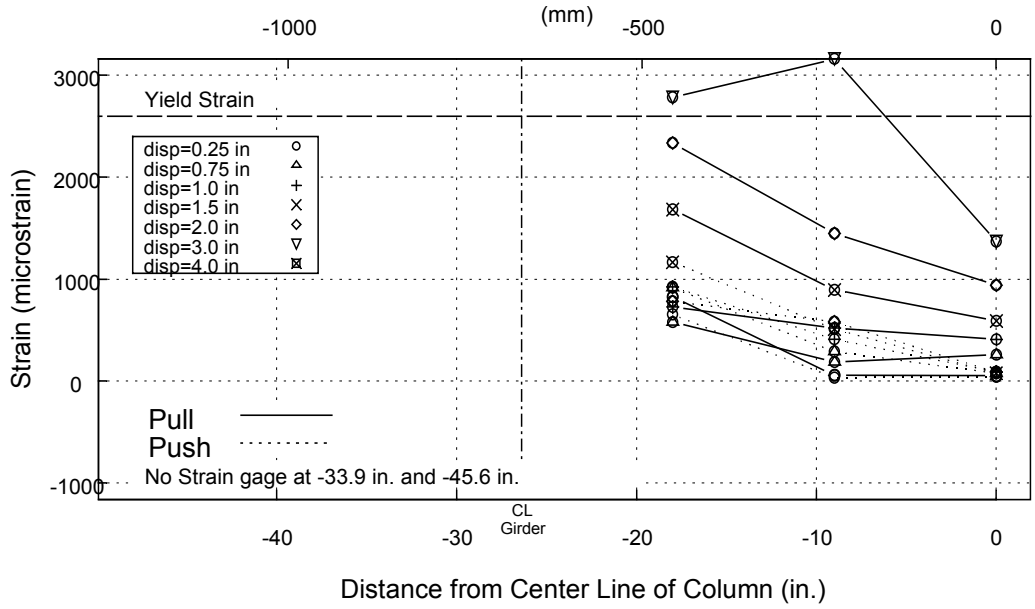

(f) Gage M

Figure 4-16 Specimen CR-NS: Measured Strain in Bent Cap Stirrups (cont.)

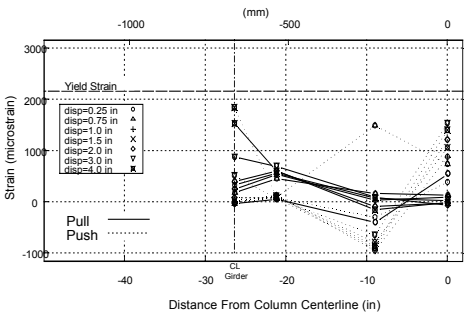

(a) Location A

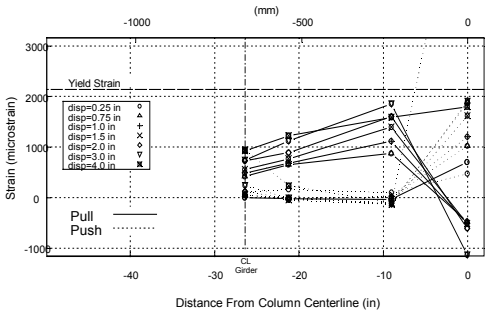

(b) Location B

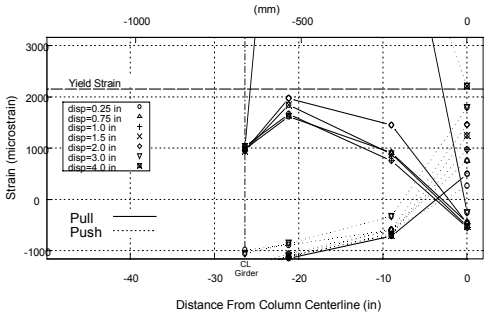

(c) Location C

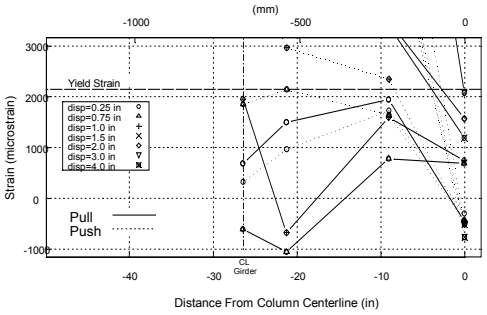

(d) Location D

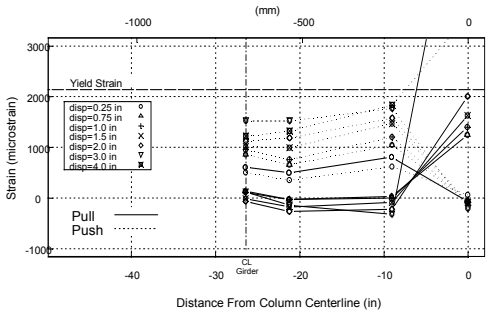

(e) Location E

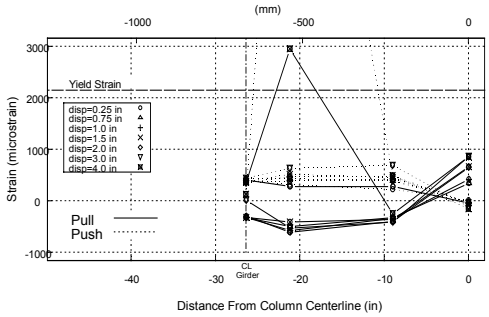

(f) Location F

Figure 4-17 Specimen CR-NS: Measured Strain in Longitudinal Deck Reinforcement

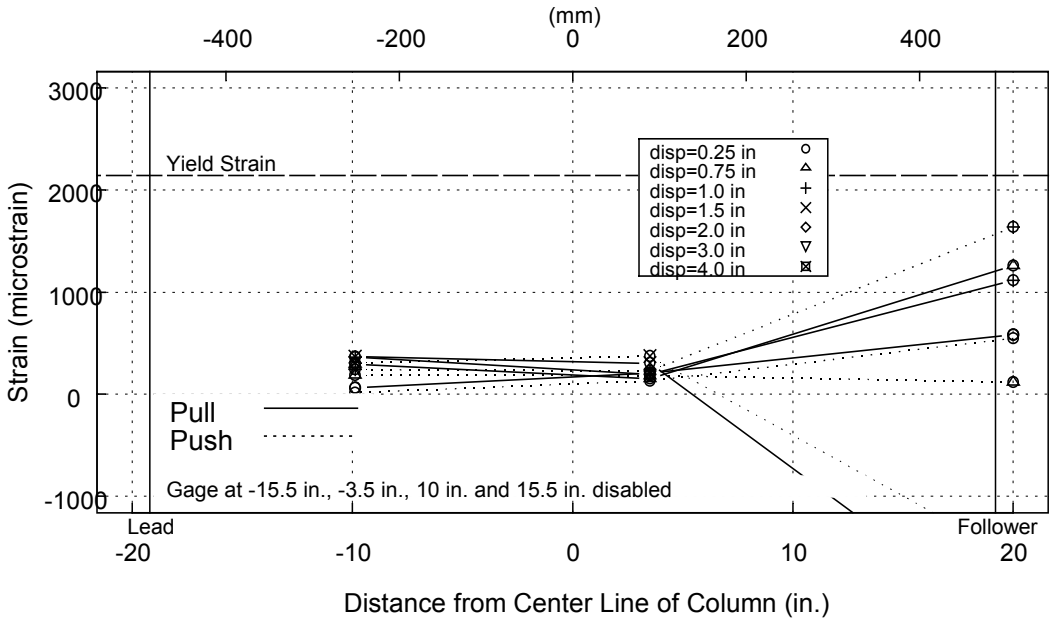

(a) Top Flange

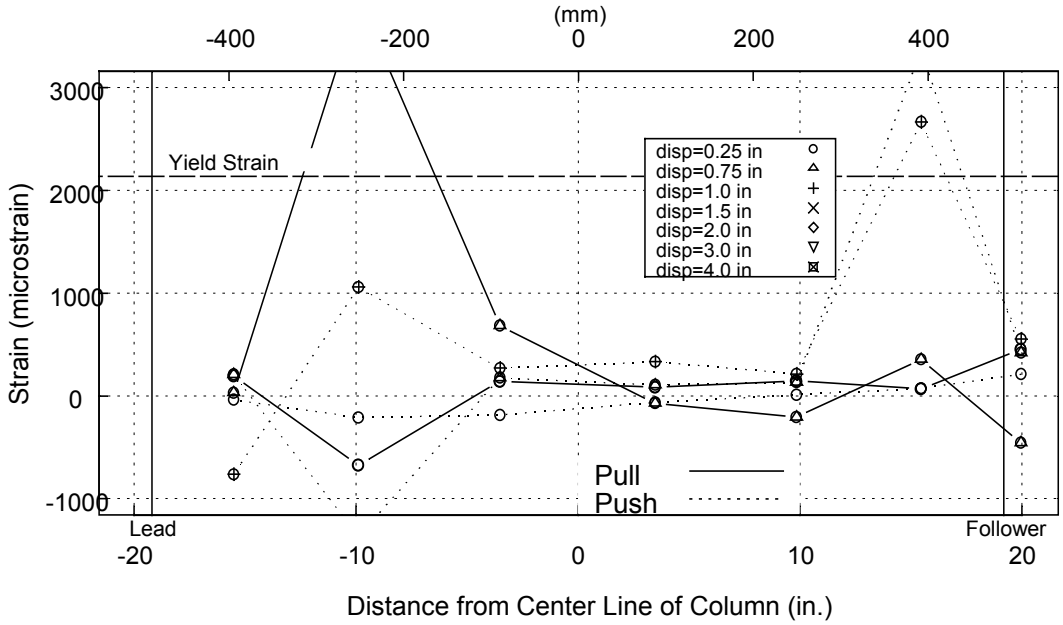

(b) Bottom Flange

Figure 4-18 Specimen CR-NS: Measured Strain in Girder Flanges

4.4 SPECIMEN 2–CONVENTIONALLY REINFORCED, STIFFENERS (CR-S)

4.4.1 Observed Performance, CR-S

The first torsional crack in the bent cap, originating at the top flange of the girder, occurred at 290 k-ft [393 kN-m], 0.0008 radians (Figure 4-19). This crack propagated at an angle of approximately fifty-five degrees, ending approximately one foot [305 mm] above the bottom of the bent cap.

Three displacement cycles after cracking, at a torsional moment of 900 k-ft [1,219 kN-m] and rotation 0.005 radians, numerous cracks developed on the bent cap face and extended the full height of the bent (Figure 4-20). Cracks also developed on the bottom of the bent cap as well as the top and underside of the deck (Figure 4-21). No spalling was observed.

At the bent cap maximum torsional moment of 1,403 k-ft [1,901 kN-m], 0.021 radians, new crack development was limited to short cracks (less than six inches [152 mm]) that developed and propagated toward each other to develop longer cracks (Figure 4-22). Spalling occurred and was concentrated at two crack locations: one vertical crack at the girder/cap interface and one diagonal crack at the location of the first crack. A major crack developed from the bottom flange and spiraled down and around the underside of the cap. A portion of bent cap concrete under the girder had separated from the girder approximately ½" [13 mm] (Figure 4-23). The underside of the bent cap had numerous torsion spiral cracks with minor damage concentrated near the column (Figure 4-24). Cracks propagated from the underside of the bent cap to the top of the column. Deck damage consisted of multiple cracking and incipient spalling. A concentration of cracks began to develop aligned with the girder, designated by the arrow shown in Figure 4-25.

The failure mechanism was a vertical torsion shear friction sliding plane in the bent cap concrete at the edge of the girder flanges (Figure 4-26). The maximum torsional rotation of 0.03 radians occurred at a torsional moment of 866 k-ft [1,173 kN-m]. All concrete on the bent cap face bound between the first diagonal crack and the girder had spalled off, exposing stirrup reinforcement as well as the sliding plane. The underside of the bent cap had significant cracking. A crack occurred on each side of the column that

extended from the column/block interface at an angle to the bent cap/girder interface. All spalling on the bent cap underside was bound between this crack and the support block (Figure 4-27). A sliding plane had developed through the top of the deck, where a well-defined failure surface parallel to the girder was exposed by major deck spalling (Figure 4-28).

Figure 4-19 Specimen CR-S: First Torsional Crack on Bent Cap Lead Face

Figure 4-20 Specimen CR-S: Bent Cap Lead Face at 0.005 radians

Figure 4-21 Specimen CR-S: Bent Cap Underside at 0.005 radians

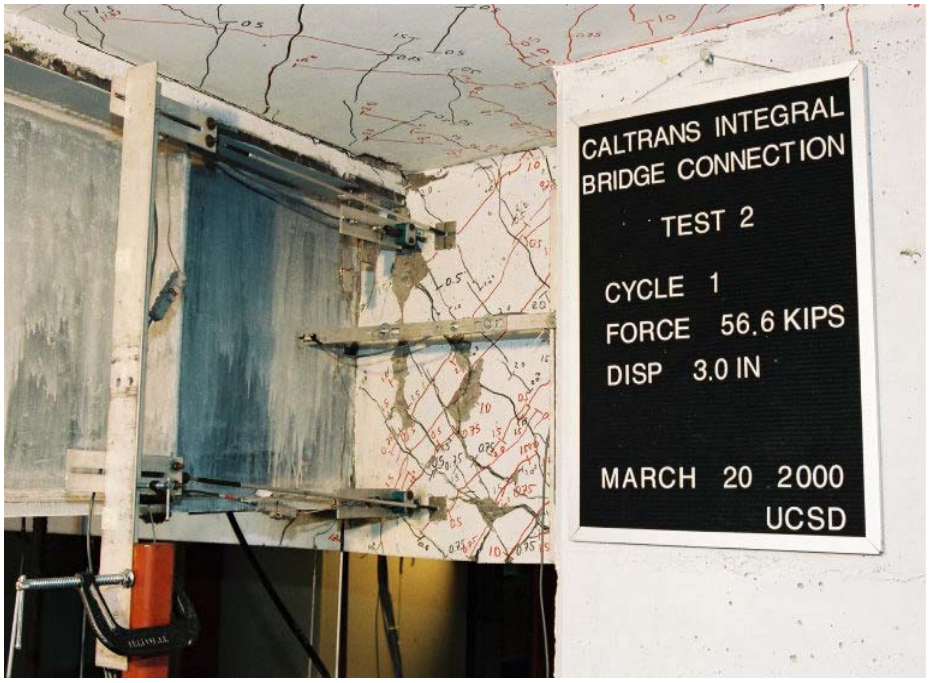

Figure 4-22 Specimen CR-S: Bent Cap Lead Face at 0.02 radians

Figure 4-23 Specimen CR-S: Bent Cap/Girder Interface at 0.02 radians

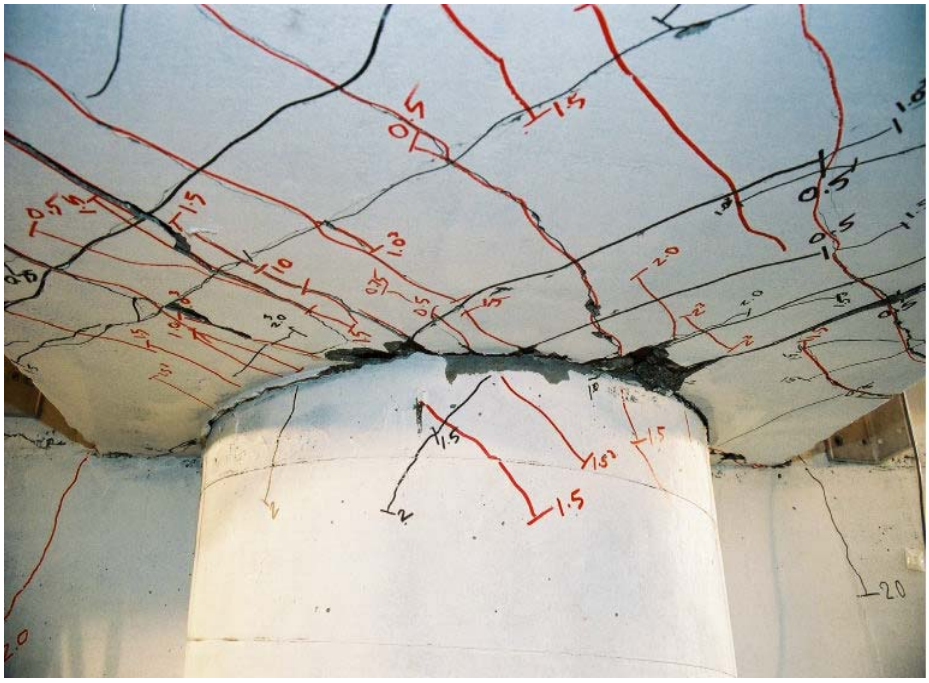

Figure 4-24 Specimen CR-S: Bent Cap Underside at 0.02 radians

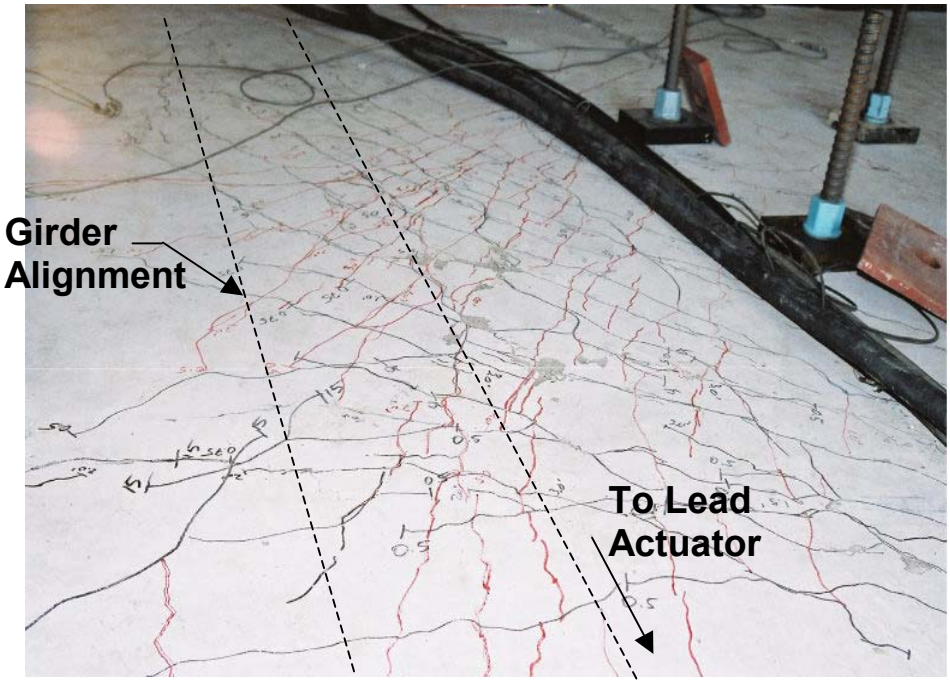

Figure 4-25 Specimen CR-S: Deck at 0.02 radians

Figure 4-26 Specimen CR-S: Bent Cap Lead Face at Ultimate Rotation, θ=0.03 radians

Figure 4-27 Specimen CR-S: Bent Cap Underside at Ultimate Rotation

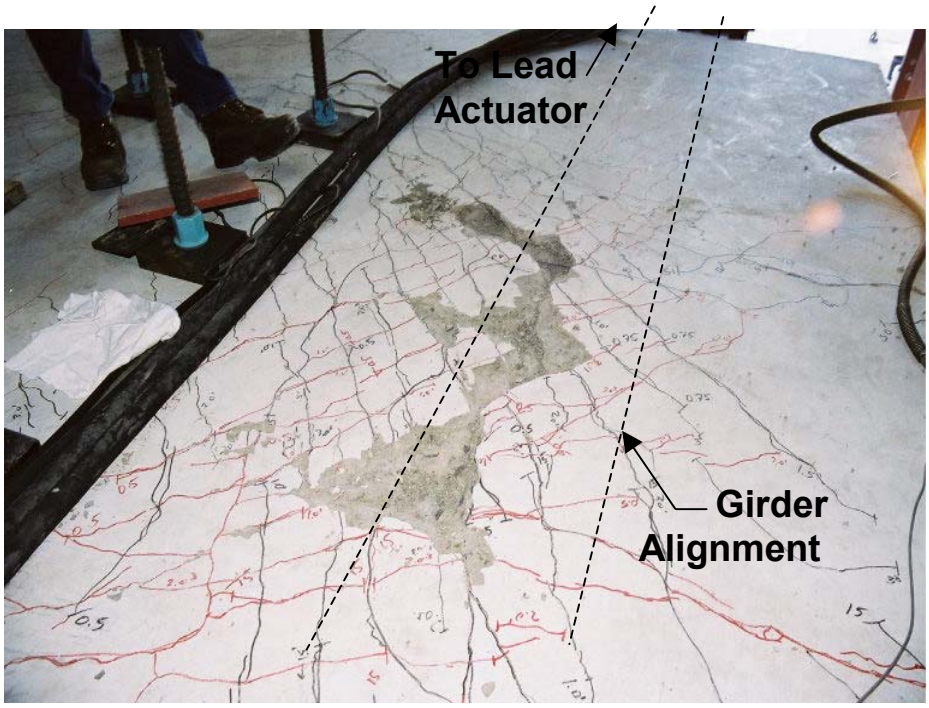

Figure 4-28 Specimen CR-S: Deck at Ultimate Rotation

4.4.2 Measured Response, CR-S

The torsional moment versus torsional rotation curve for Specimen CR-S is shown in Figure 4-29. The maximum torsional bent cap moment of 1,403 k-ft [1,901 kN-m] was twice the bent cap design torsional moment of 700 k-ft [948 kN-m]. The bent cap exhibited minimal cracking and performed nearly elastically to 700 k-ft [948 kN-m], the column overstrength moment. On both bent cap faces, total crack dilation of the bent cap was less than 0.05 in. [1.3 mm] at bent cap design moment (Figure 4-30).

Figure 4-31 shows bent cap flexural reinforcement and stirrup strain gage locations relative to the location of the lead actuator. Because the maximum strain gage readings were recorded at the corners of the bent cap, only data from strain gages located near the bent cap corners are presented. The maximum strain readings were typically obtained at locations in the joint region near the girder.

Flexural reinforcement Bars D and F, located in the bottom corners of the bent cap, yielded at the bent cap maximum torsional moment (Figure 4-32). Flexural reinforcement Bar B located in the top corner of the bent cap performed elastically throughout the loading. However, Bar H, also located in the top corner of the bent cap, yielded at the location near the girder during the maximum moment cycle.

The first occurrence of stirrup yielding was in a vertical leg at the bottom corner of the bent cap (Gage E, Figure 4-33). Strain readings showed that all other reported stirrup gage locations yielded at a torsional moment of 1,342 k-ft [1,818 kN-m], immediately before reaching the maximum torsional bent cap moment. Strains in the longitudinal deck reinforcement are plotted in Figure 4-34. Locations C and D, at the bent cap face exhibited the highest strain readings.

Strains in the top and bottom flanges of the girders are plotted in Figure 4-35. In the region near the lead actuator, both flanges are in compression during the push portion of the load cycle. During the pull portion of the same load cycle, the same region of the flanges experiences tensile strains. No location on the flanges reached yield during the loading process.

Strain readings from gages located at the top and bottom of the stiffeners are presented in Figure 4-36. During the push cycle, the top portion of the stiffeners on the

lead side is in tension and is in compression on the follower side. The bottom portion of the stiffeners on the lead side during the push cycle is in compression and tension on the follower side.

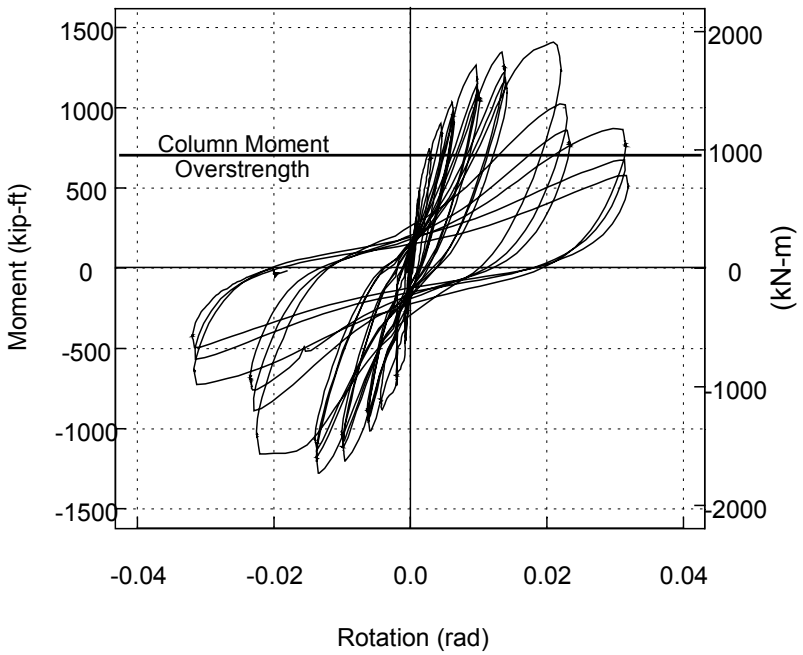

Figure 4-29 Specimen CR-S: Torsional Moment Rotation Response

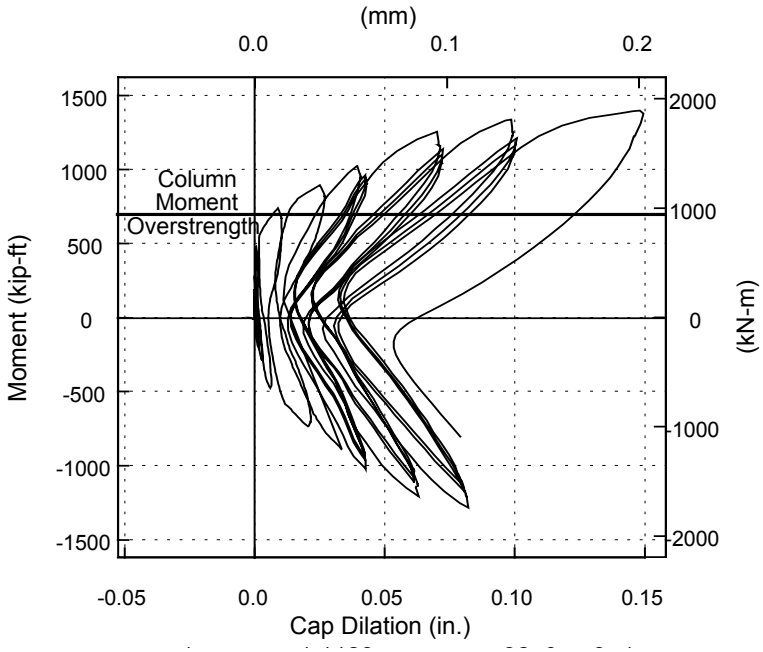

(a) Lead Face

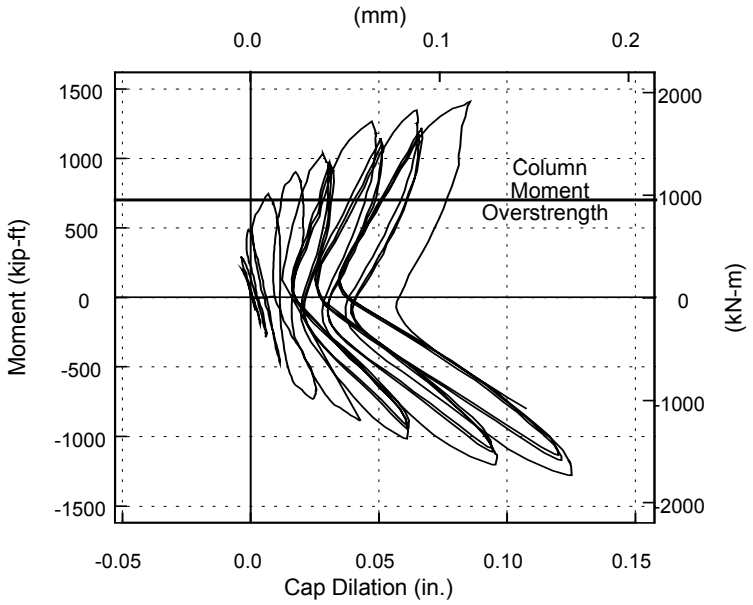

(b) Follower Face

Figure 4-30 Specimen CR-S: Measured Bent Cap Dilation

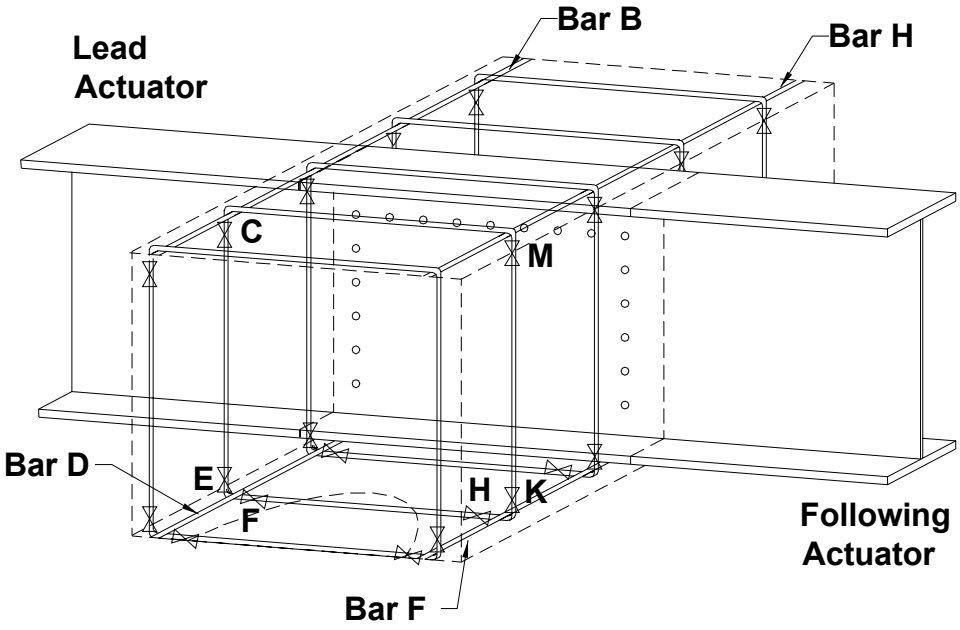

Figure 4-31 Specimen CR-S: Gage Location with Respect to Actuators

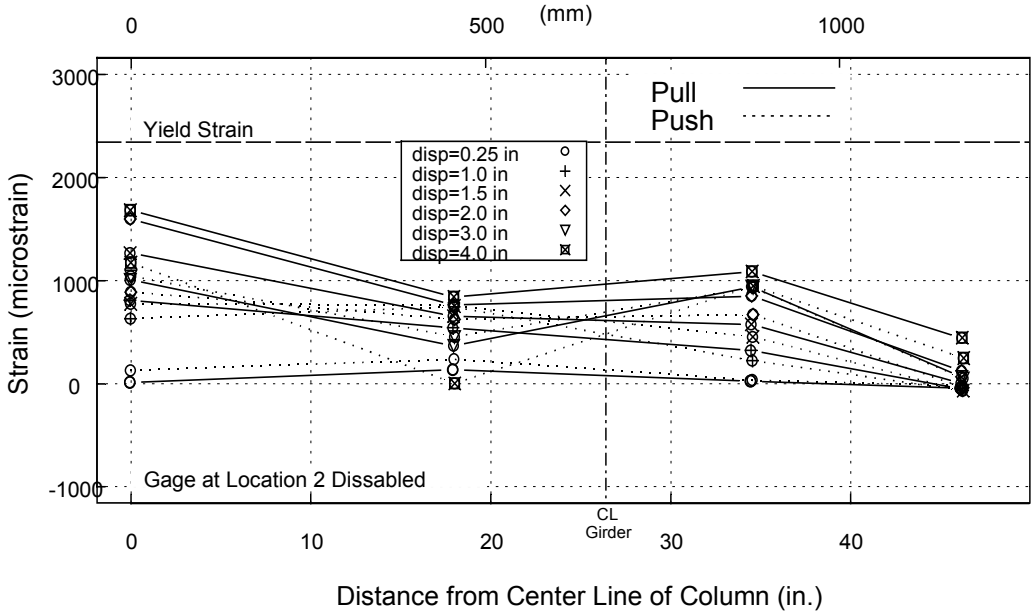

(a) Bar B

Figure 4-32 Specimen CR-S: Measured Strain in Flexural Reinforcement

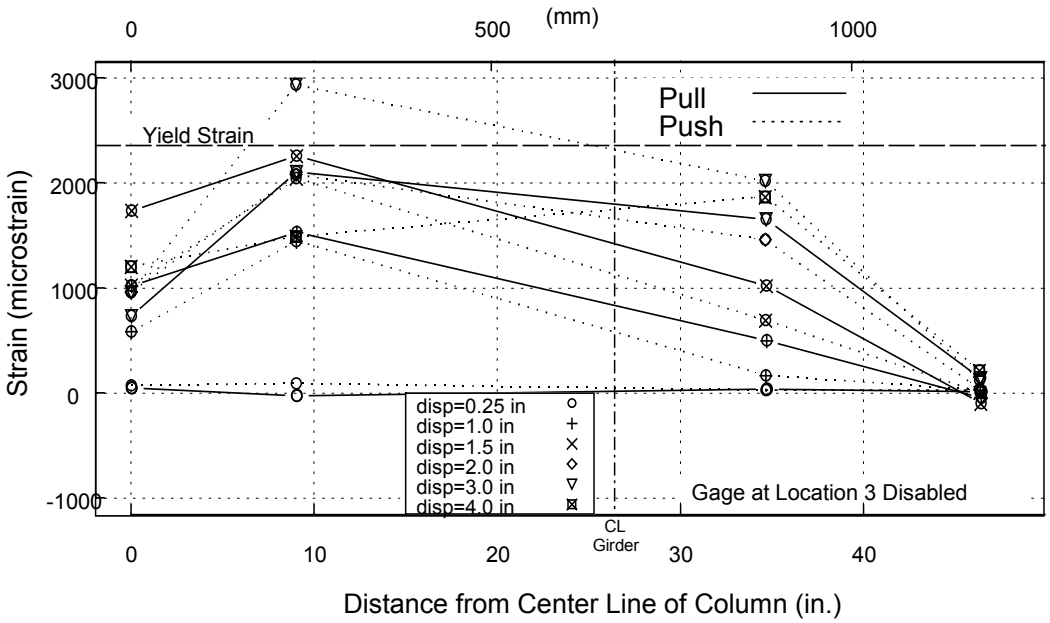

(b) Bar D

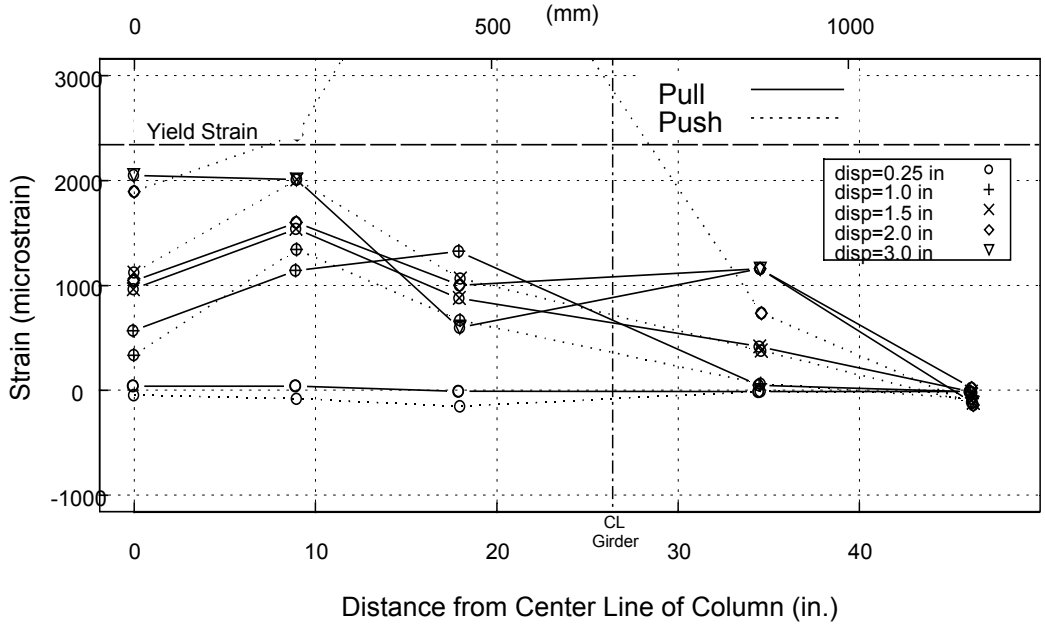

(c) Bar F

Figure 4-32 Specimen CR-S: Measured Strain in Flexural Reinforcement (cont.)

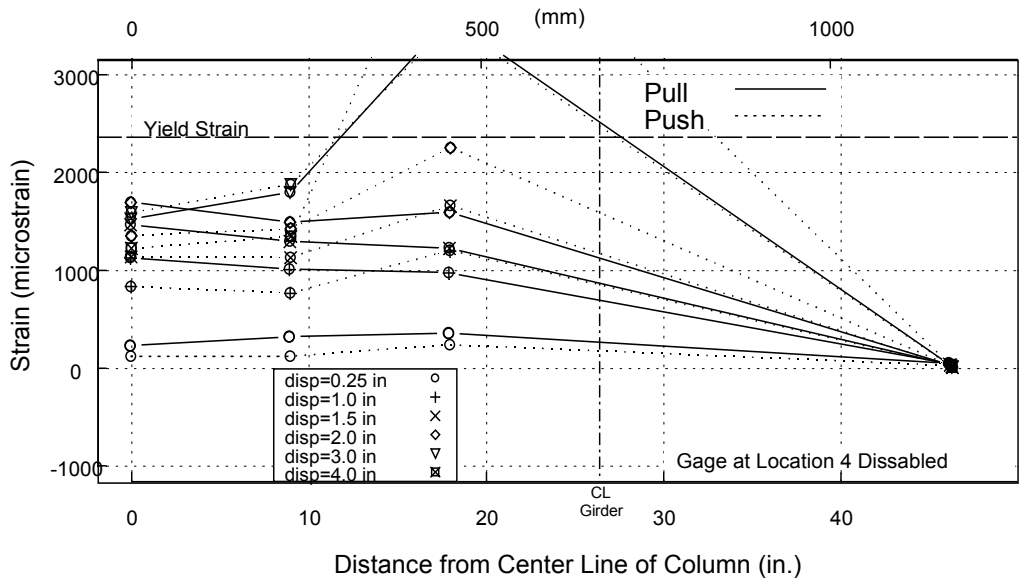

(d) Bar H

Figure 4-32 Specimen CR-S: Measured Strain in Flexural Reinforcement (cont.)

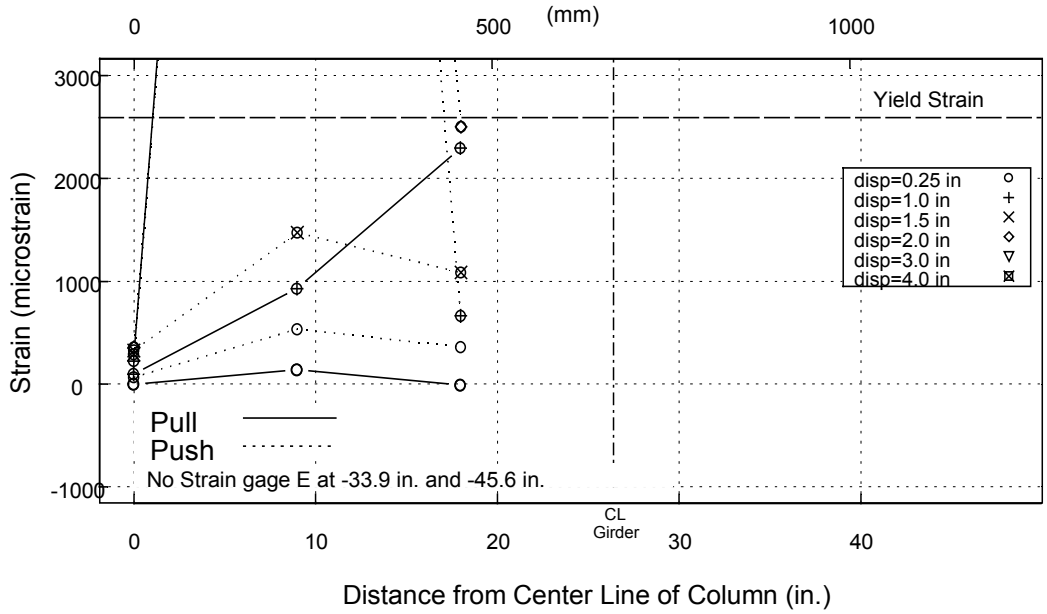

(a) Gage E

Figure 4-33 Specimen CR-S: Measured Strain in Bent Cap Stirrups

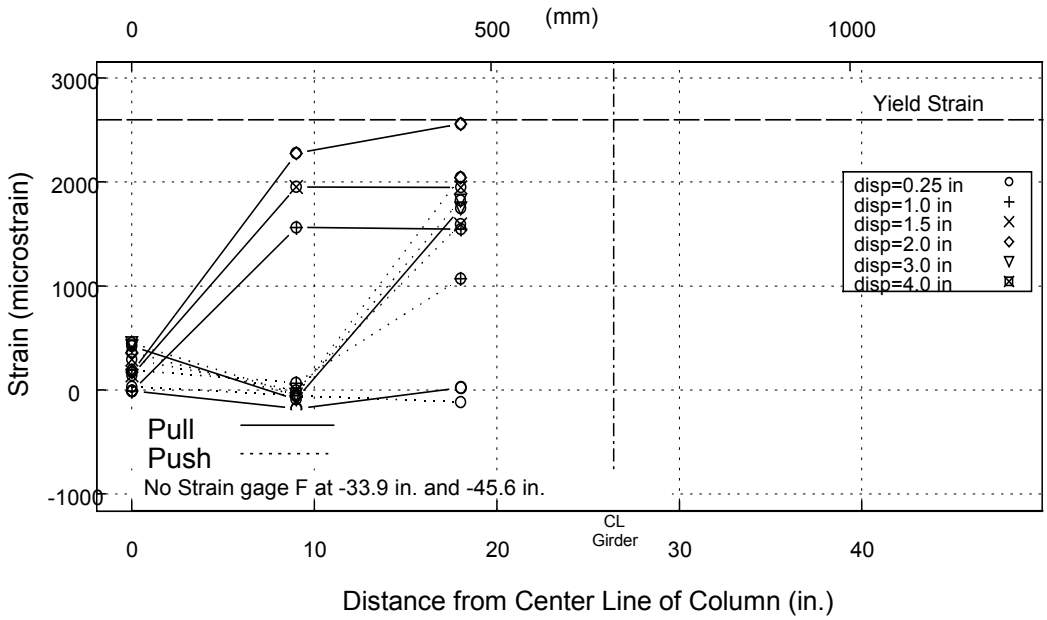

(b) Gage F

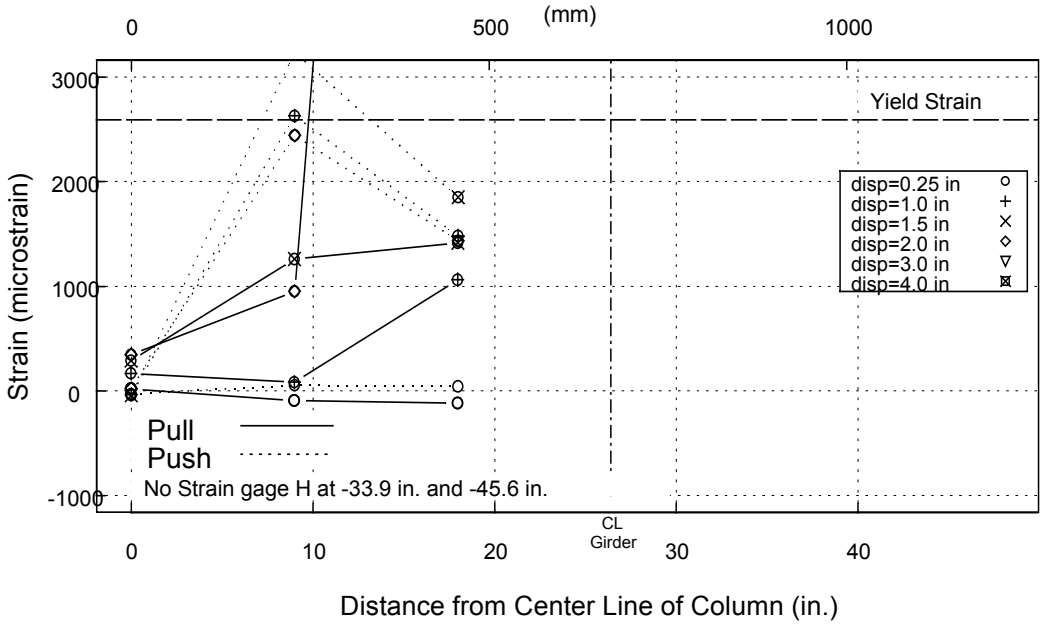

(c) Gage H

Figure 4-33 Specimen CR-S: Measured Strain in Bent Cap Stirrups (cont.)

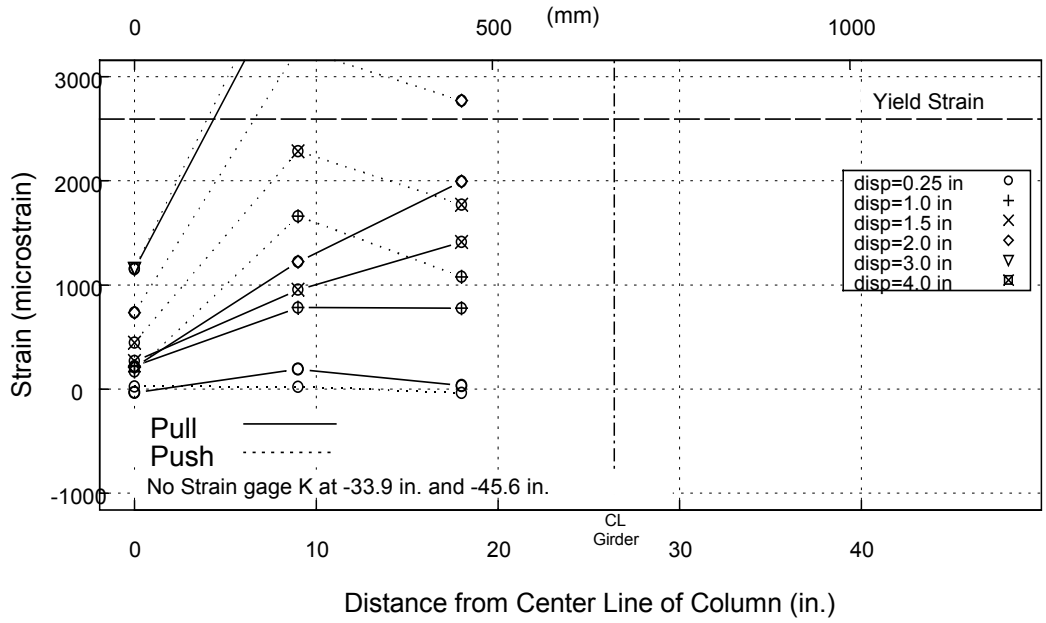

(d) Gage K

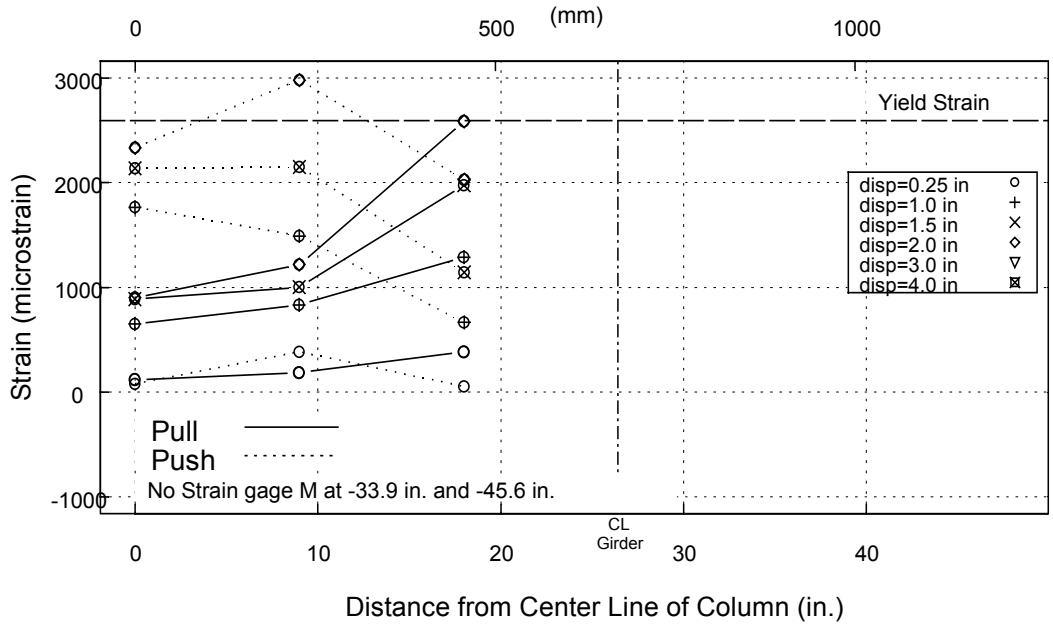

(e) Gage M

Figure 4-33 Specimen CR-S: Measured Strain in Bent Cap Stirrups (cont.)

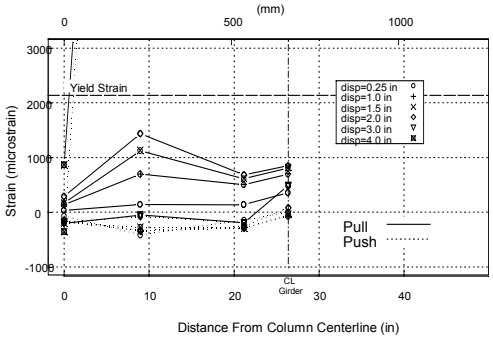

(a) Location A

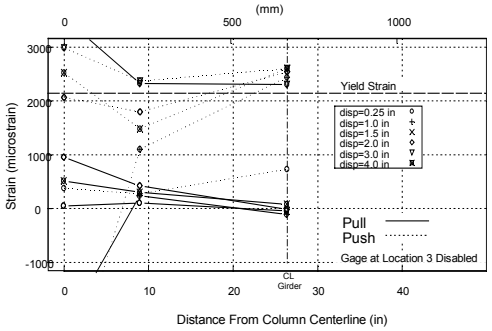

(d) Location D

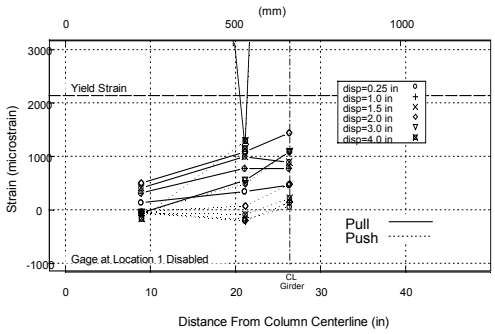

(b) Location B

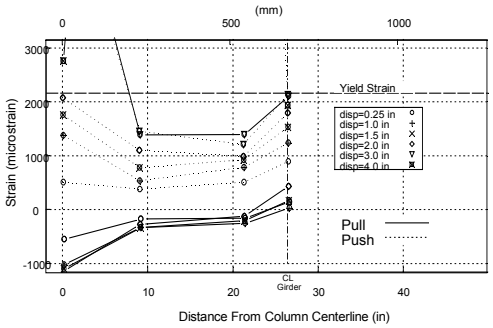

(e) Location E

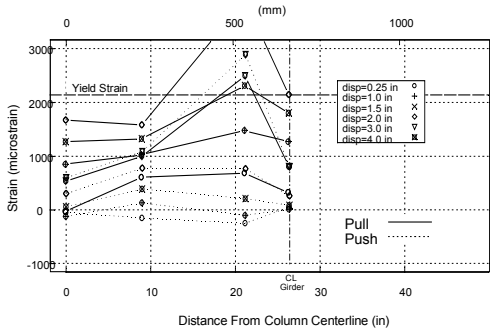

(c) Location C

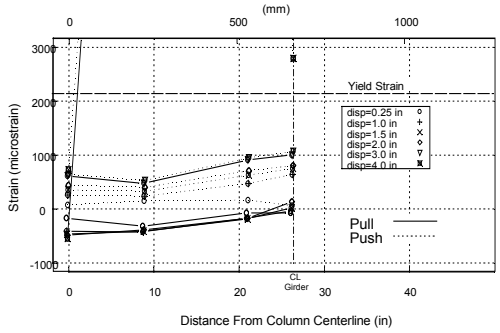

(f) Location F

Figure 4-34 Specimen CR-S: Measured Strain in Longitudinal Deck Reinforcement

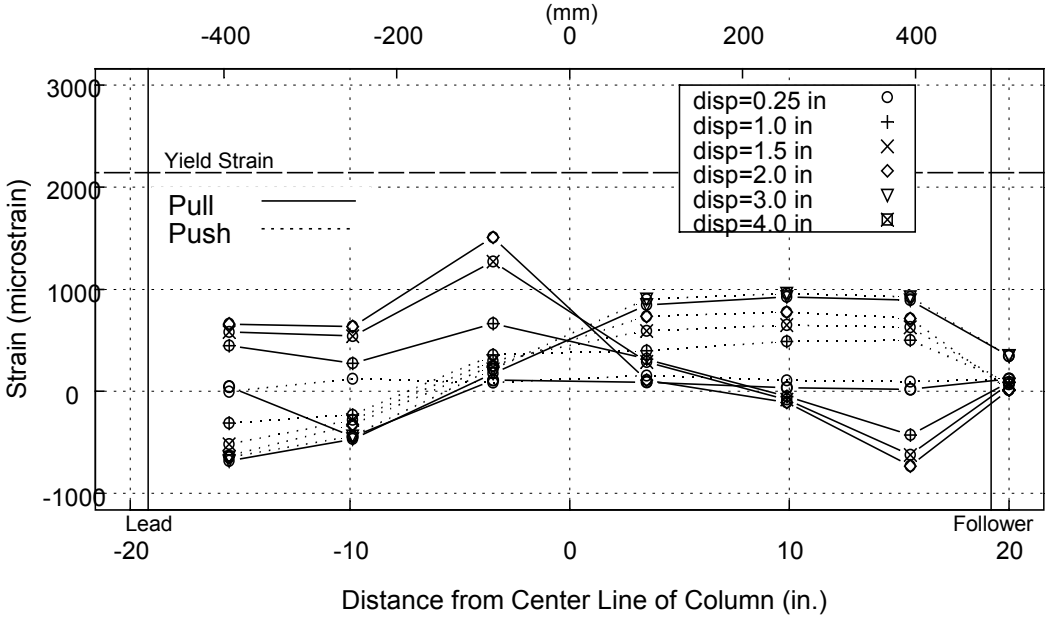

(a) Top Flange

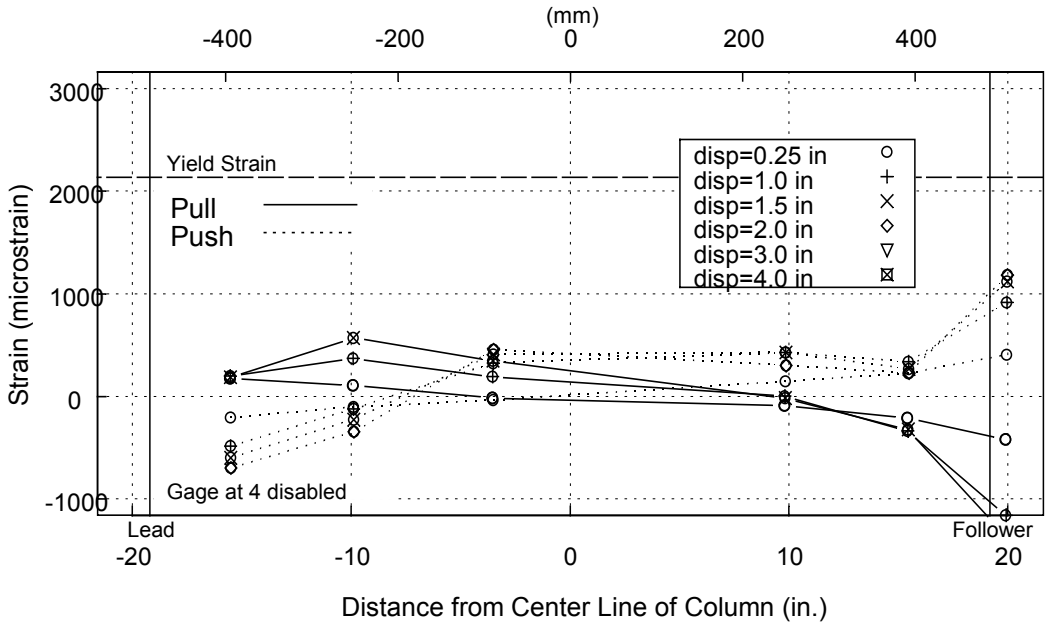

(b) Bottom Flange

Figure 4-35 Specimen CR-S: Measured Strain in Girder Flanges

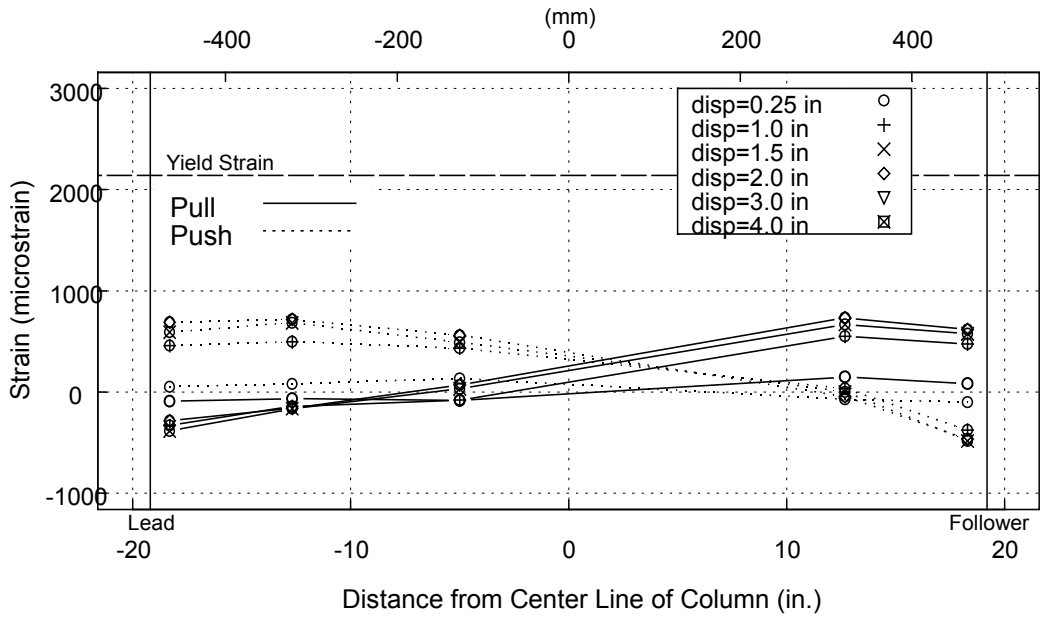

(a) Top Region

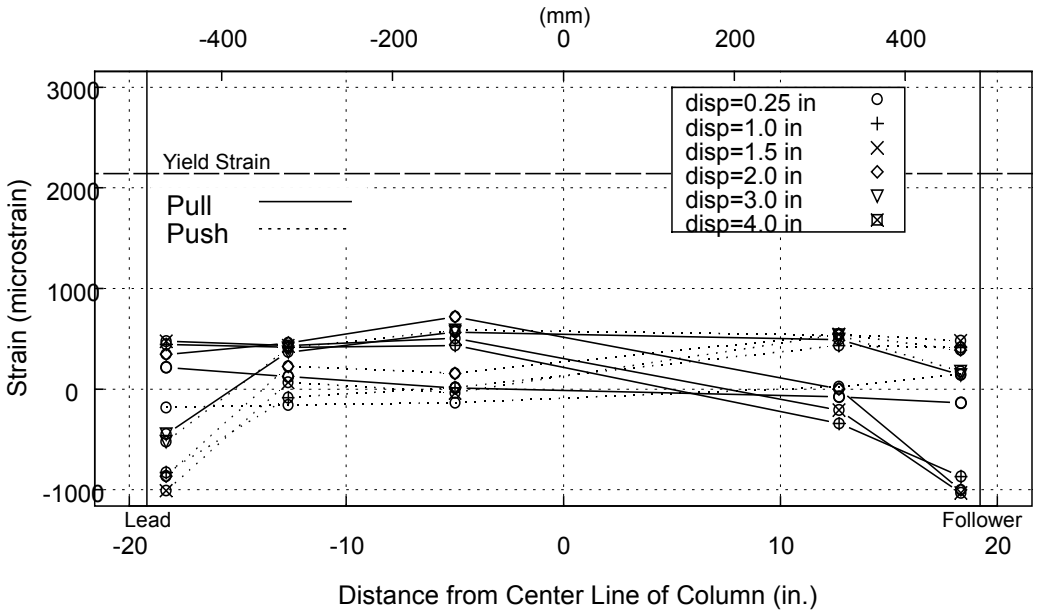

(b) Bottom Region

Figure 4-36 Specimen CR-S: Measured Strain in Girder Stiffeners

4.5 SPECIMEN 3–POST-TENSIONED, NO STIFFENERS (PT-NS)

During data reduction for Specimen PT-NS, it was discovered that strain gages were not placed on the bent cap post-tensioned bars. In an attempt to measure the actual post-tensioning force, surface gages were applied to the bent cap after load cycling and used to record strains in the bent cap while the post-tension bars were destressed. However, due to the short length of the bent cap and the extent of bent cap damage, strain readings were not precise. A statistical estimate of the actual post-tension force was obtained by repeatedly applying and averaging the measured post-tension force. However, the coarse thread of the post-tension bars used and the large diameter to length ratio resulted in large variations in seating losses. The standard deviation in the measured force was +/- 17 kip [76 kN] at a mean of 42 kips [187 kN]. The results for Specimen 3 are presented here, with the disclaimer that the post-tensioning force is not from an exact measurement.

4.5.1 Observed Performance, PT-NS

The first torsional crack initiated at the top flange of the girder and propagated toward the joint between the bottom of the bent cap and the top of the column at an angle of approximately forty-five degrees from horizontal. The torsional cracking moment of 563 k-ft [763 kN-m] corresponded to a rotation of 0.0009 radians and the crack length was approximately one foot [305 mm] (Figure 4-37).

At the maximum torsional moment of 998 k-ft [1,352 kN-m] and rotation of 0.005 radians, the initial crack extended to the support block. Only two major cracks developed on the bent cap face for each loading direction (Figure 4-38). The underside of the bent cap had numerous cracks concentrated in the region between the girder and the support block (Figure 4-39). No spalling occurred in this region.

The maximum torsional rotation of 0.03 radians occurred at a torsional moment of 694 k-ft [940 kN-m] (Figure 4-40). The bent cap concrete in the region bound by the first crack and the bottom of the bent cap was spalled completely, exposing the stirrup reinforcement. Damage on the underside of the bent cap consisted of spalling near the support block, exposing the bottom longitudinal reinforcement in the bent cap (Figure

4-41). The portion of the bent cap under the girder spalled within the joint region but remained undamaged outside the joint region (Figure 4-42).

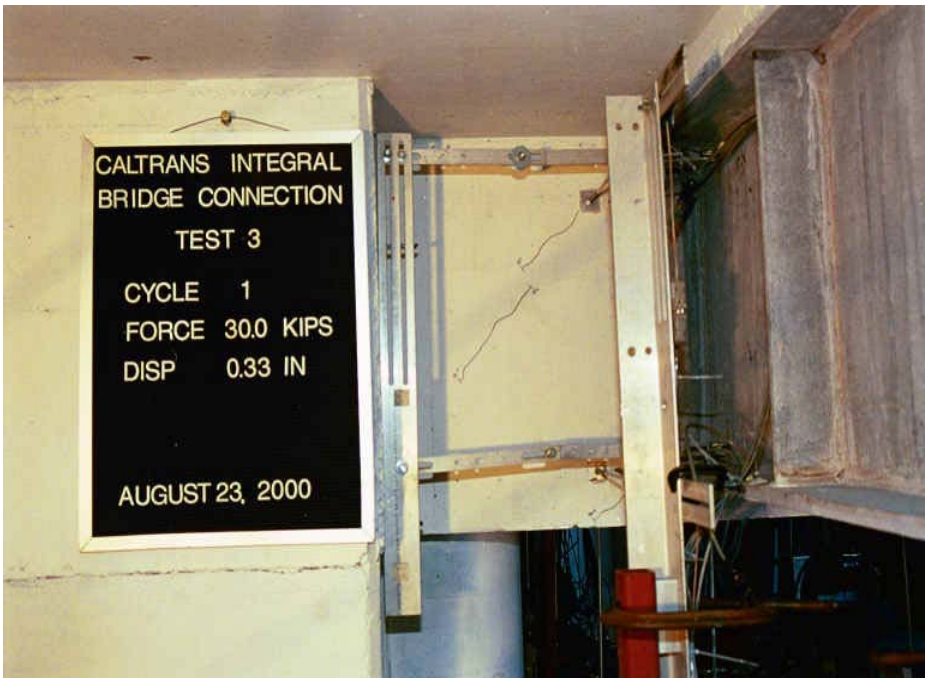

Figure 4-37 Specimen PT-NS: First Torsional Crack on Bent Cap Lead Face

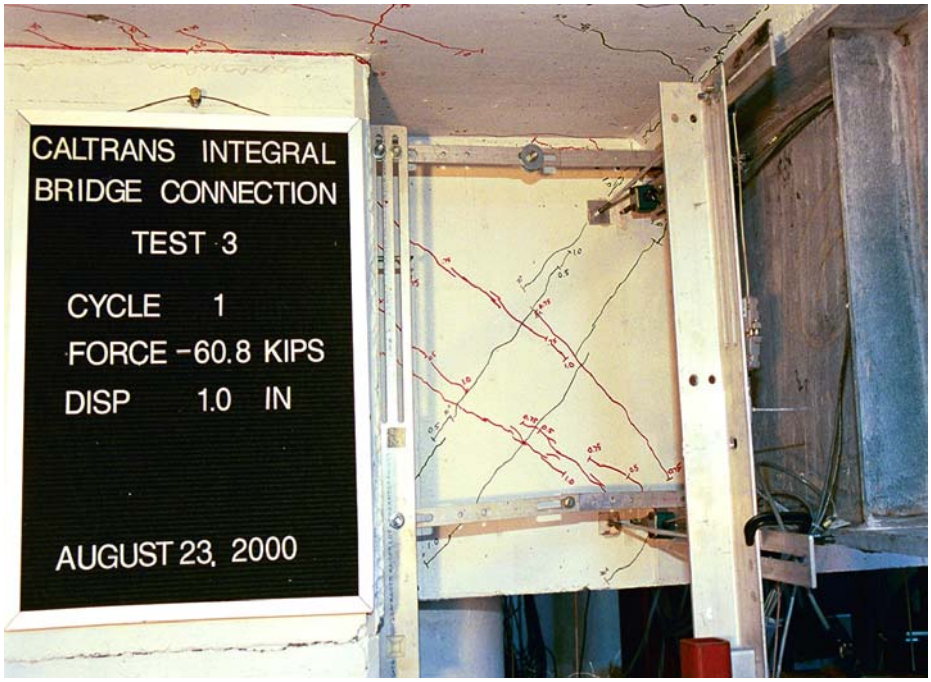

Figure 4-38 Specimen PT-NS: Bent Cap Lead Face at Maximum Torsional Moment

Figure 4-39 Specimen PT-NS: Bent Cap Underside at Maximum Torsional Moment

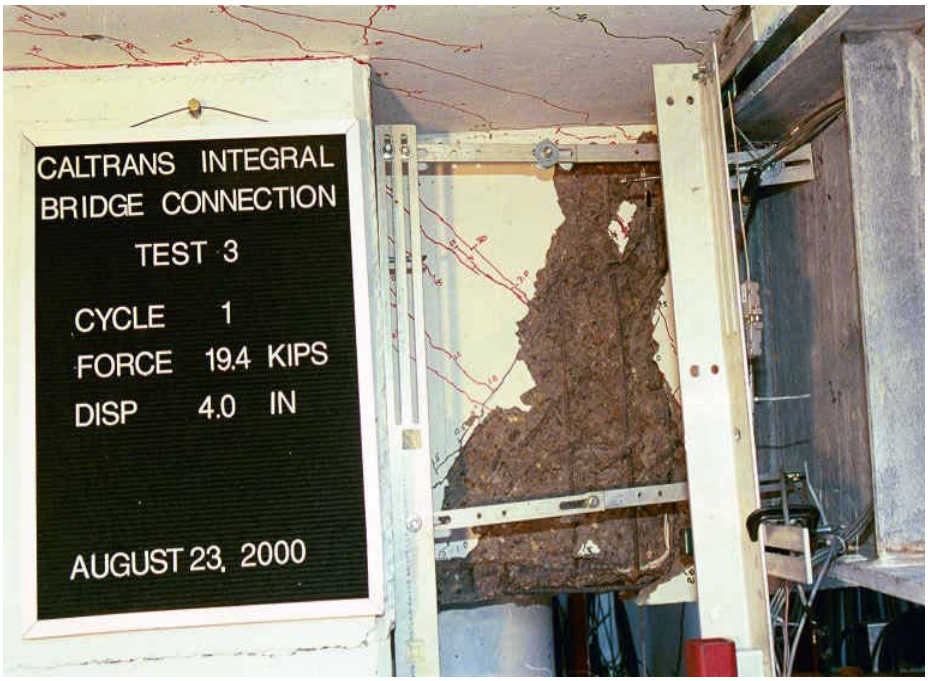

Figure 4-40 Specimen PT-NS: Bent Cap Lead Face at Ultimate Rotation, θ=0.03 radians

Figure 4-41 Specimen PT-NS: Bent Cap Underside at Ultimate Rotation (θ=0.03 radians)

Figure 4-42 Specimen PT-NS: Bent Cap/Girder Interface at Ultimate Rotation (θ=0.03 radians)

4.5.2 Measured Response, PT-NS

The torsional moment versus torsional rotation curve for Specimen PT-NS is shown in Figure 4-43. The maximum torsional moment of 998 k-ft [1,352 kN-m] exceeded the bent cap design moment of 700 k-ft [948 kN-m] by 30 percent. The bent cap exhibited minimal cracking and performed nearly elastically to 700 k-ft [948 kN-m], the column overstrength moment. Dilation of cracks in the bent cap is plotted in Figure 4-44. Crack dilations prior to reaching the bent cap design moment are less than 0.025 inches.

Strain measurements recorded from gages located on flexural reinforcement bars are presented in Figure 4-46. As seen in previous tests, the highest strains were recorded at the flexural reinforcement located at the corners of the bent cap. Figure 4-47 plots strains recorded on the stirrups in the bent cap. As with the flexural reinforcement, the strains are highest at the bent cap corners.

Strains recorded from deck reinforcement running along the longitudinal bridge axis are plotted in Figure 4-48. Maximum strains were recorded by gages located near the bent cap. Figure 4-49 plots strain measurements recorded by gages on the girder flanges. A number of gages were damaged during construction, resulting in the scattered plots shown.

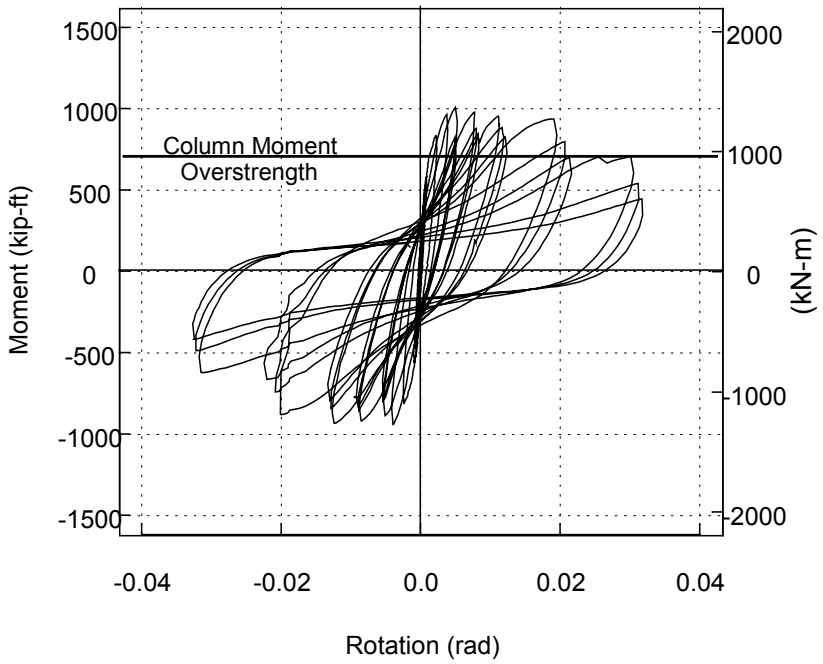

Figure 4-43 Specimen PT-NS: Torsional Moment Rotation Response

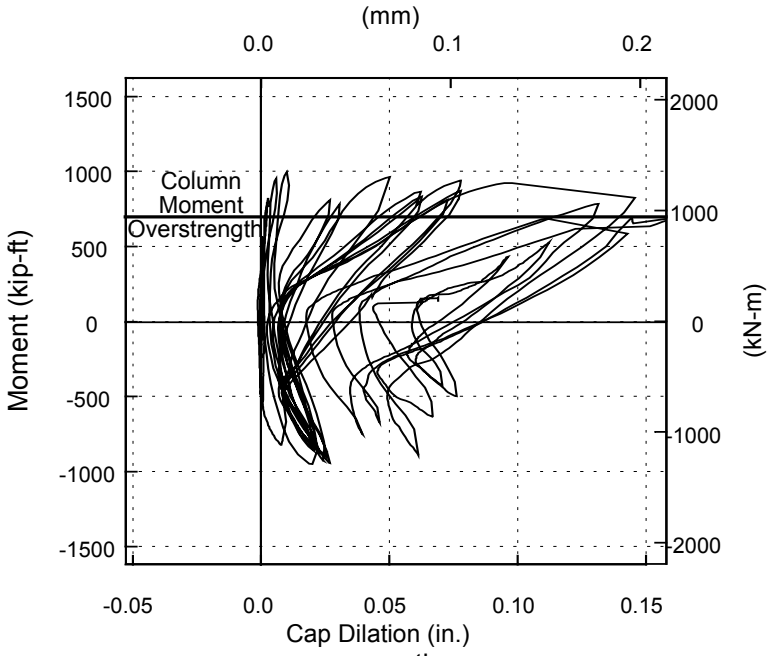

(a) Lead Face

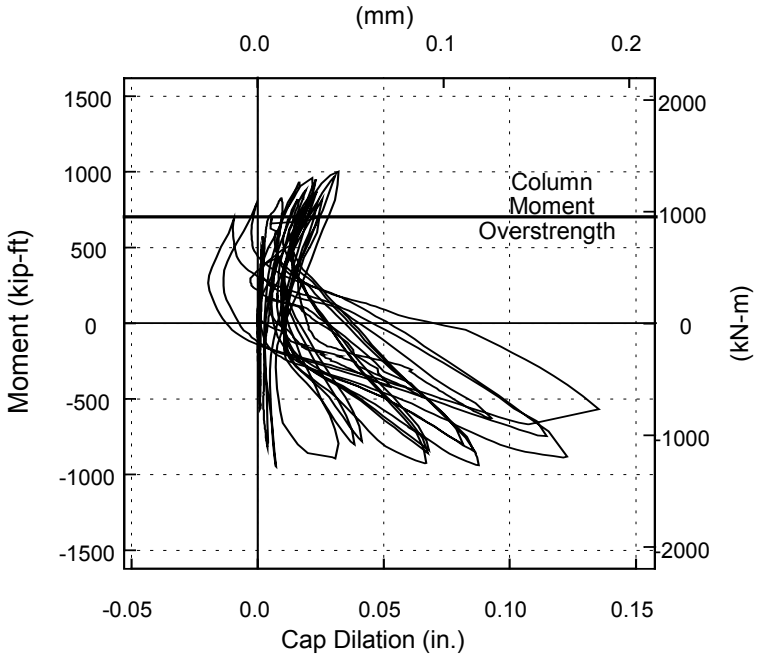

(b) Follower Face

Figure 4-44 Specimen PT-NS: Measured Bent Cap Dilation

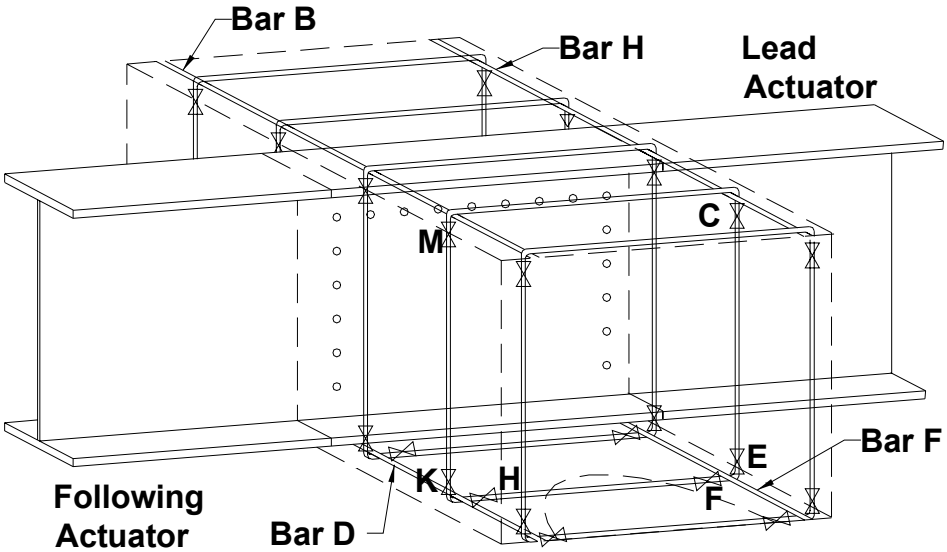

Figure 4-45 Specimen PT-NS: Gage Location with Respect to Actuators

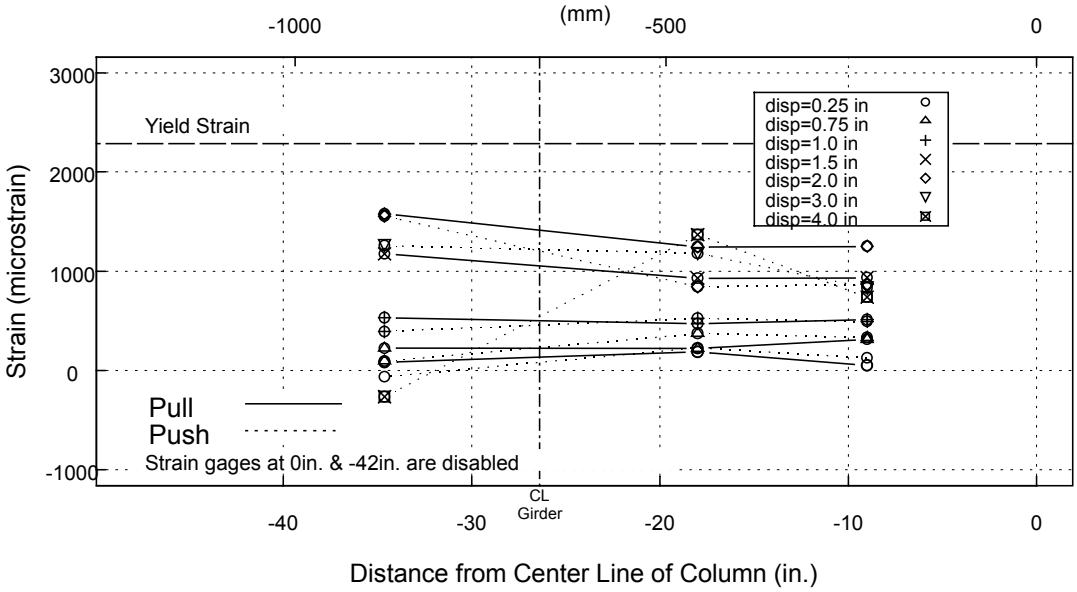

(a) Bar B

Figure 4-46 Specimen PT-NS: Measured Strain in Flexural Reinforcement

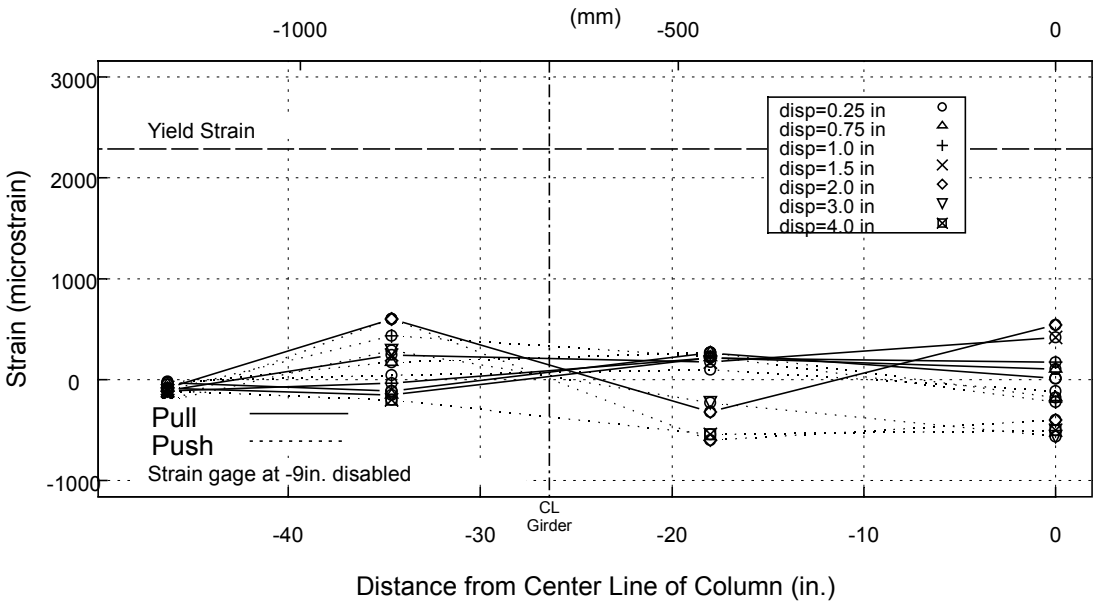

(b) Bar D

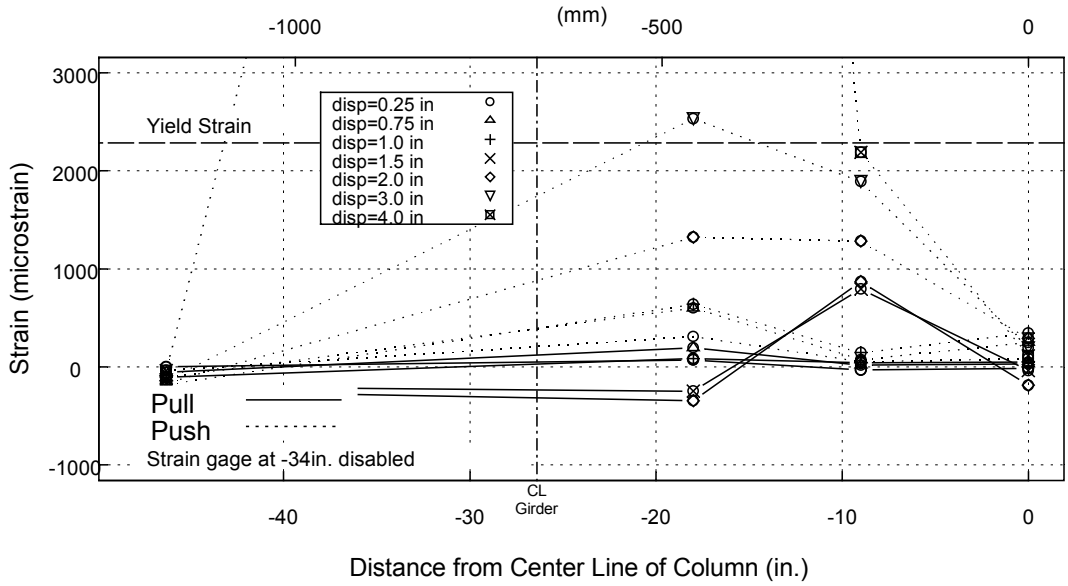

(c) Bar F

Figure 4-46 Specimen PT-NS: Measured Strain in Flexural Reinforcement (cont.)

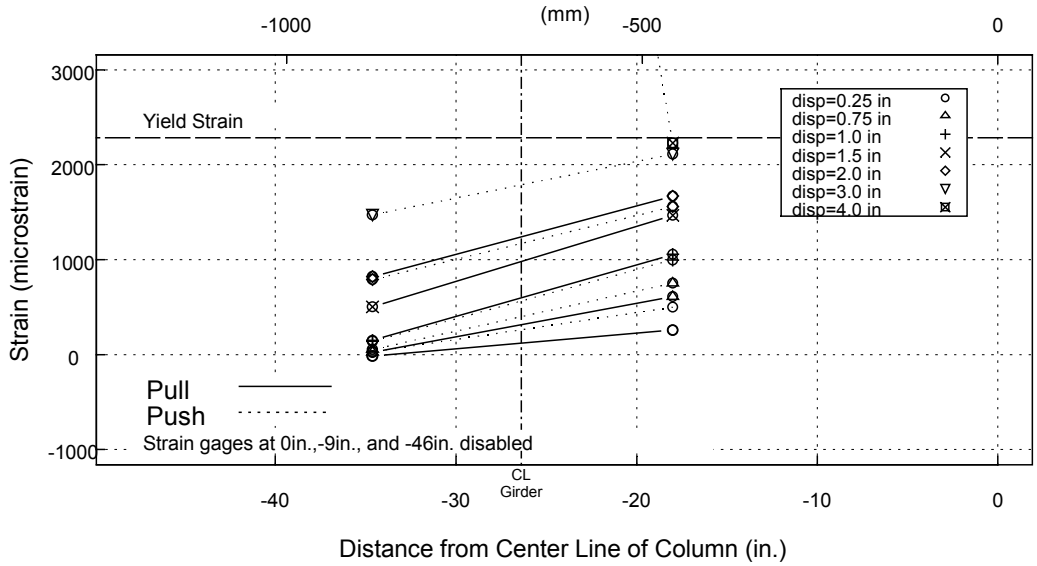

(d) Bar H

Figure 4-46 Specimen PT-NS: Measured Strain in Flexural Reinforcement (cont.)

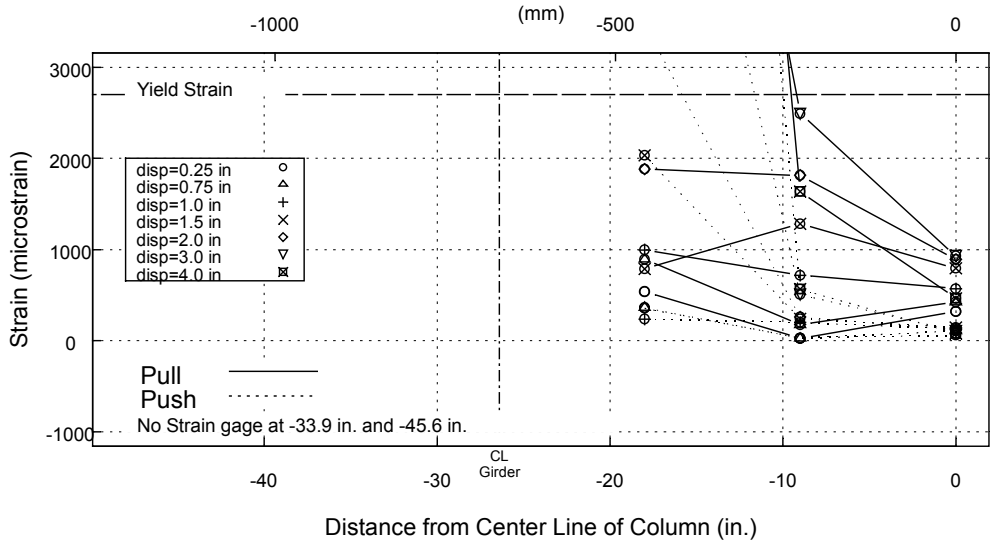

(a) Gage C

Figure 4-47 Specimen PT-NS: Measured Strain in Bent Cap Stirrups

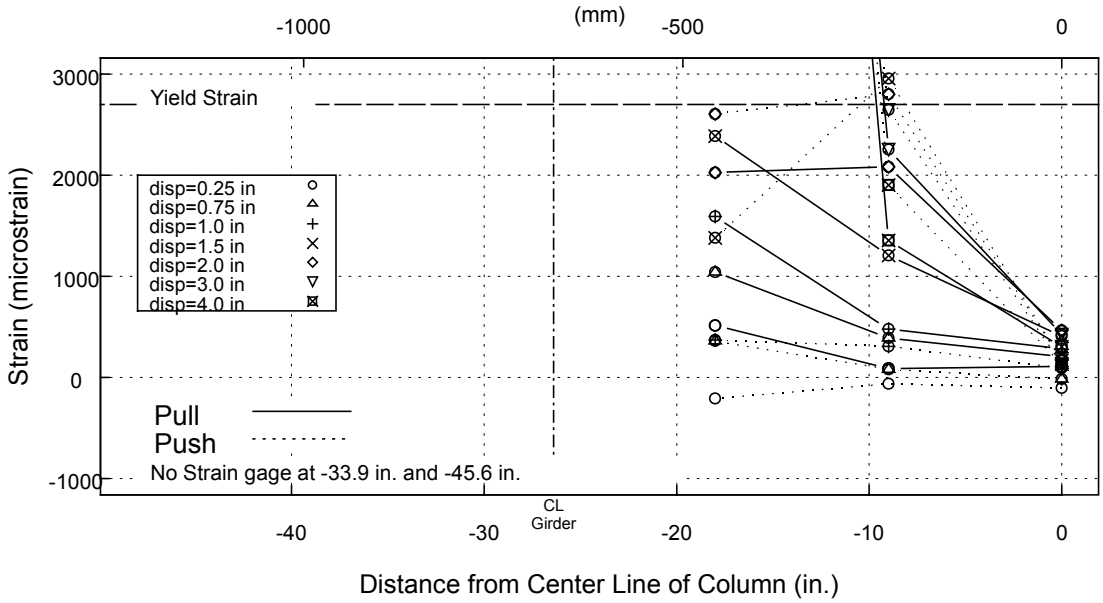

(b) Gage E

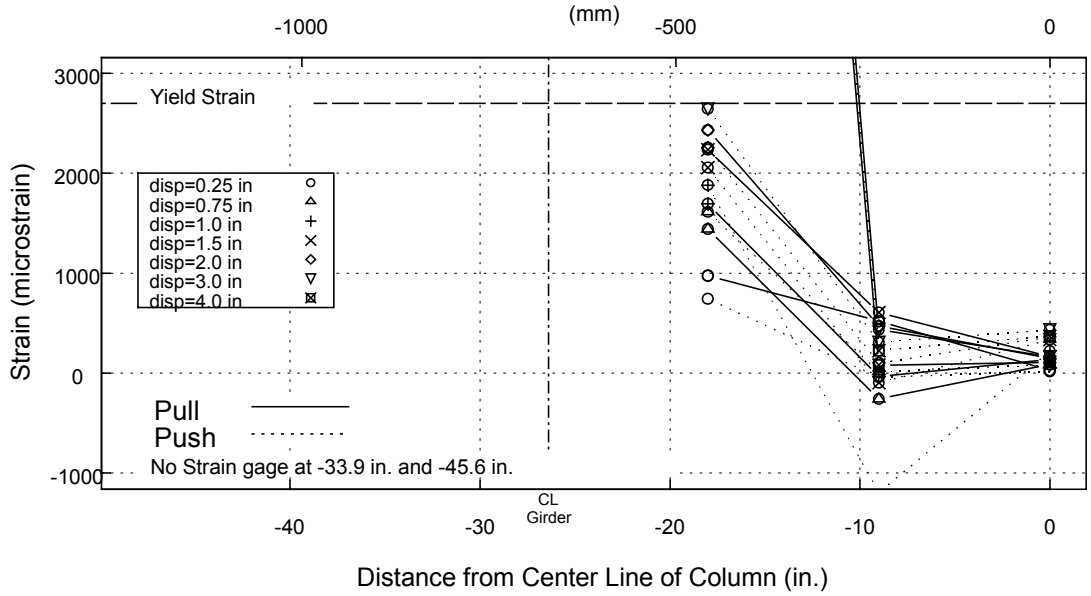

(c) Gage F

Figure 4-47 Specimen PT-NS: Measured Strain in Bent Cap Stirrups (cont.)

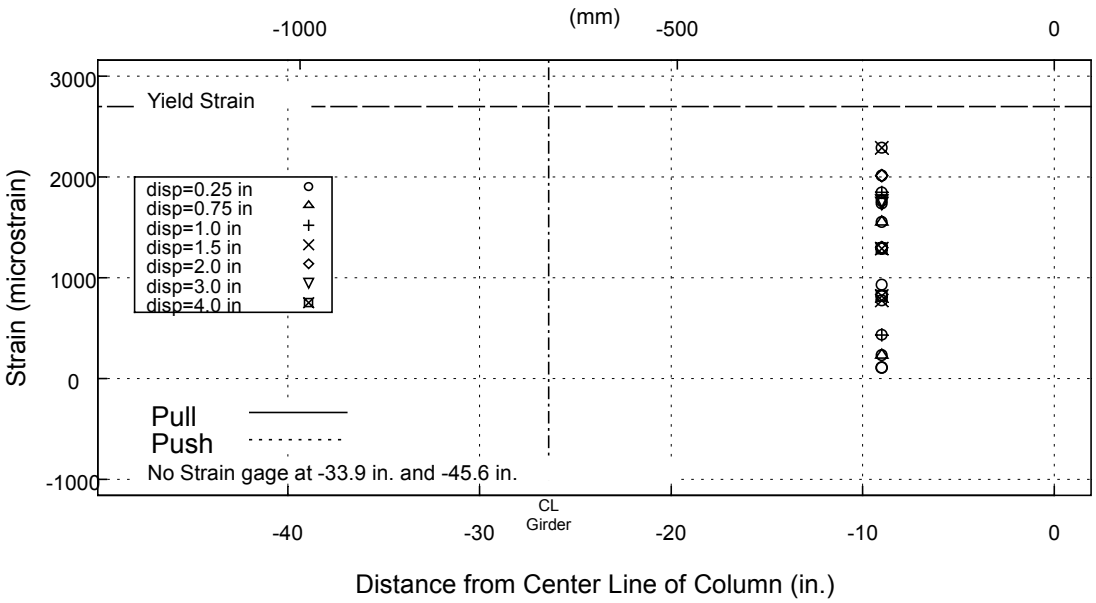

(d) Gage H

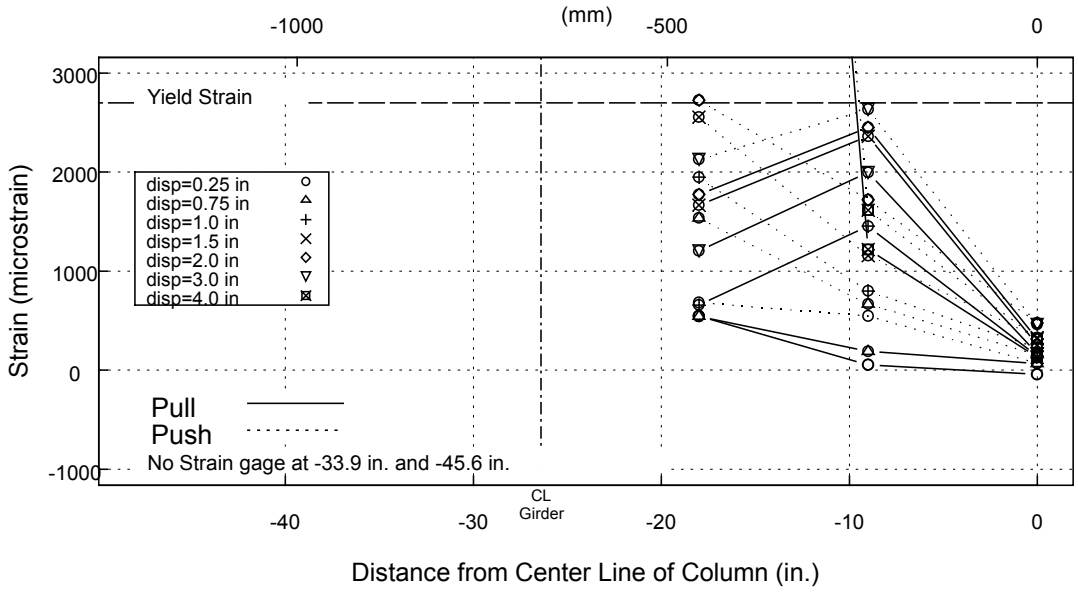

(e) Gage K

Figure 4-47 Specimen PT-NS: Measured Strain in Bent Cap Stirrups (cont.)

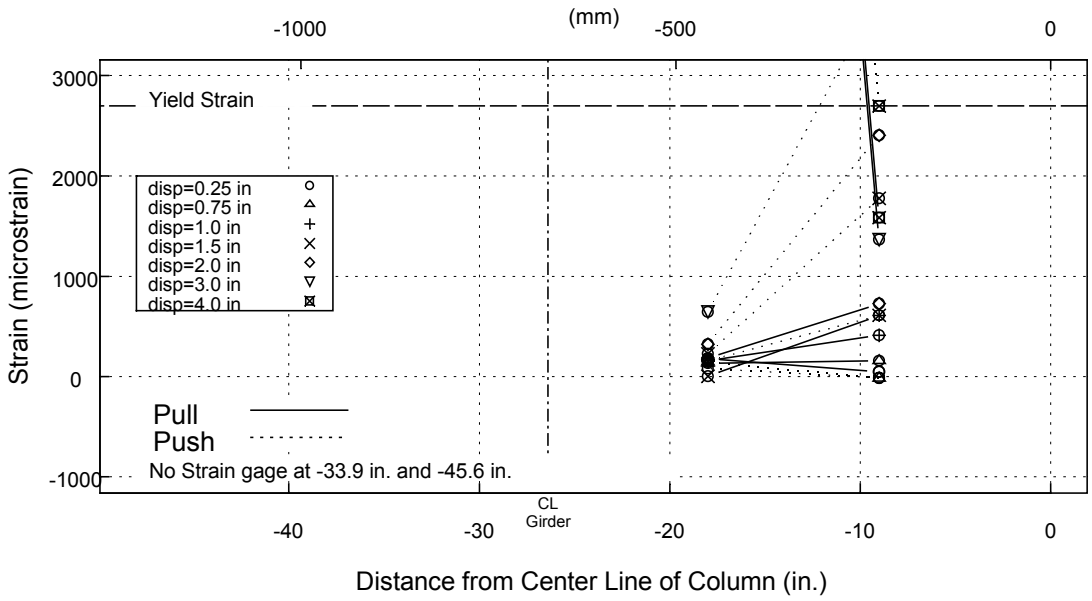

(f) Gage M

Figure 4-47 Specimen PT-NS: Measured Strain in Bent Cap Stirrups (cont.)

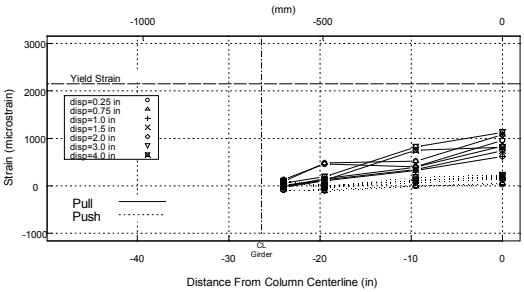

(a) Location A

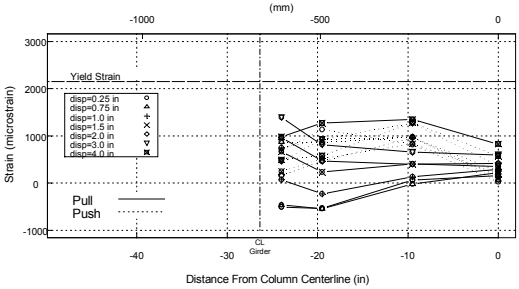

(d) Location D

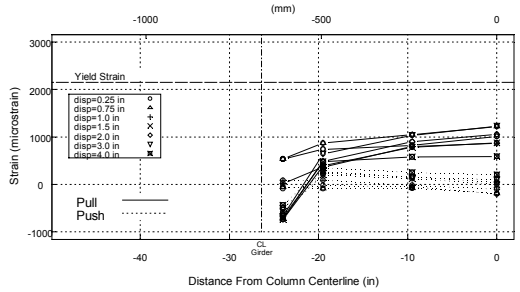

(b) Location B

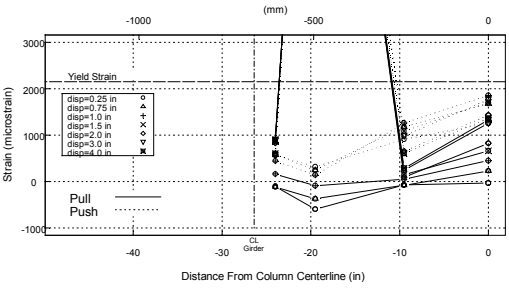

(e) Location E

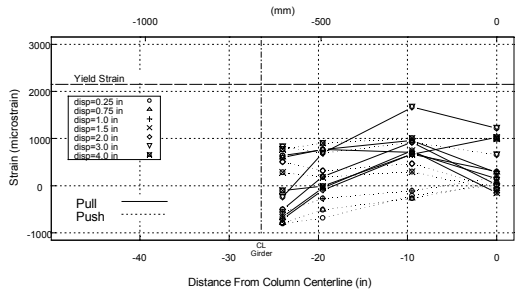

(c) Location C

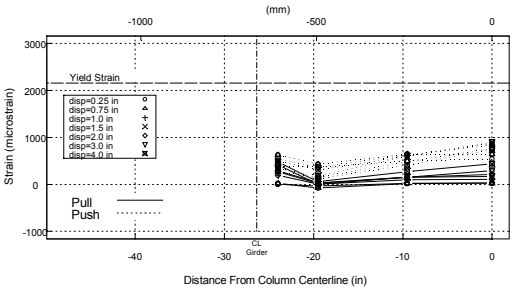

(f) Location F

Figure 4-48 Specimen PT-NS: Measured Strain in Longitudinal Deck Reinforcement

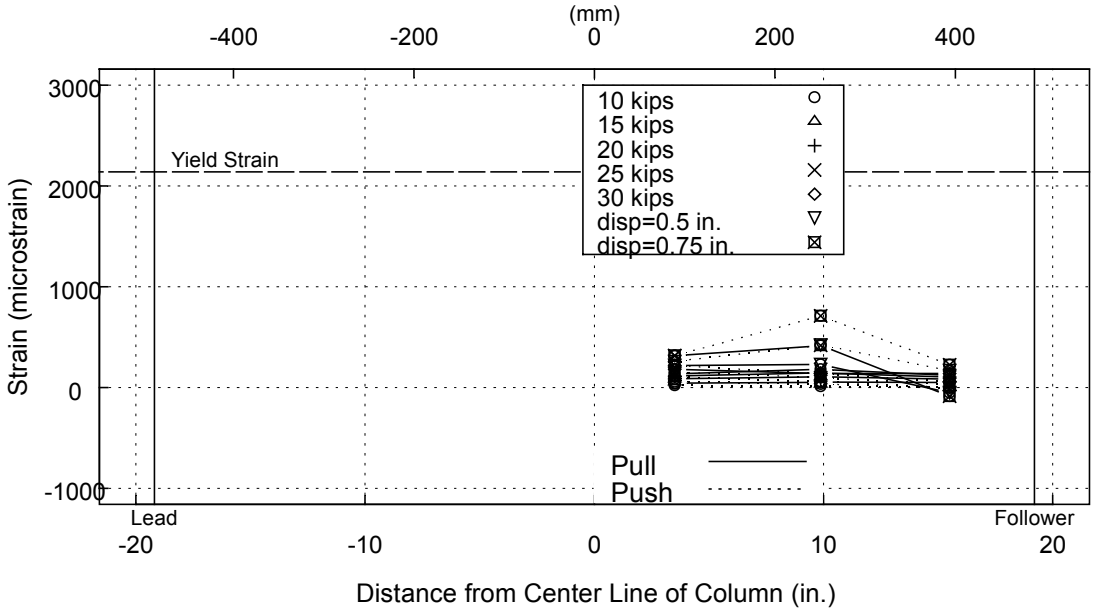

(a) Top Flange

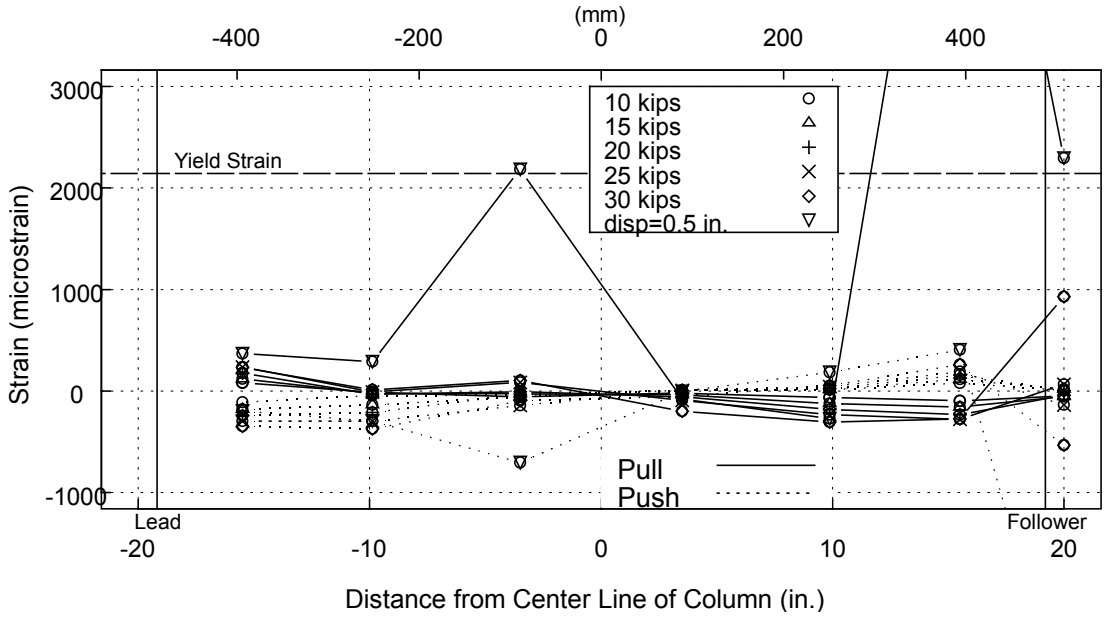

(b) Bottom Flange

Figure 4-49 Specimen PT-NS: Measured Strain in Girder Flanges

4.6 SPECIMEN 4–POST-TENSIONED, STIFFENERS (PT-S)

4.6.1 Observed Performance, PT-S

At the torsional cracking moment of 489 k-ft [662 kN-m] and corresponding rotation of 0.0006 radians, the first crack initiated at mid height of the bent cap and extended at an angle of approximately forty degrees from horizontal for about one foot [305 mm] (Figure 4-50). Cracks developed on the top and underside of the deck but were attributed to dead load application.

At a torsional moment of 1,150 k-ft [1,558 kN-m] and rotation of 0.005 radians, the first crack extended an additional 8 in. [203 mm] to the support block. An additional crack formed from the top flange of the girder and propagated to the support block at an angle of approximately forty degrees (Figure 4-51). These were the only two major cracks to develop for each direction of loading. Both the deck and the underside of the bent cap exhibited numerous, but superficial, cracks.

The maximum torsional moment of 1,347 k-ft [1,825 kN-m] was reached at a rotation of 0.012 radians (Figure 4-52). At this torsional moment, numerous new cracks formed, however spalling did not yet initiate. Minor chipping of paint was noted on the underside of the bent cap near the column and minor cracks extended from this region into the column (Figure 4-53). Deck damage was limited to superficial cracking (Figure 4-54).

Development of a failure mechanism was noted at a torsional moment of 1,316 k-ft [1,783 kN-m] and corresponding rotation 0.02 radians (Figure 4-55). The mechanism initiated from a recently developed crack that exhibited sliding plane behavior. This crack propagated from the top flange of the girder to the bottom of the cap at an angle of approximately sixty-five degrees from the horizontal. At this load level, more cracks at the underside of the bent cap and incipient spalling near the column/support block were observed (Figure 4-56).

The shear friction sliding plane was fully developed at a rotation of 0.032 radians and a corresponding torsional moment of 688 k-ft [932 kN-m] (Figure 4-57). The cap face concrete spalled in the region bound by this crack and the bottom of the bent cap. A crack extending along the width of the bent cap and running nearly parallel with the

girder also spalled. At this load level, large portions of concrete spalled off the underside of the bent cap near the support block. A large crack developed where the sliding plane extended through the bent cap (Figure 4-58). The deck concrete damage was limited to superficial cracking (Figure 4-59).

Figure 4-50 Specimen PT-S: First Torsional Crack on Bent Cap Lead Face

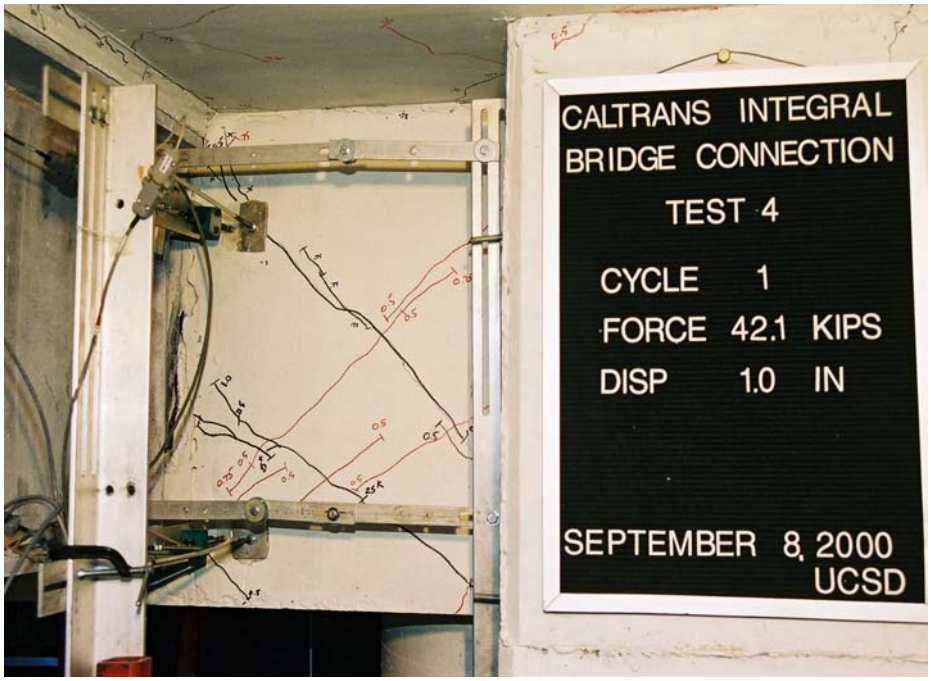

Figure 4-51 Specimen PT-S: Bent Cap Lead Face at θ=0.005 radians

Figure 4-52 Specimen PT-S: Bent Cap at Maximum Torsional Moment

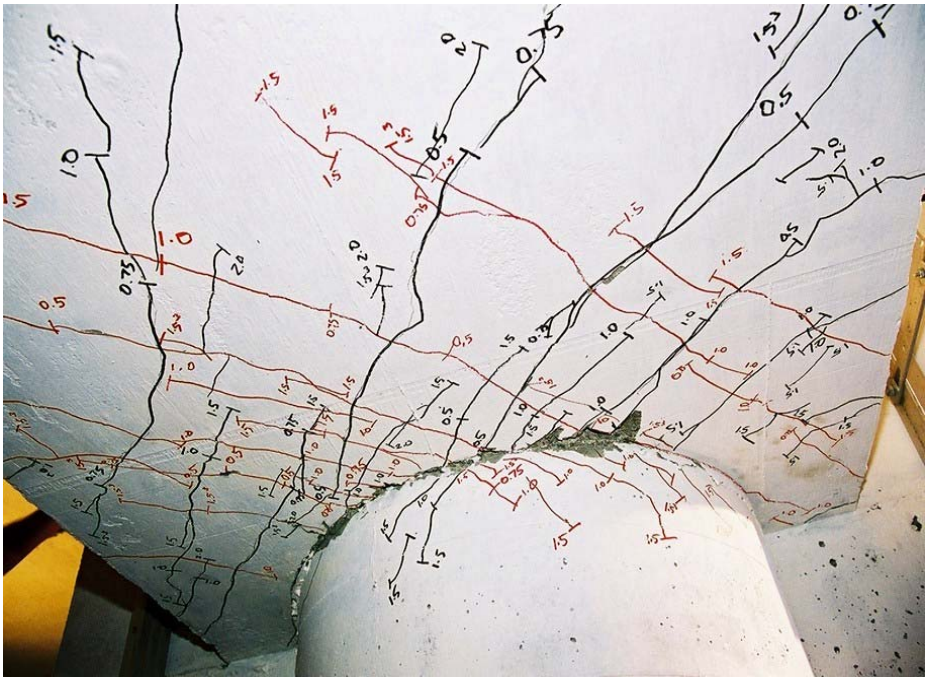

Figure 4-53 Specimen PT-S: Bent Cap Underside at Maximum Torsional Moment

Figure 4-54 Specimen PT-S: Deck at Maximum Torsional Moment

Figure 4-55 Specimen PT-S: Bent Cap Lead Face at θ = 0.02 radians

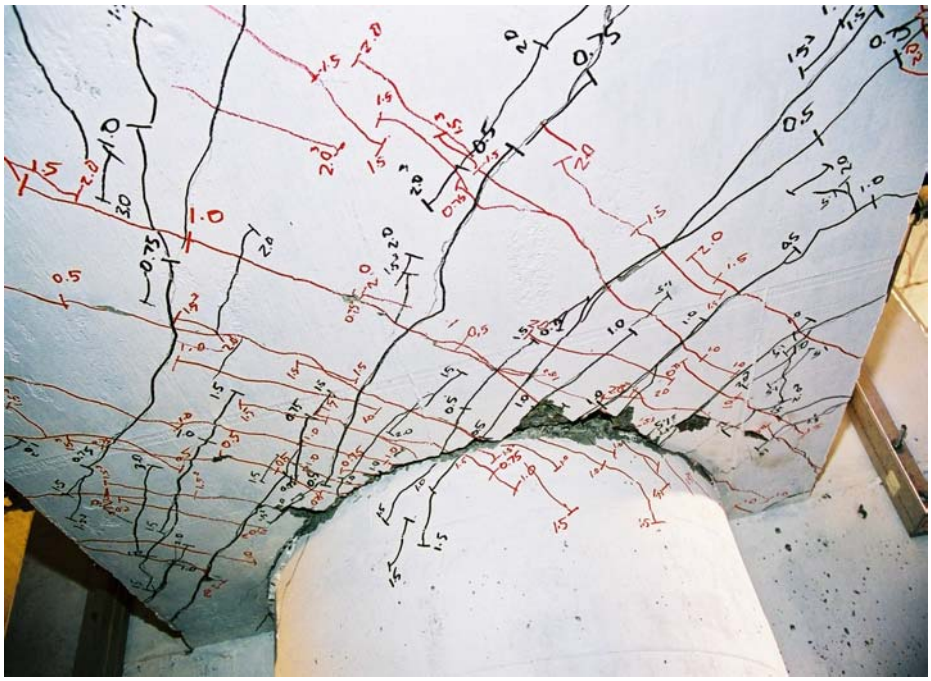

Figure 4-56 Specimen PT-S: Bent Cap Underside at θ = 0.02 radians

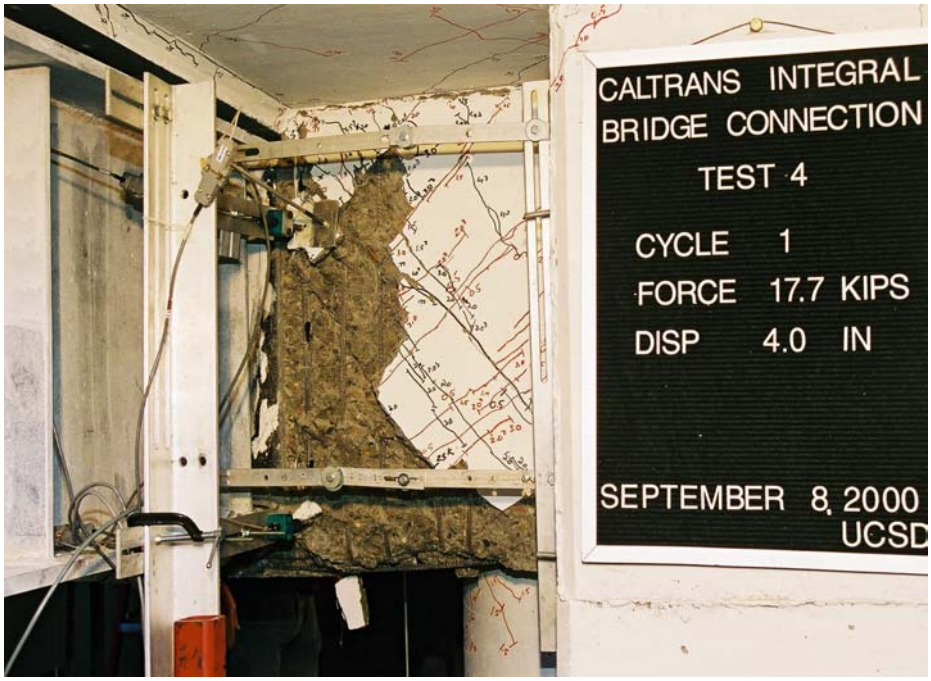

Figure 4-57 Specimen PT-S: Bent Cap Lead Face at Maximum Rotation (θ=0.03 radians)

Figure 4-58 Specimen PT-S: Bent Cap Underside at Maximum Rotation

Figure 4-59 Specimen PT-S: Deck at Maximum Rotation

4.6.2 Measured Response, PT-S

The torsional moment versus torsional rotation curve for Specimen PT-S is shown in Figure 4-60. The maximum moment of 1,347 k-ft [1,825 kN-m] exceeded the moment corresponding to the bent cap torsional design moment of 700 k-ft [948 kN-m] by 48 percent. The bent cap exhibited minimal cracking and performed nearly elastically to the column overstrength moment. The total bent cap dilation is plotted in Figure 4-61. Bent cap dilation was approximately 0.01 inches (0.254 mm) at maximum bent cap torsional moment.

Figure 4-62 shows the location of gages relative to the location of the lead actuator. The behavior of flexural reinforcement located at bent cap corners is presented in Figure 4-63. All corner bars yielded, however bars in the bottom corners of the bent cap (Bar D and Bar F) yielded before the top corner bars (Bar B and Bar H). Strain gages on the stirrups located at the face of the column and face of the bent cap reported yielding. Strains in the longitudinal deck reinforcement are shown in Figure 4-65. Yielding of the deck bars occurred at the lead face of the bent cap and at both ends of the deck. Because the actuator applied the load at the girder and not the composite section, the girder wanted to separate from the deck at the ends.

Strains in the girder flanges are shown in Figure 4-66. The highest strains in the girder flanges occurred on the portions of flanges in the middle of the bent cap. During the push cycle, the top flange at the lead face is in tension and the bottom flange at the lead face is in compression. Stiffener strains are plotted in Figure 4-67.

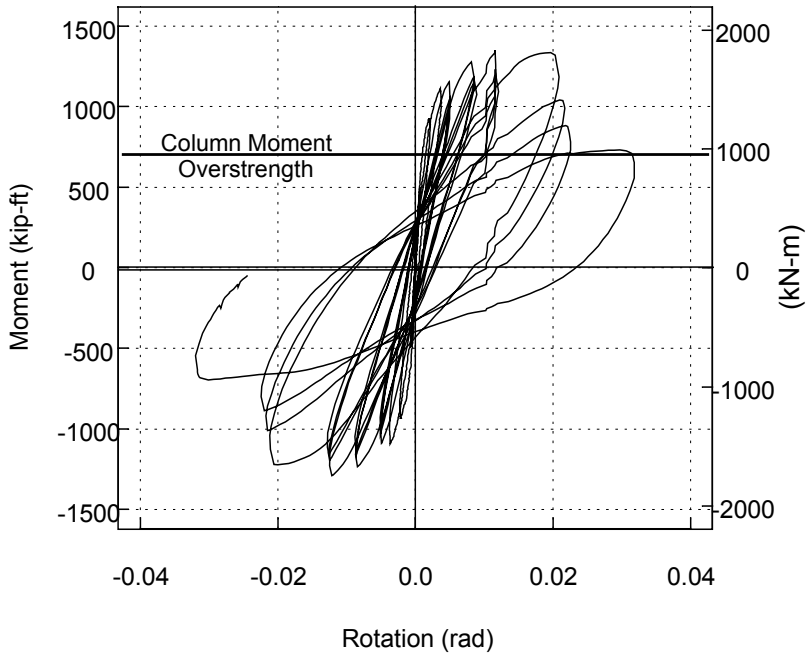

Figure 4-60 Specimen PT-S: Torsional Moment - Rotation Response

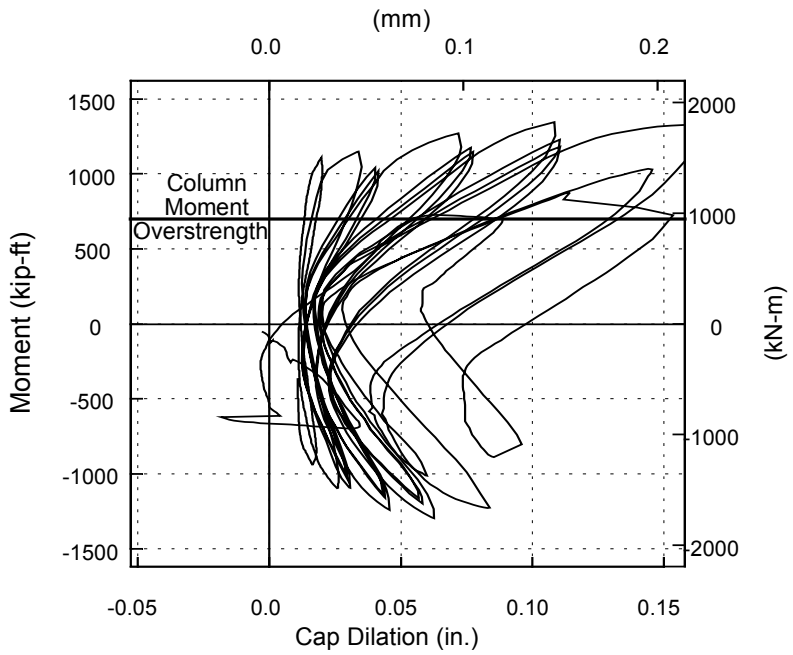

(a) Lead Face

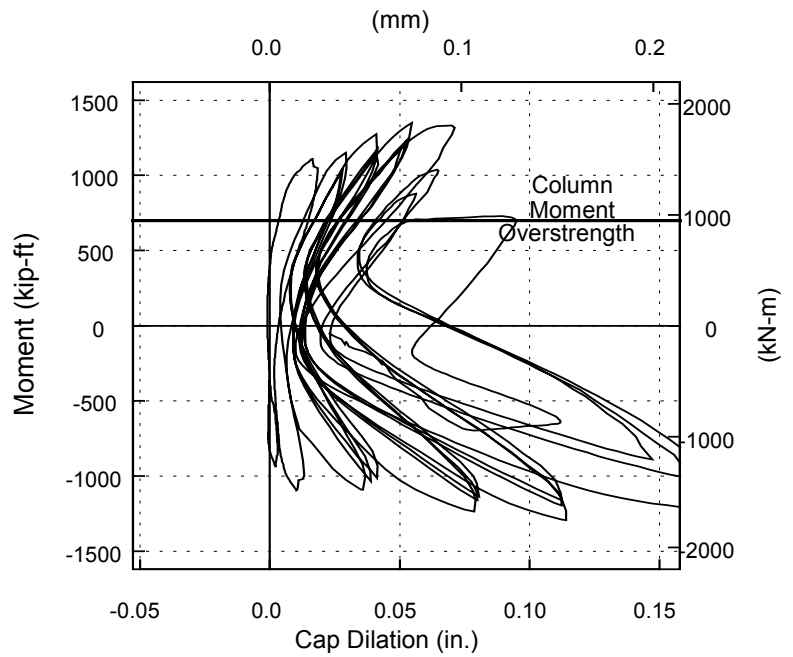

(b) Follower Face

Figure 4-61 Specimen PT-S: Measured Bent Cap Dilation

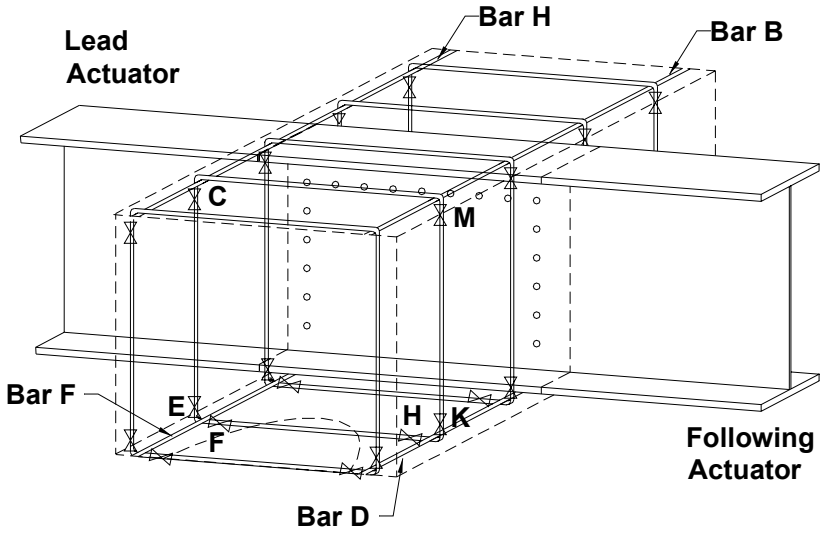

Figure 4-62 Specimen PT-S: Gage Location with Respect to Actuators

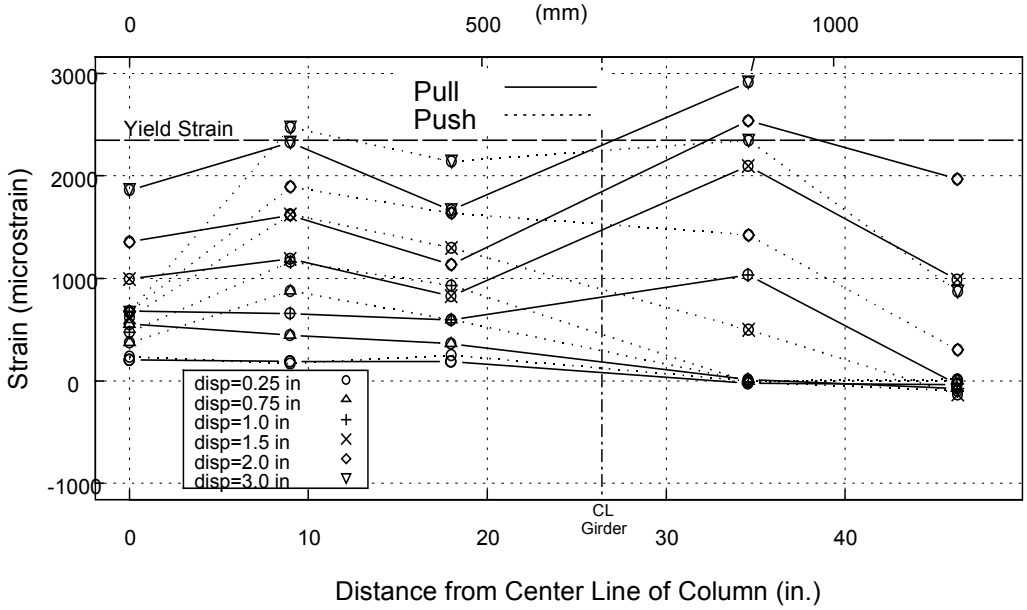

(a) Bar B

Figure 4-63 Specimen PT-S: Measured Strain in Flexural Reinforcement

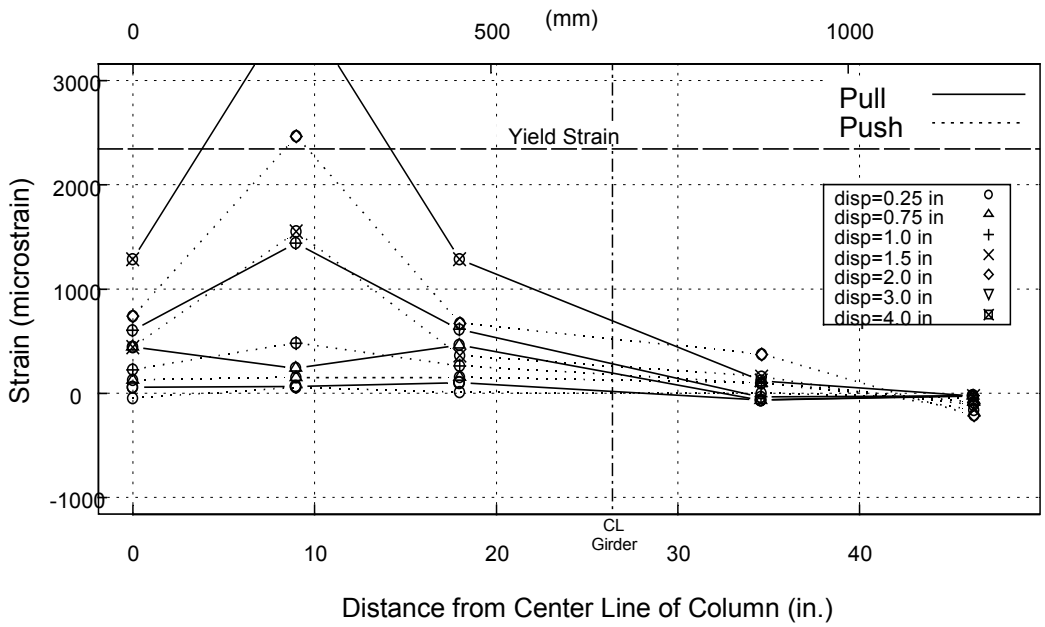

(b) Bar D

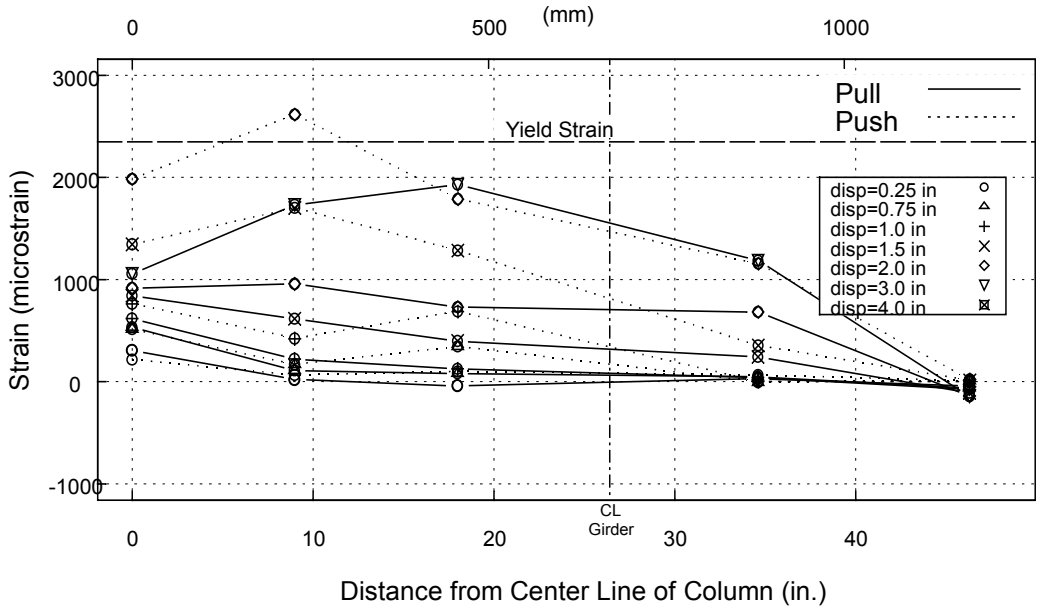

(c) Bar F

Figure 4-63 Specimen PT-S: Measured Strain in Flexural Reinforcement (cont.)

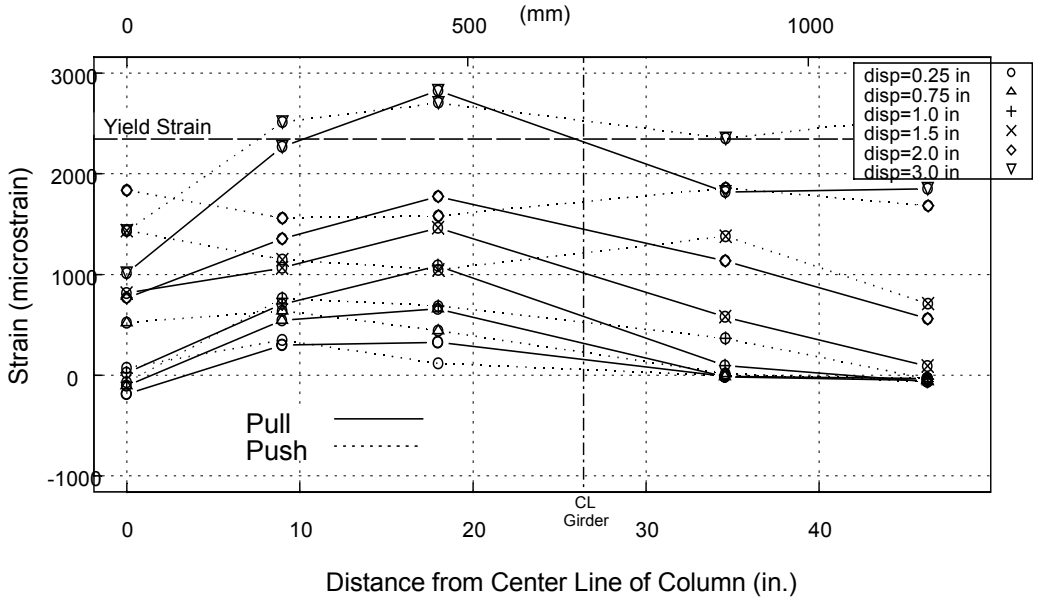

(d) Bar H

Figure 4-63 Specimen PT-S: Measured Strain in Flexural Reinforcement (cont.)

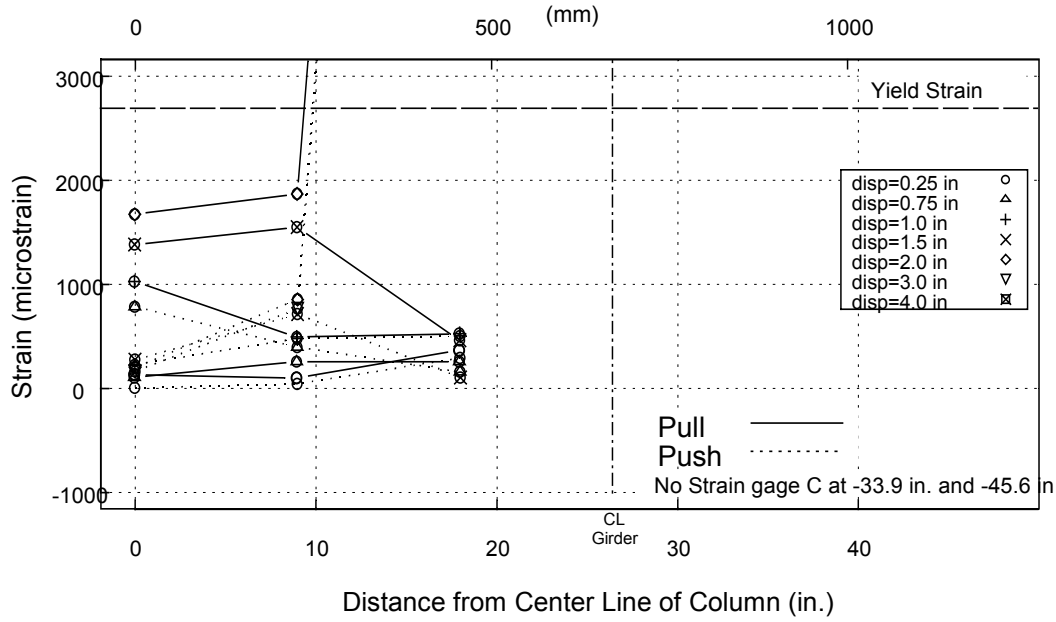

(a) Gage C

Figure 4-64 Specimen PT-S: Measured Strain in Bent Cap Stirrups

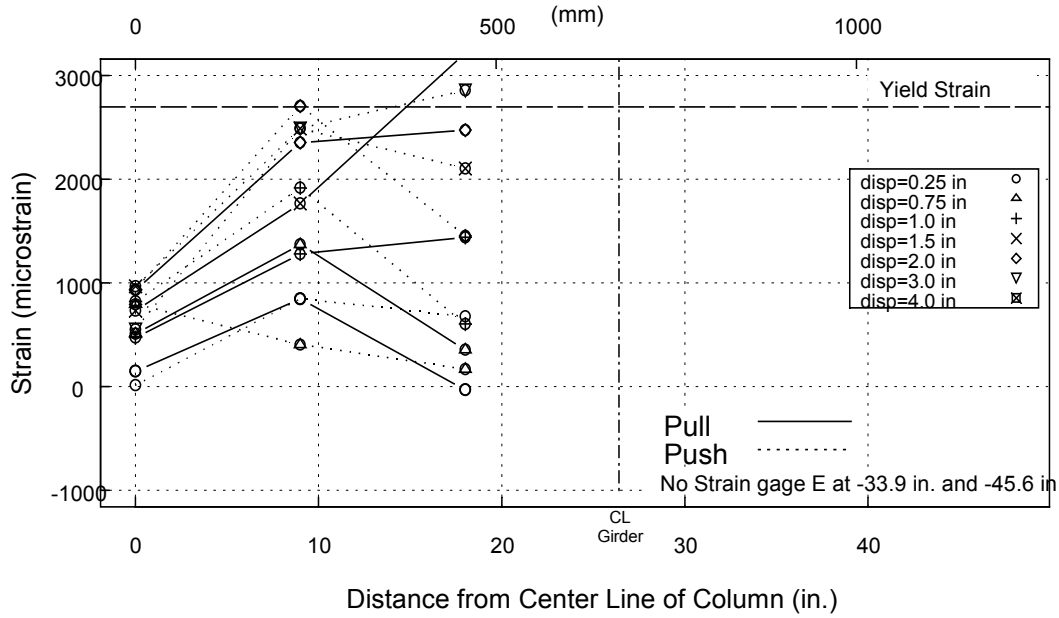

(b) Gage E

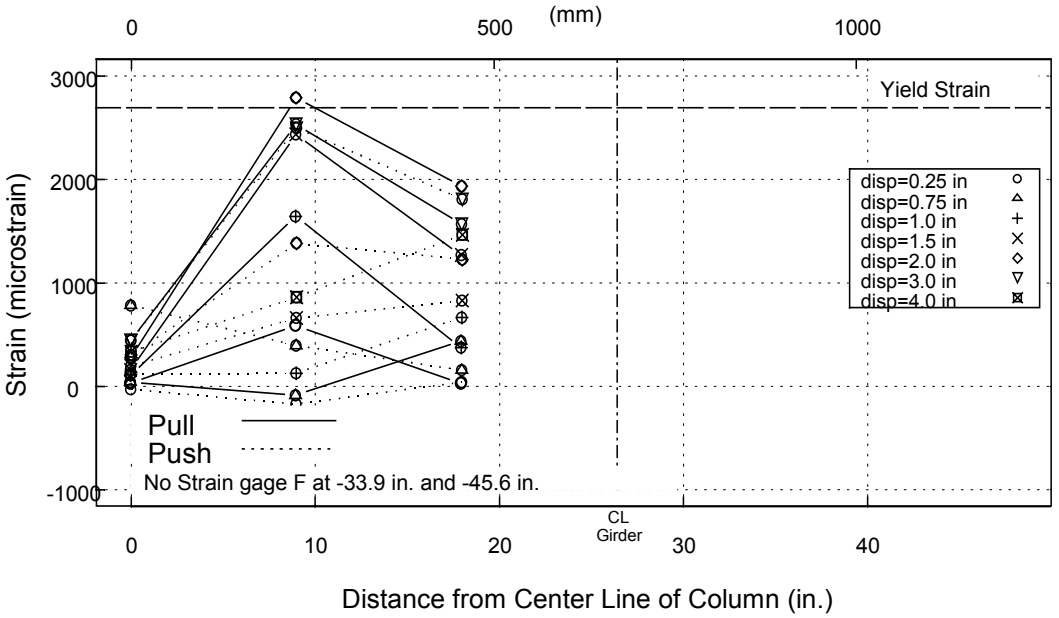

(c) Gage F

Figure 4-64 Specimen PT-S: Measured Strain in Bent Cap Stirrups (cont.)

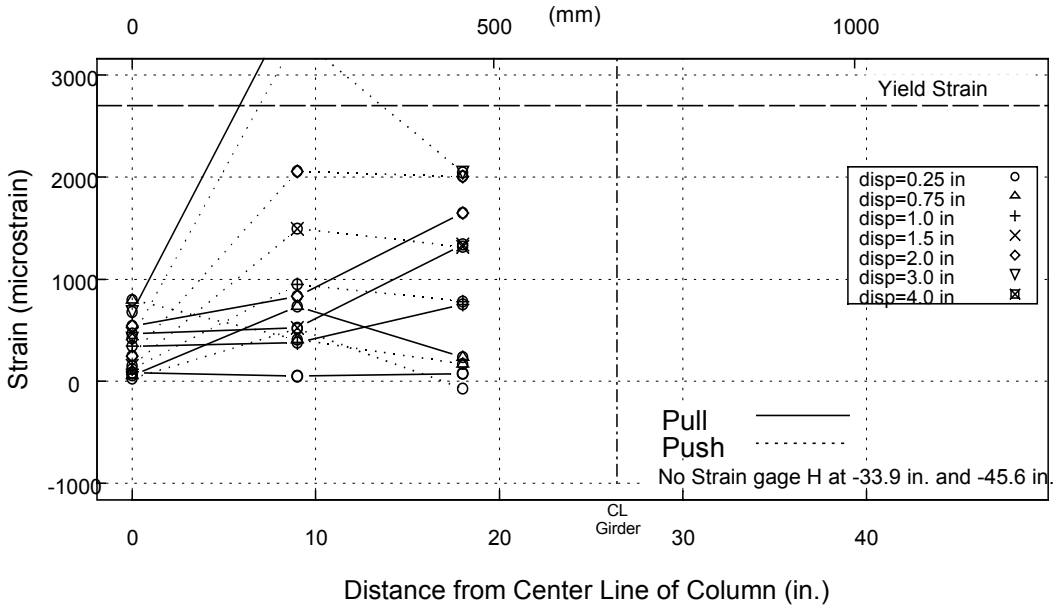

(d) Gage H

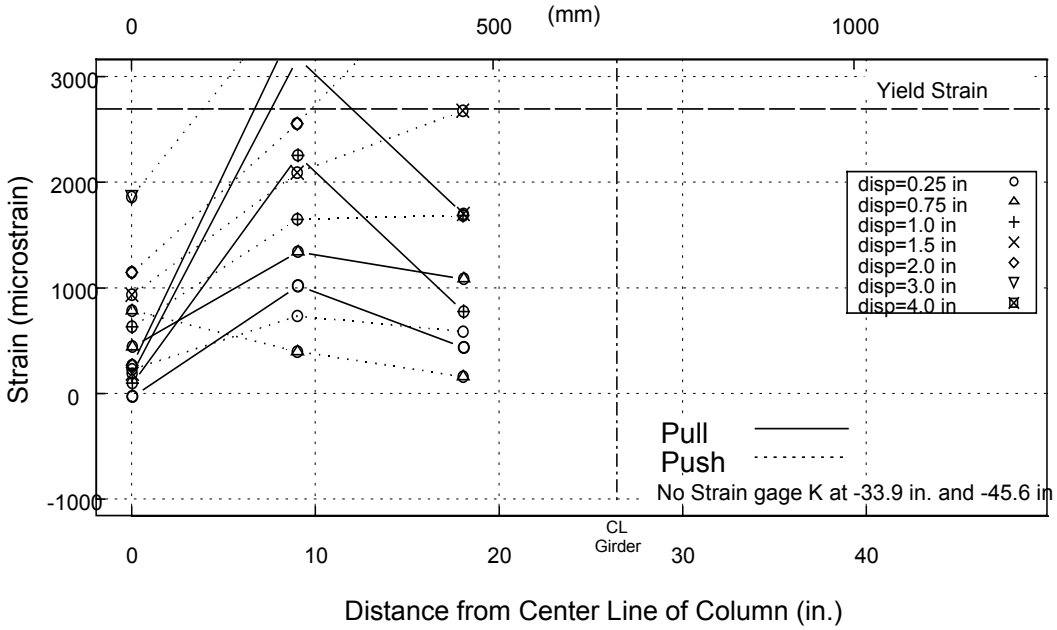

(e) Gage K

Figure 4-64 Specimen PT-S: Measured Strain in Bent Cap Stirrups (cont.)

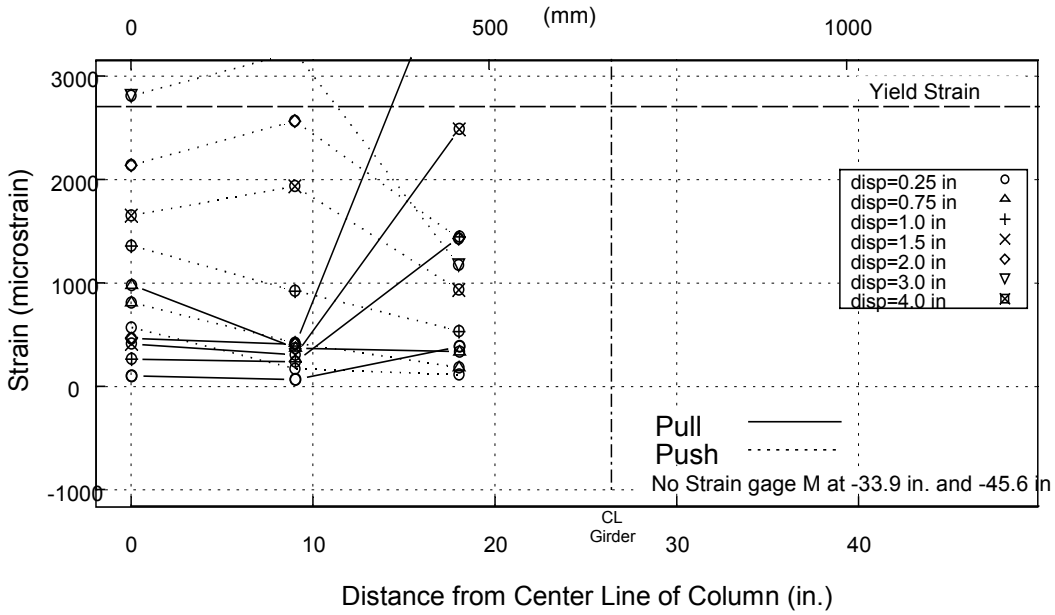

(f) Gage M

Figure 4-64 Specimen PT-S: Measured Strain in Bent Cap Stirrups (cont.)

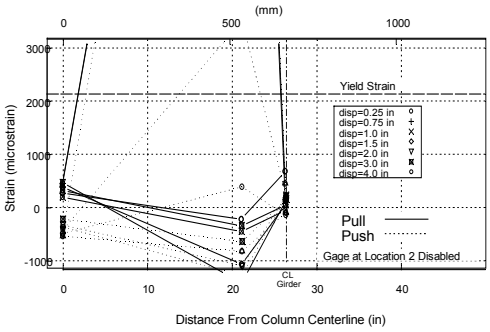

(a) Location A

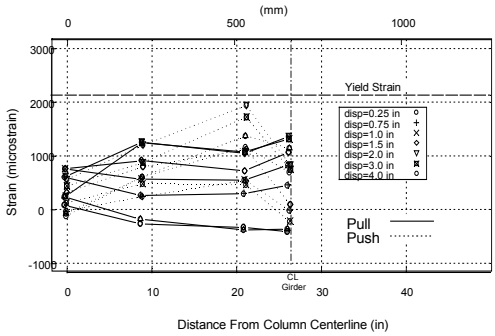

(d) Location D

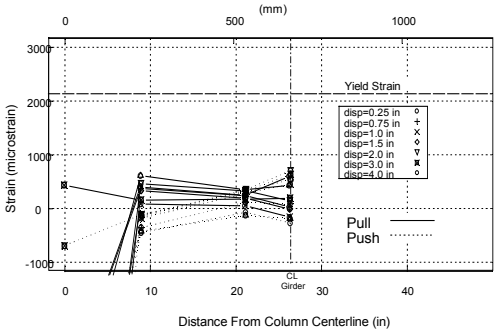

(b) Location B

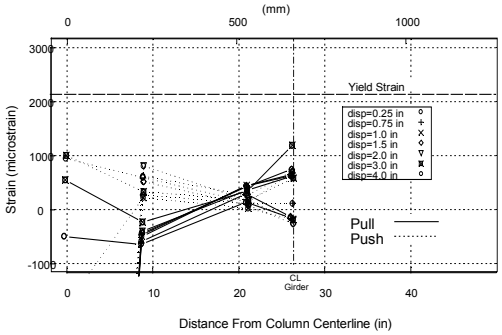

(e) Location E

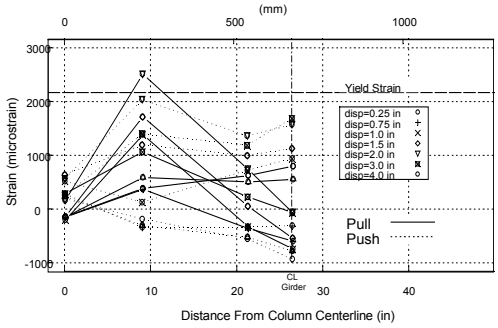

(c) Location C

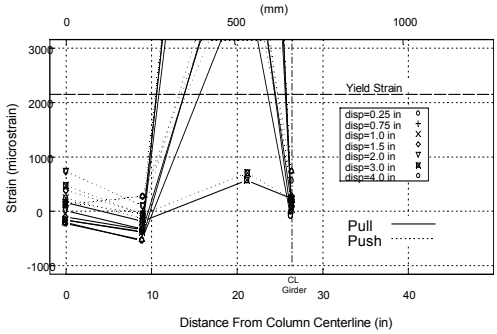

(f) Location F

Figure 4-65 Specimen PT-S: Measured Strain in Longitudinal Deck Reinforcement

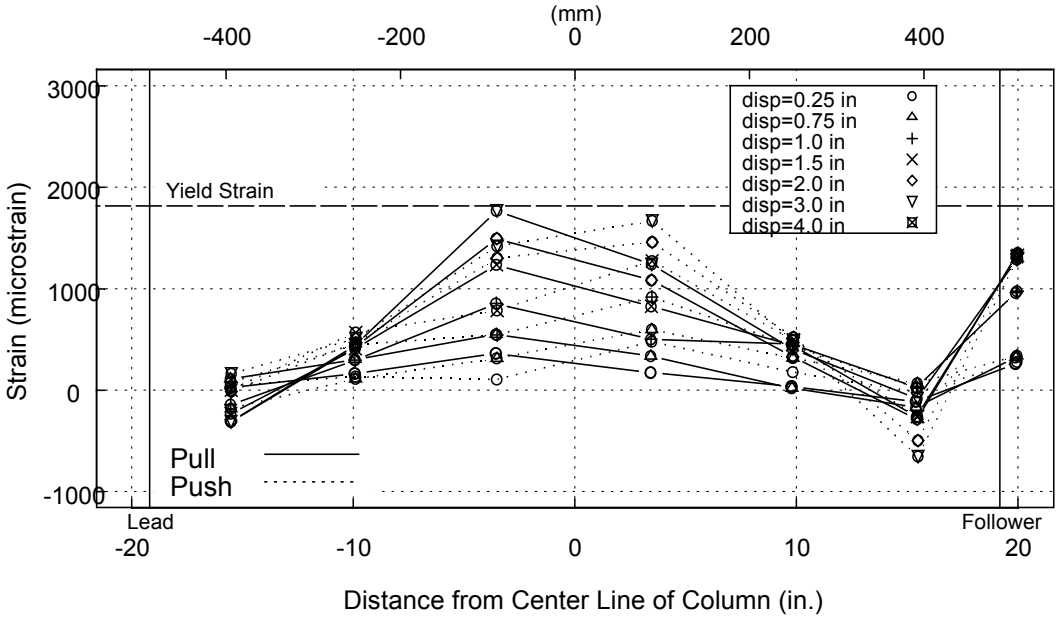

(a) Top Flange

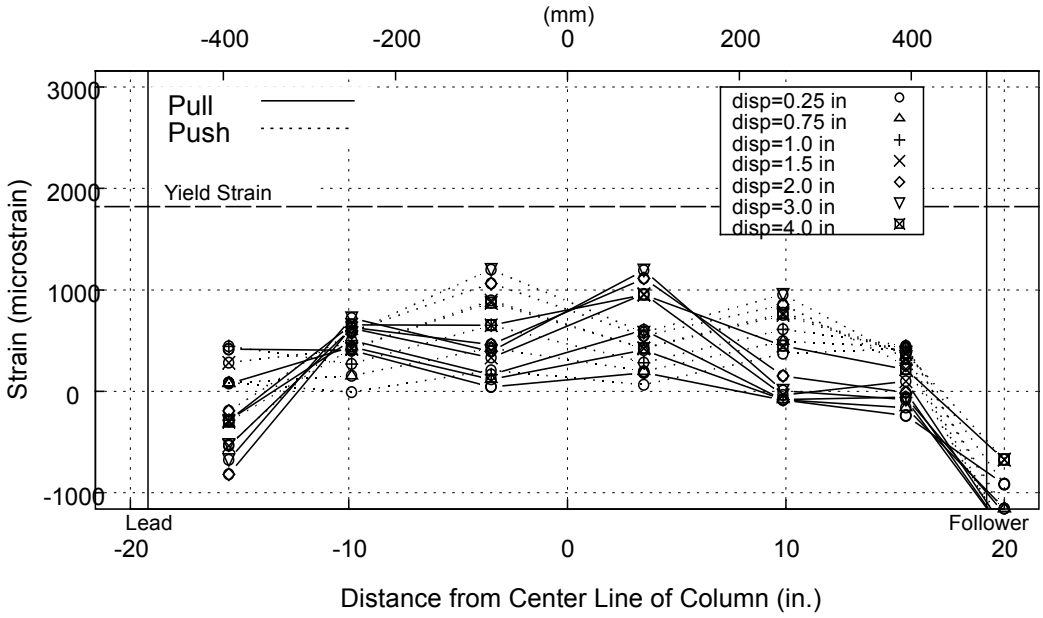

(b) Bottom Flange

Figure 4-66 Specimen PT-S: Measured Strain in Girder Flanges

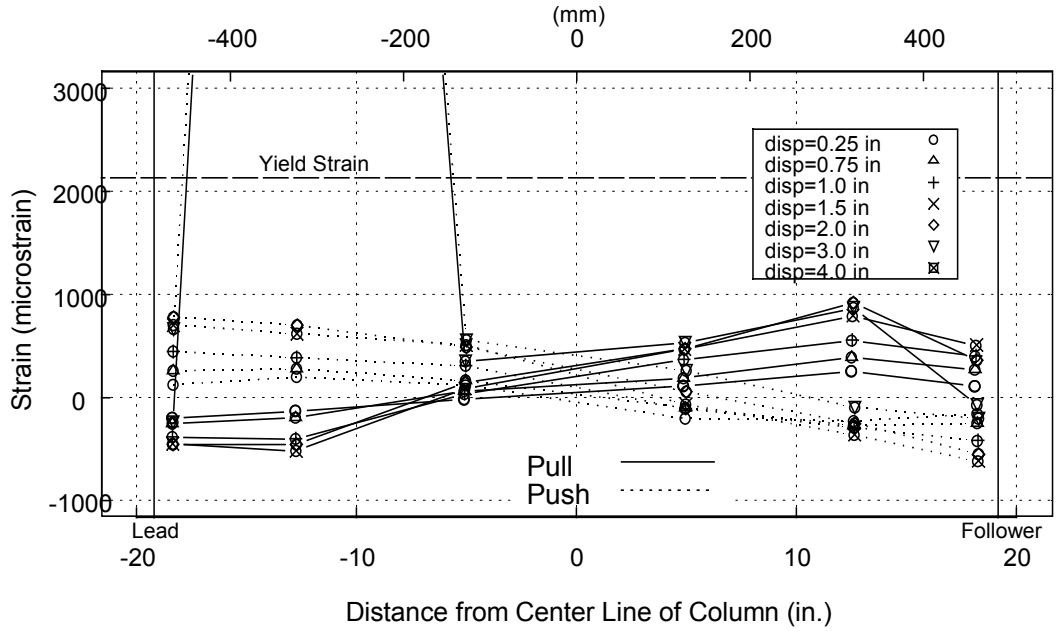

(a) Top Region

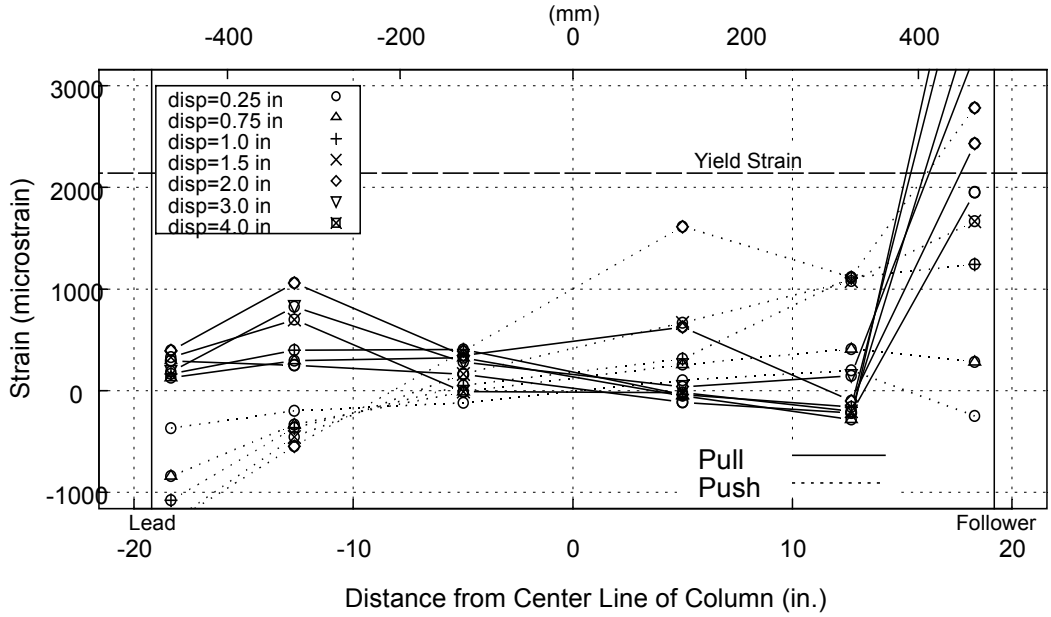

(b) Bottom Region

Figure 4-67 Specimen PT-S: Measured Strain in Girder Stiffeners

4.7 COMPARISON OF COMPONENT TEST RESULTS

All bent caps in the component tests had torsional moment capacities higher than their design torsional moment. Figure 4-68 compares the first cycle moment rotation envelopes of the four component tests. The specimens with web stiffeners on the girders in the bent cap region (Specimen CR-S and Specimen PT-S) achieved maximum torsional moments 25% higher than the specimens without bent cap region stiffeners (Specimen CR-NS and Specimen PT-NS). Strain gage readings on the stiffeners indicated that bent cap stiffeners located close to the bent cap face contributed significantly to the torsional moment transfer between girder and column. Stiffeners toward the center of the bent cap also contributed to the moment transfer, but not to such a significant extent. All four Specimens achieved approximately the same ultimate torsional rotation before reaching a torsion shear friction failure.

Figure 4-69 compares the torque-twist relationships of all four specimens. The torsional rotation plotted in all previous graphs is from an inclinometer located at the end of the bent cap. Rotations calculated from displacement readings by a pair of vertical potentiometers located under the bent cap at either bent cap face along the girder centerline were approximately the same as the rotation from the inclinometer. This indicates a rigid body rotation occurs between the girder and outer edge of the bent cap. Twist is the measure of rotation per unit length. Therefore, twist occurs only between the support block and the girder. Although the distance from center of column to center of girder is 26.4 in. [671 mm] a twist length of 24 inches [610 mm] was used. This reduction from the apparent twist length was made because of the rigid restraint provided by the support block.

In general, the post-tensioned bent caps performed better than the conventionally reinforced caps. For instance, the total bent cap crack dilation in the post-tensioned bent caps (Specimen PT-NS and Specimen PT-S) was minimal until the bent cap reached maximum torsional moment; whereas the crack dilation in the conventionally reinforced concrete bent cap increased as the torsional moment increased (Figure 4-70). Once the post-tensioned bent cap reached maximum torsional moment, the cracking of the post-

tensioned bents developed similarly to the conventionally reinforced beam. The remainder of this section presents detailed comparisons between pairs of tests.

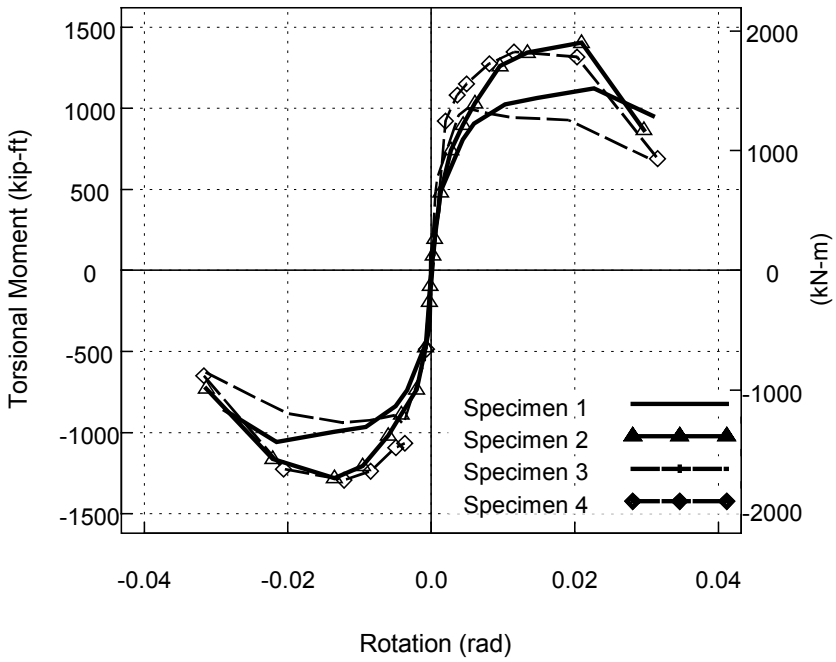

Figure 4-68 Comparison of Torsional Moment-Rotation Envelopes

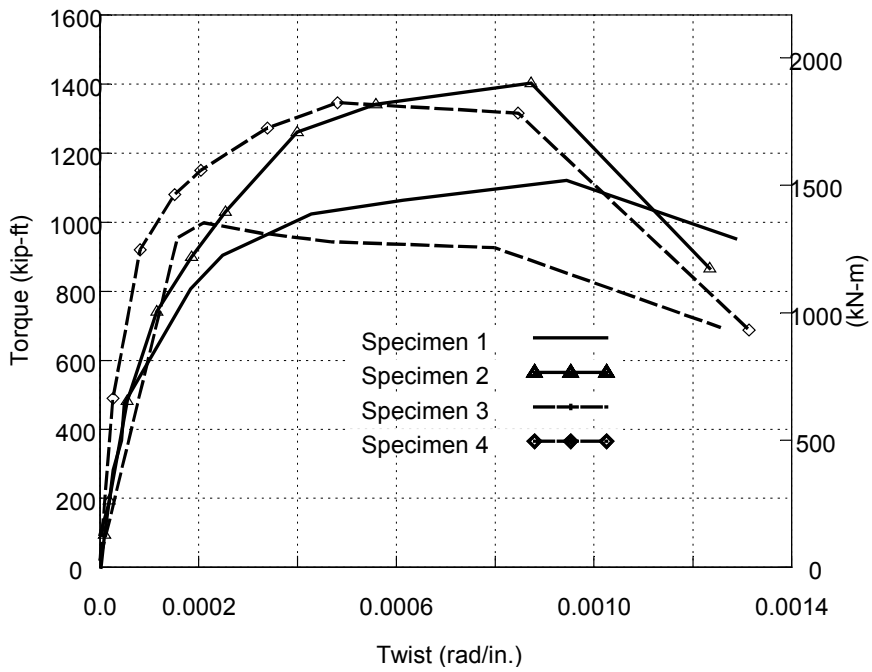

Figure 4-69 Torque-Twist Relations

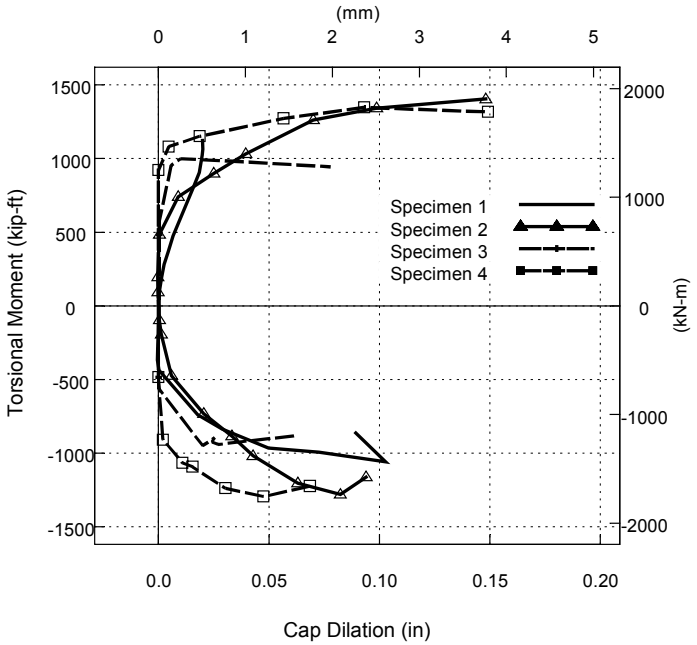

(a) Lead Face

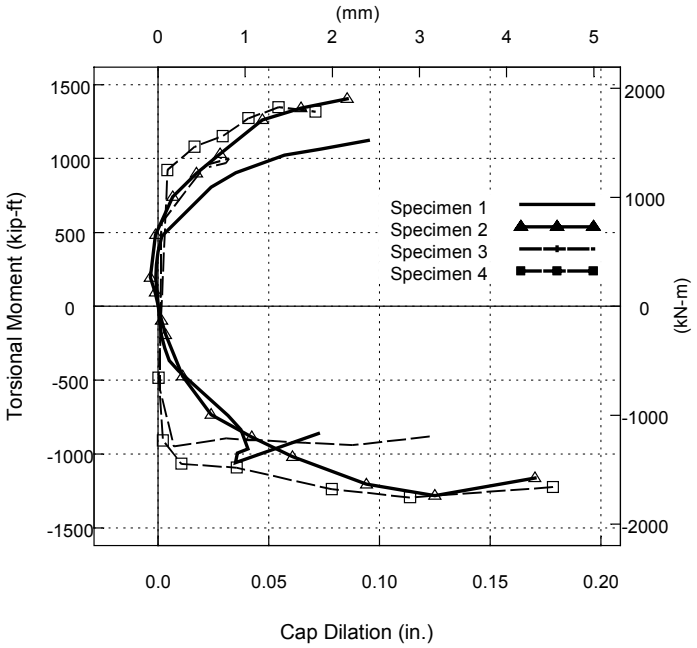

(b) Follower Face

Figure 4-70 Comparison of Bent Cap Dilation Envelopes

4.7.1 Correlation of Specimen 1 (CR-NS) and Specimen 2 (CR-S)

The only difference between Specimen 1 and Specimen 2 was that Specimen 2 had full height bearing stiffeners on the girder web in the bent cap region. Therefore, this section of the report demonstrates how the addition of full height bearing stiffeners affected the behavior of selected components.

Figure 4-71 compares bent cap damage at the design moment. Both Specimen CR-NS and Specimen CR-S have incipient spalling on the underside of the bent cap. On the lead face, Specimen CR-NS is spalling while damage to Specimen CR-S is limited to cracking. Damage at the maximum moment is compared on three faces in Figure 4-72. Both bent caps are spalling at this torsional moment. In Specimen CR-NS, significant degradation has occurred in the bent cap under the steel girder. In Specimen CR-S, the bent cap under the girder has significant cracking and the steel girder has separated from the bent cap concrete underneath. The underside of the bent cap of Specimen CR-NS has significantly degraded, with major concrete spalling occurring. The corresponding location in Specimen CR-S has spalling concentrated at the column face. Damage to the deck of Specimen CR-NS is limited to cracking, while spalling has occurred in the deck of Specimen CR-S along the girder alignment.

The specimens at their failure load are shown in Figure 4-73. Significant spalling has occurred on the lead face and bent underside in both specimens. The failure mechanism in Specimen CR-NS is a shear-friction failure plane inclined along the initial torsion spiral crack. Deck damage in Specimen CR-NS is limited to cracking. The failure mechanism of Specimen CR-S is a vertical torsion shear-friction failure plane at the edge of the girder flanges. The failure plane propagates through the deck concrete, exposing deck and main flexural reinforcement.

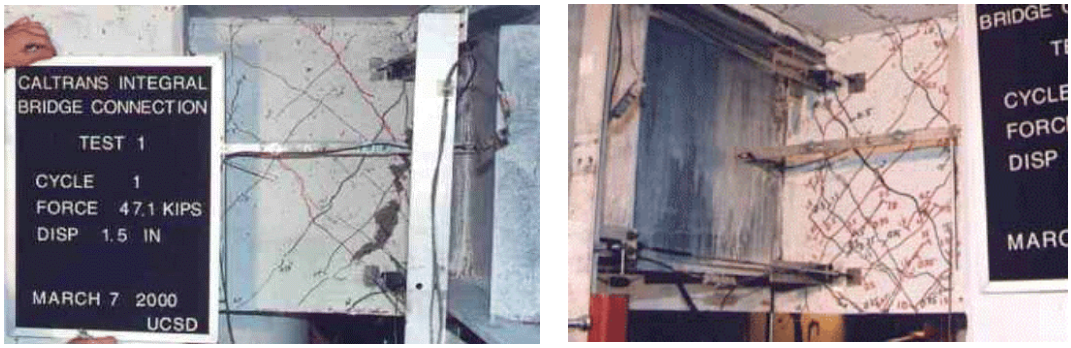

(a) Lead Face

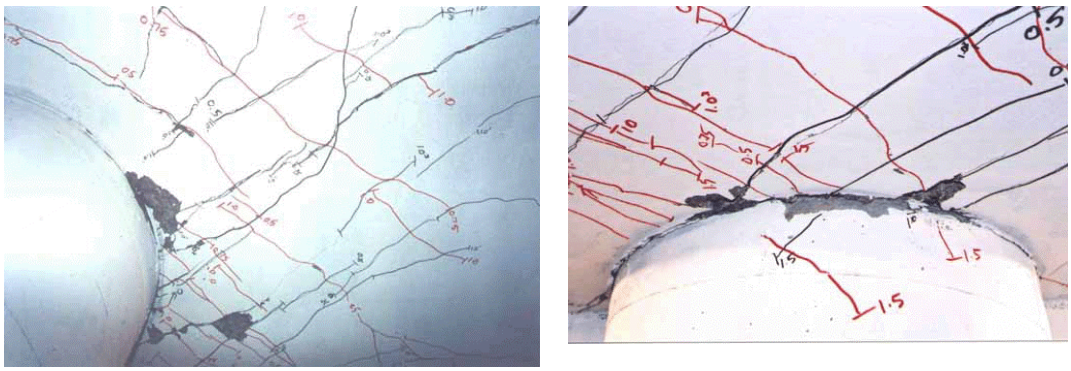

(b) Bottom Face

Specimen 1-CR-NS **Specimen 2-CR-S**

Figure 4-71 Damage Comparison at Bent Cap Rotation=0.01 radians

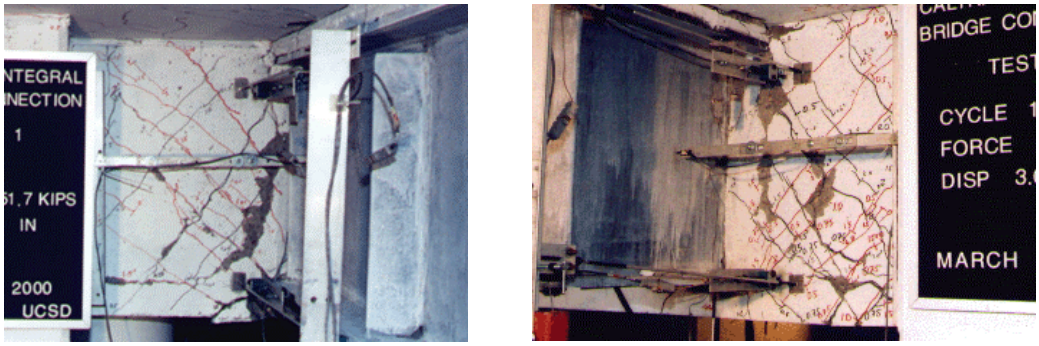

(a) Lead Face

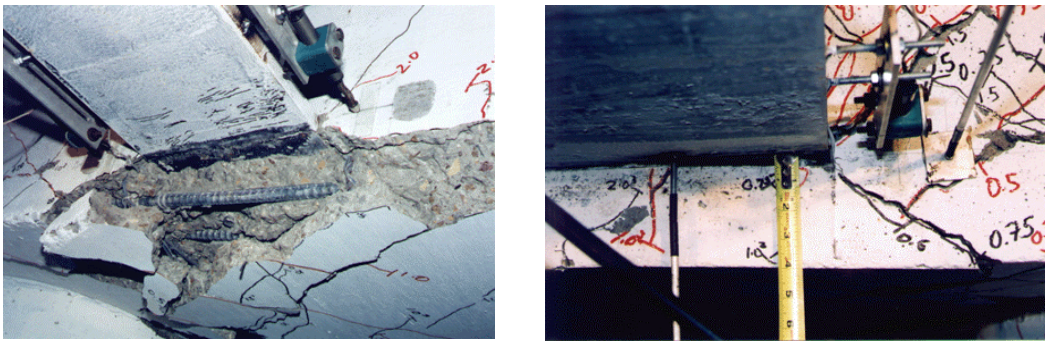

(b) Girder/Lead Face

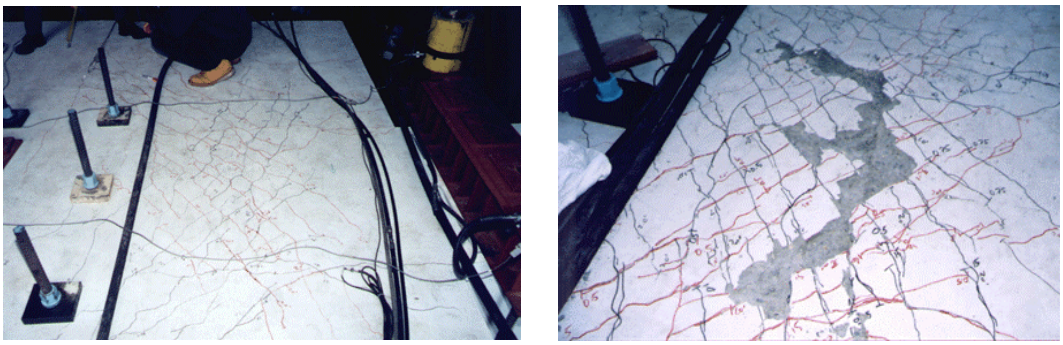

(c) Top Face (deck)

Specimen 1-CR-NS **Specimen 2-CR-S**

Figure 4-72 Damage Comparison at Bent Cap Rotation=0.02 radians

(a) Lead Face

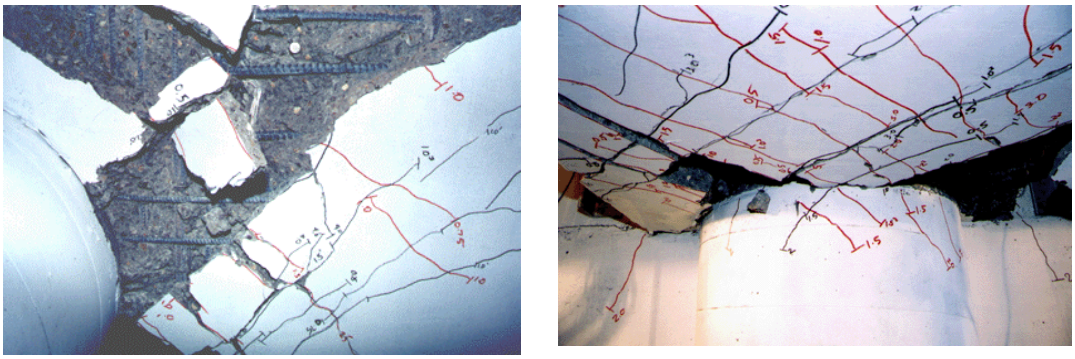

(b) Bottom Face

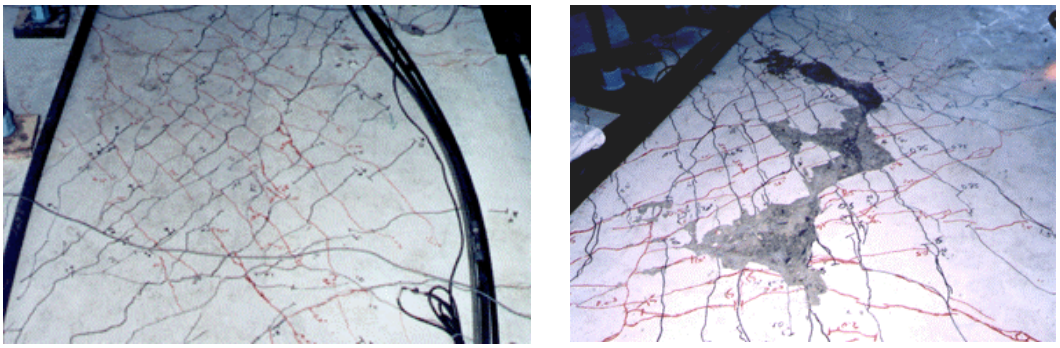

(c) Top Face (deck)

Specimen 1-CR-NS **Specimen 2-CR-S**

Figure 4-73 Damage Comparison at Bent Cap Rotation=0.03 radians (Failure)

Figure 4-74 compares the global behavior of Specimen CR-NS and Specimen CR-S. The maximum torsional moment of Specimen CR-S was approximately 25% higher than the maximum torsional moment of Specimen CR-NS. Both specimens converged to nearly the same ultimate torsional rotation and corresponding torsional moment. Initial bent cap dilation due to cracking was similar until Specimen CR-NS reached 0.05 in. [1.3 mm] at 1,000 k-ft [1,355 kN-m] while Specimen CR-S dilated to only 0.025 in. [0.6 mm]. At the bent cap maximum design moment, bent cap dilation of Specimen CR-NS was 0.09 in. [2.3 mm] while dilation in Specimen CR-NS was 0.16 in. [4 mm].

Bent cap dilation in the transverse direction (longitudinal bridge direction) of the stiffened and unstiffened Specimens are compared in Figure 4-75. The dilation is measured with a displacement transducer mounted on the bottom girder flange and targeted on the bent cap. For the same rotation, the unstiffened bent cap dilates laterally approximately 1.5 times more than in the stiffened case.

The measured strain in the flexural reinforcement at the bottom corners of both bent caps are shown in Figure 4-76. In both specimens, the maximum strains occur between the column face and girder face.

Strains at selected stirrup locations are shown in Figure 4-77. The top two graphs compare the strains in the vertical leg of stirrups near the bent cap lead actuator face. Stirrups in both specimens have the highest strains near the girders. This location in both specimens reached yield at approximately their respective maximum torsional moments. On the horizontal leg, both stirrups yielded before the maximum torsional moment was reached.

Figure 4-78 compares the flange behavior of Specimen CR-NS and Specimen CR-S. Flange strains in Specimen CR-NS were erratic. The bottom flange yielded near the bent cap face prior to reaching the maximum torsional moment. Flanges of Specimen CR-S were well behaved with no yielding recorded in the bottom flange. The top flange yielded at the ultimate rotation.

By comparing Specimen CR-NS and CR-S, the difference in performance is attributed solely to the full height bearing stiffeners on the girder web. The stiffeners increased the maximum bent cap torsional moment capacity by approximately 25%. The stiffeners did not appear to reduce bent cap dilation along the transverse bridge axis

however, they did decrease bent cap dilation along the longitudinal bridge axis. Additionally, the stiffeners delayed the onset of flange yielding.

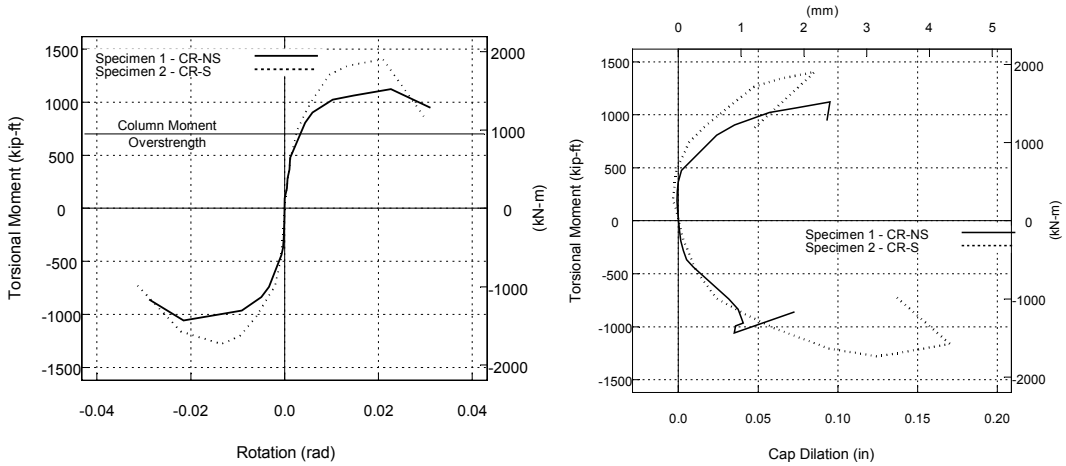

(a) Torsional Moment- Rotation Curve **(b) Torsional Moment-Dilation Curve**

Figure 4-74 Global Response Correlation

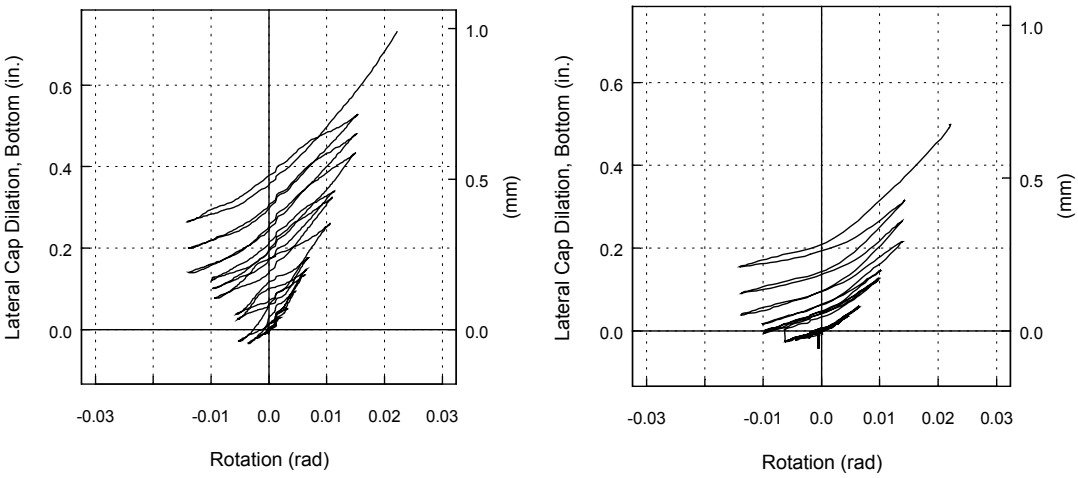

(a) Specimen 1–CR-NS **(b)** Specimen 2–CR-S

Figure 4-75 Lateral Bent Cap Dilation, Lead Face, Bottom

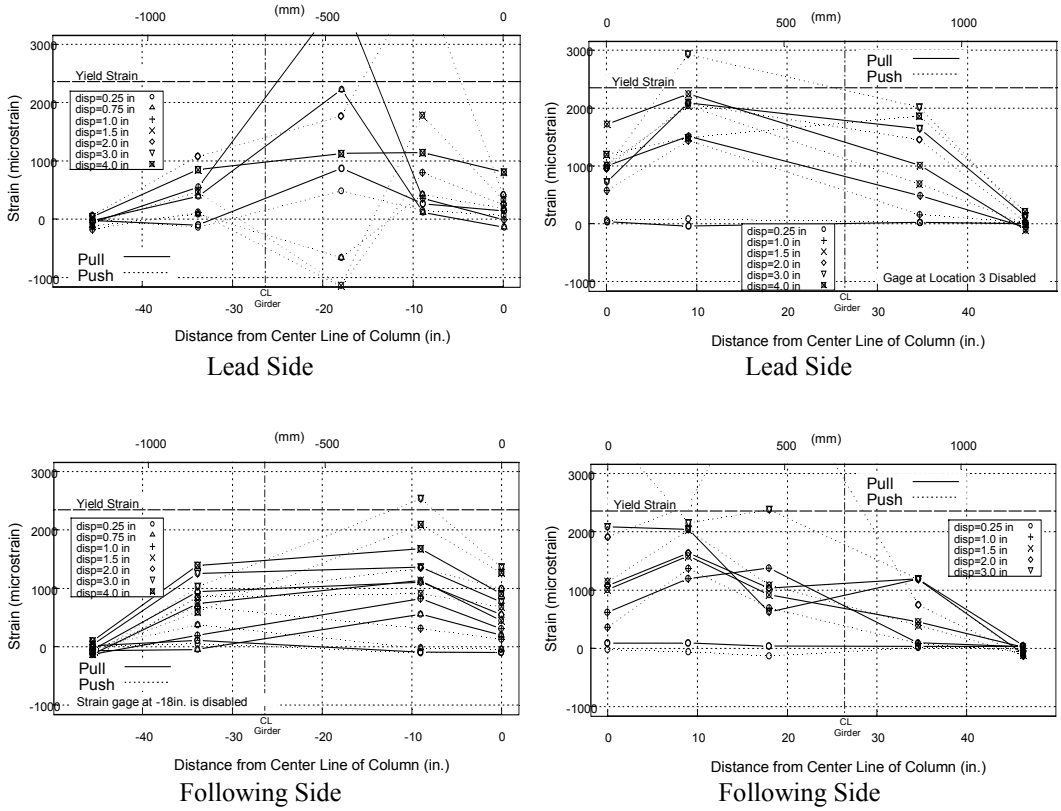

Specimen 1–CR-NS **Specimen 2–CR-S**

Figure 4-76 Measured Strain in Flexural Reinforcement at Bottom Corners of Bent Cap

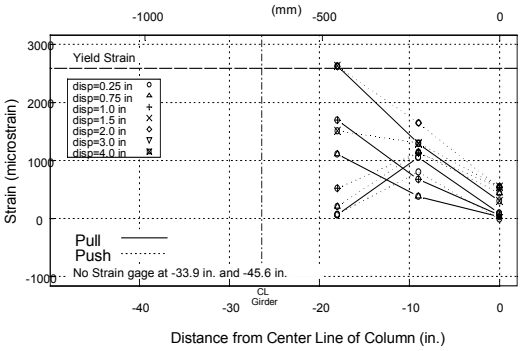

Vertical Leg, Lead Side

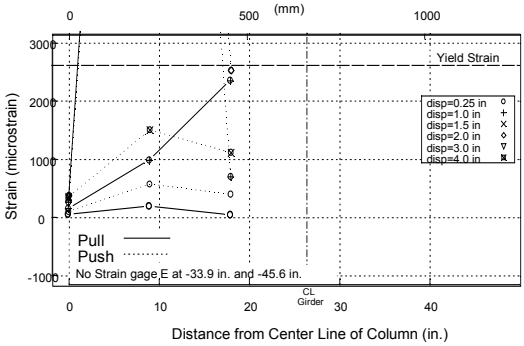

Vertical Leg, Lead Side

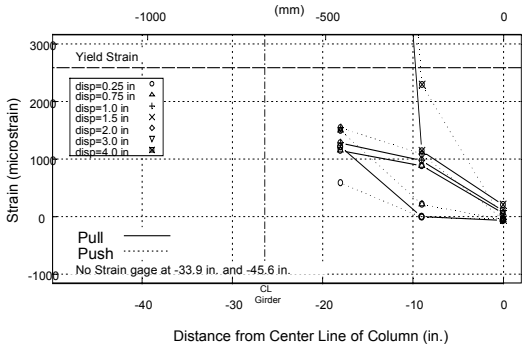

Horizontal Leg, Following Side

Specimen 1–CR-NS

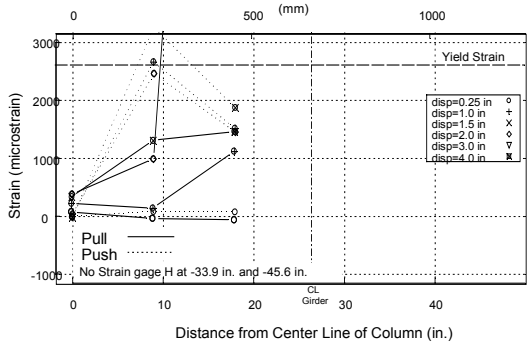

Horizontal Leg, Following Side

Specimen 2–CR-S

Figure 4-77 Measured Strain in Bent Cap Stirrups at the Bottom Corners of Bent Cap

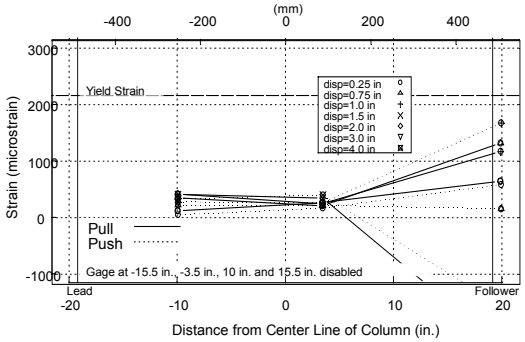

Top Flange

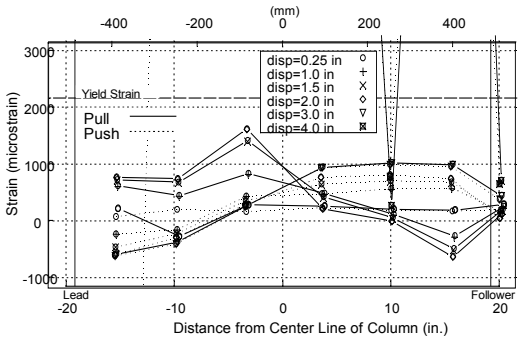

Top Flange

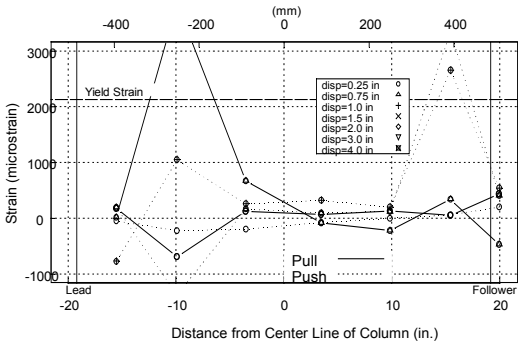

Bottom Flange

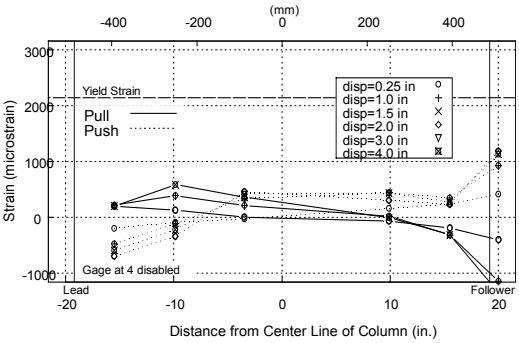

Bottom Flange

Specimen 1–CR-NS **Specimen 2–CR-S**

Figure 4-78 Measured Strain in Girder Flange

4.7.2 Correlation of Specimen 1 (CR-NS) and Specimen 3 (PT-NS)

By comparing Specimen CR-NS and Specimen PT-NS, the effect of bent cap post-tensioning can be assessed. Bent cap damage at the design level is compared in Figure 4-79. Spalling has initiated on the bent cap lead and bottom faces of Specimen CR-NS. The spalling is located near the girder flanges on the lead face and near the column on the bottom face. The lead face of Specimen PT-NS has significant cracking near the girder but no spalling. Spalling has initiated on the bottom face near the column.

The two specimens are compared at their maximum moments in Figure 4-80. Significant spalling has occurred on the lead face near the girder in both specimens. Bent cap damage of Specimen CR-NS is significant under the steel girder, with major portions of concrete spalled off exposing flexural reinforcement and girder shear studs. Damage to the underside of the bent cap in Specimen PT-NS is concentrated near the column, with the portion of concrete under the steel girder still intact. Damage to the deck of both specimens is limited to cracking.

The specimens at their failure load are shown in Figure 4-81. Significant spalling has occurred on the lead and follower faces as well as the bent underside in both specimens. The failure mechanism in both specimens is a shear-friction failure plane inclined along the initial torsion spiral crack. Deck damage in both specimens is limited to cracking.

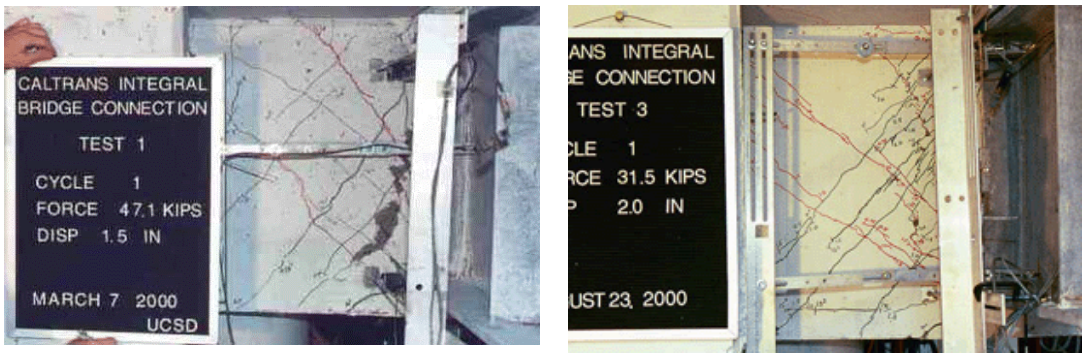

(a) Lead Face

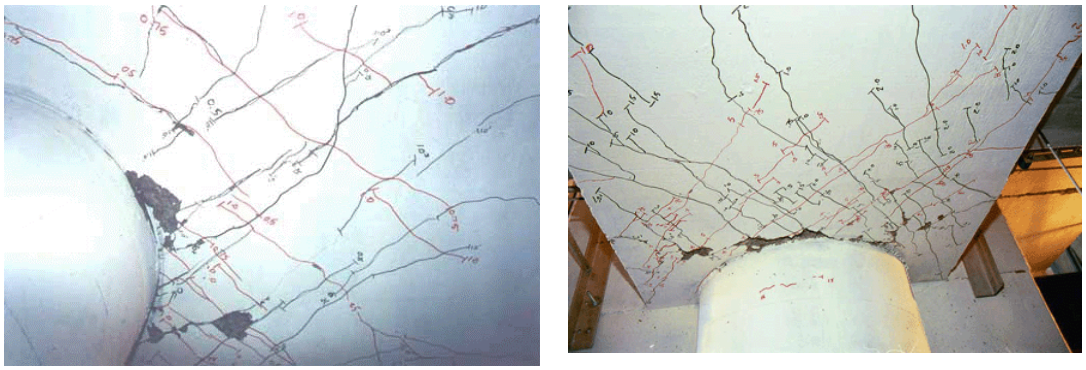

(b) Bottom Face

Specimen 1-CR-NS **Specimen 3-PT-NS**

Figure 4-79 Damage Comparison at Bent Cap Rotation=0.01 radians

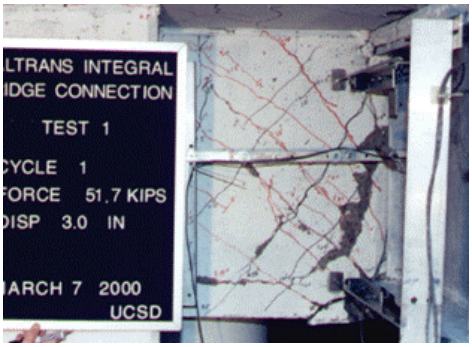

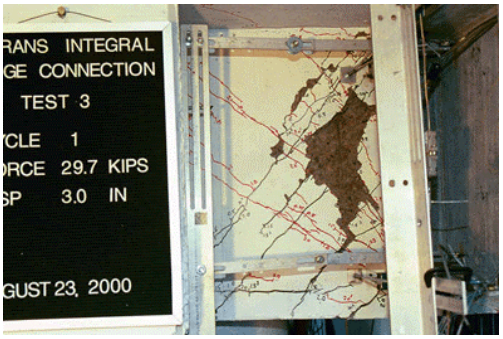

(a) Lead Face

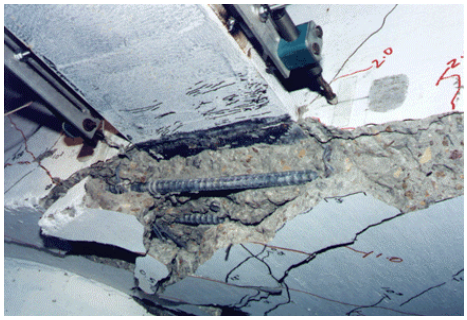

(b) CR-NS Girder/Lead Face

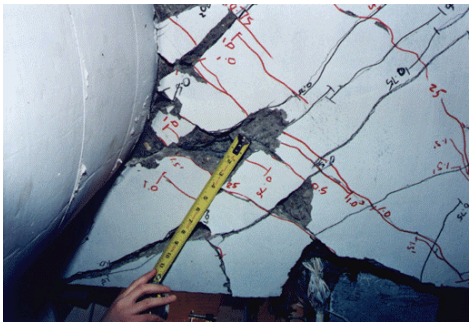

(c) CR-NS Bottom Face
Specimen 1-CR-NS

(d) PT-NS Bottom Face
Specimen 3-PT-NS

Figure 4-80 Damage Comparison at Bent Cap Rotation=0.02radians

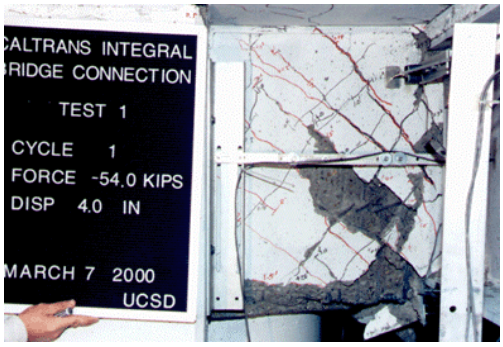

(a) Lead Face

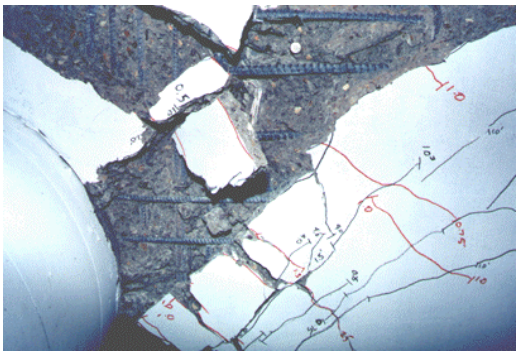

(b) Bottom Face

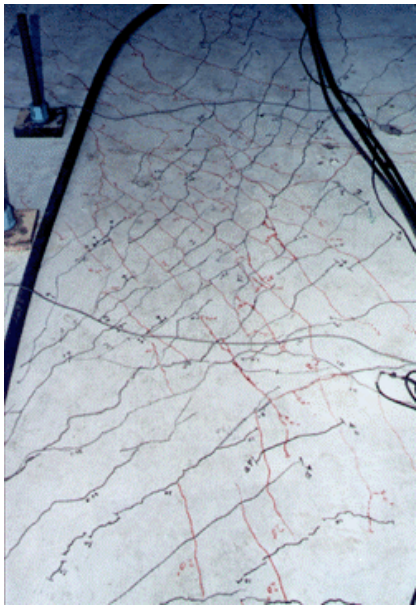

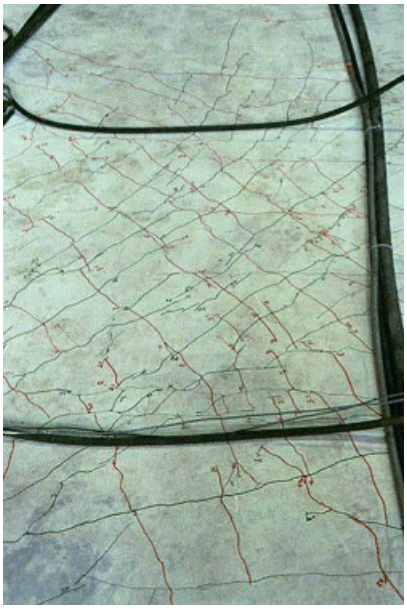

(c) Top Face (deck)

Specimen 1-CR-NS **Specimen 3-PT-NS**

Figure 4-81 Damage Comparison at Bent Cap Rotation=0.03 radians (Failure)

Figure 4-82 compares the global behavior of Specimen CR-NS and Specimen PT-NS. The maximum torsional moment of Specimen CR-NS was approximately 5% higher than the maximum torsional moment of Specimen PT-NS. This is because of the low post-tensioning force in the bent cap post-tensioning of Specimen PT-NS. Both specimens converged to nearly the same maximum torsional rotation and corresponding torsional moment. In the pull direction of loading, bent cap dilation in Specimen CR-NS began to increase immediately following first cracking. Once a maximum moment of 1,000 k-ft [1,355 kN-m] was reached, dilation of Specimen CR-NS was approaching 0.05 in. [1.3 mm]. Contrarily, dilation in Specimen PT-NS was only 0.01 in. [0.6 mm] at 1,000 k-ft [1,355 kN-m] at which point, the dilation increased while the moment remained constant.

Bent cap dilation in the transverse direction (longitudinal bridge direction) of the specimens is compared in Figure 4-83. At a corresponding rotation, the bent cap of Specimen CR-NS dilates laterally approximately 1.7 times more than the bent cap of Specimen PT-NS.

The measured strain in the flexural reinforcement at the bottom corners of both bent caps are shown in Figure 4-84. In both specimens, the maximum strains occur between the column face and girder face.

Strains at selected stirrup locations are shown in Figure 4-85. The top two graphs compare the strains in the vertical leg of stirrups near the bent cap lead actuator face. Stirrups in both specimens have the highest strains near the girders. This location in both specimens reached yield at approximately their respective maximum torsional moments.

Figure 4-86 compares the flange behavior of Specimen CR-NS and Specimen PT-NS. Flange strains in Specimen CR-NS were erratic. The bottom flanges of both specimens yielded near the bent cap face at low torsional rotation (less than 0.01 radians).

By comparing Specimen CR-NS and PT-NS, the difference in performance is attributed solely to the method bent cap reinforcement. While the conventionally reinforced bent cap achieved higher maximum moments, this conclusion is cautioned due to the level of uncertainty of the actual post-tensioning force in the bent cap. The post-tensioning was effective in reducing bent cap dilations in both the longitudinal and transverse bridge directions.

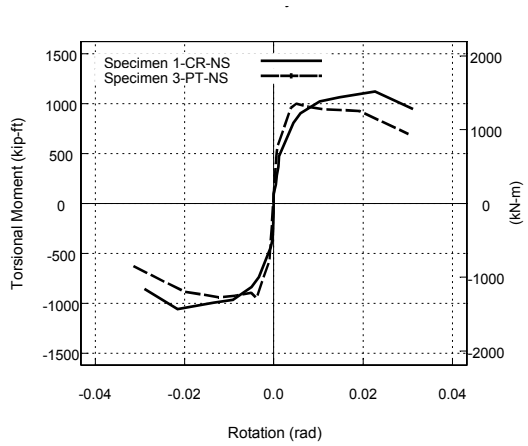

(a) Torsional Moment- Rotation Curve

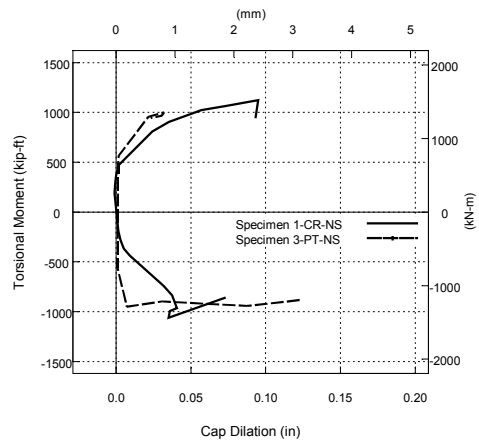

(b) Torsional Moment-Dilation Curve

Figure 4-82 Global Response Correlation

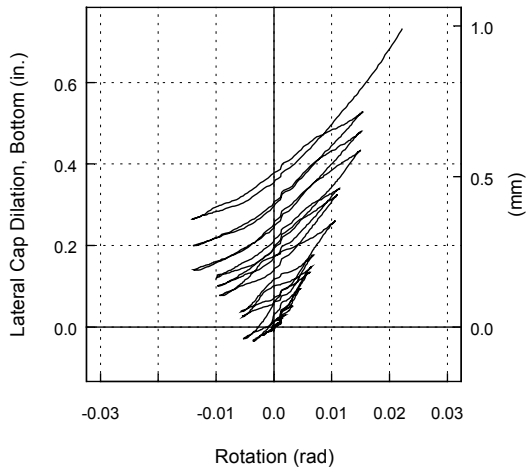

(a) Specimen 1–CR-NS

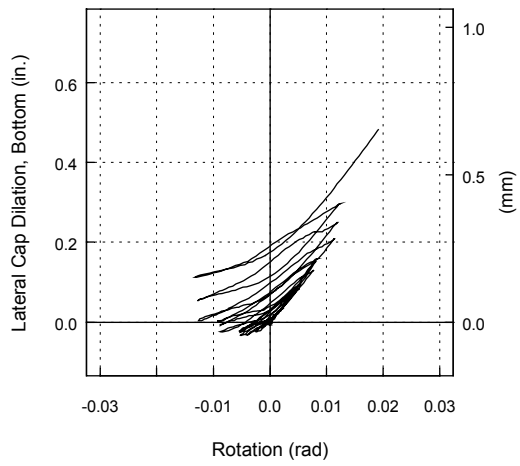

(b) Specimen 3–PT-NS

Figure 4-83 Lateral Bent Cap Dilation, Lead Face, Bottom

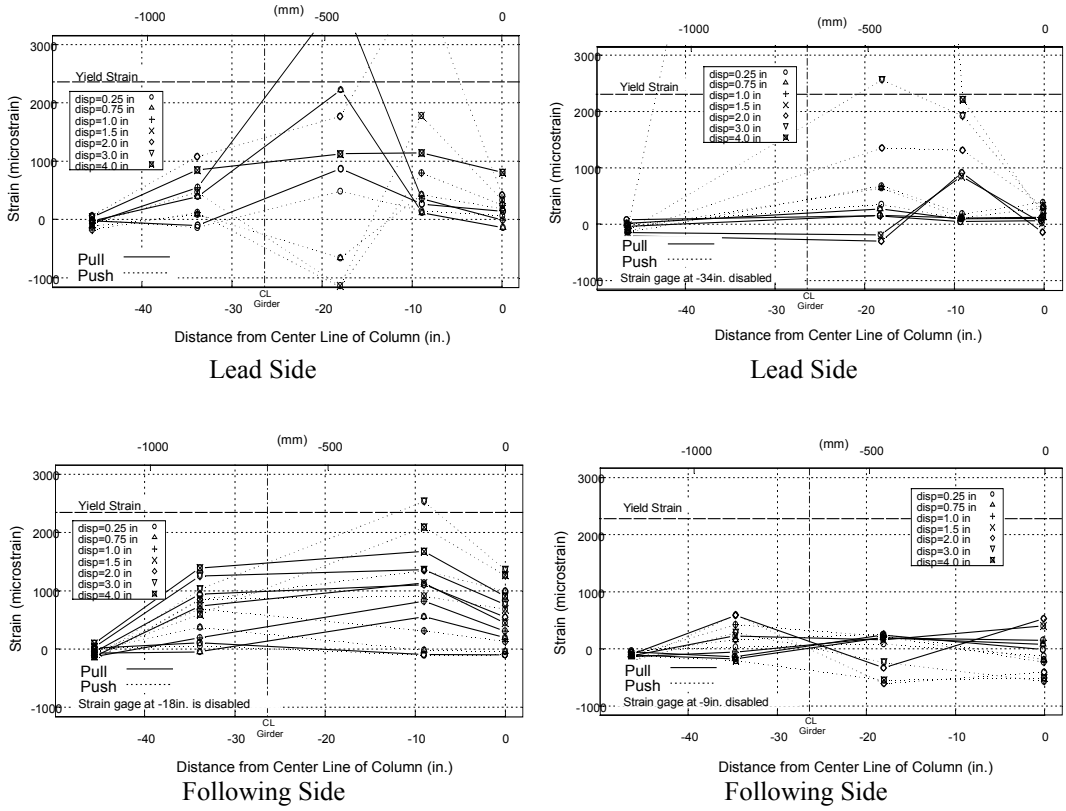

Specimen 1–CR-NS **Specimen 3–PT-NS**

Figure 4-84 Measured Strain in Flexural Reinforcement at Bottom Corners of Bent Cap

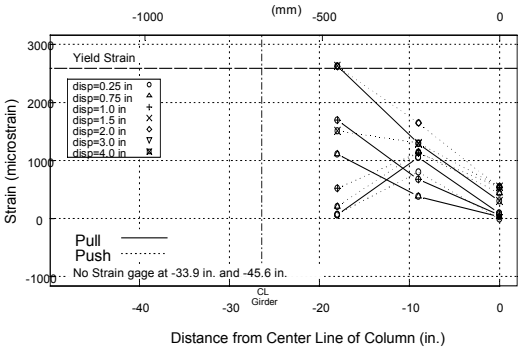

Vertical Leg, Lead Side

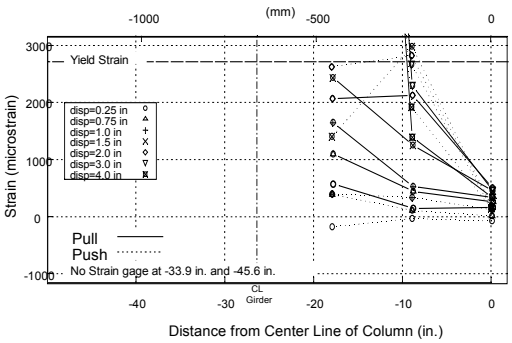

Vertical Leg, Lead Side

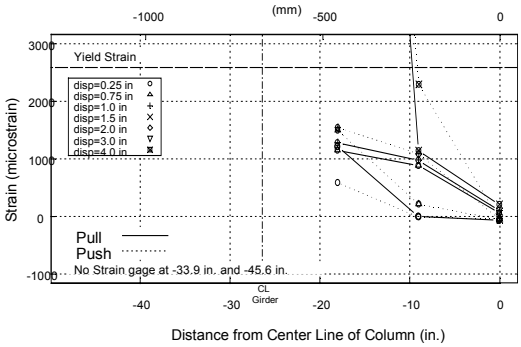

Horizontal Leg, Following Side

Specimen 1–CR-NS

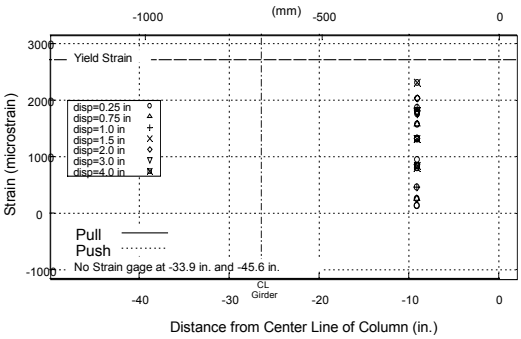

Horizontal Leg, Following Side

Specimen 3–PT-NS

Figure 4-85 Measured Strain in Bent Cap Stirrups at the Bottom Corners of Bent Cap

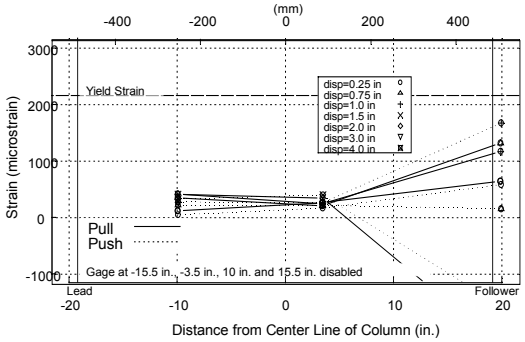

Top Flange

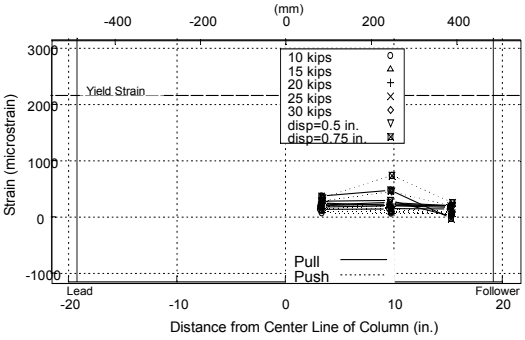

Top Flange

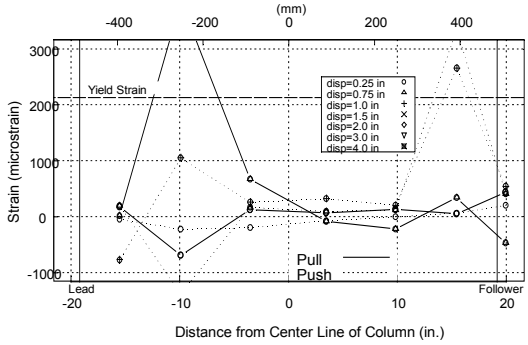

Bottom Flange

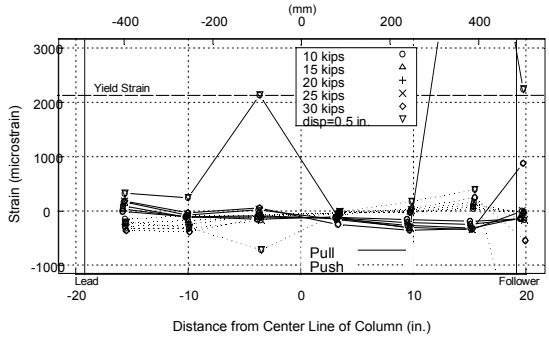

Bottom Flange

Specimen 1–CR-NS **Specimen 3–PT-NS**

Figure 4-86 Measured Strain in Girder Flange

4.7.3 Correlation of Specimen 2 (CR-S) and Specimen 4 (PT-S)

The difference between Specimen 2 and Specimen 4 was the bent cap reinforcing method. Specimen 2 was a conventionally reinforced bent cap, meaning that the flexural strength was provided by Grade 60 reinforcing steel. The bent cap flexural strength of Specimen 4 was provided by post-tensioning. This section investigates how bent cap torsional response of stiffened sections is affected by method of flexural reinforcement.

The bent caps of both specimens are shown in Figure 4-87 at the design torsional moment. Damage in both specimens is limited to cracking with the exception of minor bent cap spalling on the underside near the column of Specimen CR-S. The extent of cracking in Specimen PT-S is significantly less at this load level than in Specimen CR-S.

At the maximum moment, the failure plane in both specimens is clearly visible on the lead face (Figure 4-88). In Specimen CR-S, the failure plane is a vertical plane at the edge of the girder flanges. The failure plane of Specimen PT-S is inclined aligned with the initial spiral crack inclination. Damage on the underside of both specimens is limited spalling concentrated near the column. The failure plane in Specimen CR-S is visible on the deck surface. Deck damage in Specimen PT-S is limited to cracking.

Both specimens are shown at failure in Figure 4-89. Significant portions of concrete have spalled off the lead face of both specimens. Major spalling has also occurred on the underside of both bent caps near the column. In Specimen PT-S, major cracking on the underside of the bent is aligned with the steel girder. The vertical failure plane of Specimen CR-S is apparent from the deck while damage to the deck of Specimen PT-S is limited to cracking.

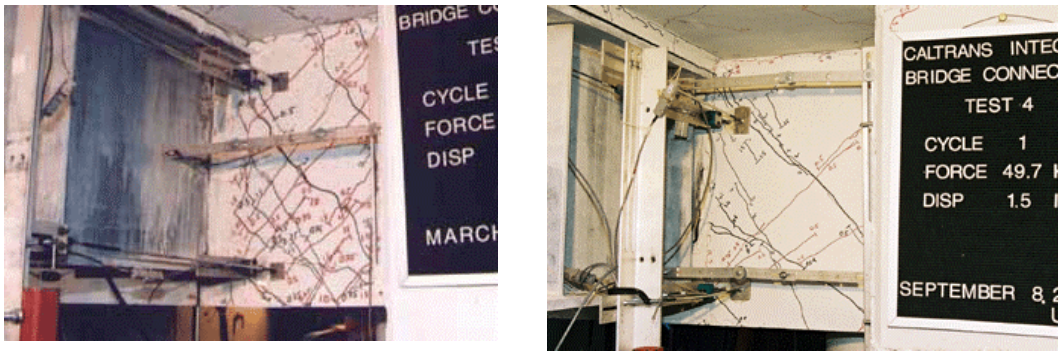

(a) Lead Face

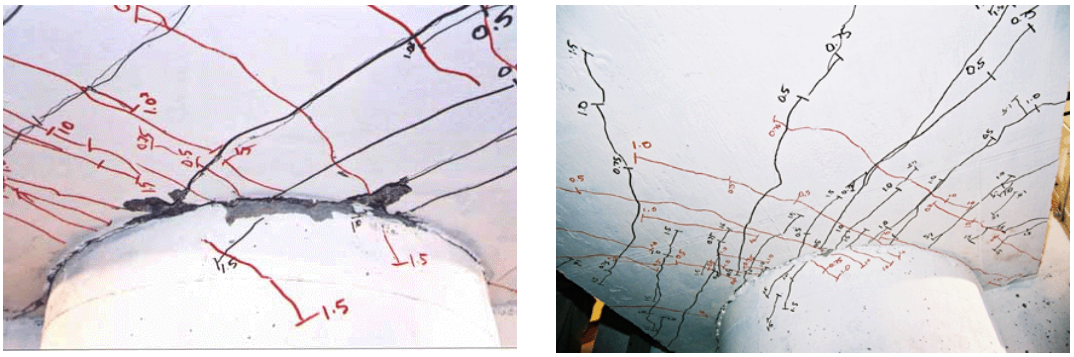

(b) Bottom Face

Specimen 2-CR-S **Specimen 4-PT-S**

Figure 4-87 Damage Comparison at Bent Cap Rotation=0.01 radians

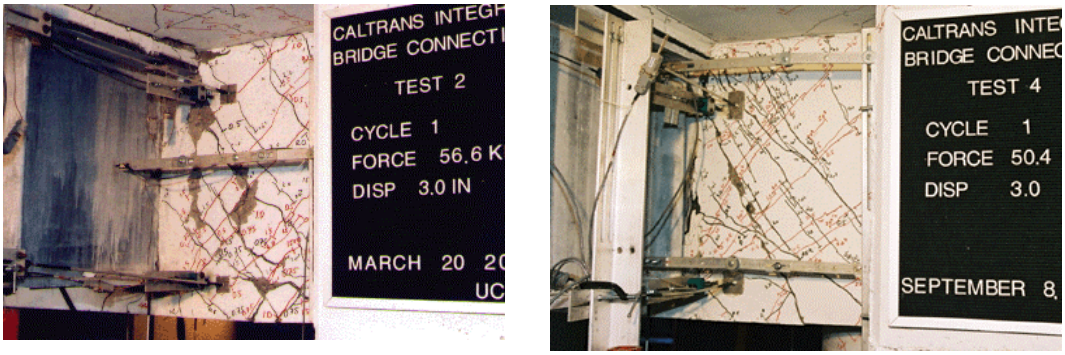

(a) Lead Face

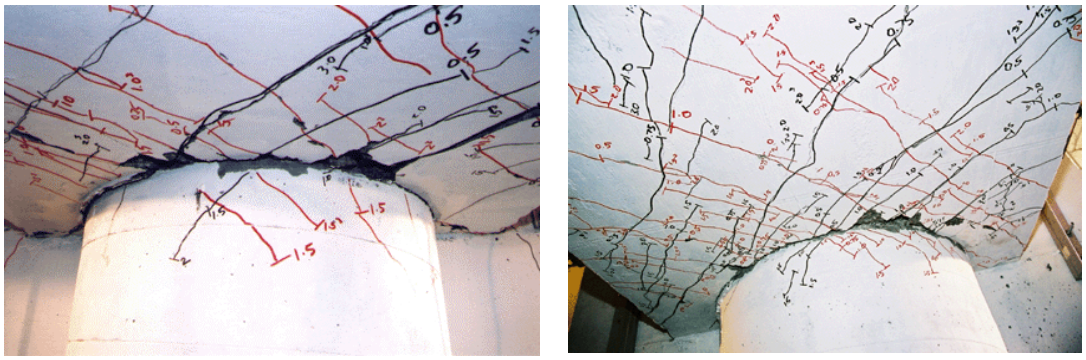

(b) Bottom Face

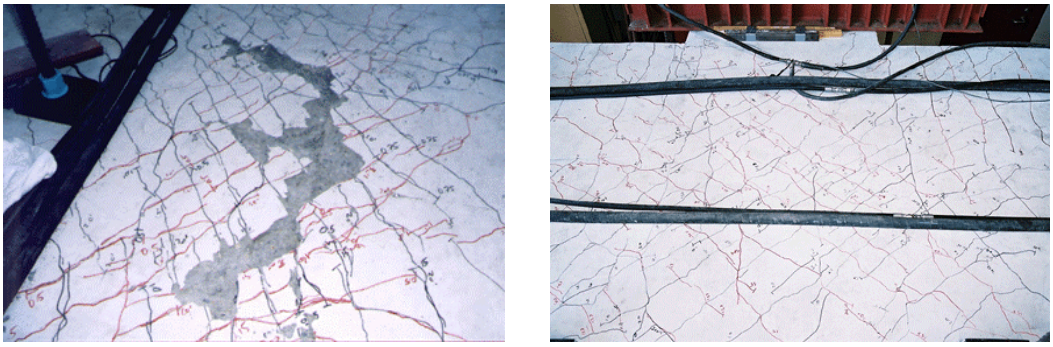

(c) Top Face (deck)

Specimen 2-CR-S **Specimen 4-PT-S**

Figure 4-88 Damage Comparison at Bent Cap Rotation=0.02 radians

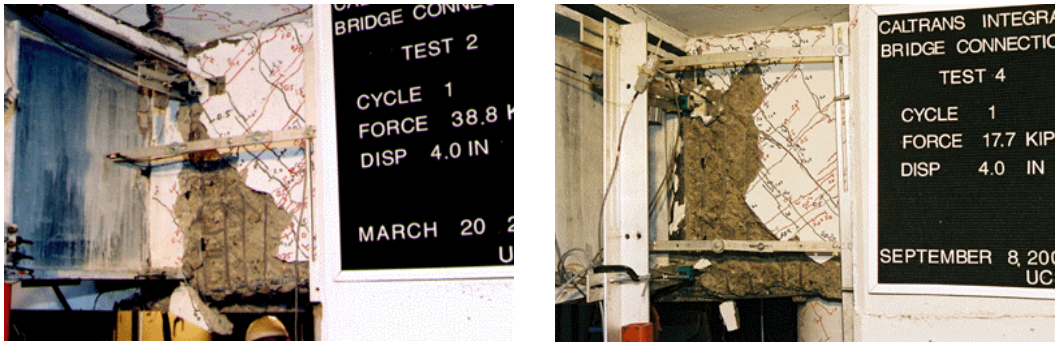

(a) Lead Face

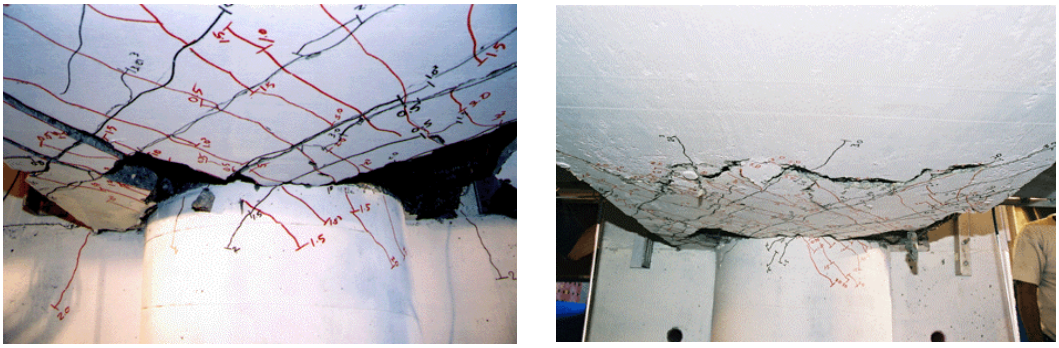

(b) Bottom Face

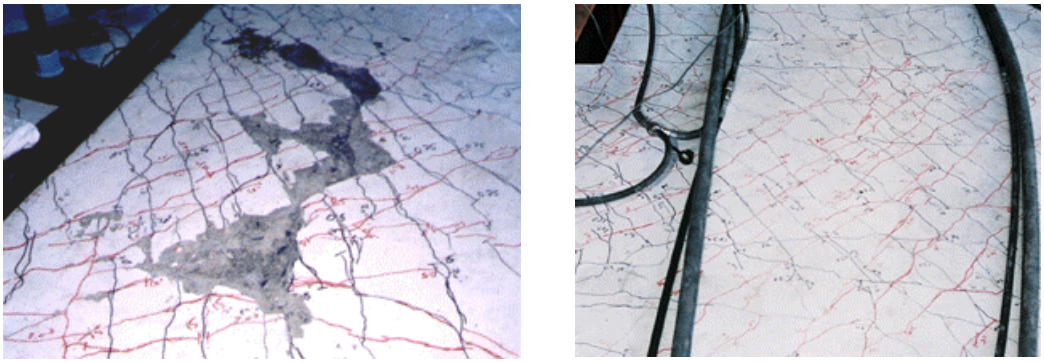

(c) Top Face (deck)

Specimen 2-CR-S **Specimen 4-PT-S**

Figure 4-89 Damage Comparison at Bent Cap Rotation=0.03 radians (Failure)

Figure 4-90 compares the global performance of the two bent caps. The maximum torsional moment and ultimate rotation of each specimen were very similar. However, the initial slope of the moment rotation response of Specimen PT-S was much steeper than that of Specimen CR-S. The advantage of the steeper moment rotation relation was less crack dilation for specimen PT-S during the initial stages of loading, as is illustrated in the torsional moment-dilation curve of Figure 4-90. The transverse bent cap dilation between Specimen CR-S and Specimen PT-S is compared in Figure 4-91. The dilation of the post-tensioned bent cap is approximately half the dilation of the conventionally reinforced bent cap.

The behavior of flexural reinforcement in the bottom corners of the bent cap is shown in Figure 4-92. Strains outside the joint region of Specimen PT-S were lower than strains at the same location in Specimen CR-S. Rebar in both specimens experienced the highest strain deformation at the column face.

Flange performance of Specimen CR-S versus Specimen PT-S is illustrated in Figure 4-93. The tensile strains in the bottom flange of Specimen PT-S were higher than in Specimen CR-S but the compressive strains were similar. The top flange of Specimen CR-S experienced the highest strains toward the center of the bent cap. The top flange of Specimen PT-S experienced the highest strains at the face of the bent cap.

Stiffener behavior of Specimen CR-S and Specimen PT-S are plotted in Figure 4-94. Stiffener deformation was greater in stiffeners located near the bent cap face.

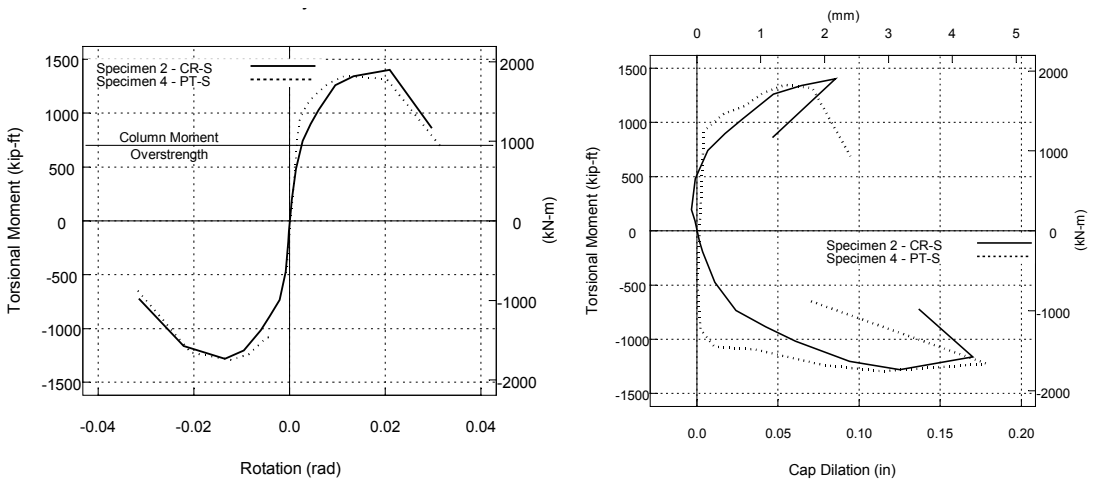

(a) Torsional Moment- Rotation Curve (b) Torsional Moment-Dilation Curve

Figure 4-90 Global Response Correlation

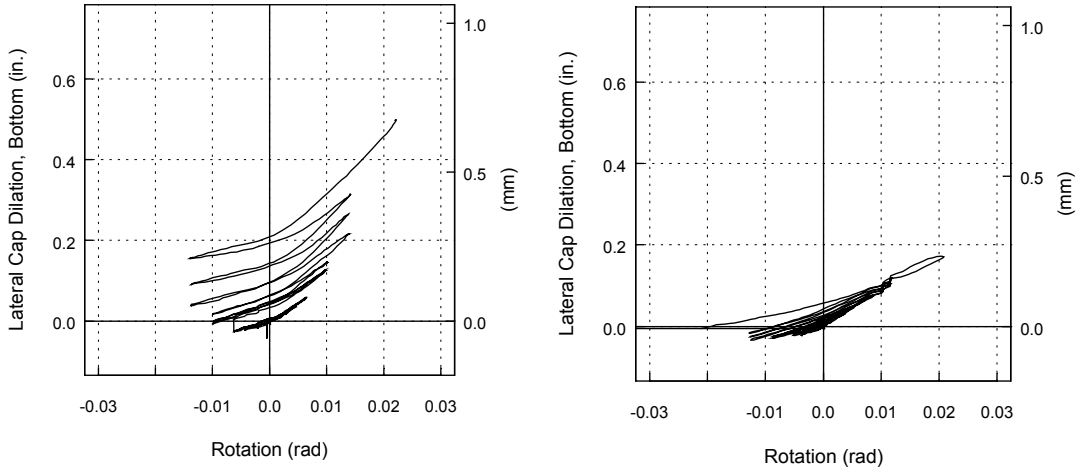

(a) Specimen 2–CR-S **(b) Specimen 4–PT-S**

Figure 4-91 Transverse Bent Cap Dilation

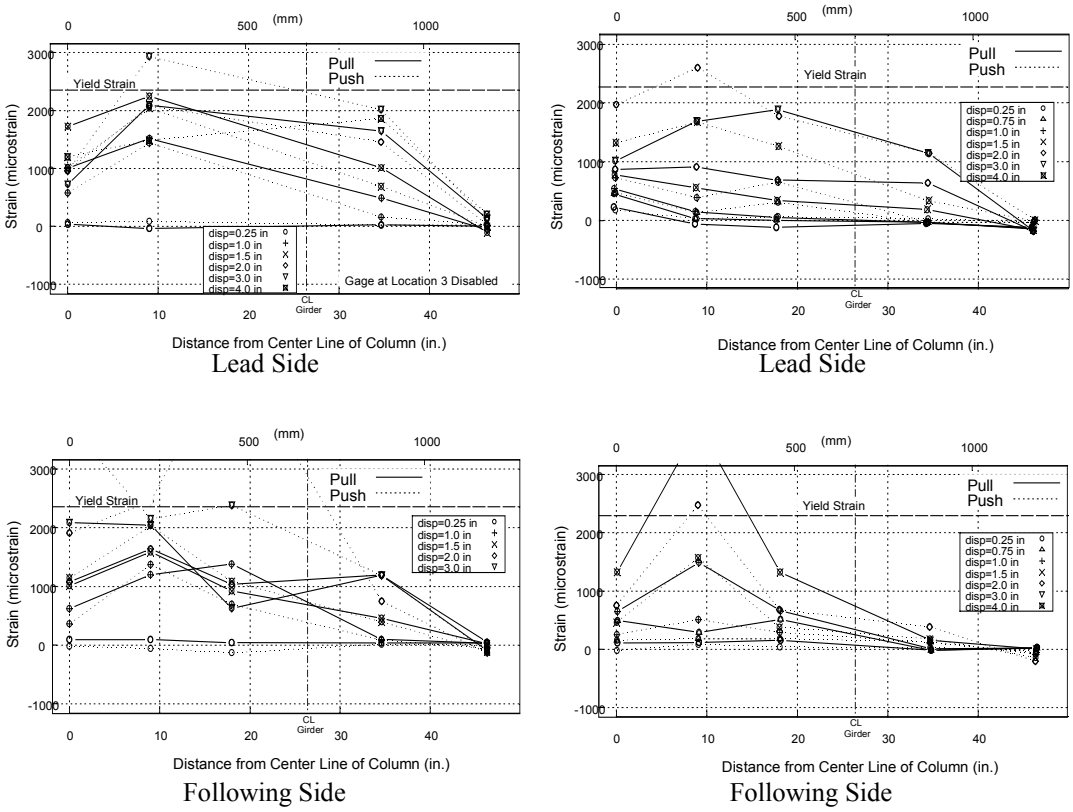

Specimen 2–CR-S **Specimen 4–PT-S**

Figure 4-92 Measured Strain in Flexural Reinforcement at Bottom Corners of Bent Cap

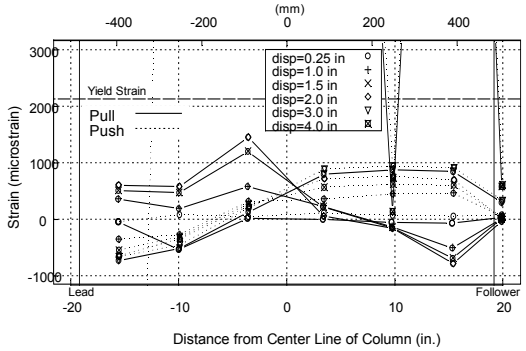

Top Flange

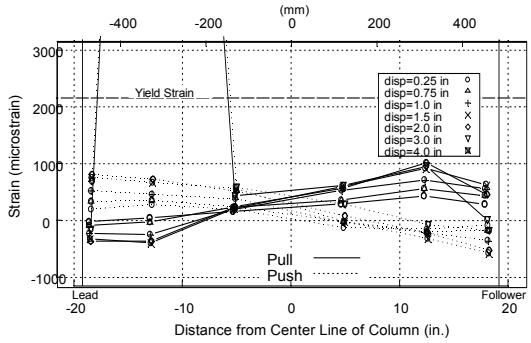

Top Flange

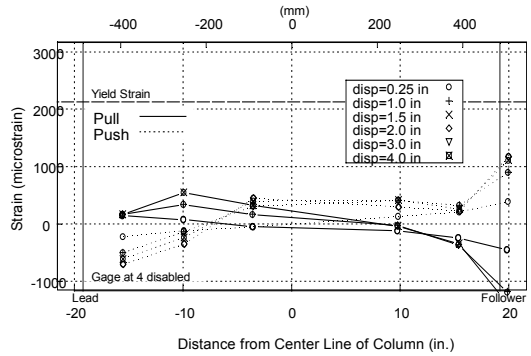

Bottom Flange

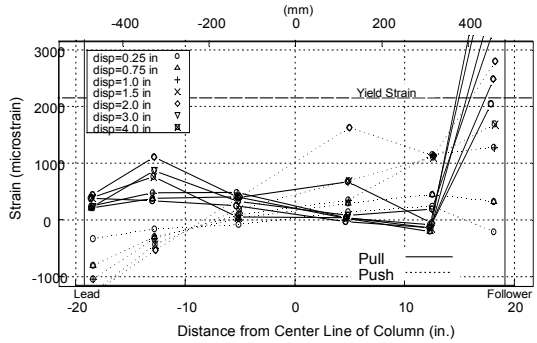

Bottom Flange

Specimen 2–CR-S **Specimen 4–PT-S**

Figure 4-93 Measured Strain in Girder Flanges

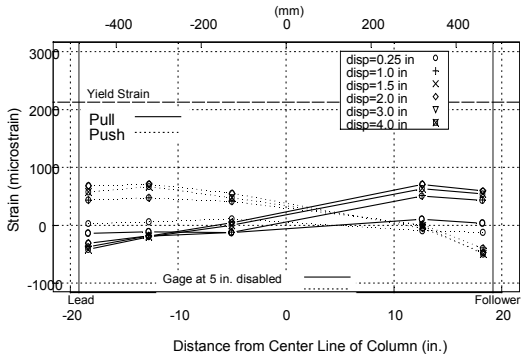

Top

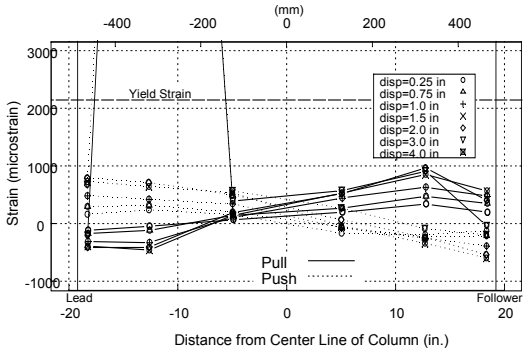

Top

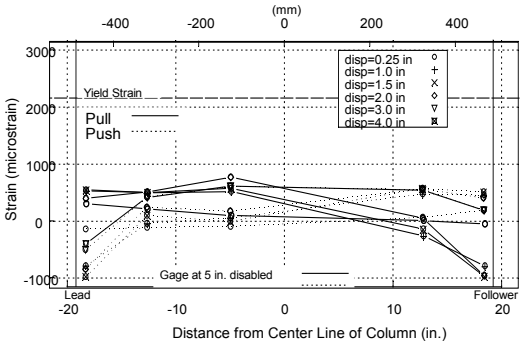

Bottom

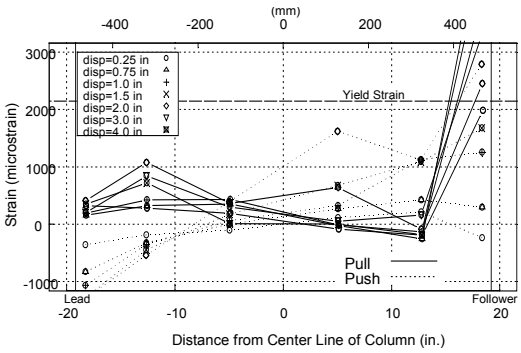

Bottom

Specimen 2–CR-S **Specimen 4–PT-S**

Figure 4-94 Stiffener Behavior

4.7.4 Correlation of Specimen 3 (PT-NS) and Specimen 4 (PT-S)

Damage to the bent caps of Specimen PT-NS and Specimen PT-S at the design moment are compared in Figure 4-95. Damage at this load level is limited to cracking with the exception of minor spalling on the bottom face near the column of Specimen PT-NS. Cracking in Specimen PT-S is minimal and cracking in Specimen PT-NS is minimal with a significant amount of cracks occurring on the bent cap face near the girder.

Specimen damage at the maximum moment is compared in Figure 4-96. Significant spalling has occurred on the lead face of Specimen PT-NS near the girder and a major crack has developed on the lead face of Specimen PT-S. Damage to the bottom face of Specimen PT-NS is a significant crack with spalling located near the column. In Specimen PT-S, damage to the underside of the bent cap is limited to minor spalling near the column. Deck damage of both specimens at this load level is limited to cracking.

At the failure load, both specimens have experienced major spalling on the bent cap face (Figure 4-89). The spalling is over the height of the girder at the girder and tapers to a point near the support block. The underside of Specimen PT-NS has spalled significantly, exposing shear reinforcement between the column and the girder. The underside of Specimen PT-S is significantly spalled near the column and a major crack aligned with the girder has developed. Damage to the deck of both specimens is limited to cracking.

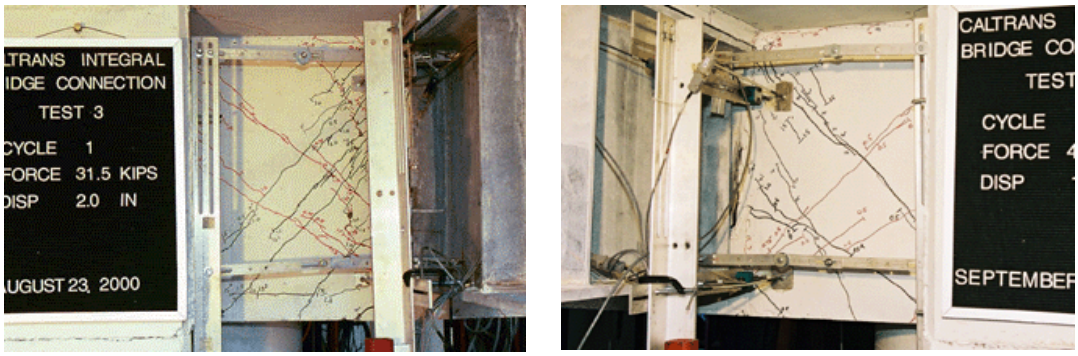

(a) Lead Face

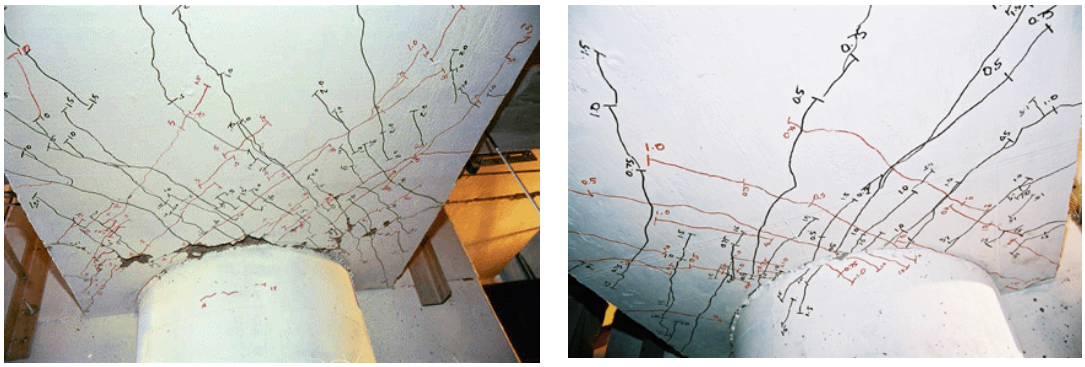

(b) Bottom Face

Specimen 3-PT-NS **Specimen 4-PT-S**

Figure 4-95 Damage Comparison at Bent Cap Rotation=0.01 radians

(a) Lead Face

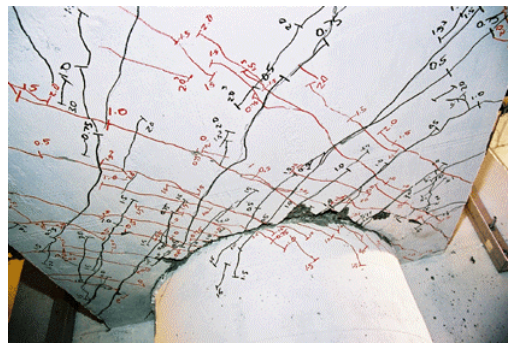

(b) Bottom Face

Specimen 3-PT-NS **Specimen 4-PT-S**

Figure 4-96 Damage Comparison at Bent Cap Rotation=0.02radians

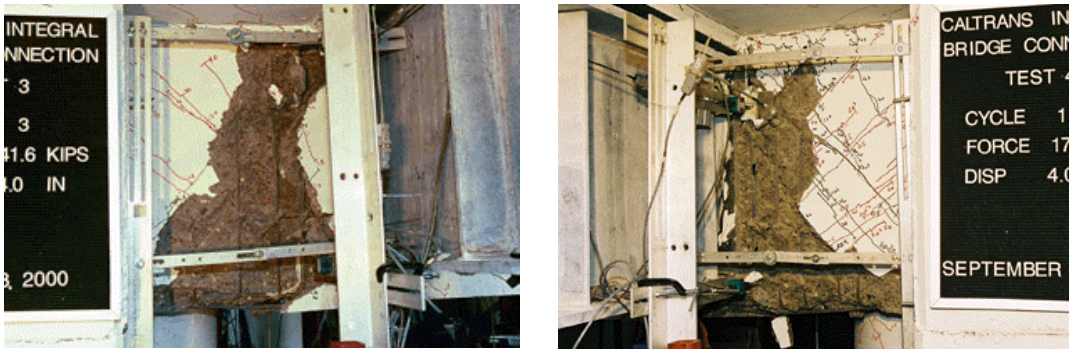

(a) Lead Face

(b) Bottom Face

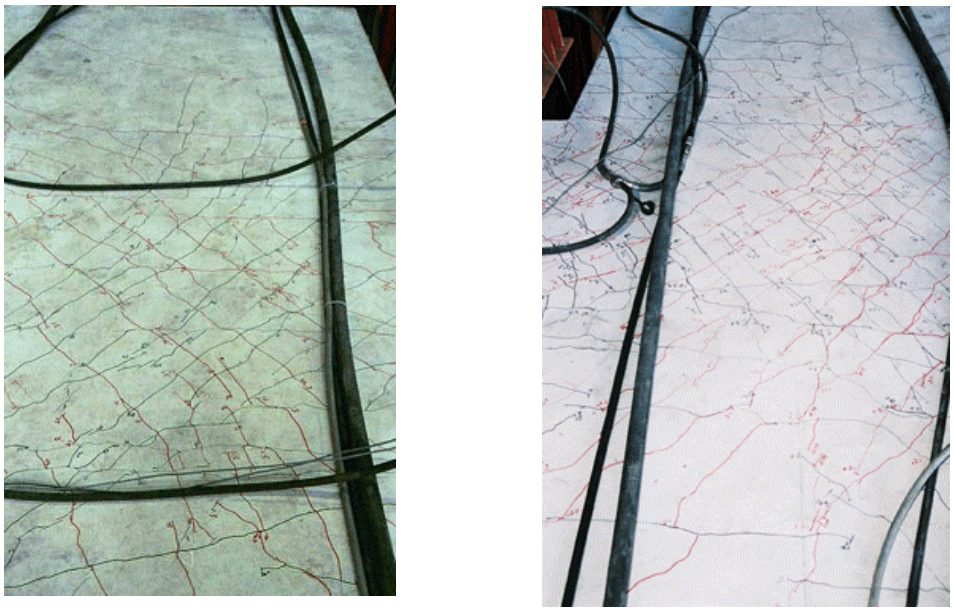

(c) Top Face (deck)

Specimen 3-PT-NS **Specimen 4-PT-S**

Figure 4-97 Damage Comparison at Bent Cap Rotation=0.03 radians (Failure)

Figure 4-98 compares the global behavior of Specimen PT-NS and Specimen PT-S. The maximum torsional moment of Specimen PT-S was approximately 25% higher than the maximum torsional moment of Specimen PT-NS. Both specimens converged to nearly the same maximum torsional rotation and corresponding torsional moment. Bent cap of both specimens was nearly zero until they reached their maximum moments, at which point, their moment leveled off while the dilation increased (Figure 4-98b).

Bent cap dilation in the transverse direction (longitudinal bridge direction) of the specimens is compared in Figure 4-99. At a corresponding rotation, the bent cap of Specimen PT-NS dilates laterally approximately 2.5 to 3 times more than the bent cap of Specimen PT-S.

The measured strain in the flexural reinforcement at the bottom corners of both bent caps are shown in Figure 4-100. In both specimens, the maximum strains occur between the column face and girder face.

Figure 4-101 compares the flange behavior of both specimens. The flanges of Specimen PT-NS yielded at very low rotations (less than 0.01 rads) while the flanges of Specimen PT-S didn't yield until near maximum torsional moment.

By comparing Specimen PT-NS and PT-S, the difference in performance due to the addition of stiffeners is assessed. The stiffeners increased the torsional moment capacity of the section by approximately 25%. The stiffeners decreased bent cap dilation in the longitudinal bridge direction however appeared to have no affect on dilation in the transverse bridge direction.

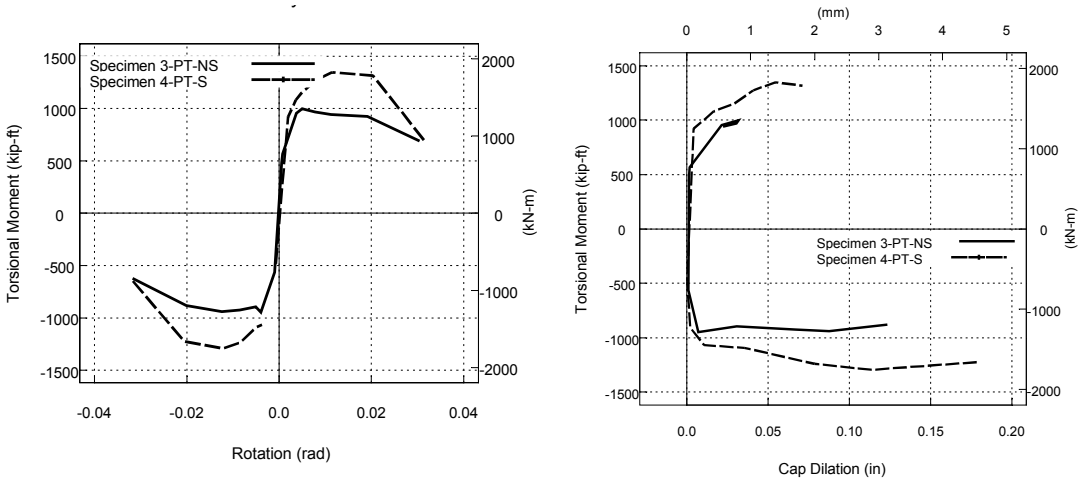

(a) Torsional Moment- Rotation Curve (b) Torsional Moment-Dilation Curve

Figure 4-98 Global Response Correlation

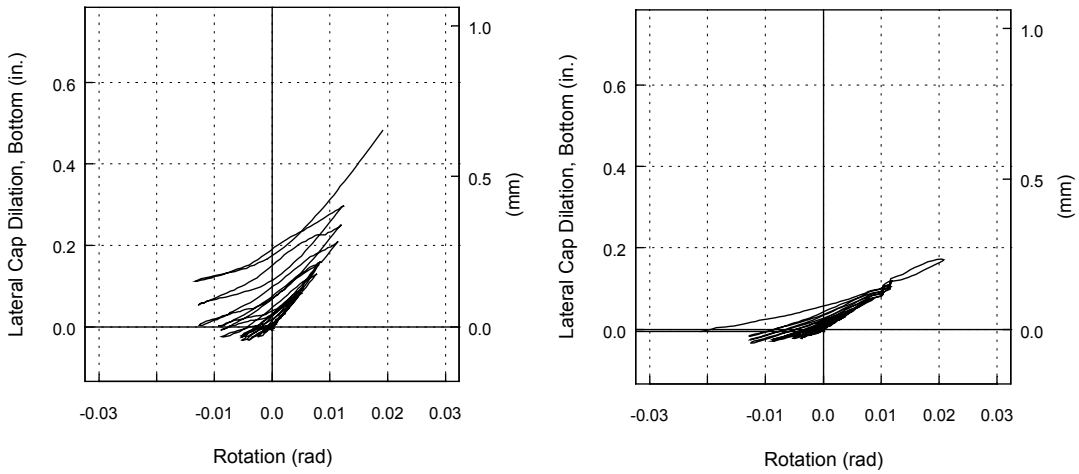

(a) Specimen 3–PT-NS **(b) Specimen 4–PT-S**

Figure 4-99 Transverse Bent Cap Dilation

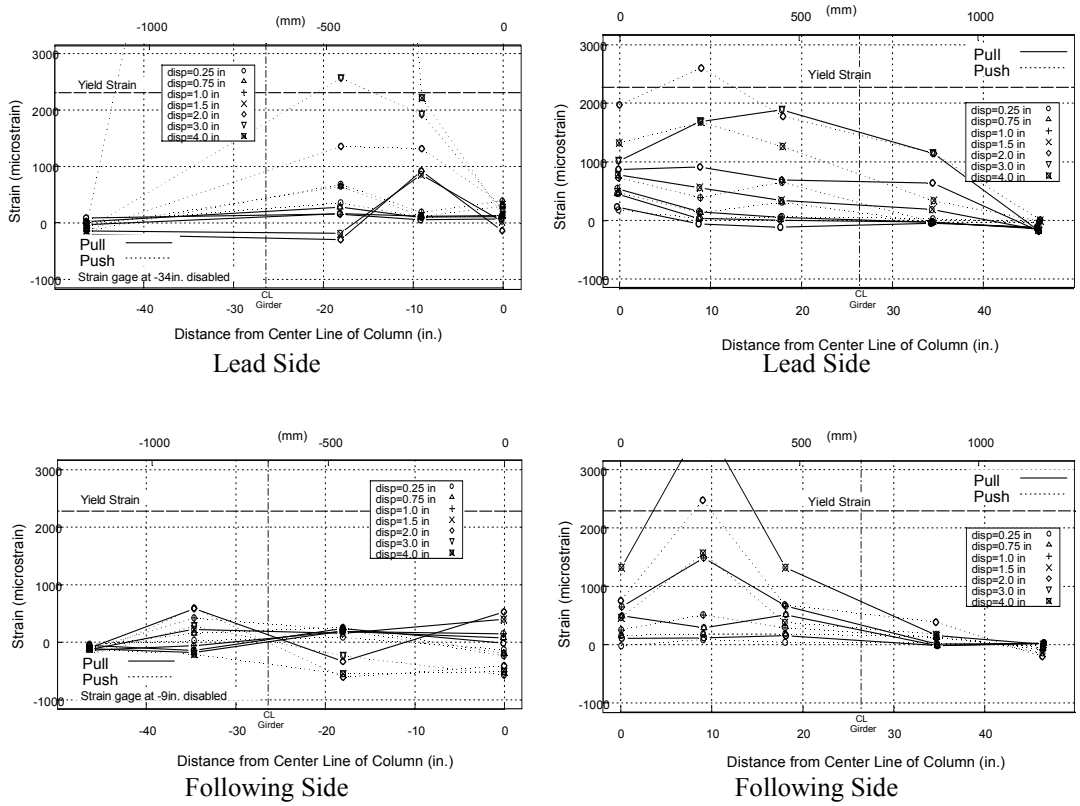

Specimen 3–PT-NS **Specimen 4–PT-S**

Figure 4-100 Measured Strain in Flexural Reinforcement at Bottom Corners of Bent Cap

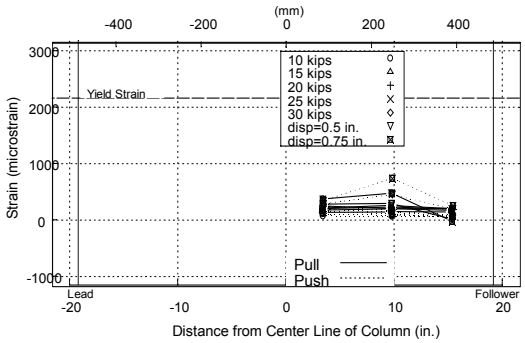

Top Flange

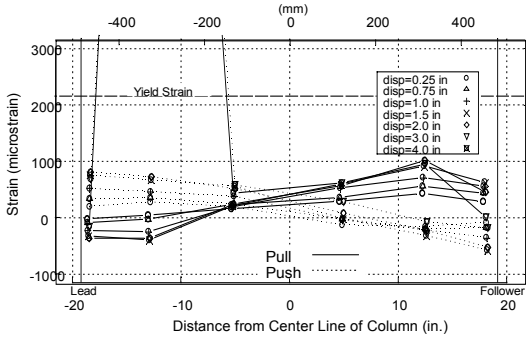

Top Flange

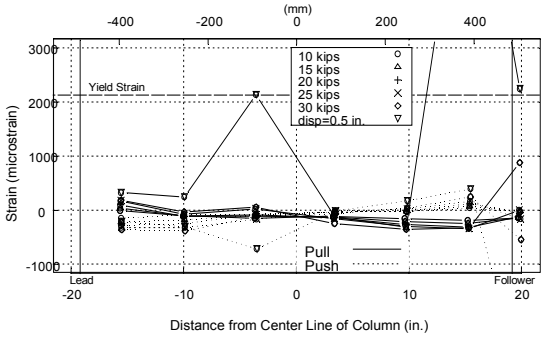

Bottom Flange

Specimen 3–PT-NS

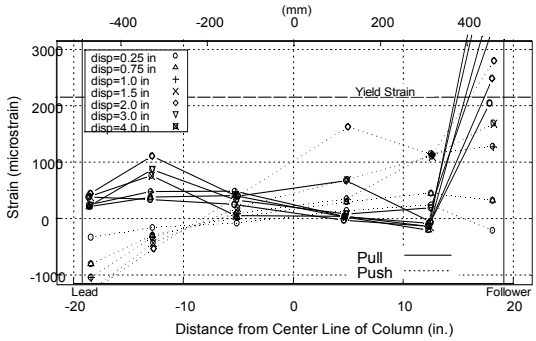

Bottom Flange

Specimen 4–PT-S

Figure 4-101 Measured Strain in Girder Flanges

4.8 SUMMARY

Based on the correlated test results presented in Section 4.7, the following conclusions can be made:

(1) Stiffeners increase the maximum torsional moment capacity of the section by approximately 25%.

(2) Strain sages on the outer stiffeners recorded the higher strains than strain gages located on the interior stiffeners, thus indicating the outer stiffeners contributed to the force transfer mechanism more than the interior stiffeners.

(3) Bent caps with stiffeners recorded approximately 1/3 of the bent cap dilation in the longitudinal bridge direction that the unstiffened sections recorded.

(4) Post-tensioned bent caps measured almost zero dilation along the transverse bridge direction up to maximum moment.

(5) Appearance of post-tensioned bent caps before maximum moment consisted of significantly less cracking.

(6) Post-tensioned bent cap is much more constructable than the conventionally reinforced bent cap.

Therefore, based on the component test findings, a post-tensioned bent cap with stiffeners on the girder in the cap region is recommended for the system test. It is recommended that the number of full height bearing stiffeners on the girder in the bent cap region be reduced from three pairs to a single pair.

Chapter 5

Development of System Test

5.1 OVERVIEW

This chapter presents the construction process and testing methods of the system test. Design of the connection detail is presented in Section 5.2. The boundary conditions used in the system test are explained in Section 5.3.1. Section 5.4 outlines the construction process of which photo documentation is presented in Appendix B. Section 5.5 presents the material properties. Section 5.6 explains the location of instrumentation and the chapter concludes with loading protocol in Section 5.7.

5.2 DESIGN OF CONNECTION DETAIL

Based on the experimental results of the component tests, a connection detail was designed to be tested in a system test. The recommendations of Chapter 4 are to post-tension the bent cap and provide a single pair of stiffeners at the face of the bent cap. The post-tensioning enhances the performance by minimizing bent cap cracking up to the maximum torsional moment. The connection detail to be tested in the system test is shown in Figure 5-1. It has a single pair of full height bearing stiffeners in the bent cap region located at the edges of the bent cap with minimal concrete cover. Post-tensioning in the form of high-strength rods provides the main flexural strength of the bent cap and is continuous over the length of the bent cap by passing through predrilled holes in the girder webs.

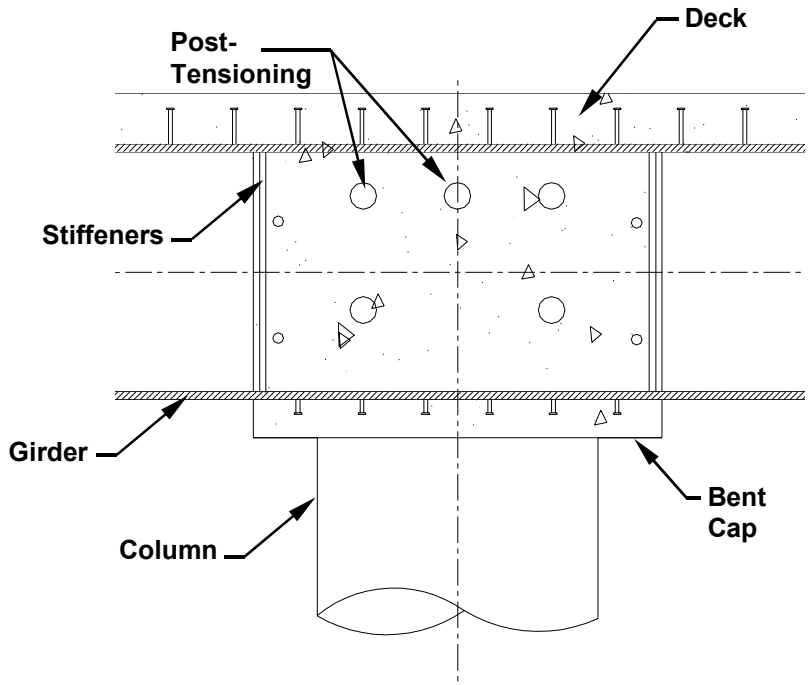

Figure 5-1 Recommended Connection Detail

5.3 DESIGN OF SYSTEM TEST SPECIMEN

The goal of the component tests was to load the bent cap to torsional failure in order to develop complete behavior profiles including failure mechanisms. In contrast, the goal of the system test was to have a flexural column failure and to record and observe bent cap damage levels as they corresponded to increasing column ductility levels. Where the component tests consisted of the bent cap with a single girder and an artificially stiffened column to prevent column failure, the system test featured the full bent cap width, four steel girders and a single column designed for flexural failure.

The system test specimen was constructed at 40% scale of Bent 3 of the prototype as in the component tests and was designed from recommendations based on the most promising component test results. The specimen was constructed in an inverted orientation (Figure 5-2 and Figure 5-3), with the specimen resting on rollers at the girder dead load inflection points.

The inverted setup was first designed by Dowell et al. (47) for testing the Terminal Separation Replacement structure. The advantage of the inverted test setup is that it is supported at the superstructure dead load inflection points (one fifth of the span) rather

than the superstructure seismic inflection points (one half the span). In addition to being compact, the setup is advantageous because one actuator, located at the column seismic inflection point (column mid-height), applied the seismic load to the system. Since the dead load moment is created by stressing vertical rods from the column load stub to the laboratory strong floor, application of the dead load and seismic load is separate and effectively uncoupled. Applying the load at the column seismic inflection point also reduces the vertical dimension of the setup.

Figure 5-2 System Test Specimen

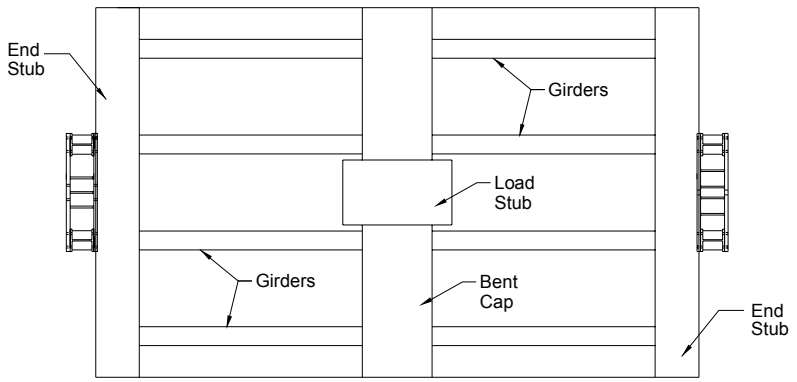

Plan

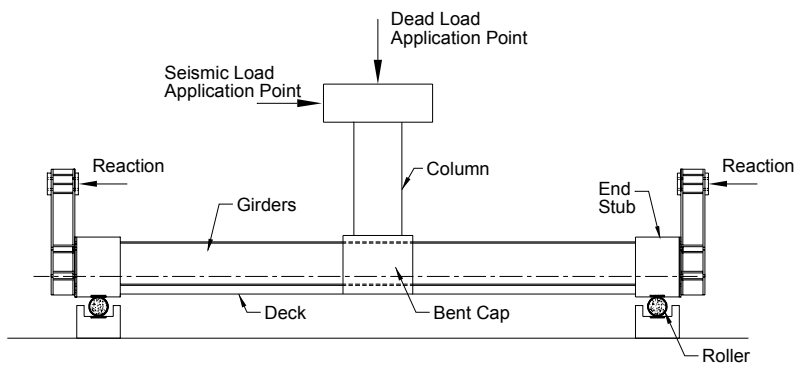

Elevation

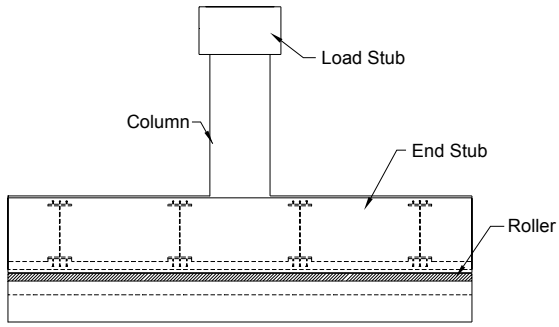

End View

Figure 5-3 System Test Specimen Geometry

5.3.1 Boundary Conditions

A schematic of the test setup with all the loading fixtures is shown in Figure 5-4. To understand the system test boundary conditions, the prototype dead load deflected shape and moment diagrams are shown in Figure 5-5a and Figure 5-5b. Between the inflection points, the deflected shape due to self-weight can be approximated as a simply supported beam with an upward point load at the center (Figure 5-5c). The value of the point load required to produce the moment, M is solved for in $M=PL/4$. The dead load moment is created in the test specimen by stressing post-tensioning bars to a value of P from the top of the column load stub to the laboratory strong floor (Figure 5-4). With the specimen horizontally restrained at the strong wall and vertically supported at both rollers, the specimen is free to translate horizontally, thus inducing no moment in the superstructure. For the dead load to remain constant during seismic loading, the rods were attached to a rocker at the top of the column (**Error! Reference source not found.**). The load was monitored with a load cell on one rod.

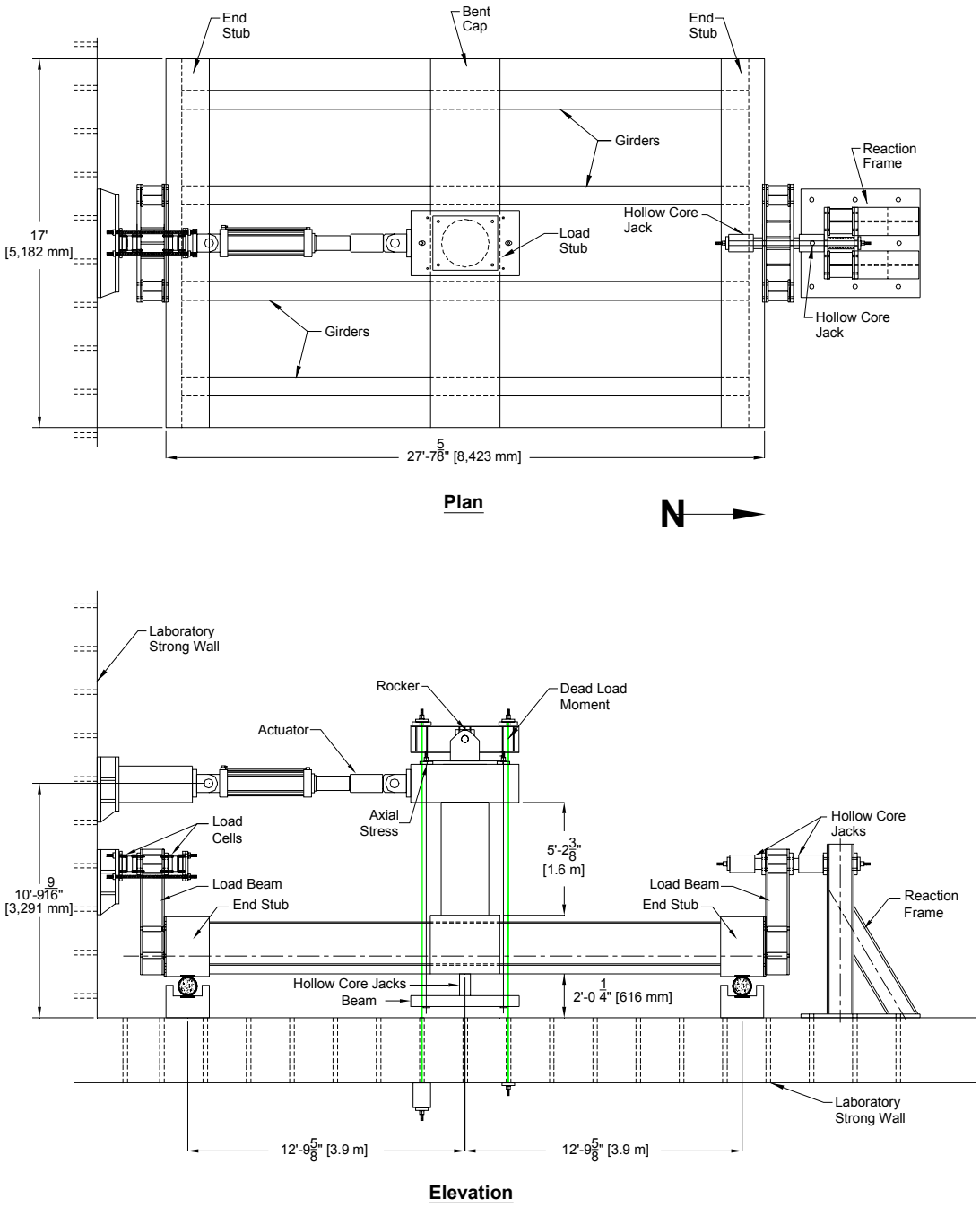

Figure 5-4 System Test Setup

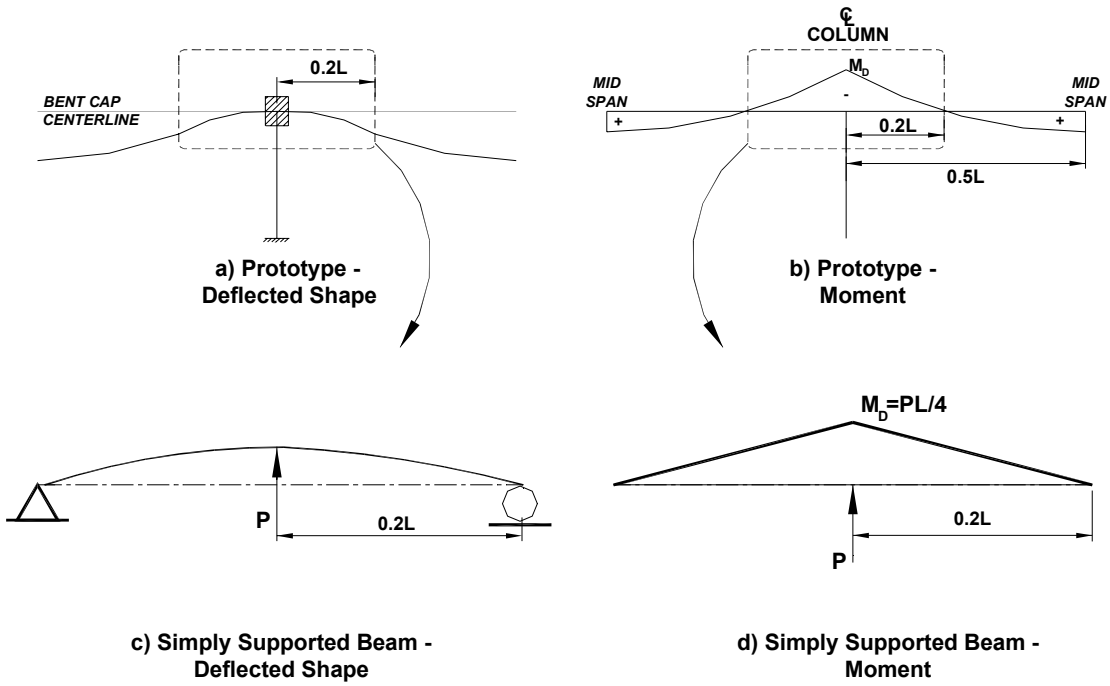

Figure 5-5 Moment and Deflected Shape Due to Gravity Loads

Using the dead load inflection points as a boundary condition, the shear to moment ratio in the column is ill proportioned and the axial force required to correctly model the dead load moment is smaller than that required to correctly model the axial stress in the column. Four bars extending from the top of the column and stressed under the deck with a jack reacting against the specimen induce no bending moment in the superstructure. Strain gages on each bar recorded strain levels in the bars throughout the test. Once all dead load modeling is complete, pressure in the hollow core jacks at the reaction frame was increased to connect the load beam to the reaction frame (Figure B. 28).

In the longitudinal direction of the bridge, the column of the prototype structure is fixed-fixed. Therefore, the column deforms in double bending when the bridge is subjected to a longitudinal seismic event (Figure 5-6a). The column moment diagram between the seismic inflection point and the bent cap centerline is similar to a cantilevered beam with a point load at the end (Figure 5-6b). The column seismic moment could be created with a horizontal load applied at the column seismic inflection

point. With the column seismic moment correctly modeled, the seismic moment into the superstructure would be correct.

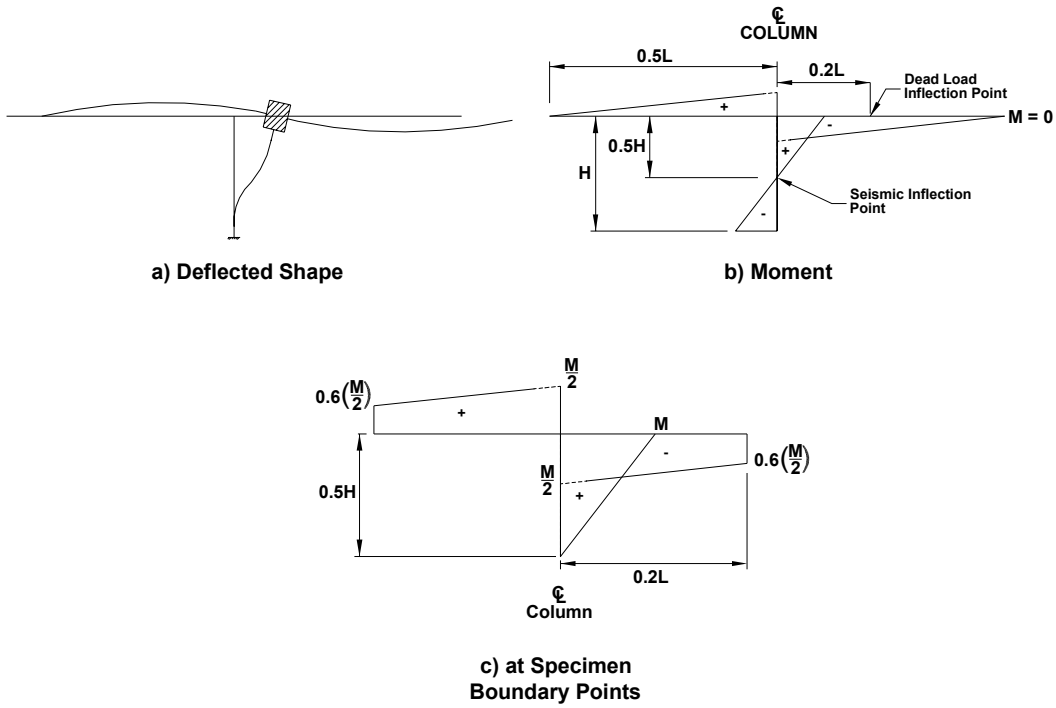

Figure 5-6 Prototype Moment and Deflected Shape Due to Seismic Loads

Because the superstructure of the specimen ended at the dead load inflection points and not at the seismic inflection points, a moment existed at the ends of the specimen (Figure 5-6c). From similar triangles, the superstructure seismic moment at the dead load inflection points was always 60% of the superstructure seismic moment at the centroid of the superstructure. This moment was created by locating the horizontal reactions a distance *h* from the superstructure centroid. Assuming equal horizontal reaction, the distance *h* was solved from $0.6(M/2)=(V/2)h$ (Figure 5-7, Figure B. 25, **Error! Reference source not found.**).

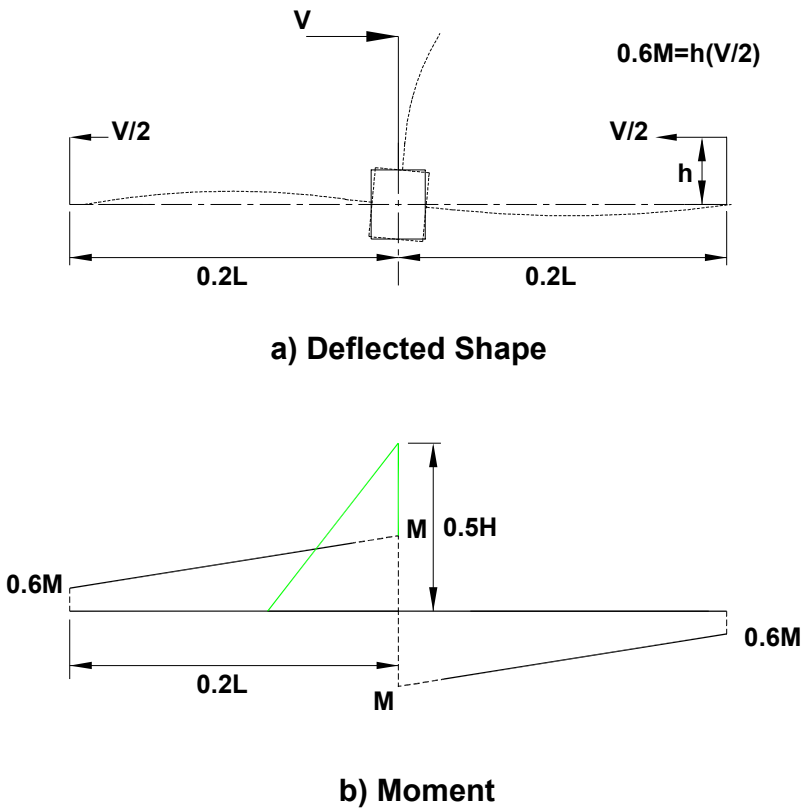

Figure 5-7 Seismic Load Modeling

5.4 CONSTRUCTION OF SYSTEM TEST SPECIMEN

The system test was constructed in the Charles Lee Powell Structural Research Laboratories. The girders were delivered by a commercial fabricator to the laboratories. Steel tubes and plates for the rollers were constructed off site and delivered to the laboratories. The loading fixtures, including the rocker at the top of the column, the load beams at the girder ends, and the reaction frame at one girder end were constructed at the Campus Research Machine Shop on the University of California San Diego campus.

All steel reinforcement was fabricated and formed off site. Strain gages were applied to the reinforcing bars and girders on site at the Powell Laboratories. Construction of test specimens, including building of formwork, tying of steel reinforcement and casting of concrete was also executed at the Powell Laboratories.

5.4.1 Construction of Deck, Girders and End Stub for System Test Specimen

Casting of concrete inside the two steel rollers and their supports was done in the laboratory yard. Steel plates cast into the supports were greased to provide a smooth sliding surface for the roller (Figure B. 24). The roller was a concrete filled steel tube. Once constructed, the rollers and supports were located on the laboratory strong floor and the formwork for the deck was constructed on top of them. A steel plate would also be cast in the deck concrete above each roller in the deck to provide a frictionless surface. The deck reinforcement was tied and the girders were located on top.

Once the girders were in place, the end stub reinforcement was tied. Because the end stubs would be subjected to torsion, the reinforcement needed to be continuous along their length, therefore, end stub reinforcement and post-tensioning ducts passed through predrilled holes in the girder web (**Error! Reference source not found.**).

5.4.2 Construction of Column and Bent Cap for System Test Specimen

The column rebar cage was assembled in a horizontal position by supporting the ends of the cage and allowing the assembly to rotate. The column longitudinal reinforcement was distributed around the circumference to allow bent cap post-tensioning ducts to pass through. The column was lowered into position on top of the deck once all deck reinforcement was tied in place (**Error! Reference source not found.**).

The bent cap transverse reinforcement consisted of tightly spaced, rectangular-shaped stirrups. The stirrups were three legged with the vertical legs terminating in seismic hooks. In construction of a prototype bridge, the stirrups are oriented with the open side on top. This opening allows reinforcement to be placed under and around the seismic hooks. Once all other reinforcement is in place, specifically the main flexural reinforcement and column shear reinforcement, the stirrups are closed by j-hooks tied across the top.

Because the test specimen was constructed in an inverted orientation, the deck reinforcement was in place when the column and stirrups were located. Therefore, the j-hooks and stirrup seismic hooks of the stirrups needed to be looped under the deck reinforcement. Additionally, the column hoops in the joint region could not be slid over the top of the column once in place (**Error! Reference source not found.**). The hoops

had to be on the column while locating the stirrups, further contributing to the congestion in stirrups already tightly spaced stirrups to satisfy joint region requirements.

The inverted test setup also required ingenious methods of haunch construction between the girders and the deck. Therefore, the deck was cast to the haunch level, with the concrete surface under the girders left unfinished and rough. After the deck had cured for four days, a grout was mixed and compacted under all four girders. The bent cap and end stub formwork was constructed with the formwork for the bottom deck surface still in place.

Throughout construction, the specimen was continuously supported on falsework. Prior to removing the falsework, the post-tensioning bars in the bent cap were stressed to their design loads. Strain gages on the bent cap post-tensioning bars recorded the strain levels in the bars throughout the test. The load beam and load cells at the south end of the specimen were connected to the laboratory strong wall (**Error! Reference source not found.**) and the falsework was removed.

Figure 5-8 Bent Cap Reinforcement

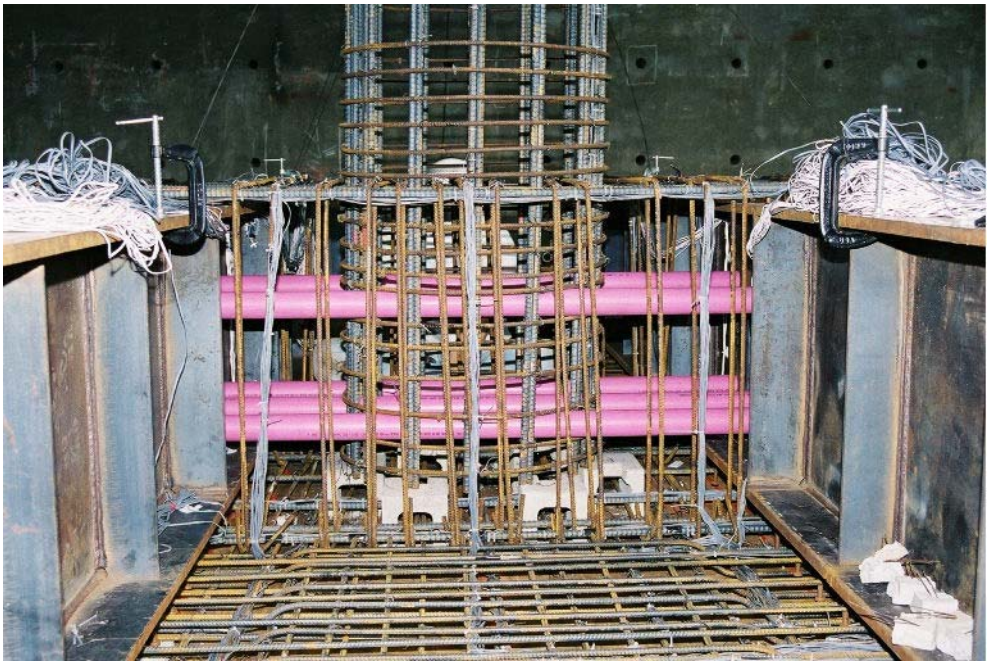

Figure 5-9 Joint Region

5.5 PROPERTIES OF SYSTEM TEST SPECIMEN MATERIAL PROPERTIES

5.5.1 Steel Reinforcement Material Properties, System Test

The steel reinforcement bar properties derived from tensile tests are tabulated in Table 6.1. The reinforcement supplier was unable to deliver A706 reinforcing bars in No. 3 [10 mm], so Grade 60 [414 MPa] was used. The stirrup bars used in the bent cap and the hoops used for transverse column reinforcement did not exhibit any yielding plateaus. The rebar specified was A706, Grade 60 [414 MPa]. The hoops were butt-welded to conform to the Ultimate Splice Requirements outlined in 52ULTS of the Caltrans Bridge Design Specifications (14).

Table 5.1 Measured Reinforcement Properties

Item		Yield Stress, f_y ksi [MPa]	Ultimate Stress, f_{ult} ksi [MPa]	Elongation* ε_{su} %
Bentcap:	Stirrup #3 [10 mm]	yielded	111.0 [765]	7.3
	Flexural #3 [10 mm]	66.2 [456]	107.0 [738]	9.1
	Flexural #5 [16 mm]	68.7 [474]	97.9 [675]	12.61
Column:	Hoop #3 [10 mm]	yielded	99.3 [685]	8.8
	Longitudinal #5 [16 mm]	66.9 [461]	94.6 [652]	13.2
Deck:	Truss #3 [10 mm]	62.2 [429]	103.3 [712]	10.2
	Transverse #3 [10 mm]	82.0 [565]	117.4 [809]	9.4
	Longitudinal #3 [10 mm]	80.7 [556]	115.7 [798]	10.0

* based on 8 in. (203 mm) gage length

5.5.2 Concrete Material Properties, System Test

All concrete was specified to have a compressive strength of 4 ksi [27.6 MPa], ½" [13 mm] aggregate and a design slump of 4" [102 mm]. The mix design for the concrete is summarized in Chapter 3. The measured compressive strengths at 7-days, 28-days and day of test were determined from standard cylinder compression tests and are presented Table 5.2.

Table 5.2 Concrete Compressive Strength

Location	7 Days ksi [MPa]	28 Days ksi [MPa]	Day of Test ksi [MPa]	Age (Days)
Column	4.68 [32]	5.6 [39]	5.37 [37]	26
Bent Cap	3.81 [26]	5.26 [36]	4.96 [34]	32
Deck	3.51 [24]	4.86 [34]	5.2 [39]	51

5.6 INSTRUMENTATION OF SYSTEM TEST SPECIMEN

The girder flanges, webs and stiffeners were instrumented with post-yield strain gages. The girder webs of the two interior girders were instrumented with strain rosettes. Selected reinforcement bars in the column, bent cap and deck were instrumented with strain gages. The specimen's performance was also recorded with linear displacement transducers, inclinometers and actuator readings.

5.6.1 Strain Gage Locations in System Test

Figure 5-10 shows the strain gage locations on the column longitudinal reinforcement. Five levels up the column were instrumented on six column longitudinal bars. Strain gages recorded behavior at three stirrups in the joint region and two stirrups on either side of the joint region as shown in **Error! Reference source not found.**. Each stirrup inside the joint region was instrumented with ten strain gages, with one at each center point and the remaining six located toward the stirrup locations near the corners of the bent cap. Stain gages on stirrups outside the joint region were instrumented only at the corners with the exception of one at the top center.

Bent cap flexural reinforcement was instrumented with strain gages at five locations in the joint region and six locations outside the joint region (**Error! Reference source not found.**). Inside the joint region, gages were applied to flexural reinforcement bars at all four bent cap corners and of center of the four bent cap faces. Outside the joint region, gages C and G were omitted.

Seven longitudinal deck bars were instrumented with six strain gages each, shown in Figure 5-13. Strain gages were located at each bent cap face, one strain gage one foot [305 mm] away and one strain gage two feet [610 mm] away from the bent cap face on both the push and pull sides of the specimen. Strain gages were applied to two transverse deck reinforcement bars on either side of the transverse bridge axis but only one side of the longitudinal bridge axis. The layout is shown in Figure 5-13.

5.6.2 External Displacement Measurement Devices in System Test

Figure 5-14 and Figure 5-15 show the locations linear potentiometers, curvature rods, and inclinometers. Potentiometers were located under each girder and column centerline at five transverse cross-sections of the bridge (Figure 5-14). Longitudinal translation of the superstructure was measured by two string potentiometers mounted on two free-standing columns with the end stub as the target. Load stub displacement at the top of the column was measured by a string potentiometer mounted on the free stranding reference columns at the end.

One rotational device was mounted on the end of the bent cap and one was mounted on the bent cap at the column centerline. Rotation values could also be obtained

from the vertical linear potentiometers located under the deck. Multiple rotation measurement locations were used in hopes of capturing twist values along the beam length.

Curvature measurements were taken at four heights up the column on both the push and pull face of the column (Figure 5-15). One diagonal, two horizontal and two vertical displacement transducers were located on one face of the bent cap in the joint region to measure any crack dilation of the bent cap.

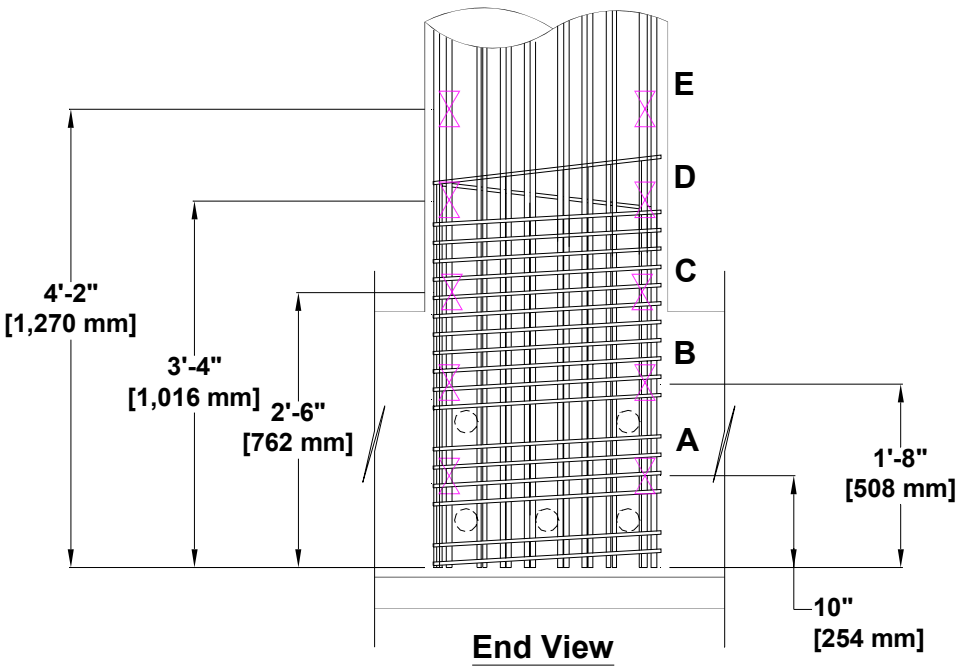

LEGEND
S=REGULAR STRAIN GAGE
COL=COLUMN GAGES
#=BAR LOCATION
A=LOCATION ON BAR

EXAMPLE:
SCOL1A

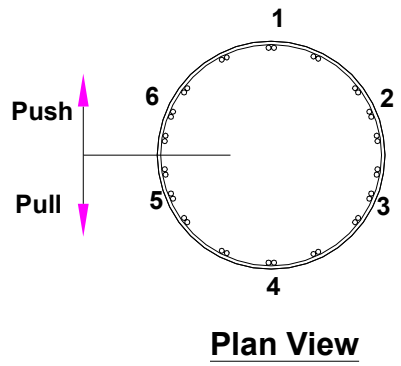

Figure 5-10 Location of Strain Gages on Column Reinforcement

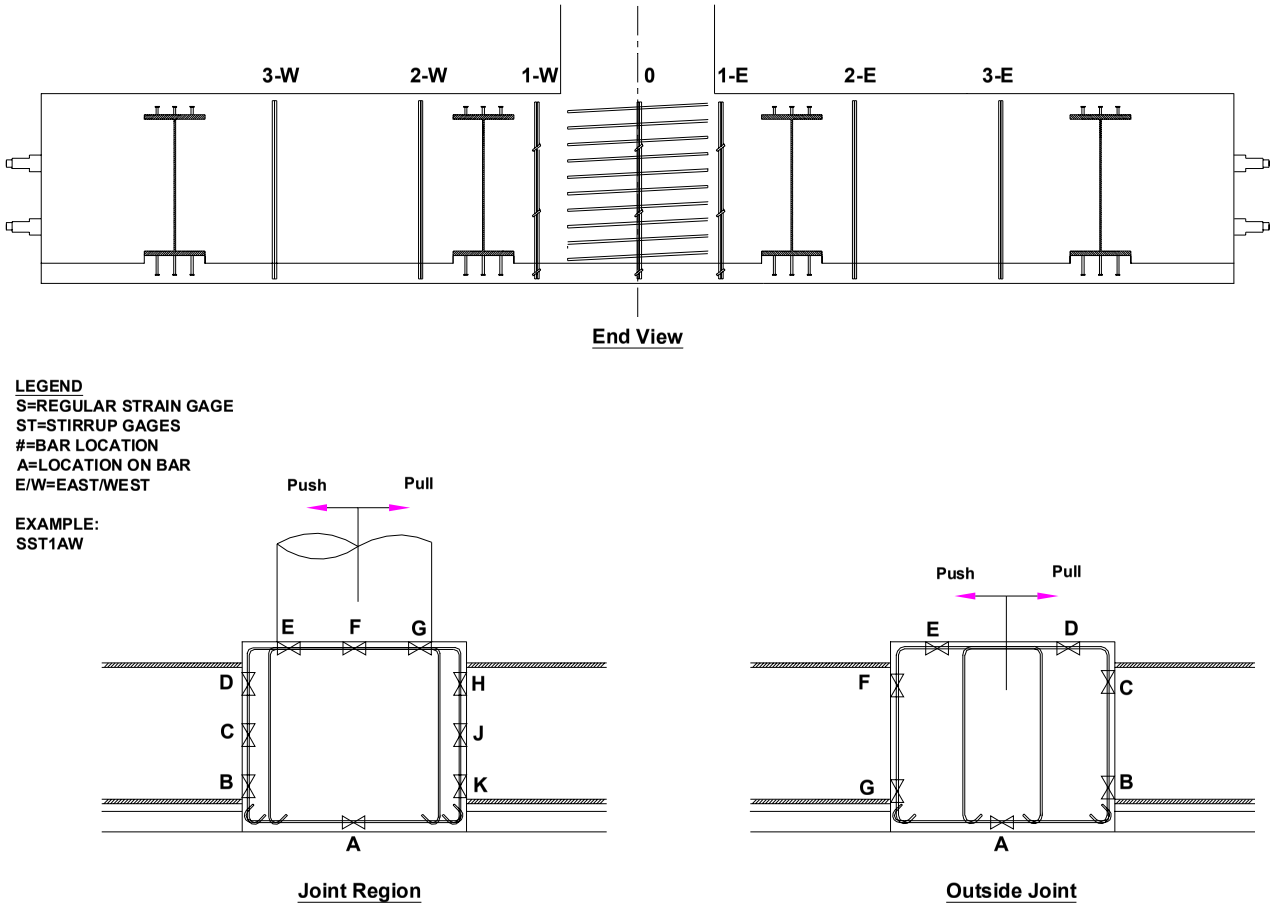

Figure 5-11 Location of Strain Gages on Bent Cap Stirrups

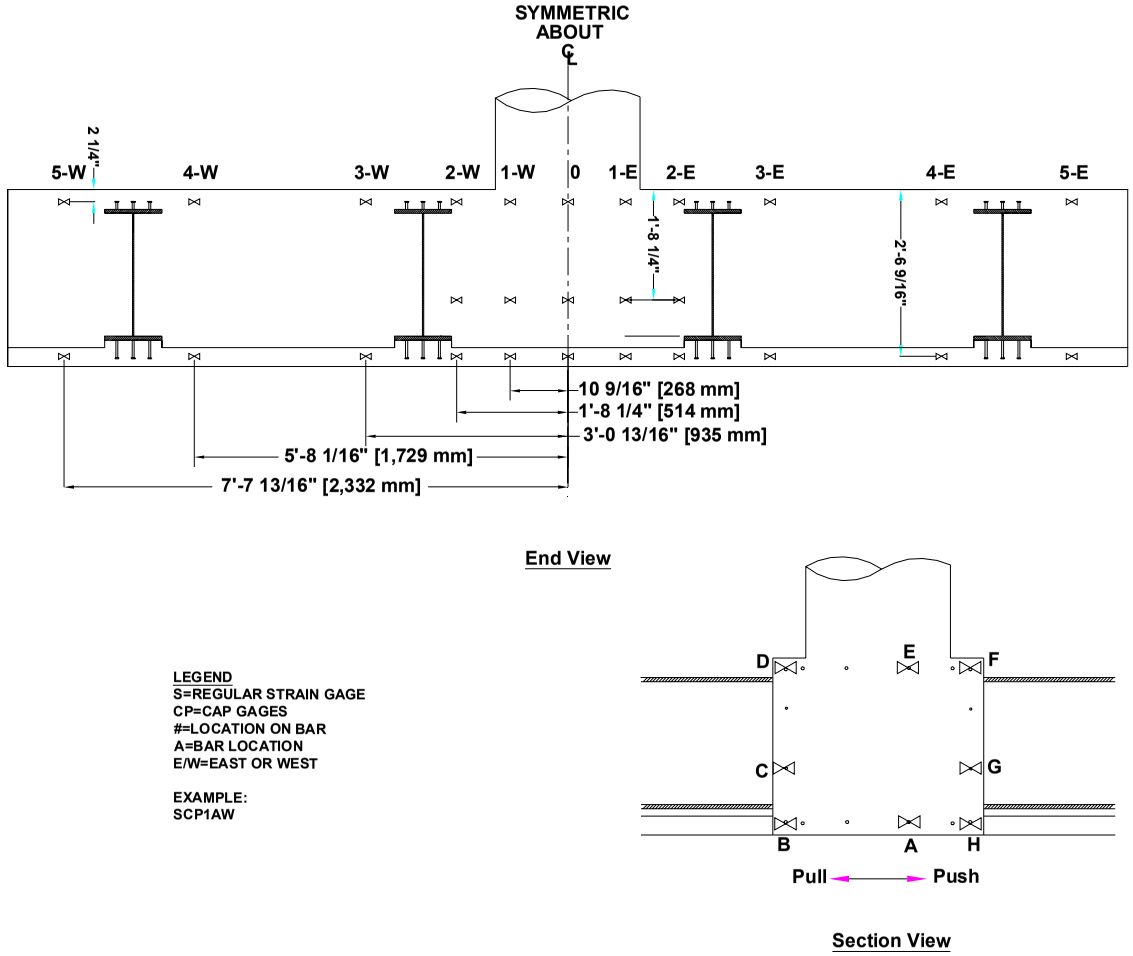

Figure 5-12 Location of Strain Gages on Flexural Reinforcement

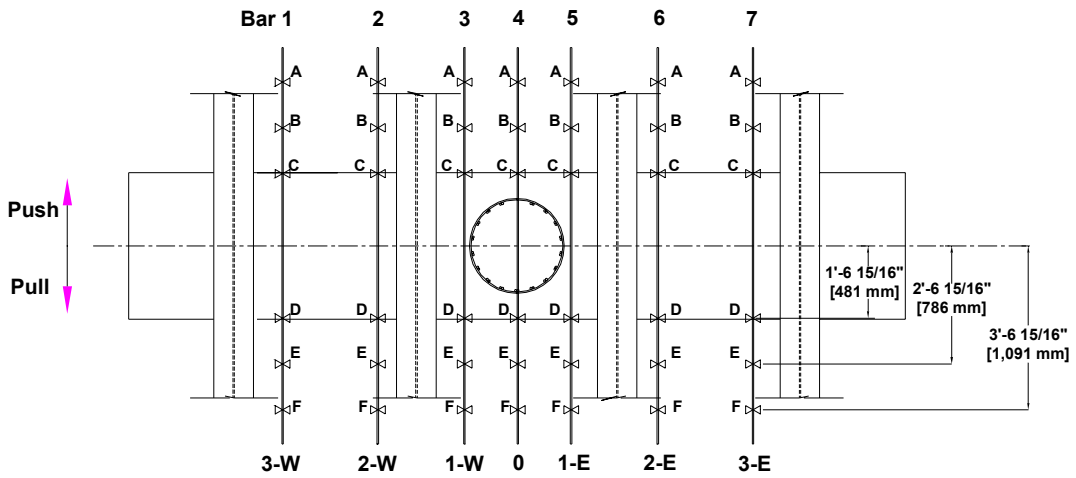

LEGEND
S=REGULAR STRAIN GAGE
DK=DECK GAGES
#=BAR LOCATION
A=LOCATION ON BAR
E/W=EAST OR WEST

EXAMPLE:
SDK1AW

Plan View - Longitudinal Gages

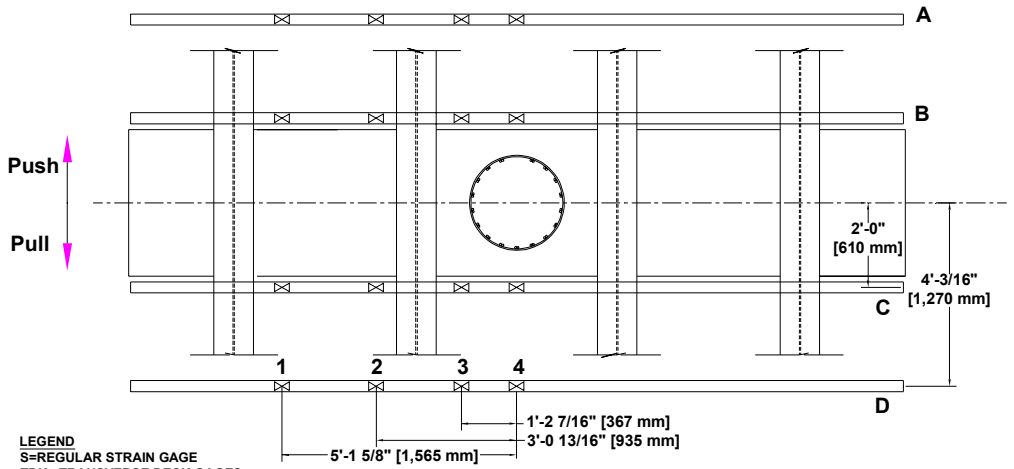

LEGEND
S=REGULAR STRAIN GAGE
TDK= TRANSVERSE DECK GAGES
#=LOCATION ON BAR
A= BAR LOCATION
W=WEST

EXAMPLE:
STDK1AW

Plan View - Transverse Gages

Figure 5-13 Location of Strain Gages on Deck Reinforcement

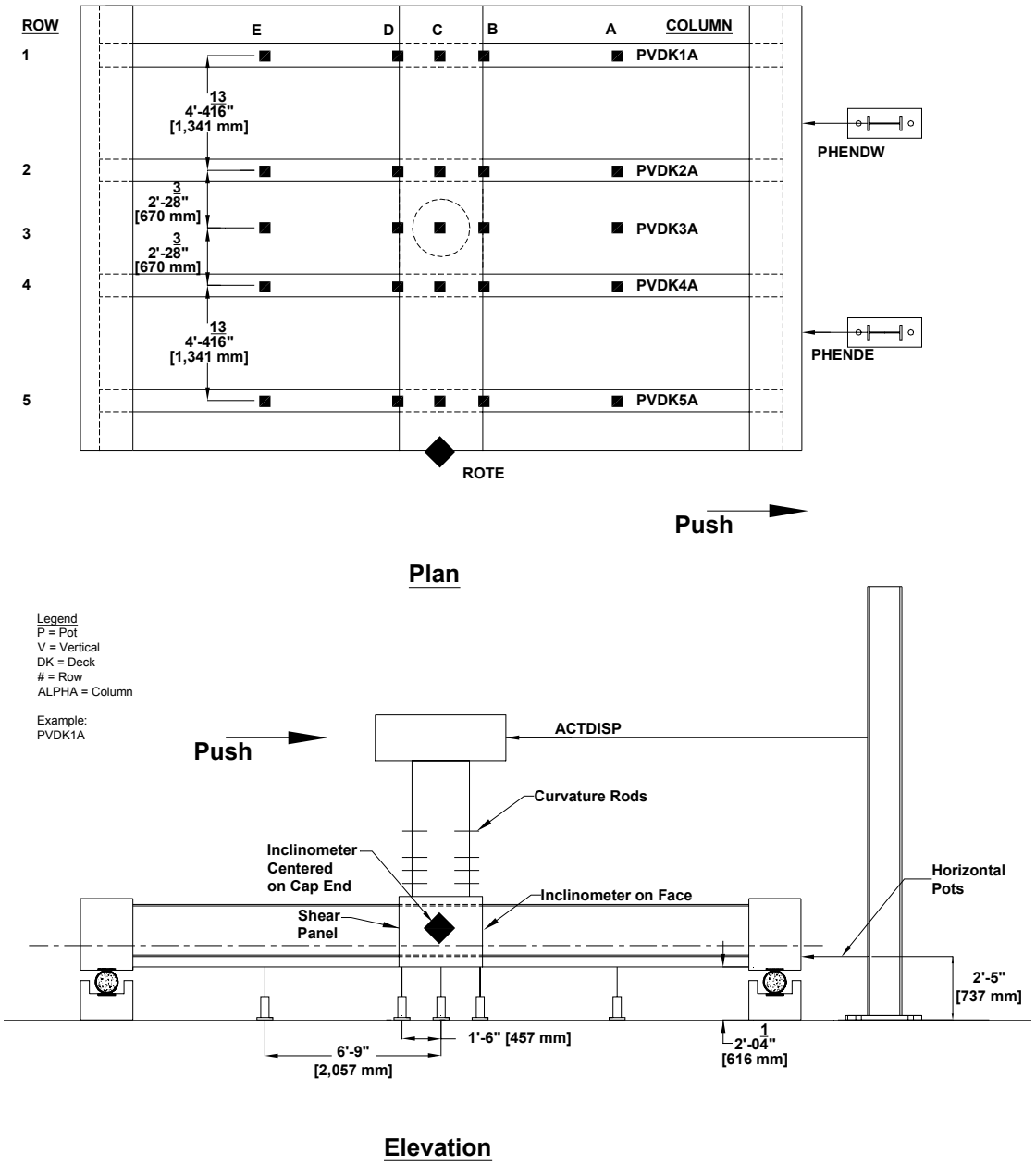

Figure 5-14 Displacement Measurement Locations

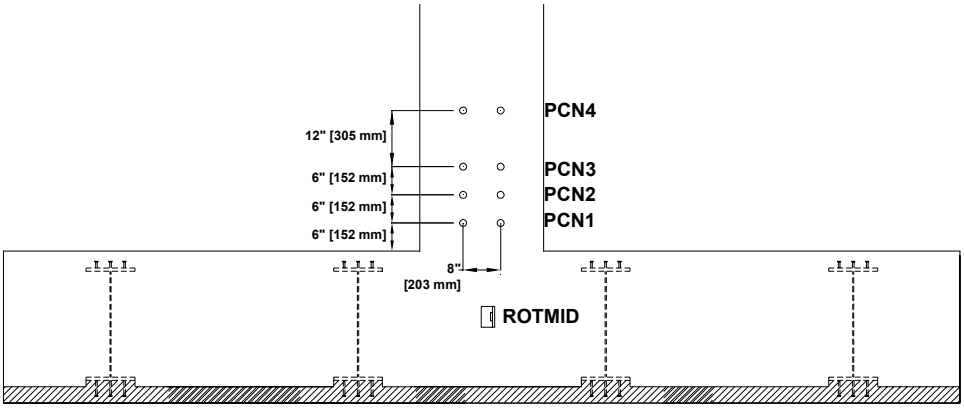

Inclinometer and Curvature Rods

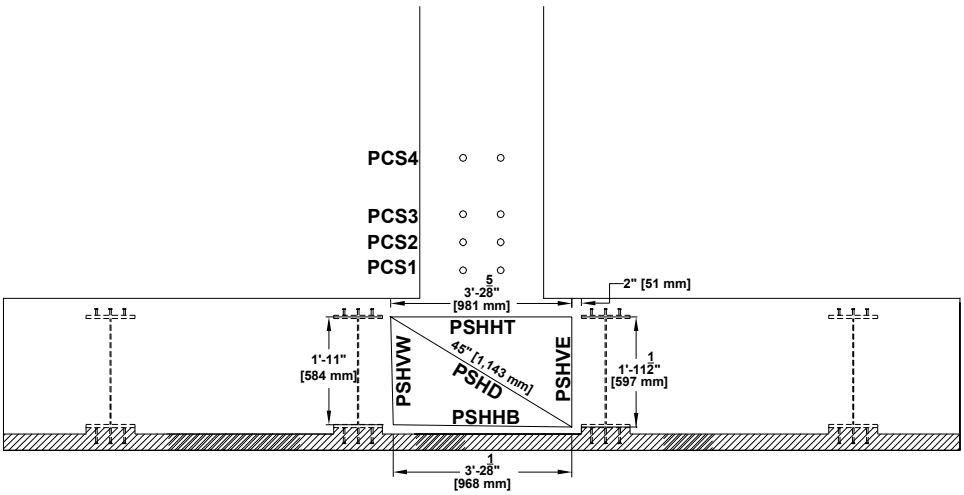

Shear Panel

Figure 5-15 Bent Cap Face Instrumentation

5.7 LOADING PROTOCOL FOR SYSTEM TEST

The seismic load was applied via a servo-controlled hydraulic actuator located at the column seismic inflection point under a quasi-static, fully reversed cyclic testing protocol (Figure B. 29). Loading began as single-cycle, 5 kip [22 kN] load intervals until column cracking was observed. Post-cracking, single-cycle load intervals were increased to 20 kip [89 kN] up to theoretical first yield of longitudinal column reinforcement bars. Strain gages on the column longitudinal reinforcement indicated the occurrence of first yield. The value of column displacement at first yield for the positive and negative directions were averaged and multiplied by the ratio of ideal column capacity to theoretical column capacity. The displacement calculated from this ideal first yield is defined Displacement Ductility One.

After reaching first yield, loading protocol was switched to displacement control. Each displacement interval was no great than 1.5 times its preceding displacement. Each displacement level was for three cycles. The seismic loading protocol curve is shown in Figure 5-16.

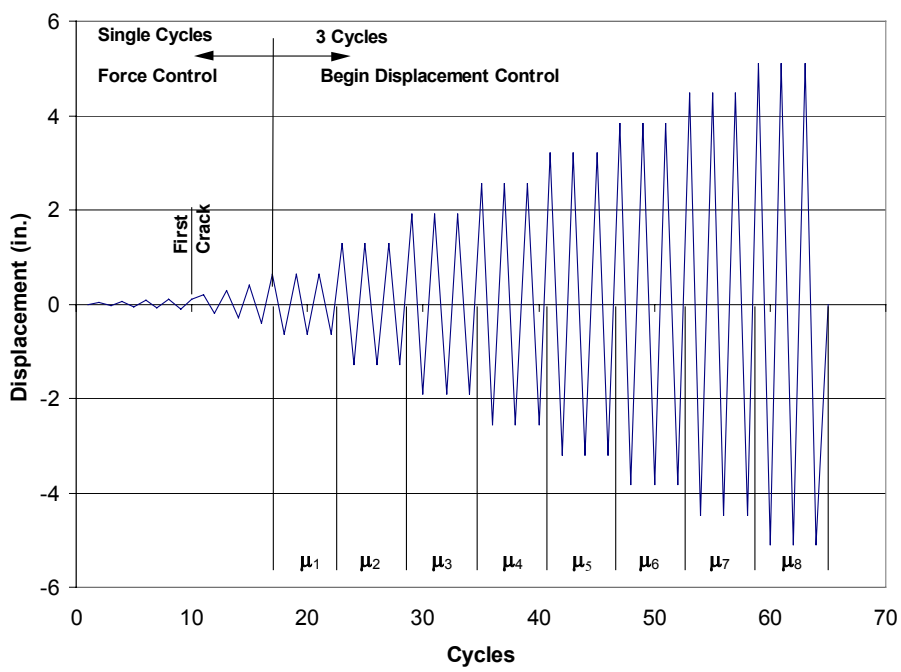

Figure 5-16 System Test Loading Sequence

Chapter 6

Experimental Results of System Test

6.1 OVERVIEW

This chapter presents the results from the system test. Section 6.2 of this chapter presents a qualitative summary of the test results. Section 6.3 presents the measured response of the test. The chapter concludes with a comparison of system test results with results from component test Specimen PT-S. Bridge components of the test specimen, tested in the upside down position, are referred to as they would be in the prototype structure. For instance, the "top of the column" is where the column joins the bent cap.

6.2 OBSERVED PERFORMANCE, SYSTEM TEST

Before seismic loading began, cracks were noticed on both sides of the deck. These cracks resembled flexural cracks and were presumably from the application of the dead load.

The first crack to form due to seismic loading was a flexural crack in the column during the push portion of the 50 kip [222 kN] loading cycle. Displacement at the load stub centerline was 0.2 in. [5 mm]. The crack was approximately eight inches [203 mm] from the bottom of the bent cap (Figure 6-1). The bent cap was undamaged. On the pull portion of the same load cycle, three flexural cracks developed in the top of column on the opposite face (Figure 6-2).

The first column longitudinal bar yield was recorded by strain gage scol4d (chp5 fig ref) and occurred on the push portion of the 100 kip [444 kN] loading cycle. Torsional cracking initiated on the bottom of the bent cap, presumably from column longitudinal reinforcement strain penetration (Figure 6-3). At this load level, ideal first yield column displacement was calculated as describe in Section 5.7, thus defining the first ductility level and hence the start of three cycle loading.

On the first cycle of Displacement Ductility One (μ_Δ = 1) (Figure 6-4), two torsional cracks developed on the bent cap face (Figure 6-5). One crack was

approximately four inches long [102 mm] and the other was approximately eight inches [203 mm]. Both cracks initiated approximately 9 in. [229 mm] from the bottom of the bent cap on either side of the column longitudinal reinforcement and extended down at an angle of approximately 45° from the vertical. By the third cycle of μ_Δ= 1, a spiral crack on the bent cap face had extended toward the girder and a new crack had developed (Figure 6-6). At the first cycle of μ_Δ = 1.5, cracks on the bottom of the bent cap previously described as strain penetration cracks began to resemble torsion spiral cracks as they extended toward the girders (Figure 6-7 and Figure 6-8).

During the first cycle of μ_Δ = 2, spiral cracks on the bent cap face continued to develop (Figure 6-9). Existing cracks extended toward the girders and the bottom of the bent cap at the column. Torsion spiral cracks initiated from the girder and spiraled toward the bottom of the bent cap (Figure 6-10). Spiral cracks on the bottom of the bent cap continued to form through the third cycle of μ_Δ= 2 (Figure 6-11). Spiral cracks on the face of the bent cap extended toward the girder web (Figure 6-12). Incipient spalling at the top of the column was observed and is shown during the first load cycle of μ_Δ = 3 in Figure 6-13. The south bent cap face is shown in Figure 6-14.

At μ_Δ = 4, there is little additional degradation of the bent cap faces (Figure 6-15, Figure 6-16). Incipient spalling of cover concrete at the top end of the column can be seen in Figure 6-17. Figure 6-18, Figure 6-19, Figure 6-20 and Figure 6-21 show the progression of the failure mechanism development at the top of the column. Reinforcement failure occurred during the third cycle of μ_Δ = 8. The specimen reached its ultimate strength when buckling of seven column longitudinal bars occurred successively in addition to hoop fracture. Figure 6-22, Figure 6-23, Figure 6-24, and Figure 6-25 show the specimen at μ_Δ = 10, the final load level. It can be seen that little additional bent cap degradation occurred after the column hinge mechanism began to develop at μ_Δ = 4. Bent cap damage on the face is limited to superficial cracking (Figure 6-22). Damage on the bottom face of the bent cap was concentrated near the top of the column and limited to cracking and minimal spalling (Figure 6-23, Figure 6-24, and Figure 6-25).

Figure 6-26 shows the bridge after sustaining a simulated longitudinal seismic event. The structural damage was concentrated at the designated failure mechanism

location at the top of the column. Superstructure damage was limited to cracking on the bottom and side faces of the bent cap in the joint region. The bent cap outside of the joint region was undamaged.

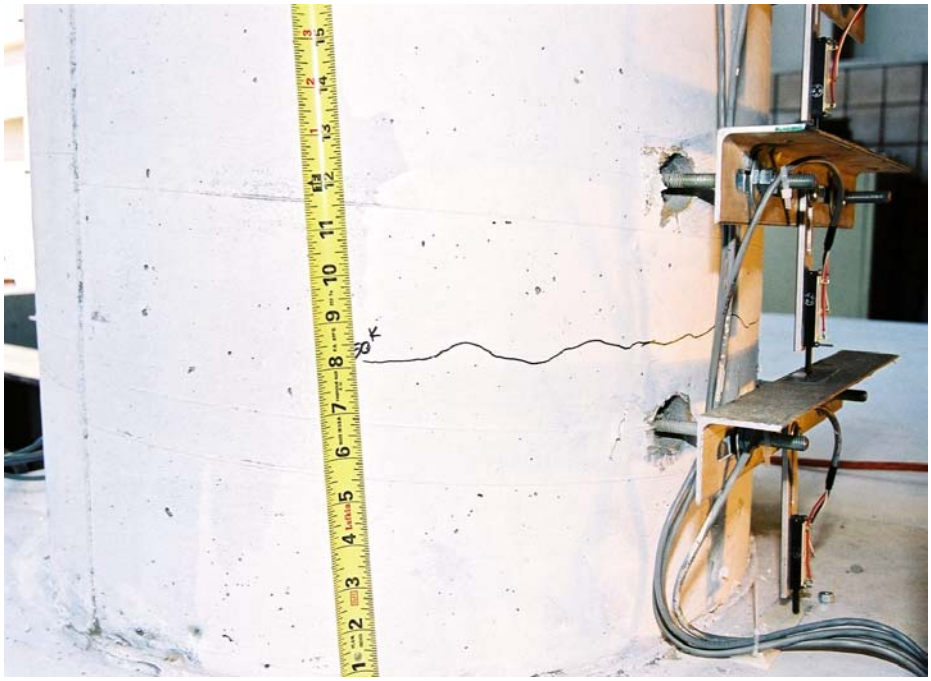

Figure 6-1 First Column Crack

Figure 6-2 First Flexural Cracks on Negative Loading

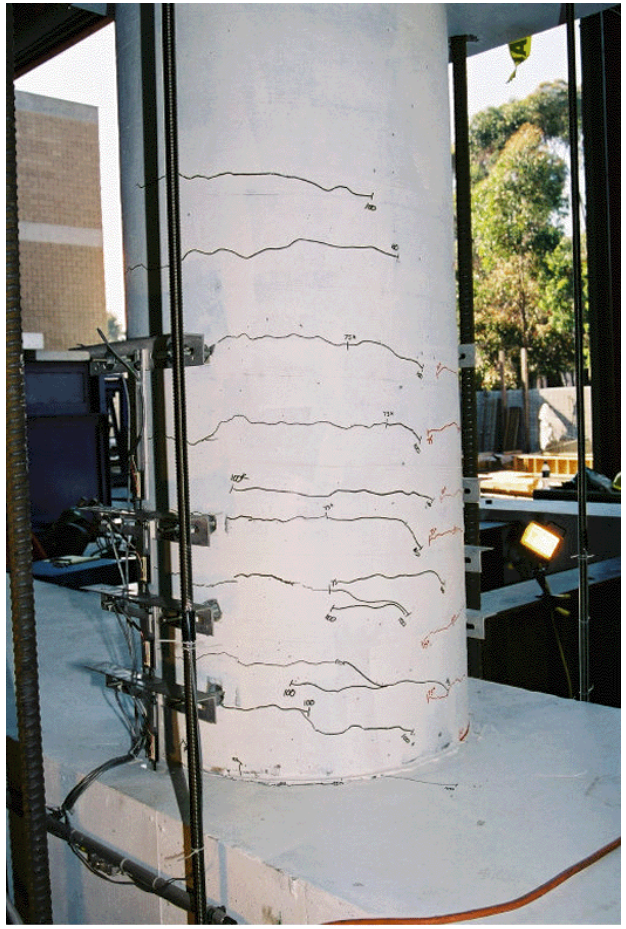

Figure 6-4 Column at First Column Longitudinal Yield

Figure 6-3 $\mu_\Delta = 1$

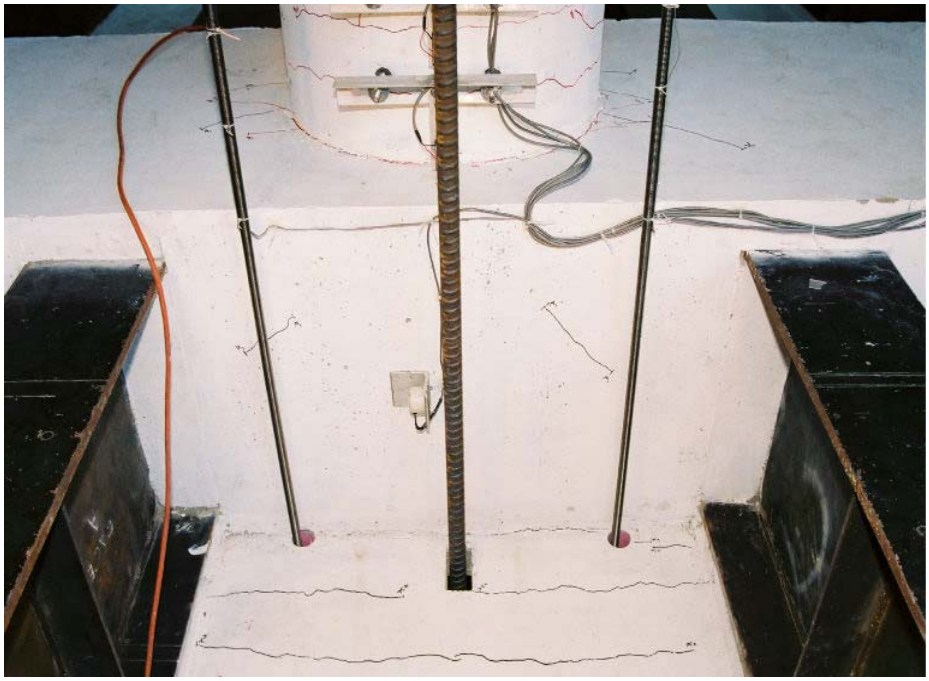

Figure 6-5 First Bent Cap Torsional Crack, μ_Δ = 1, Cycle One

Figure 6-6 Torsional Crack Development, μ_Δ = 1, Cycle Three

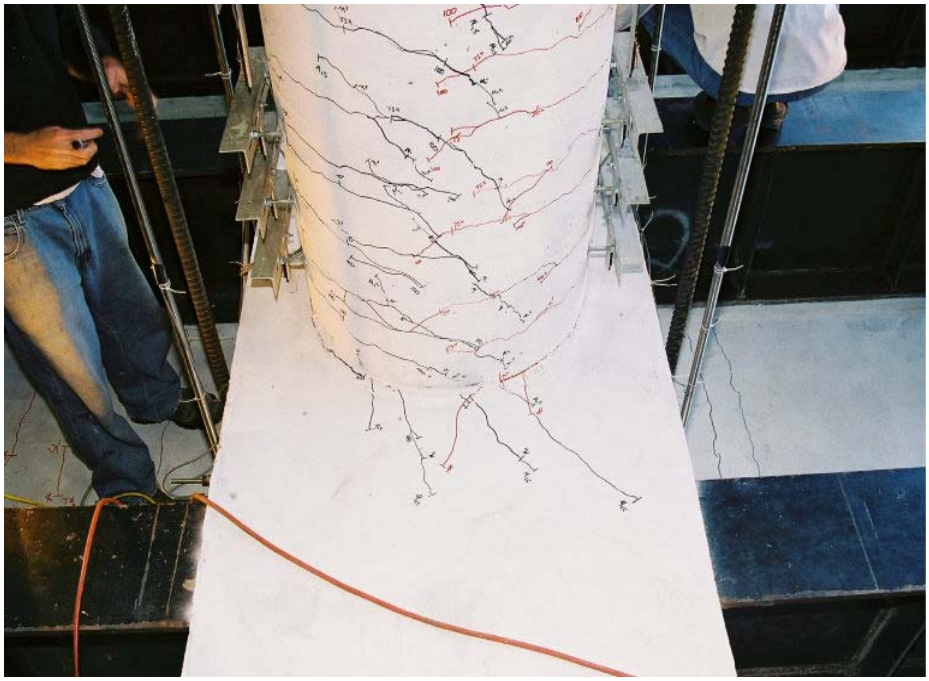

Figure 6-7 East Side of Bent Cap at μ_Δ = 1.5, Cycle One

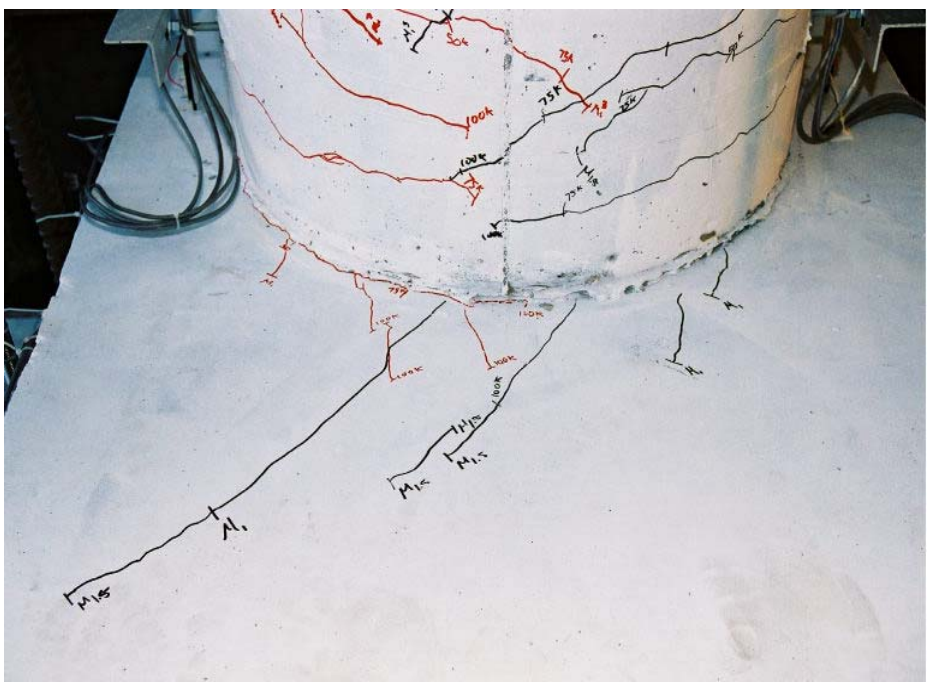

Figure 6-8 West Side of Bent Cap at μ_Δ = 1.5, Cycle One

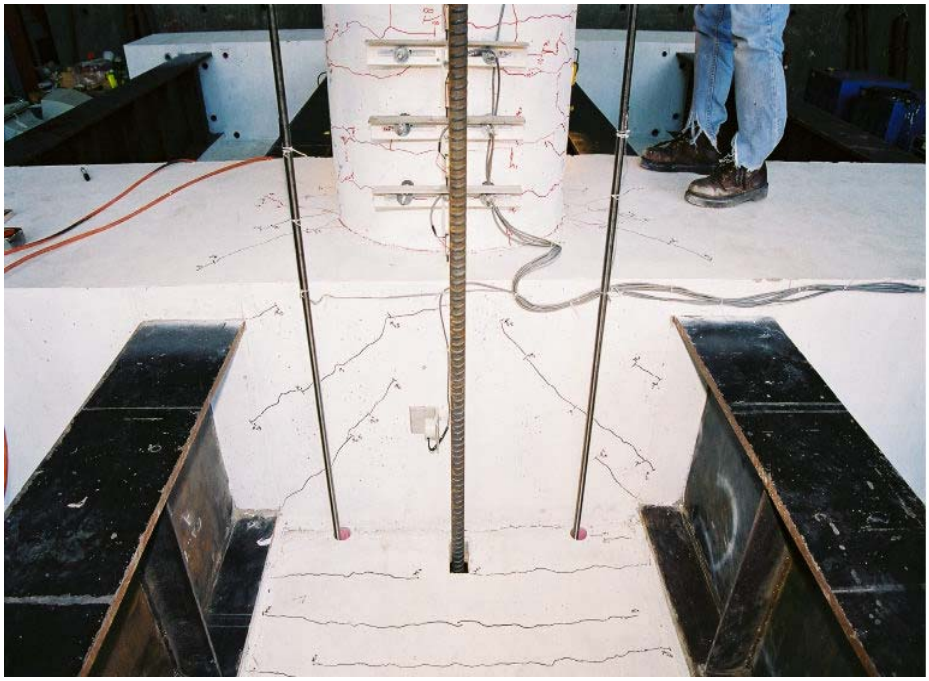

Figure 6-9 North Bent Cap Face, μ_Δ = 2, Cycle 1

Figure 6-10 Cracks in North Bent Cap Face at μ_Δ = 2, Cycle 1

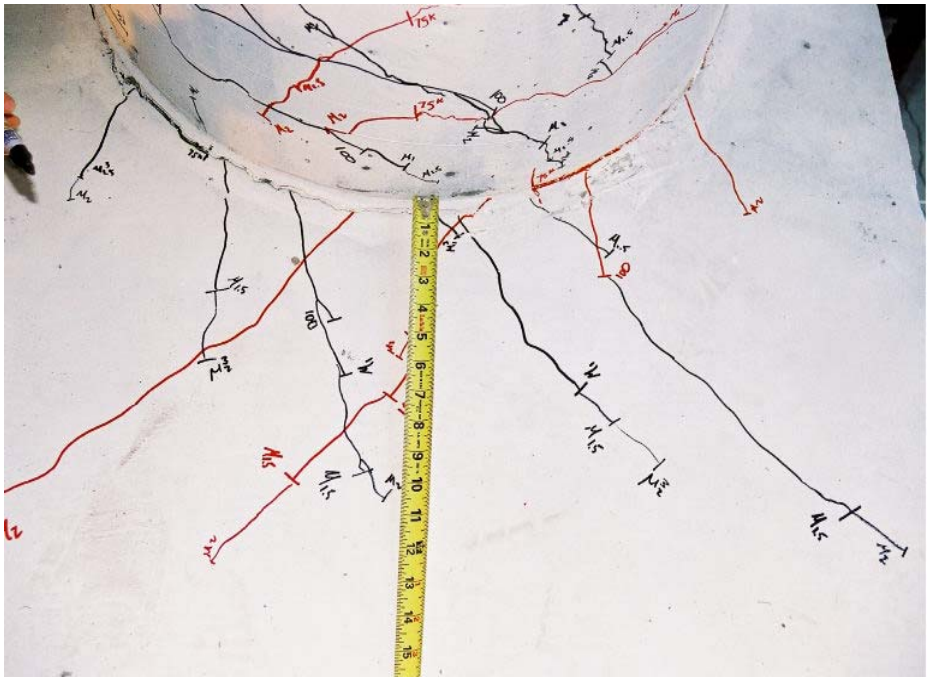

Figure 6-11 East Side, Bottom of Bent Cap at $\mu_\Delta = 2$, Cycle Three

Figure 6-12 Girder-Cap Interface at $\mu_\Delta = 2$, Cycle Three

Figure 6-13 South Face of Column/Bent μ_Δ = 3, Cycle One

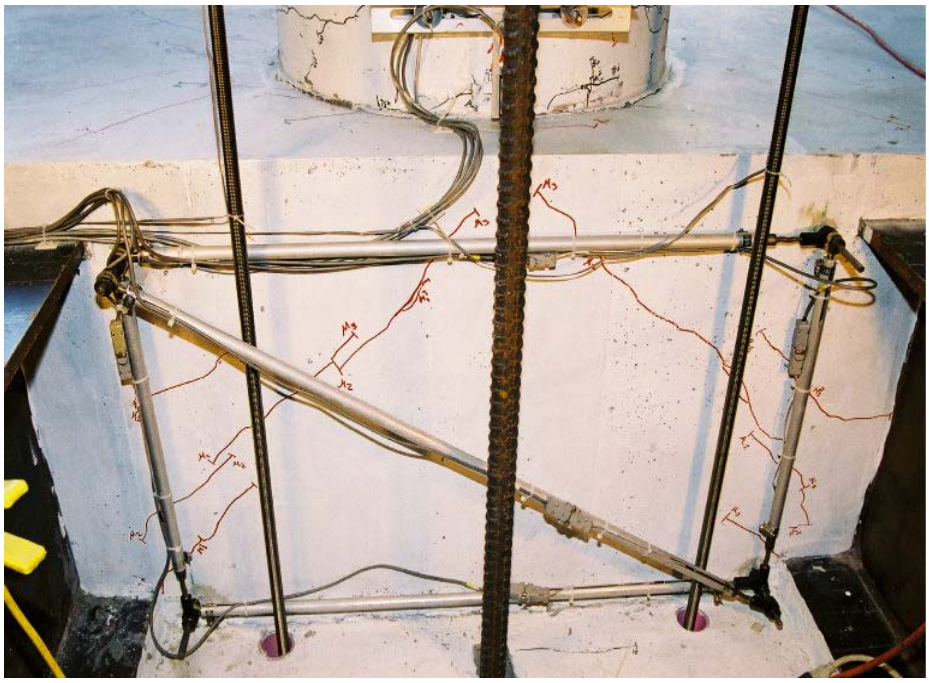

Figure 6-14 South Bent Cap Face μ_Δ = 3, Cycle One

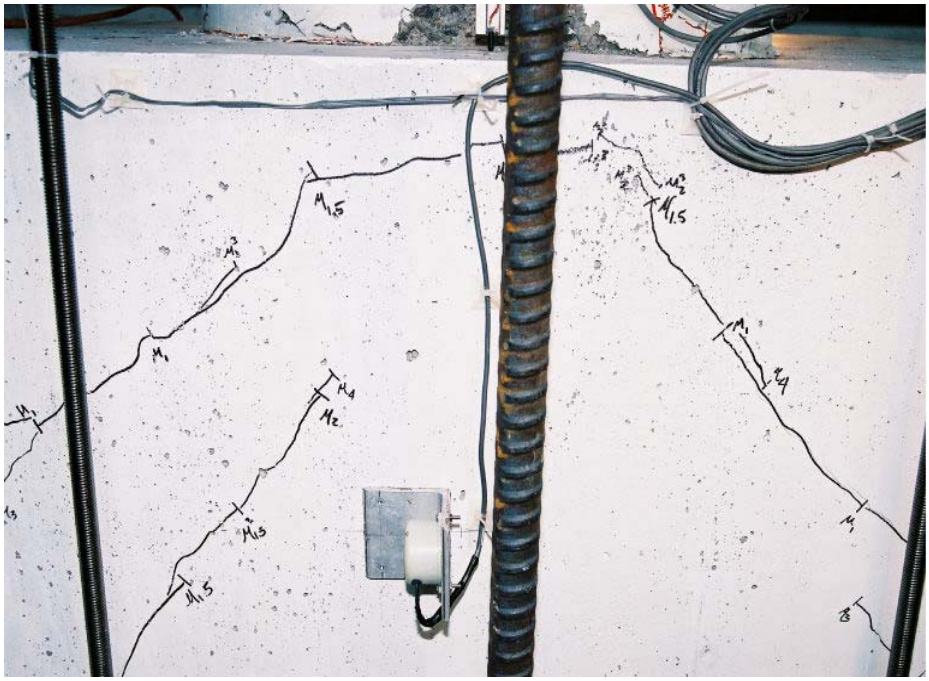

Figure 6-15 North Bent Cap Face at μ_Δ = 4, Cycle One

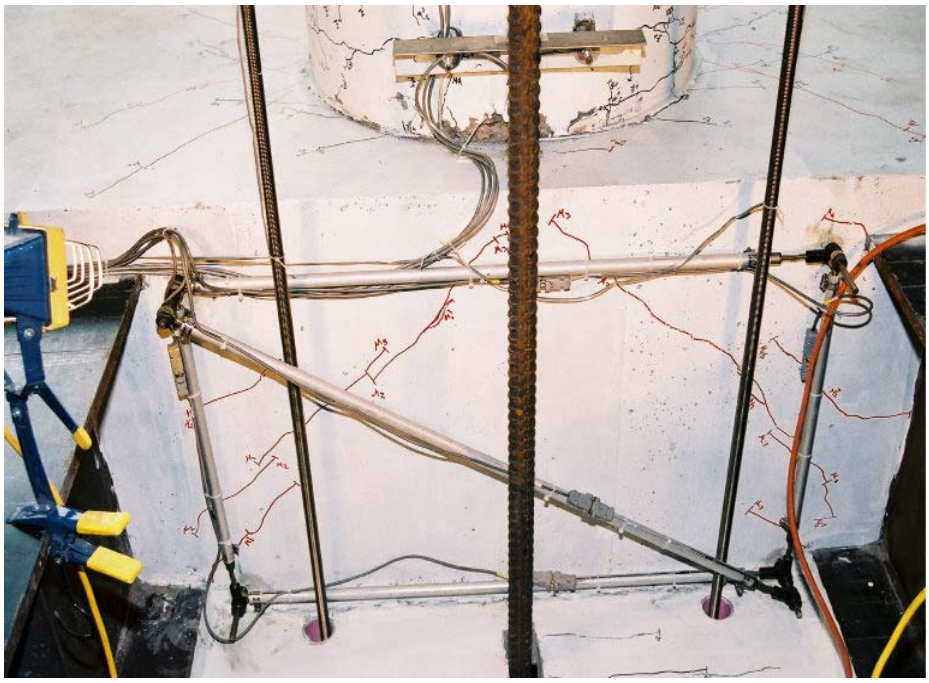

Figure 6-16 South Bent Cap Face at μ_Δ = 3, Cycle One

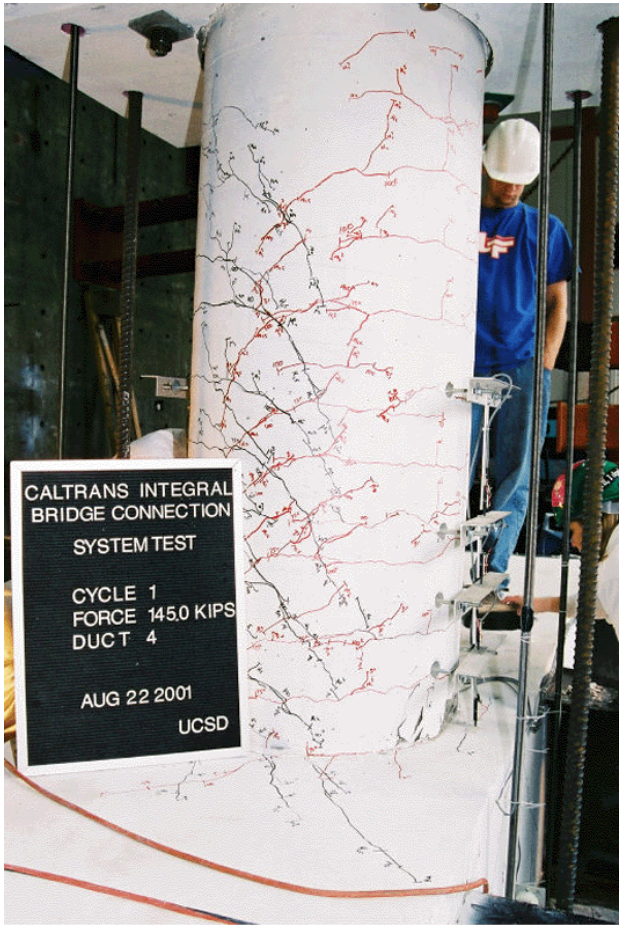

Figure 6-18 $\mu_\Delta = 4$, Cycle One

Figure 6-17 $\mu_\Delta = 6$, Cycle One

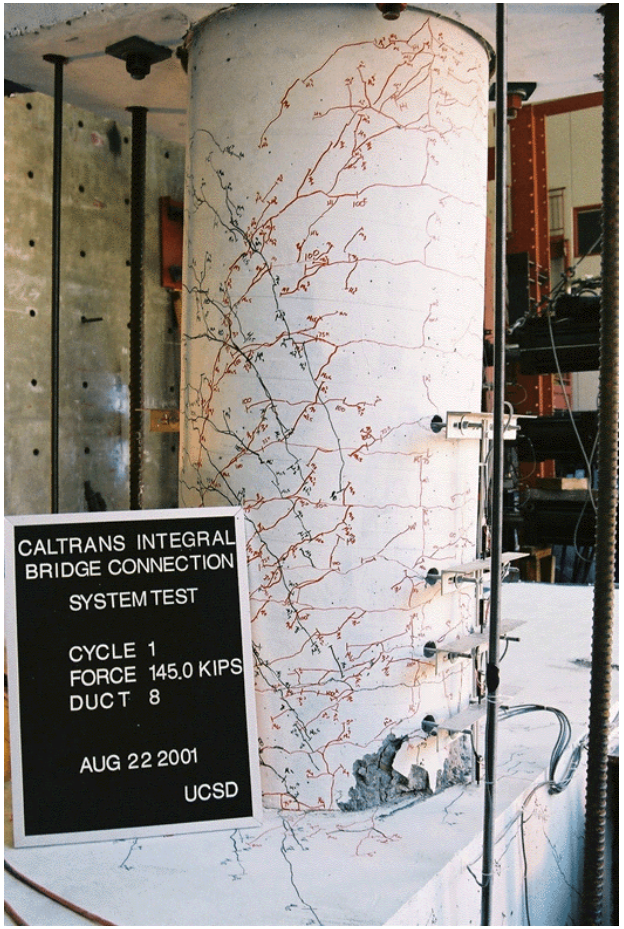

Figure 6-20 μ_Δ = 8, Cycle One

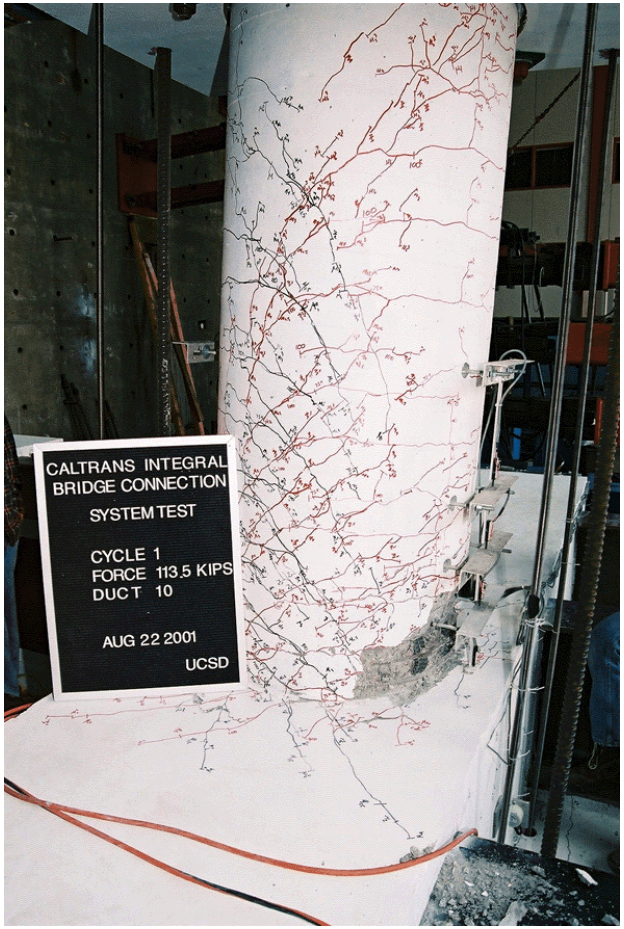

Figure 6-19 μ_Δ = 10, Cycle One

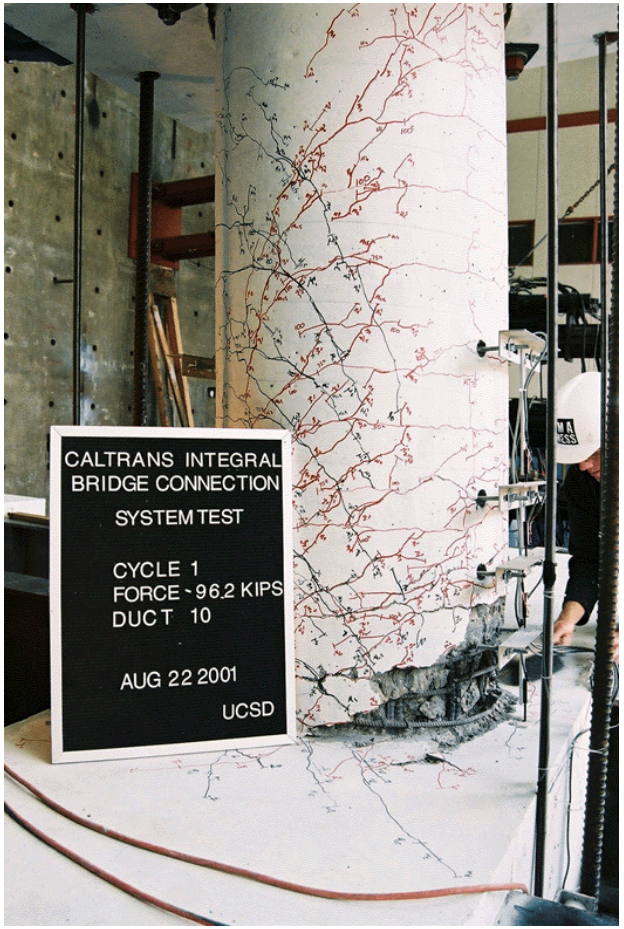

Figure 6-22 μ_Δ = 10, Final Displacement Cycle

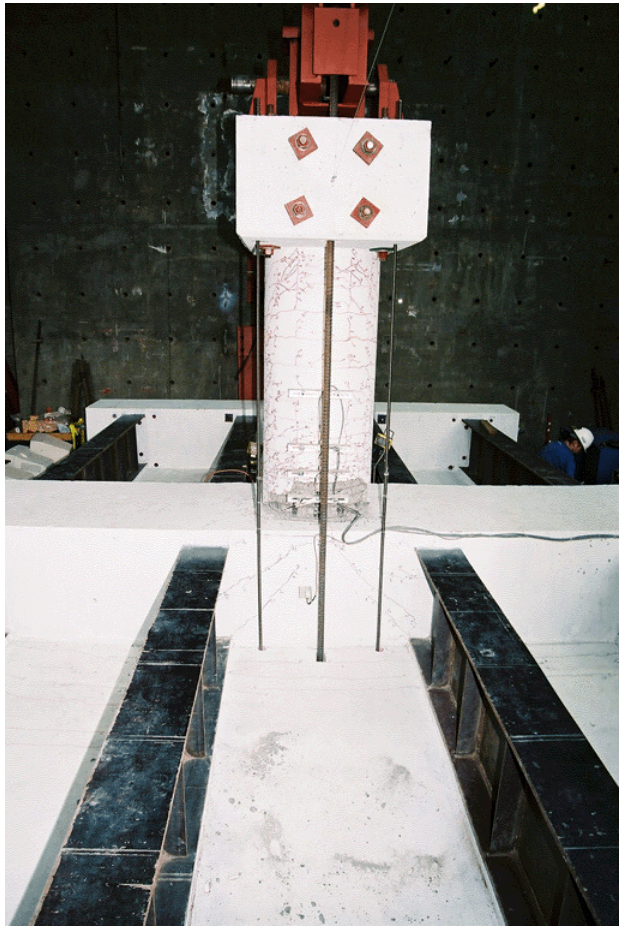

Figure 6-21 μ_Δ = 10, North Bent Cap Face

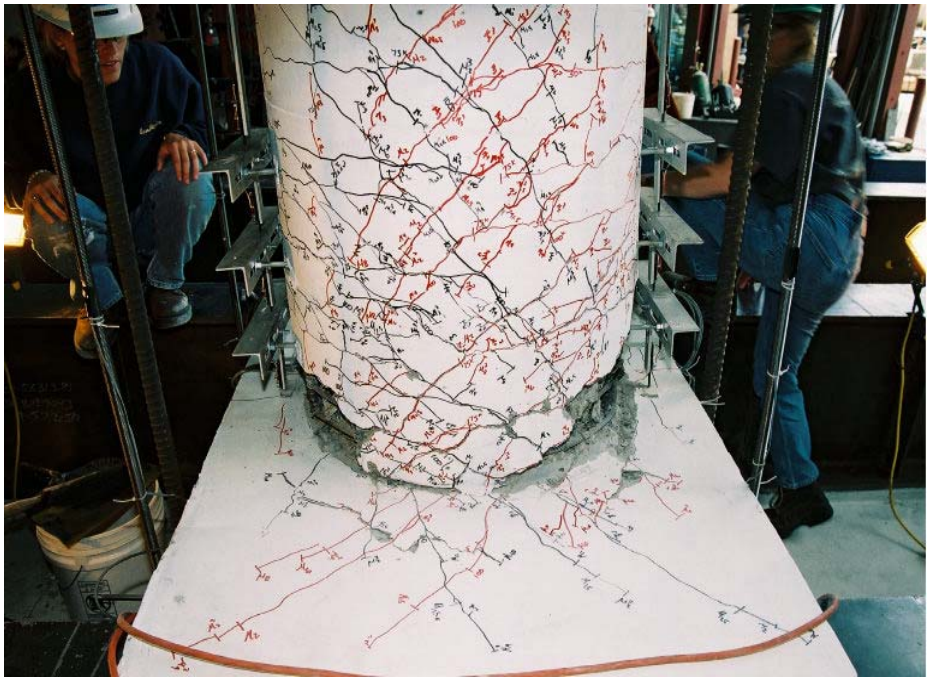

Figure 6-23 East Bent Cap Bottom Face $\mu_\Delta = 10$

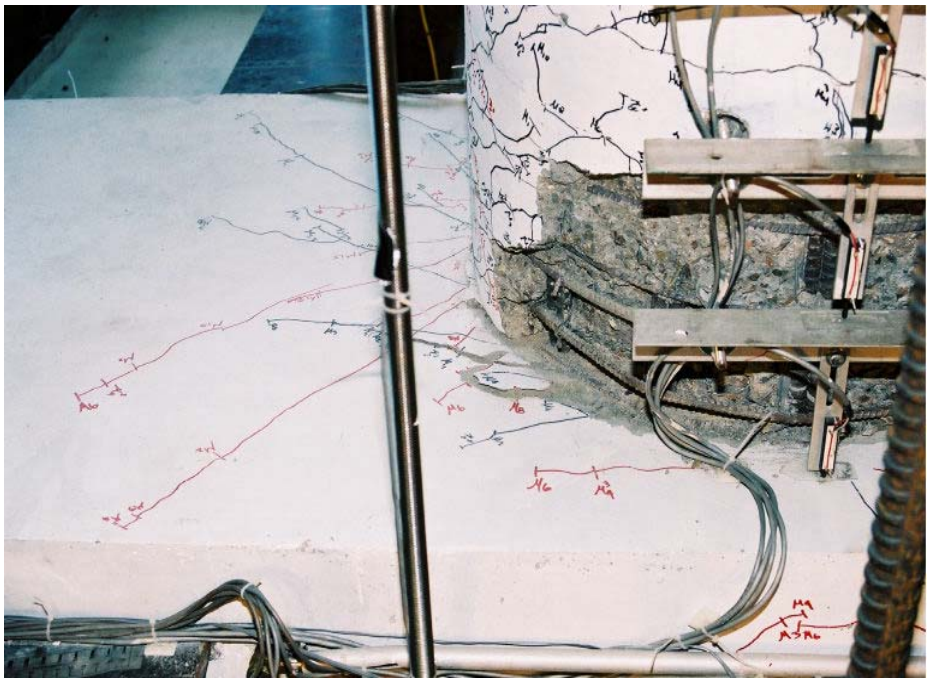

Figure 6-24 West Bent Cap Bottom Face $\mu_\Delta = 10$

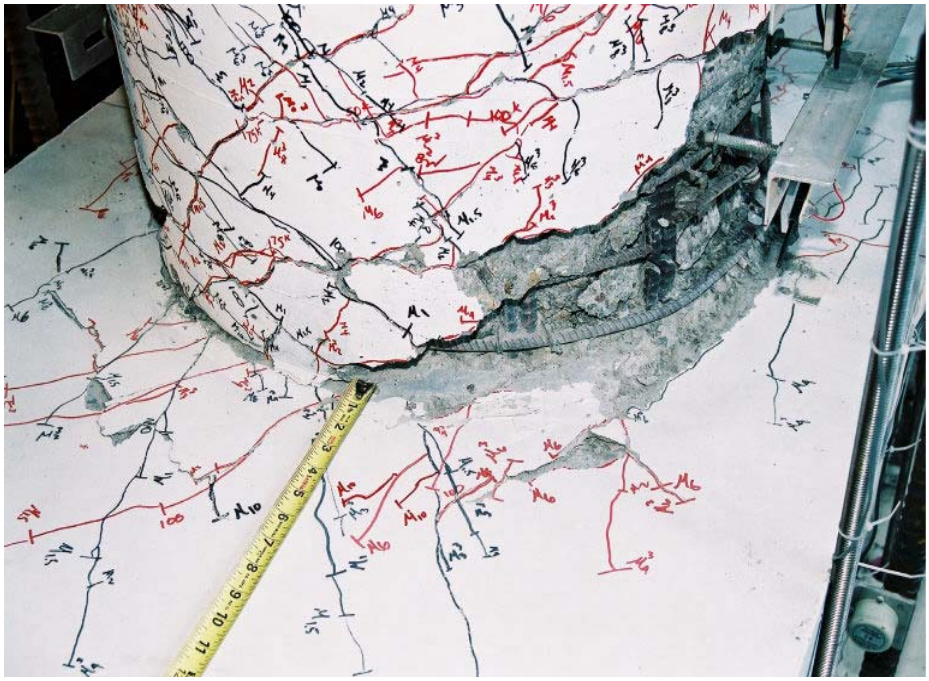

Figure 6-25 East Bent Cap Bottom Face at $\mu_\Delta = 10$

Figure 6-26 End of Test

6.3 MEASURED RESPONSE, SYSTEM TEST

The force versus displacement hysteresis of the column is shown in Figure 6-27. The force plotted is the actuator force and the plotted displacement is the column displacement measured at the load stub. Figure 6-28 shows the three components of column displacement at the load stub. The top displacement is a sum of displacement due to bent cap rotation, superstructure translation, and column deformation. All column displacements reported are located at the centerline of the load stub.

As presented in the observed performance section of this chapter, bent cap damage was concentrated in the joint region with no cracking of the bent cap outside the joint region. In addition to this visual assessment, rotation measurements at the end and middle of the bent cap substantiate that the entire superstructure is not effective in carrying the torsional moment. Figure 6-29 plots torsional moment versus bent cap rotation at the bent cap ends and at the column centerline. Rotation of the bent cap at the center is approximately five times greater than bent cap rotation at the end.

The column moment versus the column displacement is plotted in Figure 6-30. The displacement plotted is due to column deformation only. The figure plots the column overstrength design moment. This design moment was extrapolated to the centerline of the bent cap and multiplied by a capacity protection factor of 1.2 to obtain the superstructure torsional design moment.

As explained in Chapter *2,* this torsional moment is equally resisted on either side of the column. Therefore, the bent cap design moment plotted in Figure 6-31 is half of the design moment in Figure 6-30. The bent cap torque-twist behavior as predicted by equations from Hsu [26] and Collins and Mitchell [27] are plotted in the figure. The torsional shear friction capacity [18] of the section was predicted and is represented by a straight line in the graph. The twist is calculated by dividing the rotation by the length the rotation occurs over. The column centerline to girder centerline distance was equal to 26.4 in. [671 mm]. Because girder flanges and half the column encroach this length, using the exact center to center distance was not appropriate. Until further analysis is done to obtain a more precise twist length, the twist length was taken to be 24 in. [610 mm]. The first bent cap crack occurred at a bent cap torsional moment of 429 k-ft [582

kN-m]. The initial slope of the bent cap outside the joint region matches the initial slope from Collins and Mitchell [27] but the inside slope inside the joint region is flatter (lower torsional rigidity) The cracking strength was also well predicted by Collins and Mitchell's equation [27] for a prestressed beam. Because the Hsu [26] equation used did not account for additional strength due to post-tensioning, its predicted cracking strength was slightly lower than that measured in the test. The graph also illustrates that the bent cap design moment was never reached.

Performance of gravity load corrections at the column is plotted in Figure 6-32. Both axial loads were well maintained throughout the test.

Column curvature measurements are plotted in Figure 6-33. Curvature rods were located on the north and south face of the column.

Longitudinal deck deformation profiles obtained from linear displacement transducers located beneath the specimen are plotted in Figure 6-34. The deformed shape of the deck is appropriate for the seismic loading imposed on the test. Transducers at locations A and B were hooked up to a faulty box in the data acquisition system and were therefore not included in the graphs. The transverse deck deformation profiles are shown in Figure 6-35. At the bent cap centerline, a twisting of the bent is observed.

Figure 6-36 shows the column longitudinal reinforcement bars prior to yield. The first location to yield was in bar four on the push portion of the 100 kip [445 kN] cycle. Strain measurements in the bars after the first yield are shown in Figure 6-37. Ductility levels with readings beyond gage limits were omitted from the graphs.

Strain measurements in the bent cap main flexural reinforcement are shown in Figure 6-38. Reinforcement outside the joint region in the bent cap remained elastic throughout the test.

When the specimen is in the push cycle, deck reinforcement is in tension on the north side and compression on the south side (Figure 6-40). When the specimen is in the pull cycle, longitudinal deck reinforcement is in compression on the north end of the deck and tension on the south end. At the face of the bent cap, the longitudinal deck bars experience high strain deformations at the column centerline. Strain measurements of transverse deck reinforcement are plotted in Figure 6-41. Gages were applied to transverse deck reinforcement on the west side of the specimen only.

Strain measurements were taken from the top and bottom flanges of all girders. The two interior girders were instrumented with six strain gages on the top and bottom flanges in the joint region. All other flanges were instrumented with two strain gages each. Figure 6-42 and Figure 6-43 show strain measurements from the flanges of the two interior girders. The top flange is the flange nearest the deck and the gages are located on the inside of the girders. When the specimen is in the push stage of the cycle, the bottom flange is in compression on the north side and tension on the south. The top flange, composite with the deck maintains a relatively constant state of tension throughout the loading cycles.

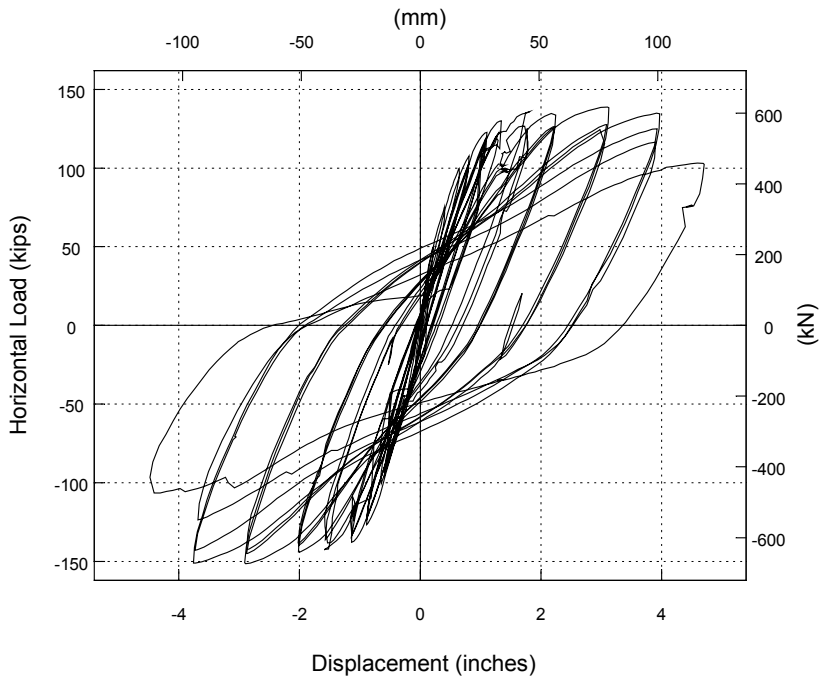

Figure 6-27 Column Force versus Displacement Response

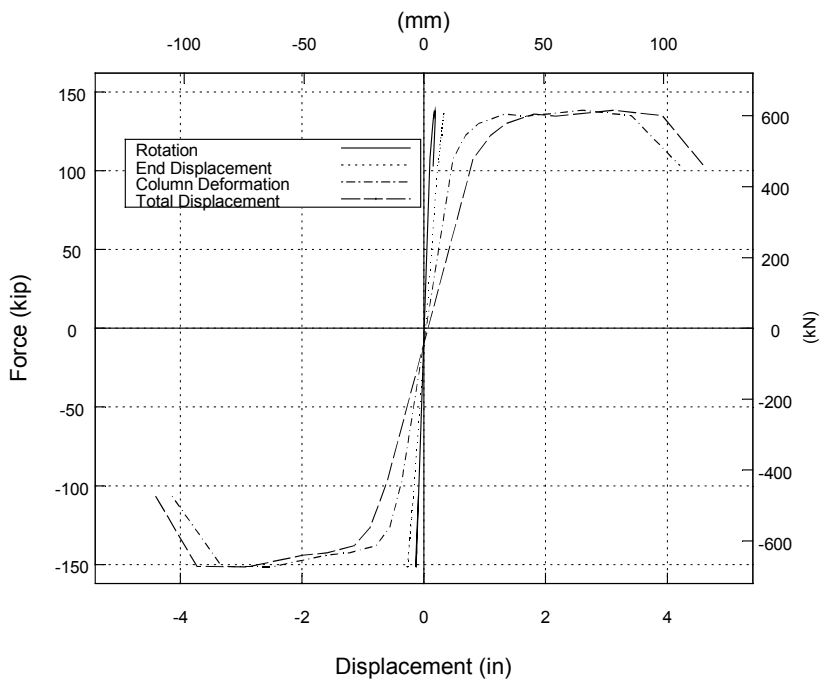

Figure 6-28 Components of Column Displacement

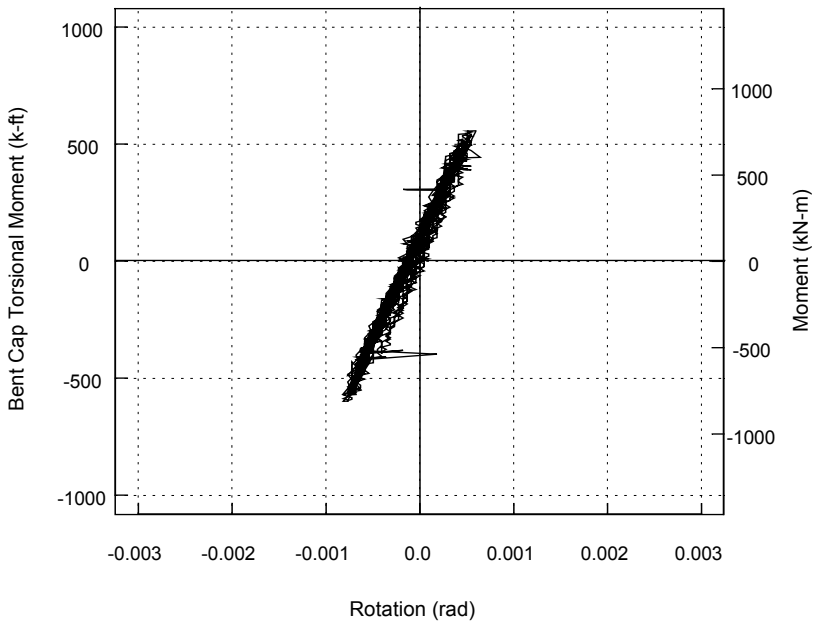

(a) at Bent Cap End

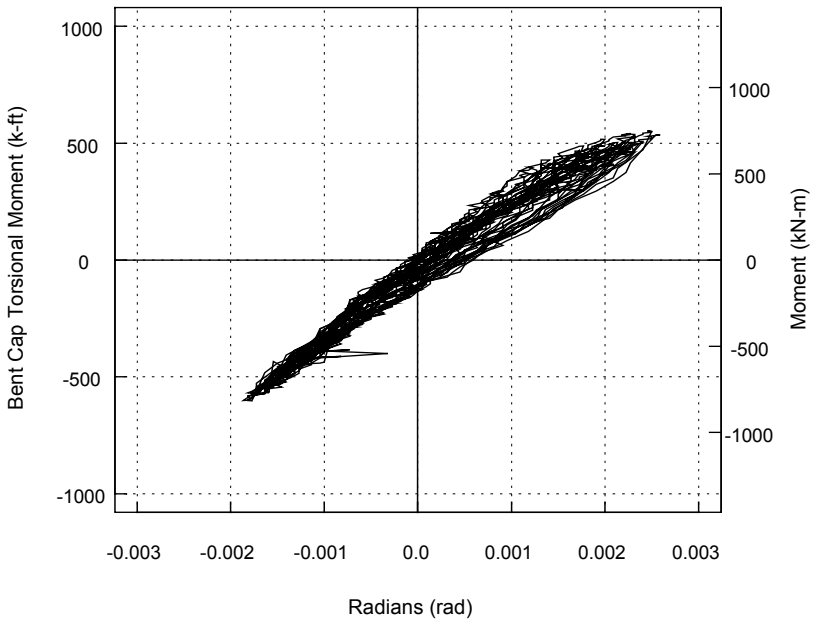

(b) at Column Centerline

Figure 6-29 Bent Cap Torsional Moment versus Rotation

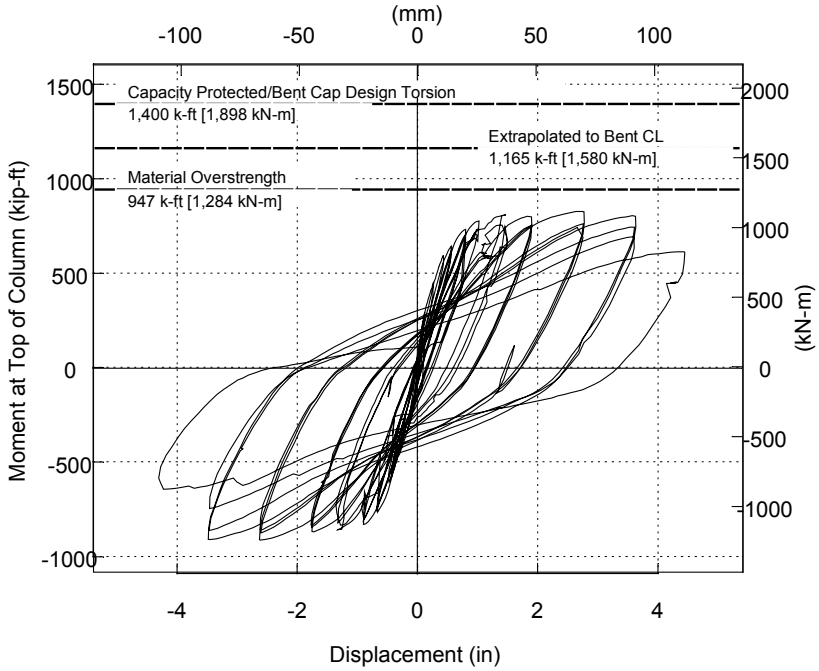

Figure 6-30 Column Moment versus Displacement

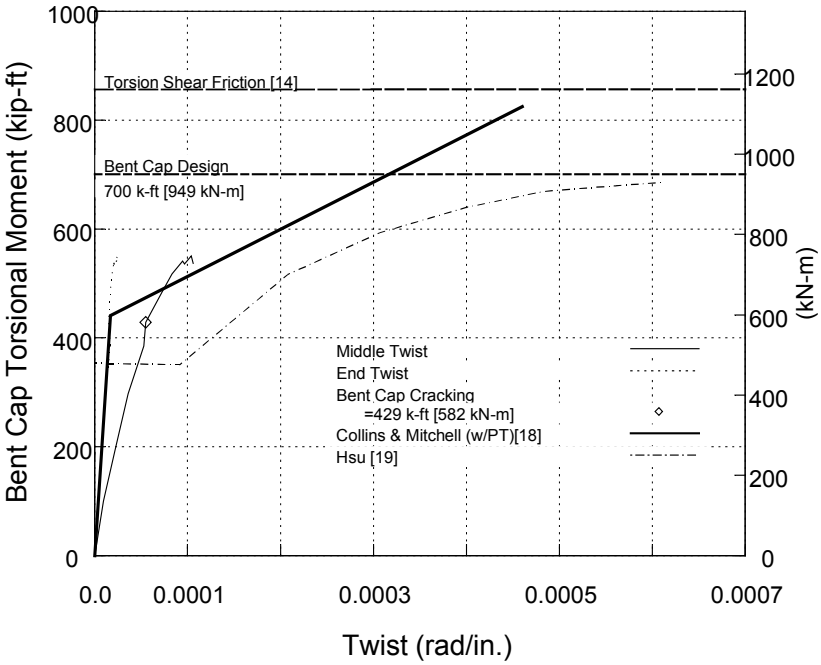

Figure 6-31 Torsional Moment at Superstructure Centroid

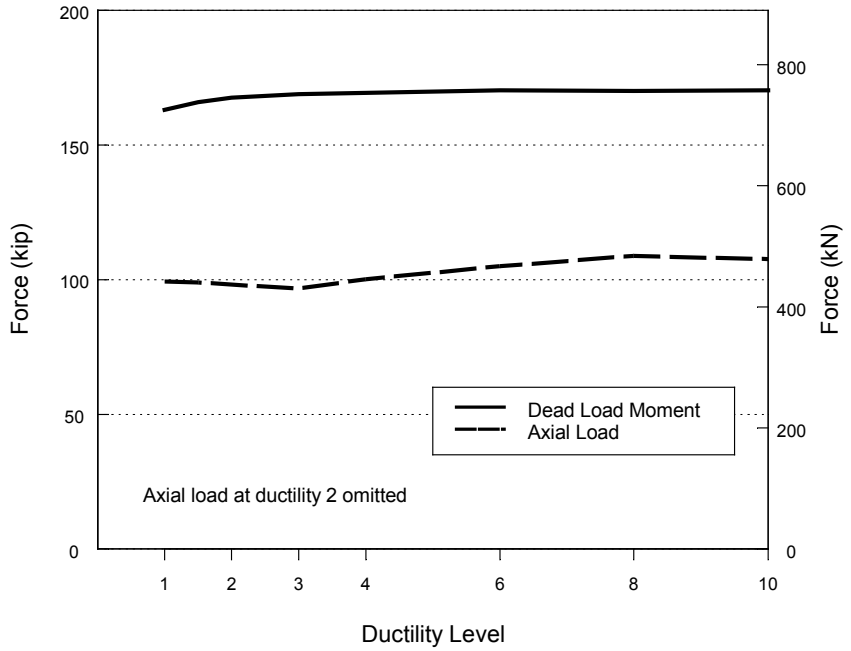

Figure 6-32 Dead Load Moment and Axial Load Performance

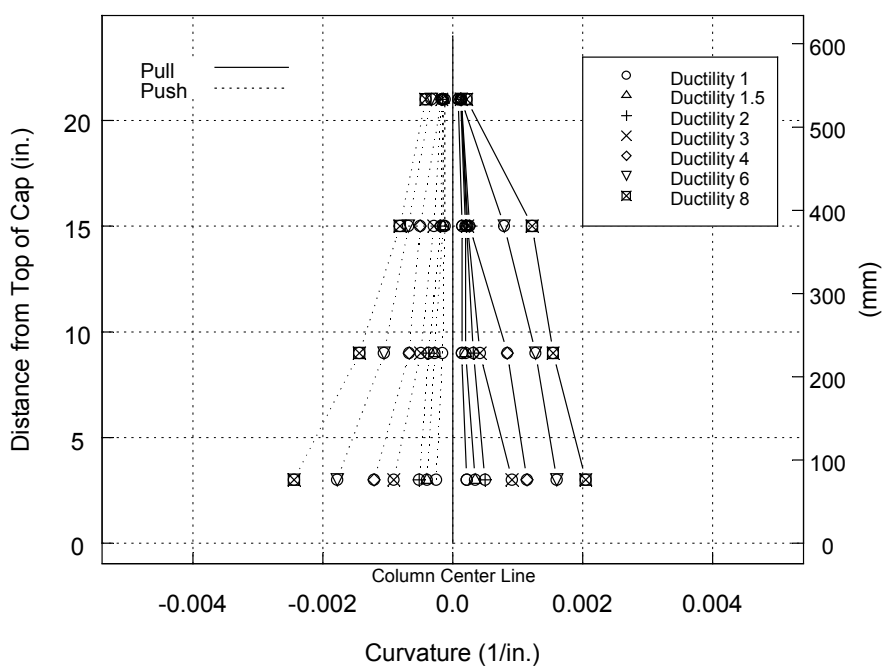

Figure 6-33 Column Curvatures

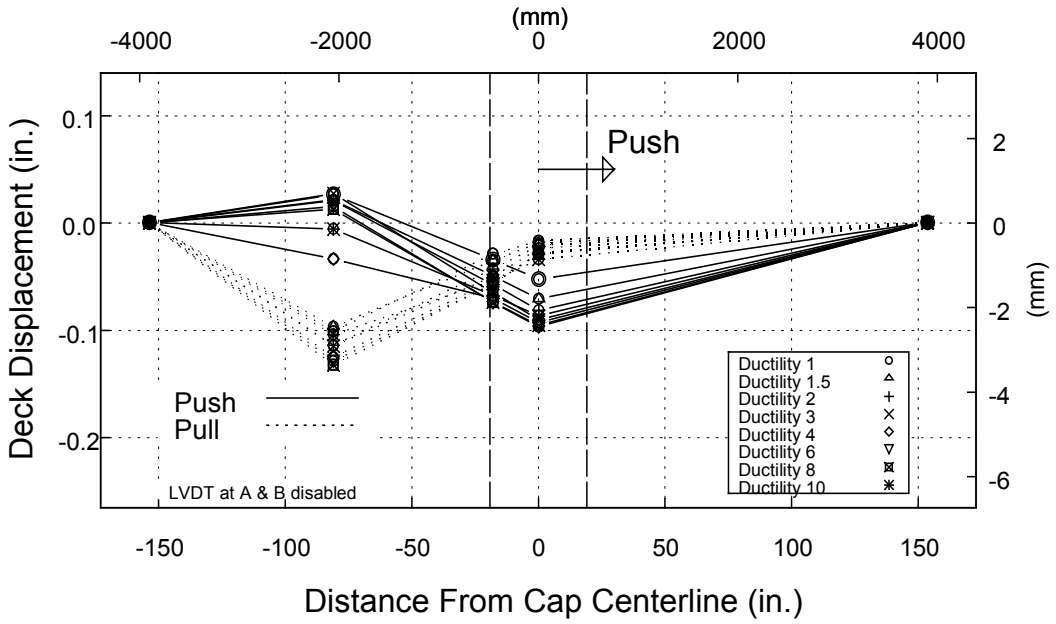

(a) Row One

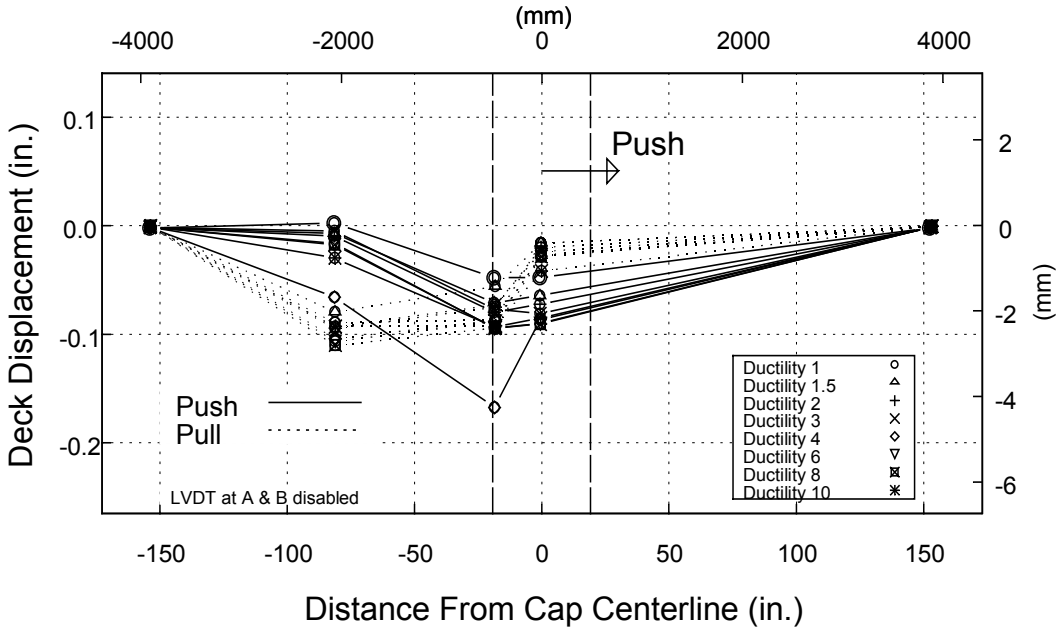

(b) Row Two

Figure 6-34 Measured Longitudinal Deck Deformation

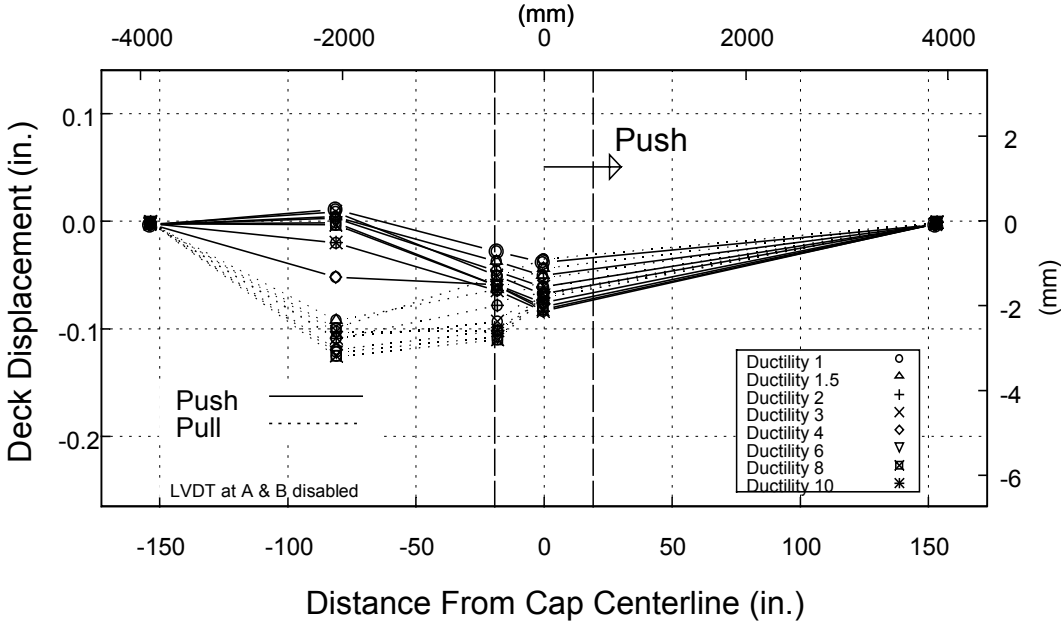

(c) Row Three

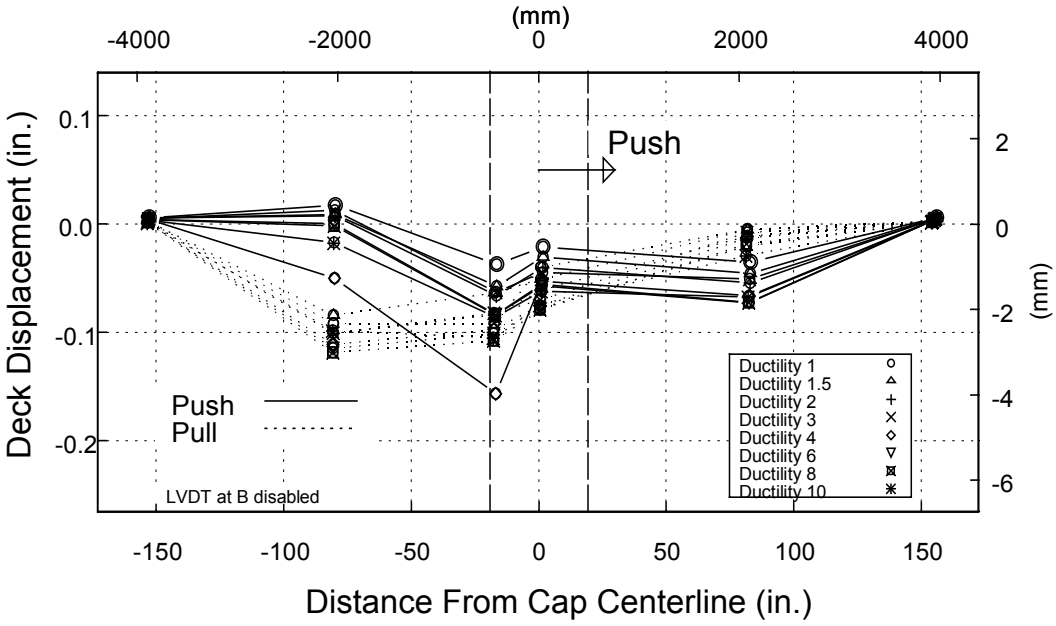

(d) Row Four

Figure 6-34 Measured Longitudinal Deck Deformation (cont.)

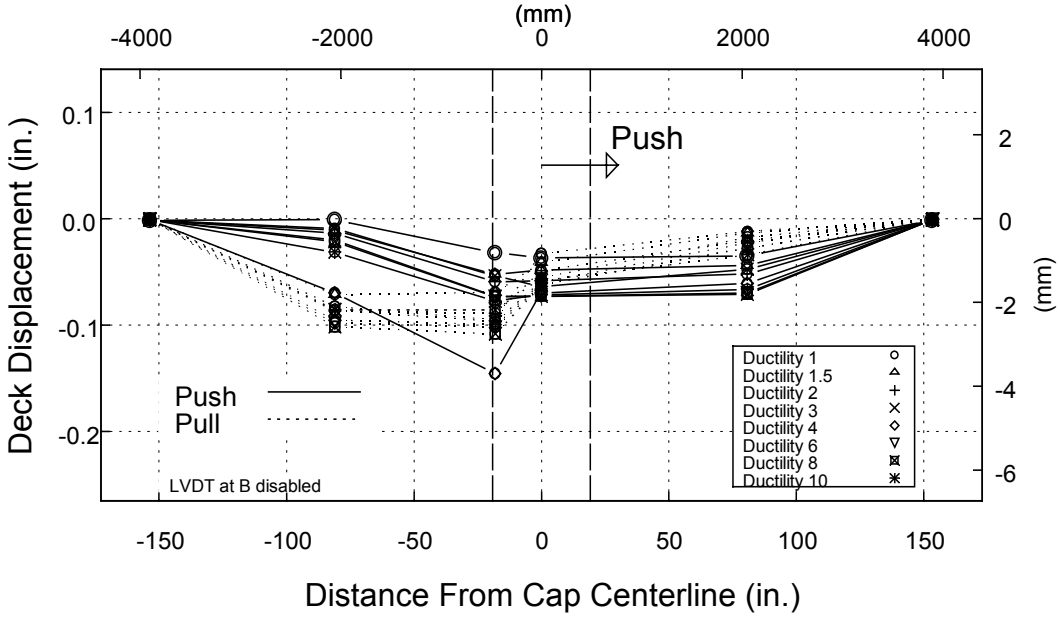

(e) Row Five

Figure 6-34 Measured Longitudinal Deck Deformation (cont.)

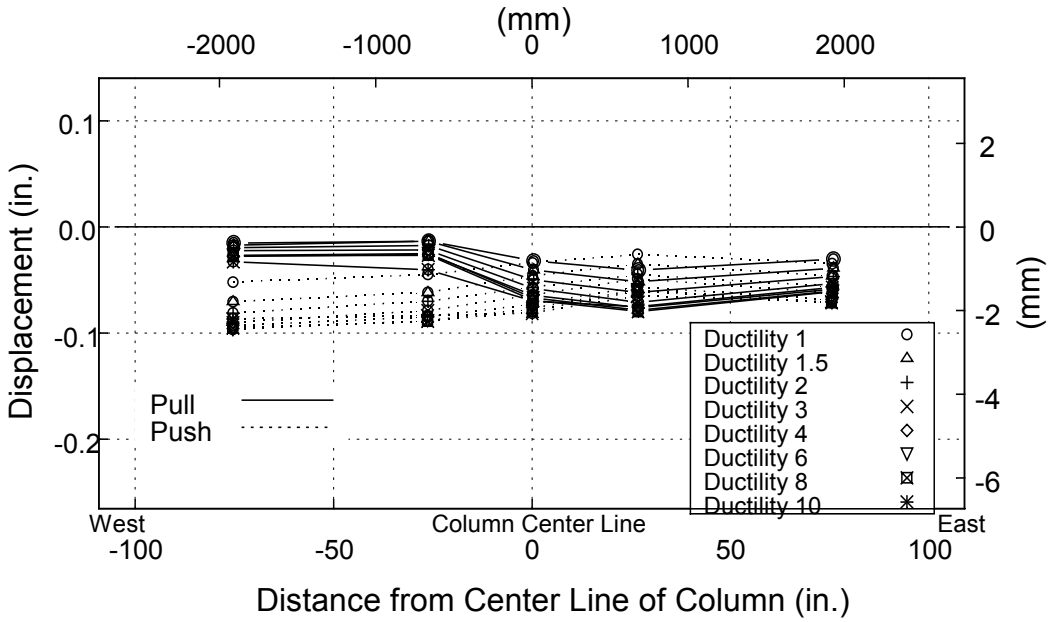

(a) Row C

Figure 6-35 Measured Transverse Deck Deformation

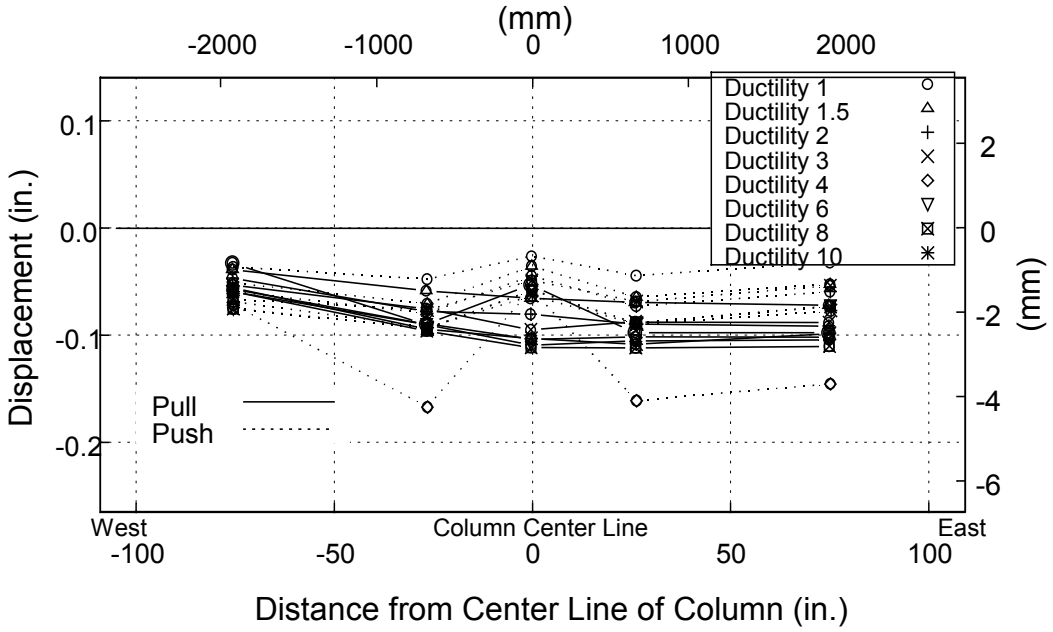

(b) Row D

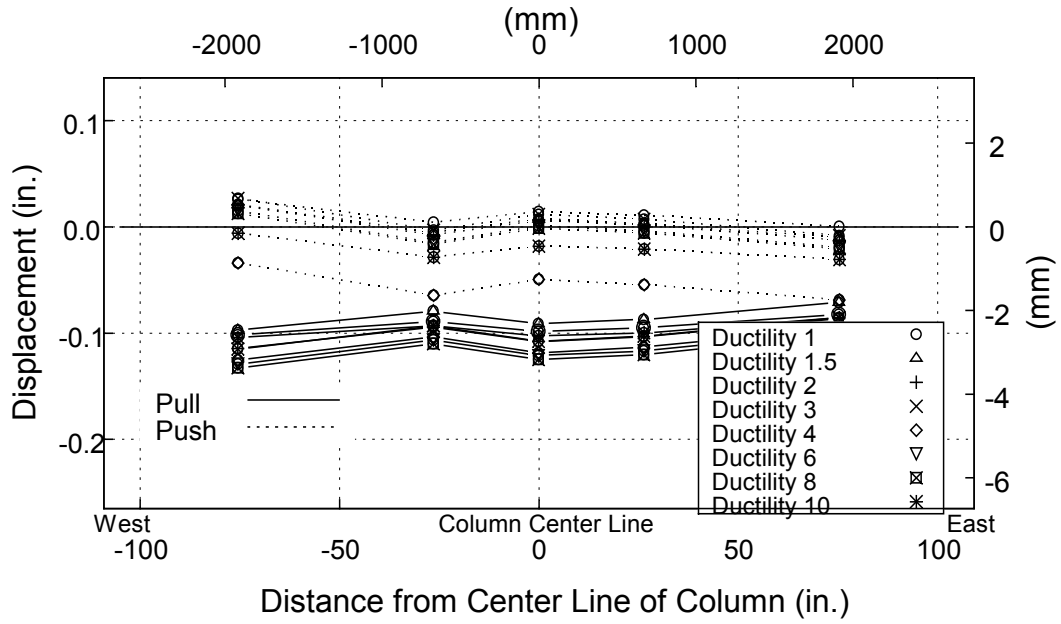

(c) Row E

Figure 6-35 Measured Transverse Deck Deformation (cont.)

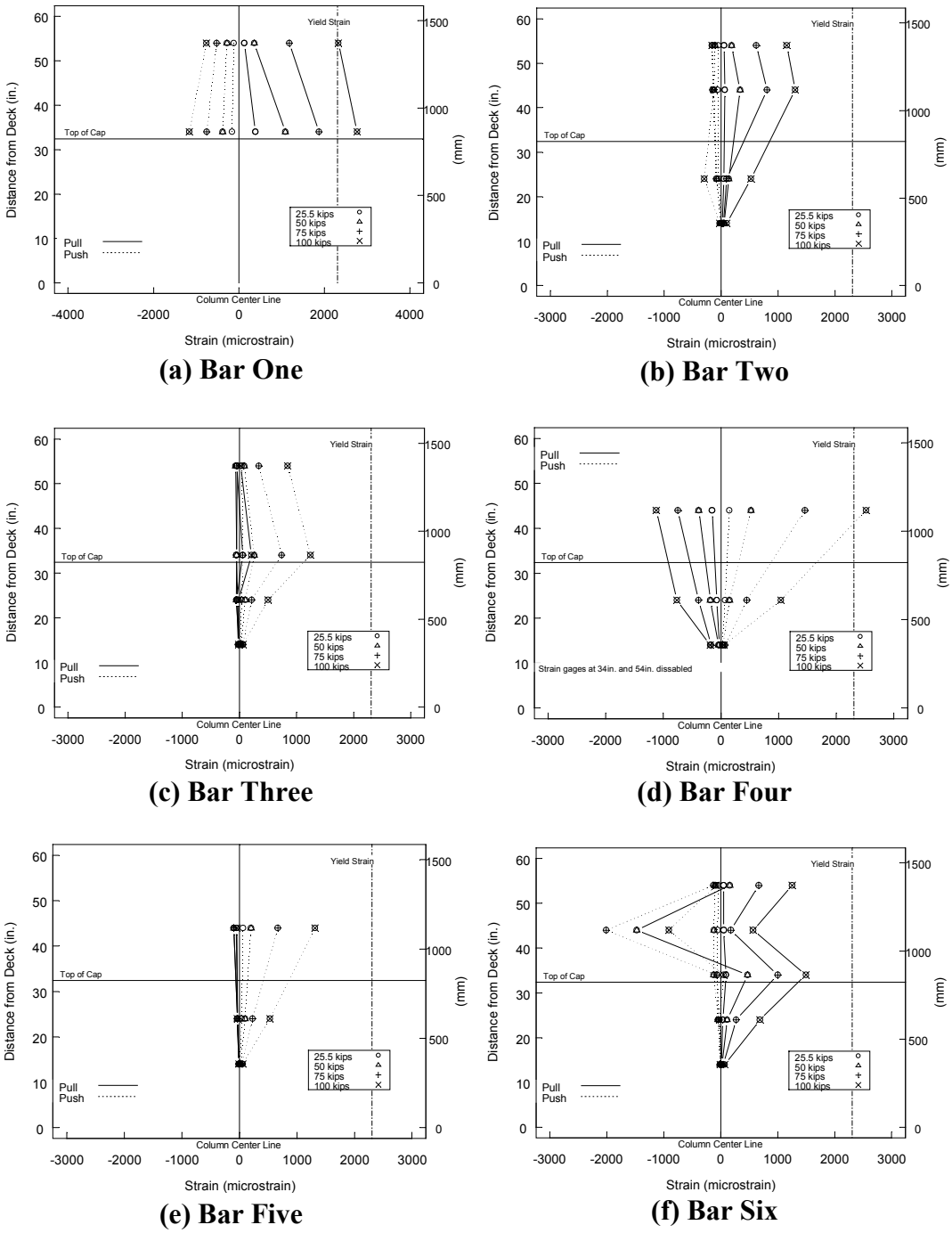

(a) Bar One

(b) Bar Two

(c) Bar Three

(d) Bar Four

(e) Bar Five

(f) Bar Six

Figure 6-36 Measured Strain in Column Longitudinal Bars Prior to First Yield

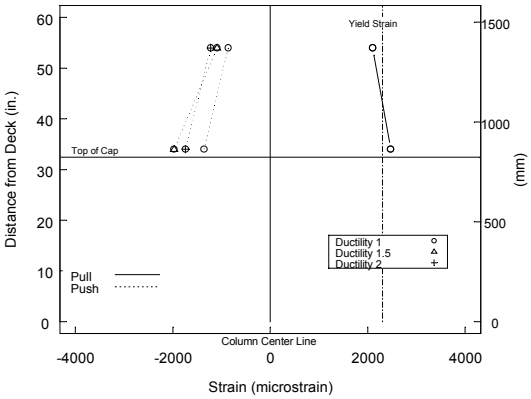

(a) Bar One

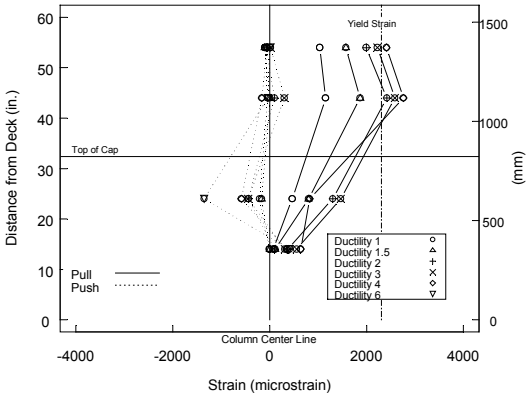

(b) Bar Two

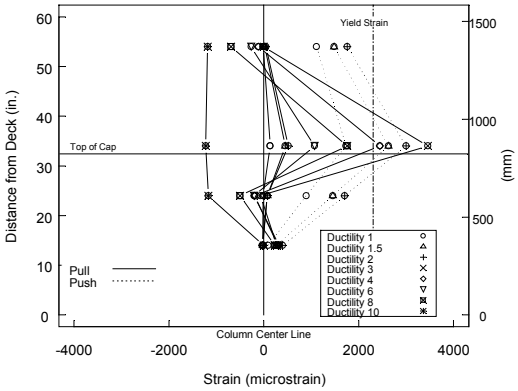

(c) Bar Three

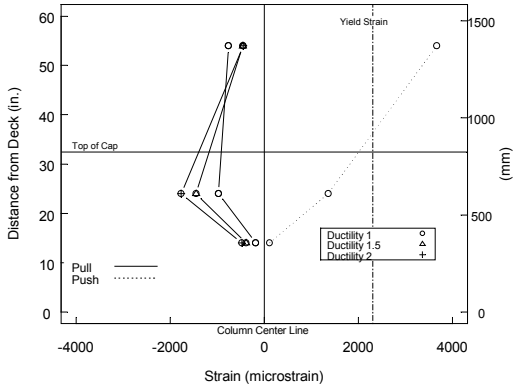

(d) Bar Four

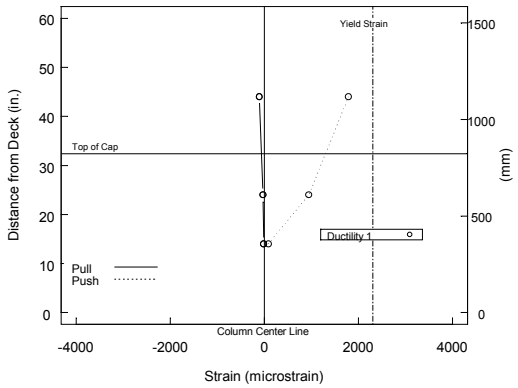

(e) Bar Five

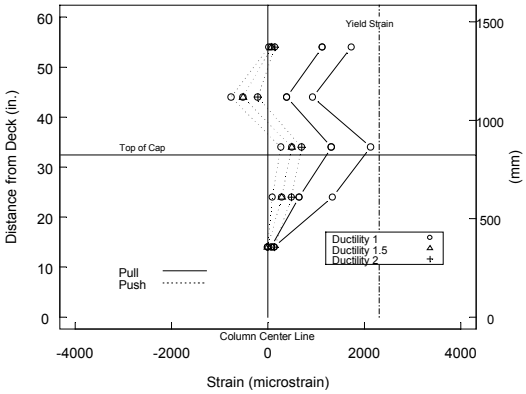

(f) Bar Six

Figure 6-37 Measured Strain in Column Longitudinal Bars Post-Yield

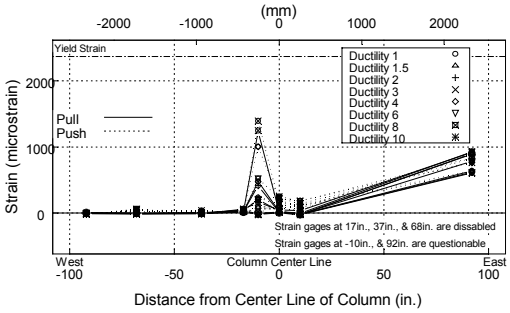

(a) Bar A

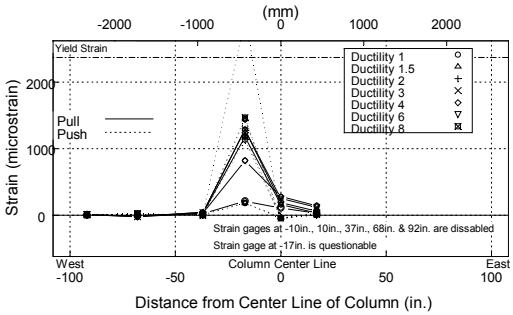

(b) Bar B

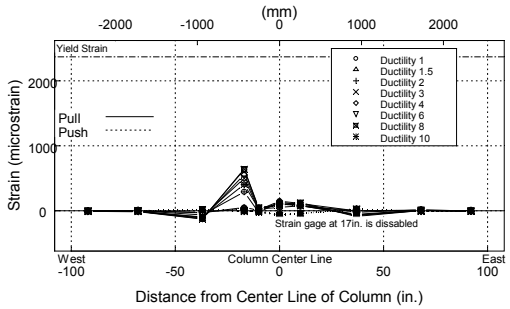

(c) Bar C

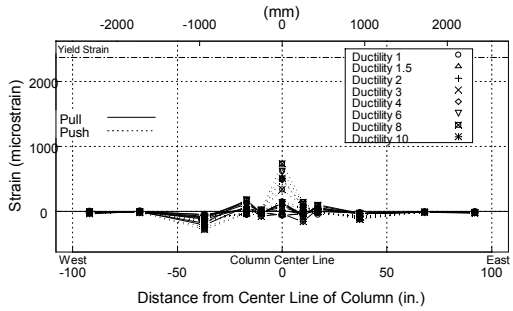

(d) Bar D

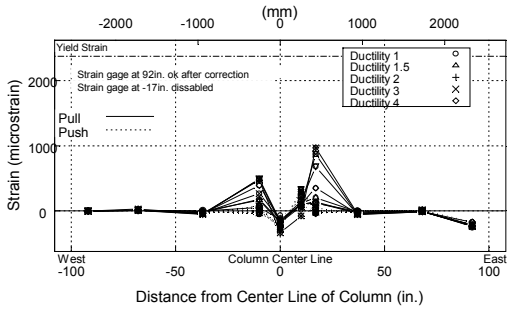

(e) Bar E

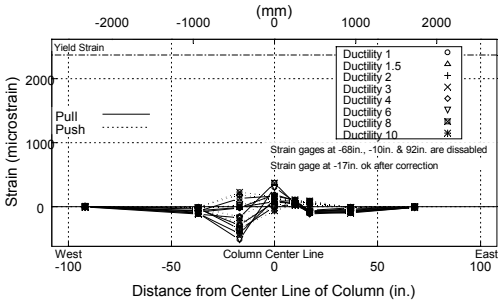

(f) Bar F

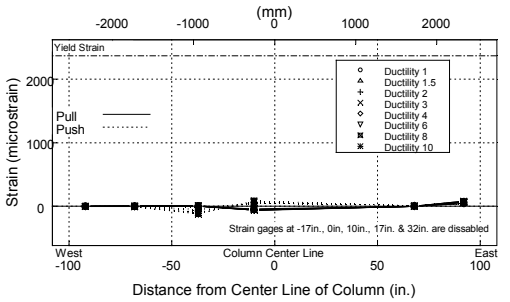

(g) Bar G

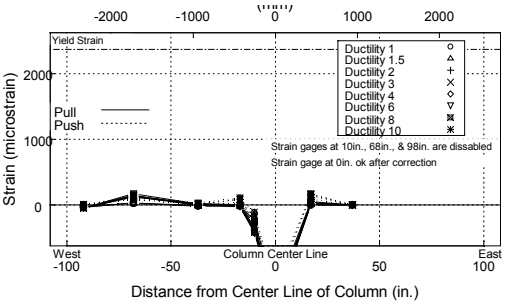

(h) Bar H

Figure 6-38 Measured Strain in Flexural Reinforcement

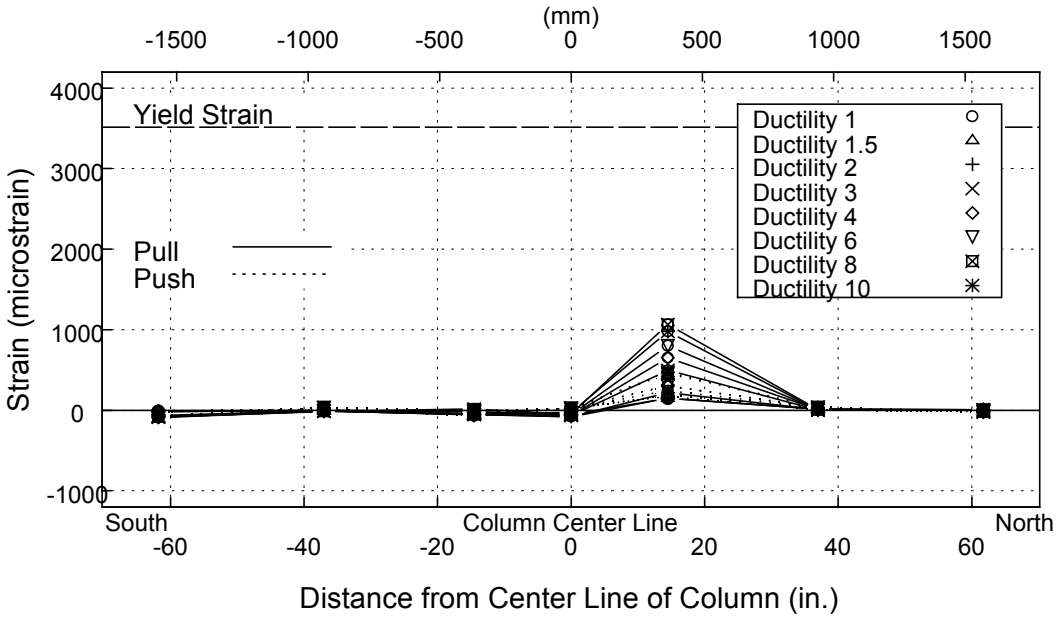

(a) Bottom South Corner

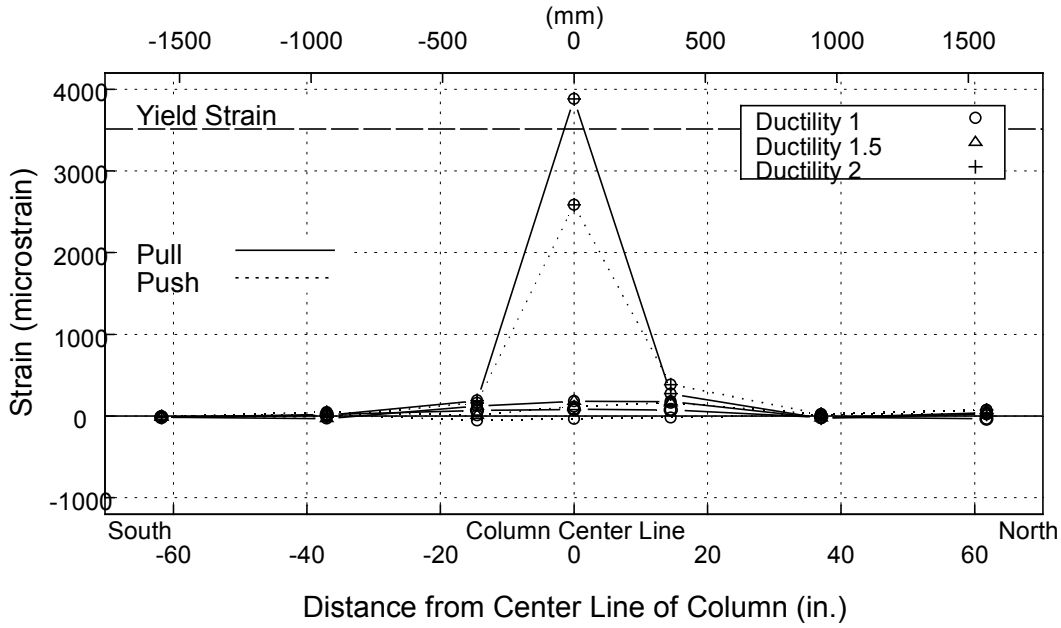

(b) Top North Corner

Figure 6-39 Measured Strain in Bent Cap Stirrups

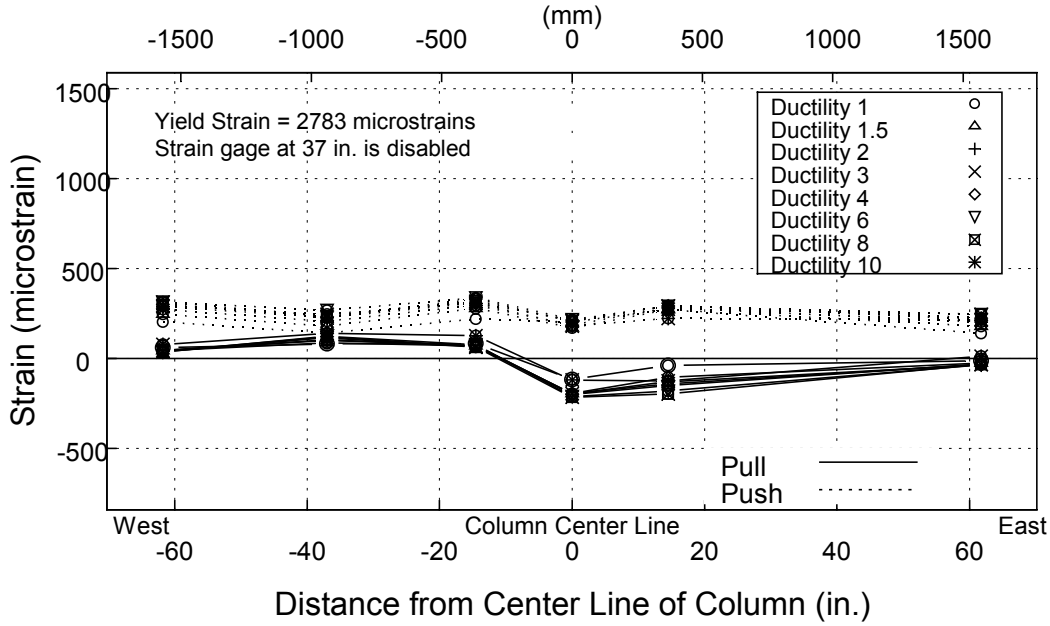

(a) Location A

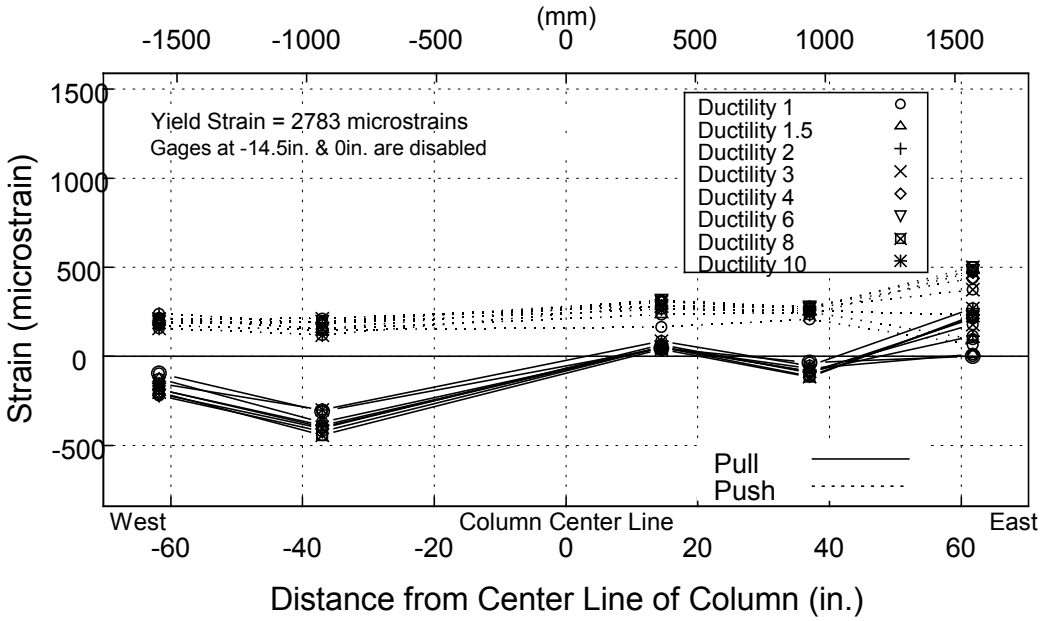

(b) Location B

Figure 6-40 Measured Strain in Longitudinal Deck Reinforcement

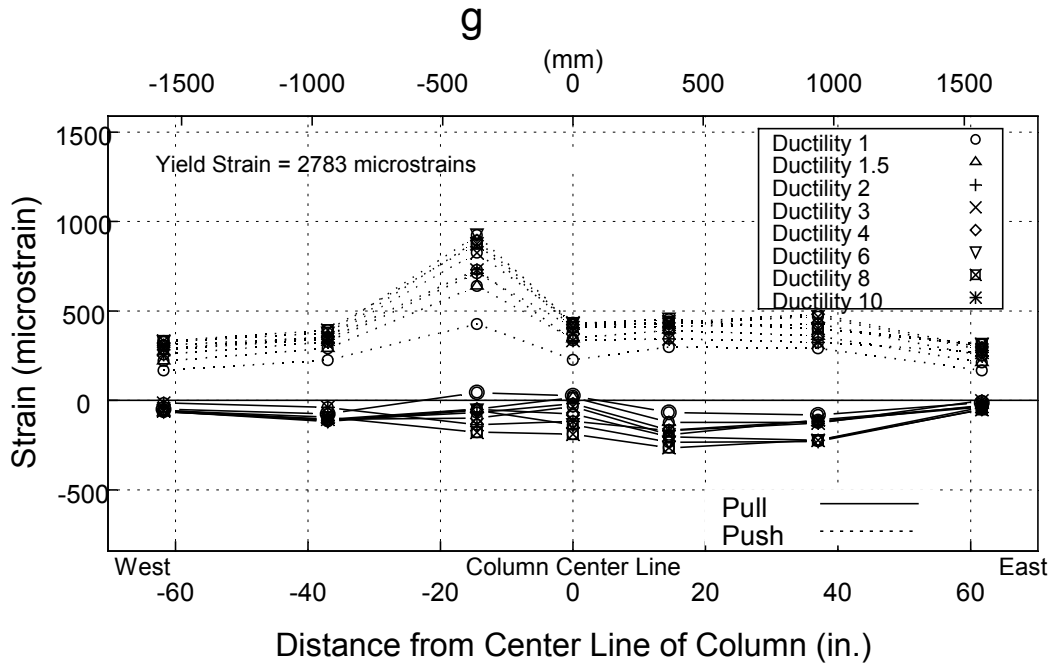

(c) Location C

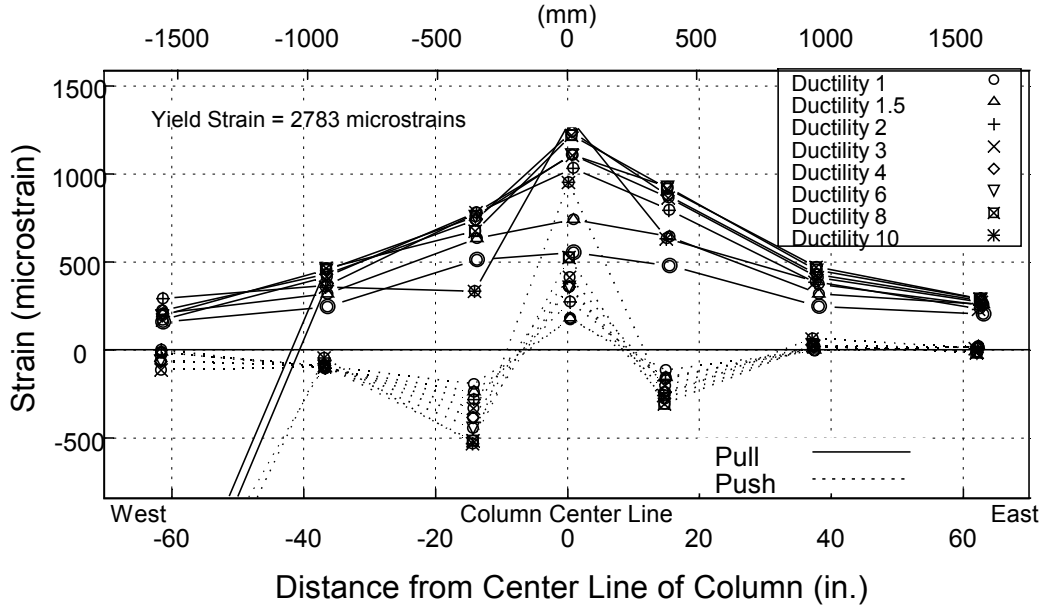

(d) Location D

Figure 6-40 Measured Strain in Longitudinal Deck Reinforcement (cont.)

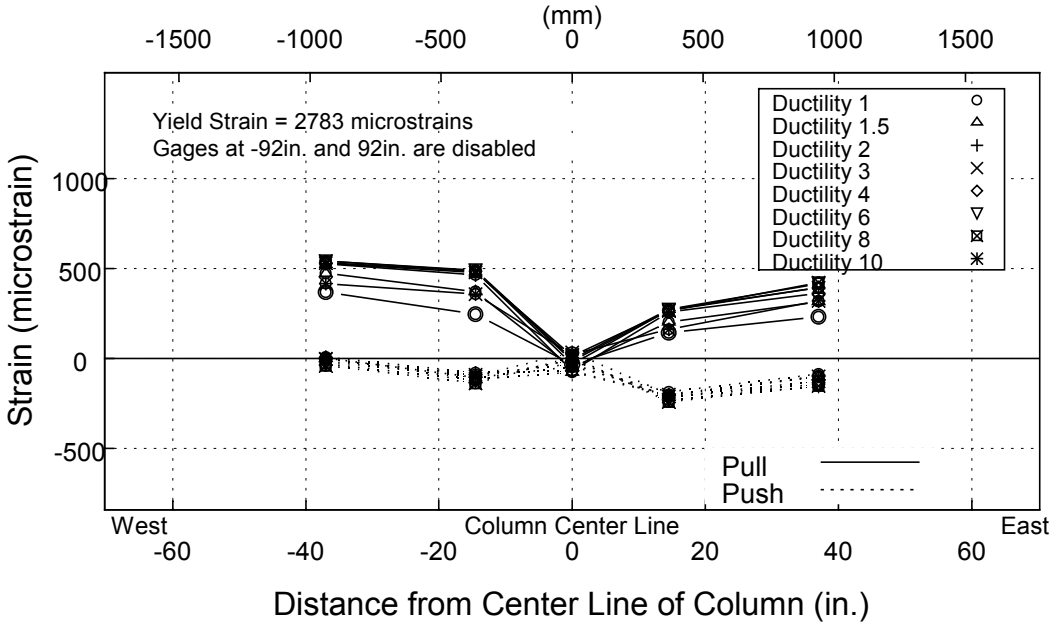

(e) Location E

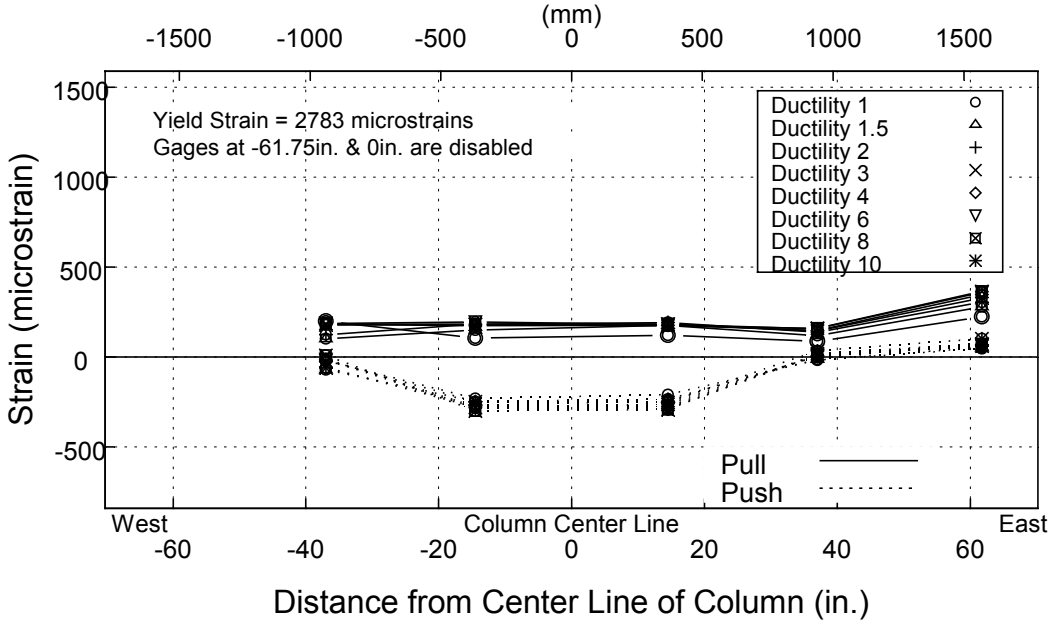

(f) Location F

Figure 6-40 Measured Strain in Longitudinal Deck Reinforcement (cont.)

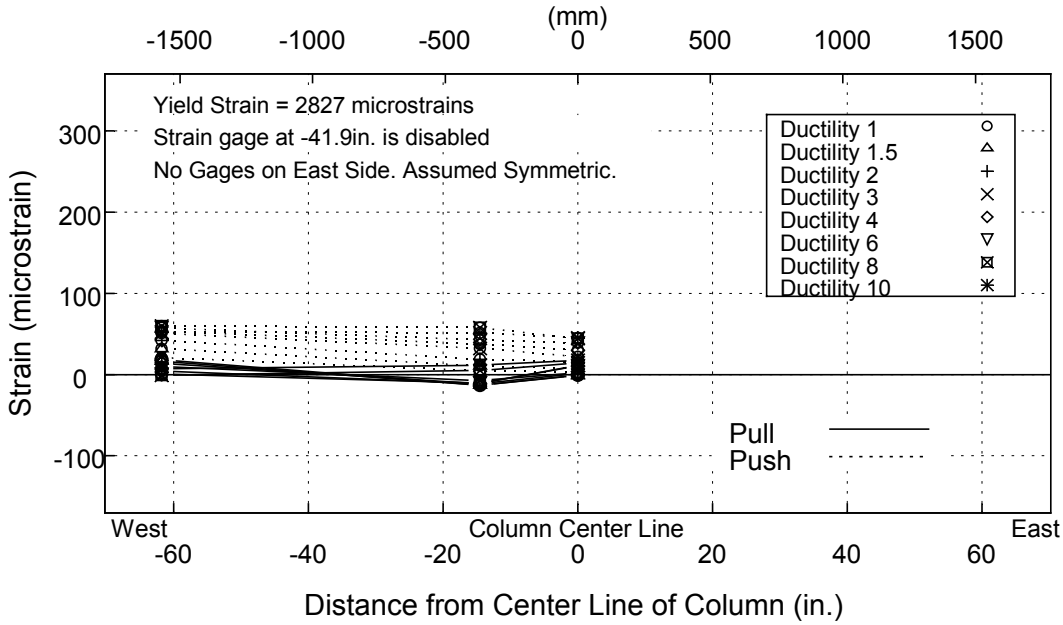

(a) Row A

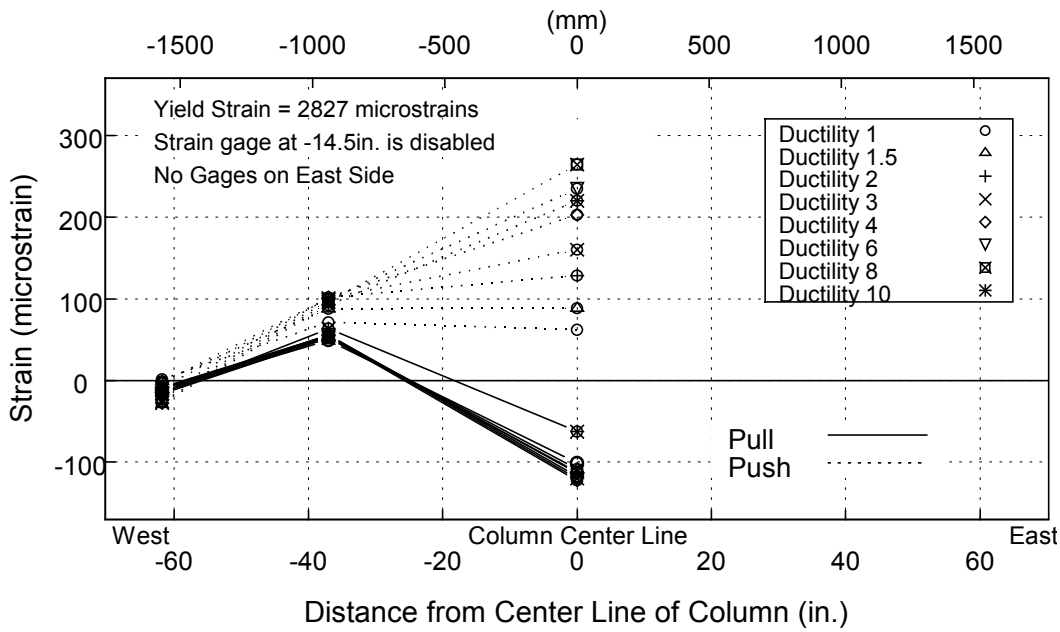

(b) Row B

Figure 6-41 Measured Strain in Transverse Deck Reinforcement

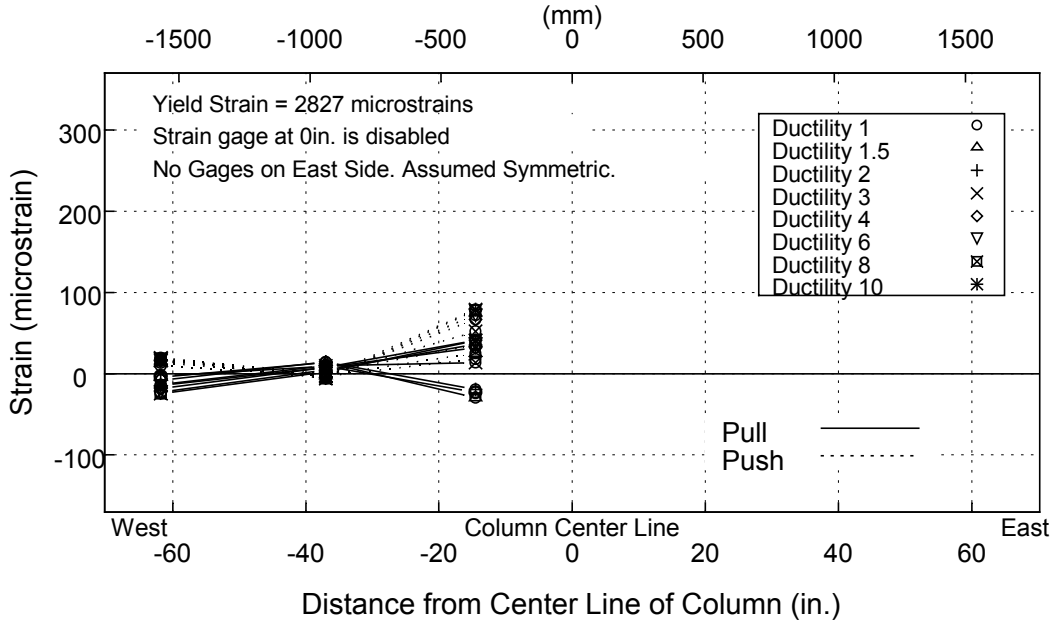

(c) Row C

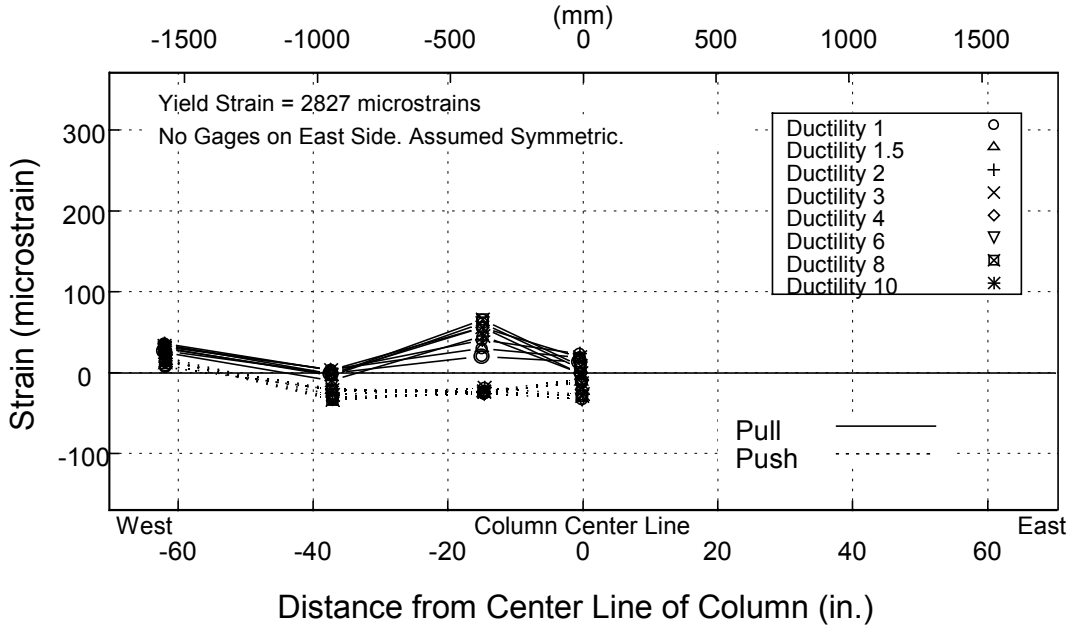

(d) Row D

Figure 6-41 Measured Strain in Transverse Deck Reinforcement (cont.)

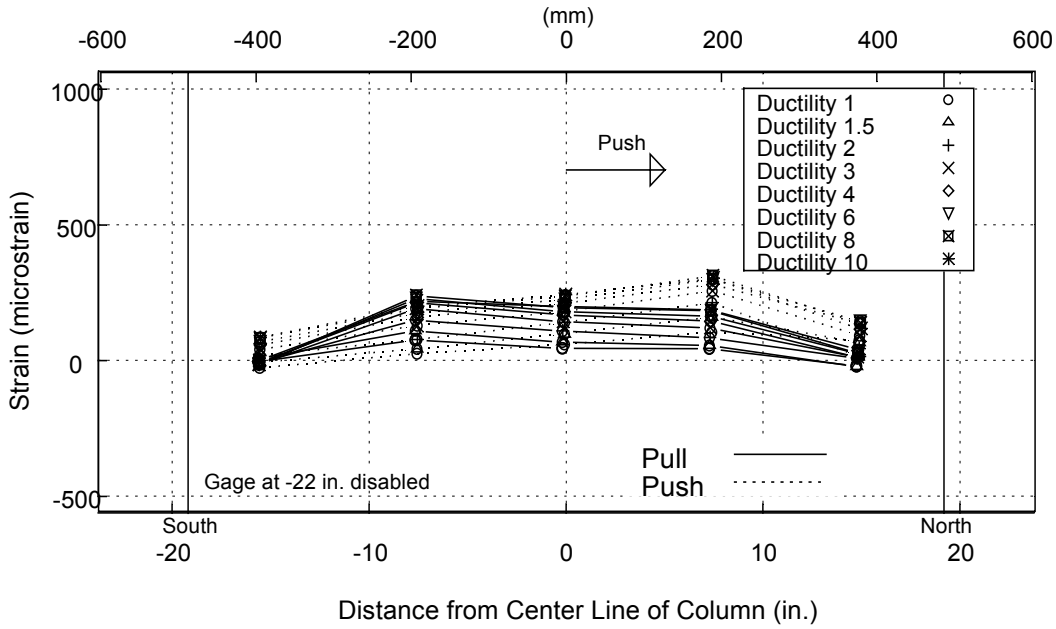

(a) Top Flange

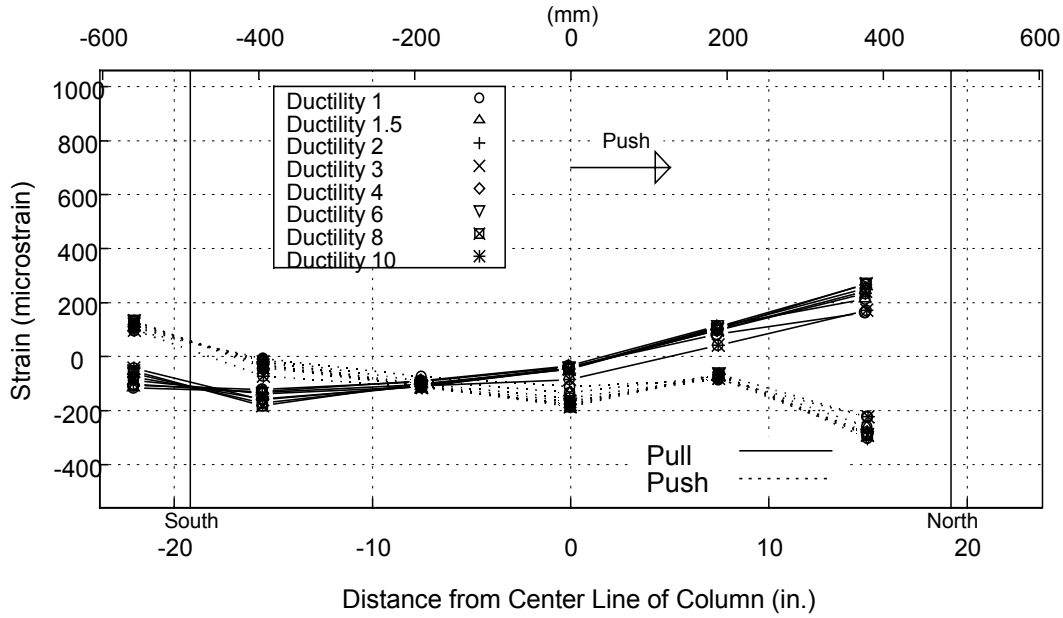

(b) Bottom Flange

Figure 6-42 Measured Strain in Flanges Girder Two, Joint Region

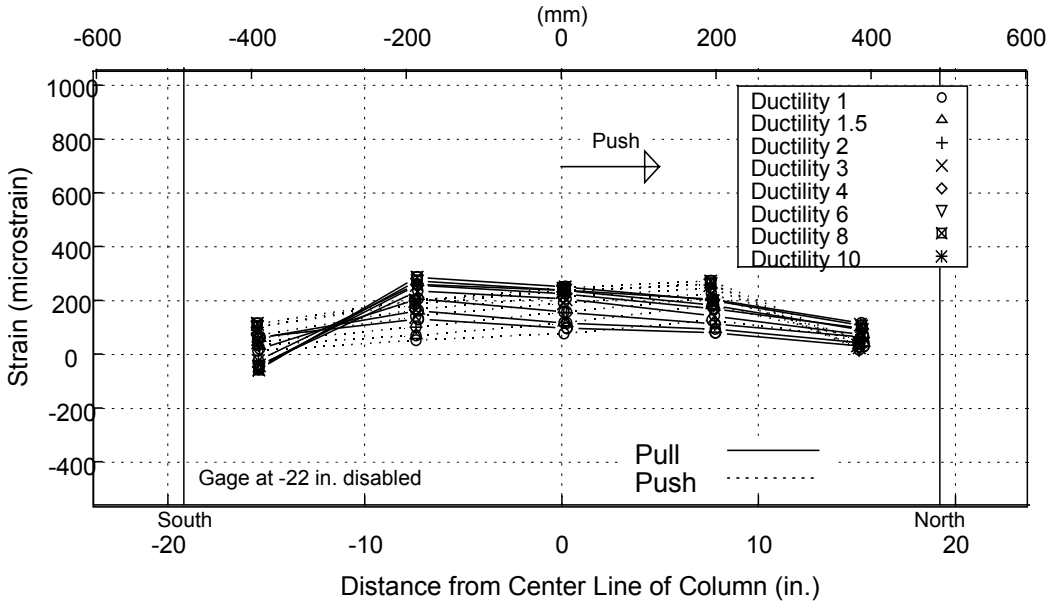

(a) Top Flange

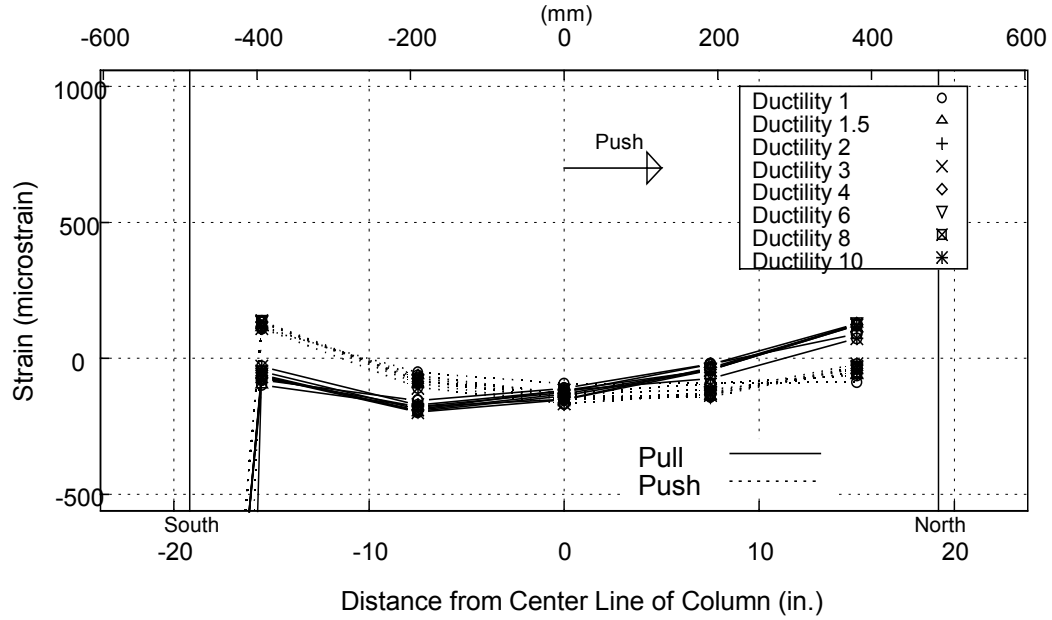

(b) Bottom Flange

Figure 6-43 Measured Strains in Flanges Girder Three, Joint Region

Chapter 7

Development of Design Model

7.1 OVERVIEW

This chapter presents preliminary design recommendations and construction considerations. Section 7.2 presents the recommended design procedure for integral connections. Section 7.3 outlines design specifications. Section 7.4 suggests design issues to consider for alternative bent cap configurations. Construction and maintenance considerations are presented in Section 7.5. The chapter concludes with a summary in Section 7.6

7.2 RECOMMENDED BENT CAP DESIGN PROCEDURE

This section outlines the recommended seismic design process of an integral bent cap. The first portion of the section outlines the procedures for determining the demands on the bent. The second portion outlines the procedure for determining the capacities. The bridge used for the design example is a single-column, post-tensioned bent cap with four steel plate girders (Figure 7-1). A single pair of full height bearing stiffeners is located on the girder web in the bent cap region on all four girders. The bridge is a four span bridge.

The design process presented is based on recognizing that the bent cap between the interior girders and the column is essentially a "deep beam". Using this analogy, the force is transferred through a compression field between the interior girders and the column. Therefore, one step of the design process limits the compressive strength of the concrete based on this assumption.

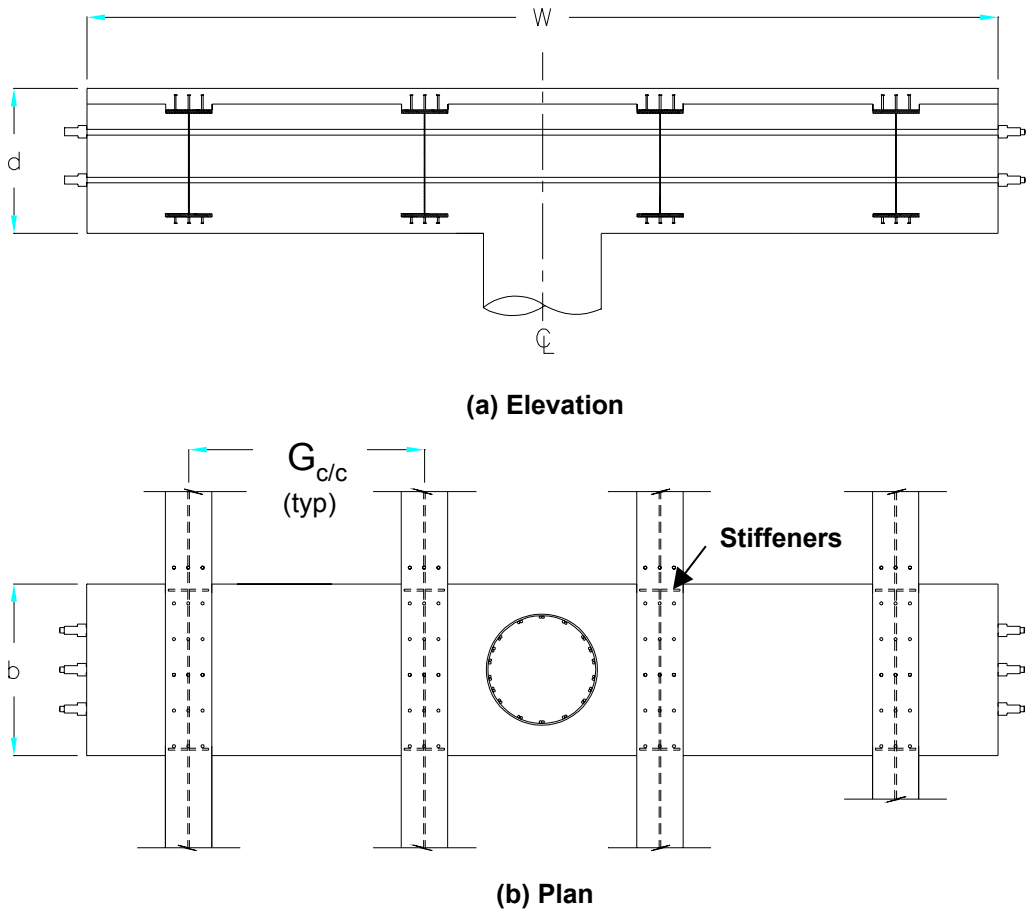

Figure 7-1 Design Example Bridge

Only torsional loads induced by a longitudinal seismic event are considered in this section. This portion of the design example assumes that the design earthquake is specified, all components are preliminarily sized, and the required load combinations as specified in AASHTO have been considered.

7.2.1 Bent Cap Torsional Moment Demand

Column Moment Overstrength (M_{max})

The overstrength moment, M_{max}, for the column as designed is determined at the top of the column from a moment curvature analysis with appropriate material overstrength moments applied (Figure 7-2). An overstrength factor of 1.3 applied to the concrete compression strength, steel yield strength and steel ultimate strength is recommended ($1.3f_y$ and $1.3f'_c$) (*priestley class notes* ref).

Capacity Protected Overstrength (M_T)

Extrapolate the column overstrength moment M_{max} at the top of the column to the superstructure centerline to get M'_{max} (Figure 7-2):

$$M'_{\max} = M_{\max}\left(\frac{d/2 + l_c/2}{l_c/2}\right) \tag{7-1}$$

Apply a component overstrength factor of 1.2 (20) to M'_{max} to obtain the superstructure torsional moment demand, M_T.

Bent Cap Torsional Design Moment, $M_T/2$

For a symmetric, single column bent, the torsional moment is equally split to either side of the superstructure. Figure 7-3 illustrates the recommended distribution of the torsional moment to the superstructure. With girders straddling the column, the torsional bent cap design moment is half the superstructure torsional moment demand, $M_T/2$.

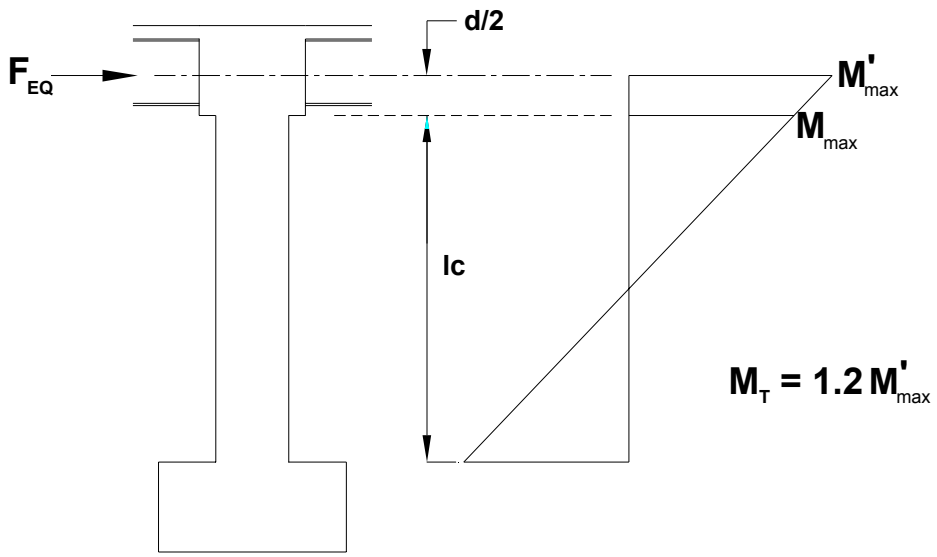

Figure 7-2 Superstructure Design Moment

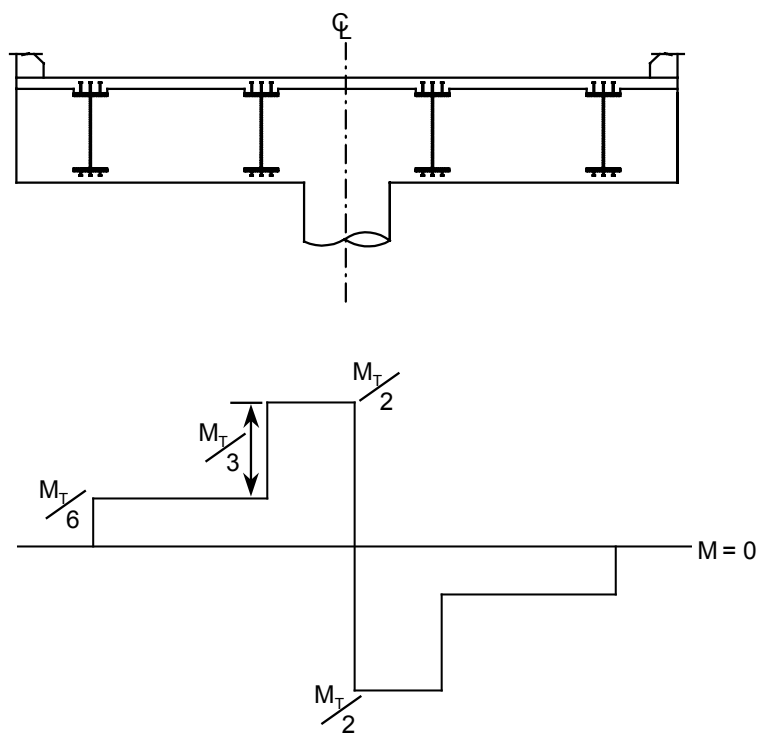

Figure 7-3 Distribution of Design Moment Along Bent Cap

Girder Demands/Effective Superstructure Width

As explained in the previous section, the torsional moment is distributed to the bridge abutments over the entire superstructure width. As shown in Figure 7-3, the torsional moment is distributed along the bent cap with a higher proportion of the moment being resisted by the interior girders. The worst case scenario would be to design the interior girders for the entire moment, resulting in overdesign of the exterior girders. Assuming the torsion is equally distributed between the interior and exterior girder is inappropriate because of the relative bent cap torsional stiffness. Previous research (9) has recommended that the torsional moment be split 2/3-1/3 between the interior and exterior girder. Based on the experimental and analytical results of the system test, the same recommendation is used for superstructure moment distribution of an integral bridge.

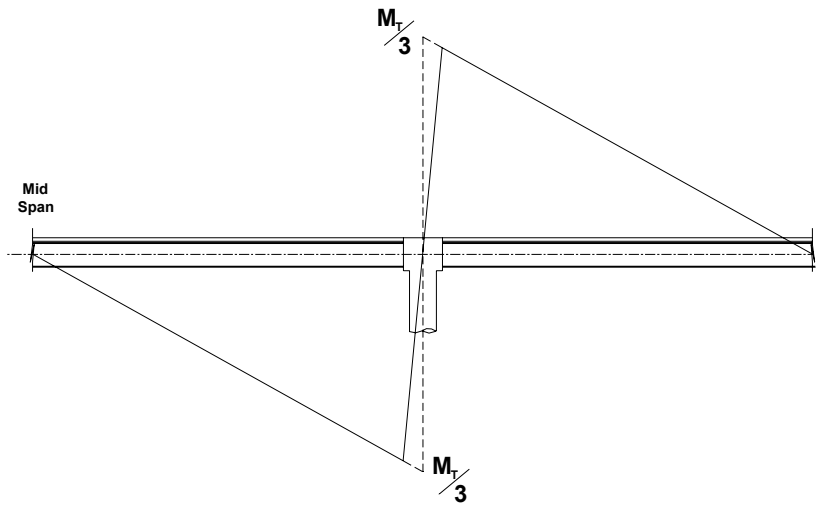

(a) Interior Girder

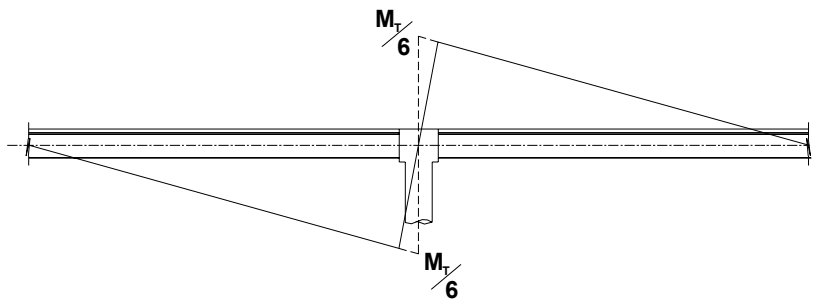

(b) Exterior Girder

Figure 7-4 Girder Moment Profiles

7.2.2 Bent Cap Torsional Moment Capacity

Bent Cap Cracking Moment (M_{cr}).

The cracking torque for a prestressed section is calculated from Collins and Mitchell's equation (27):

$$T_{cr} = \frac{A_c^2}{p_c} f_{cr} \sqrt{1 + \frac{f_{pc}}{4\sqrt{f_c^{'}}}} \tag{7-2}$$

In the system test, this cracking moment occurred at 60% of the bent cap design moment, therefore the following limit is placed on the cracking torque:

$$T_{cr} \geq 0.6 \frac{M_T}{2} \tag{7-3}$$

Concrete Compressive Stress (σ_{st}).

At the bent cap torsional design moment, $M_T/2$, the compressive stress in the bent cap concrete should be limited to $0.5f'_c$. The bent cap concrete compressive stress is checked by considering a compression strut that extends from the compression zone of the column to the intersection of the top girder flange, web and stiffener. Following is a step-by-step procedure to obtain the compresive stress in the bent cap concrete.

(a) The moment is resolved into a T-C couple at the column. The distance between the T-C forces is approximated as two-thirds the column diameter (Figure 7-5a). The total T-C force is then obtained from the superstructure torsional moment demand:

$$T = C = \frac{3M_T}{2D_c} \tag{7-4}$$

(b) As shown in Figure 7-3, the torsional moment is distributed to either side of the column. Therefore the compression and tension force to be resisted by the bent cap on either side of the column is half the force obtained in Step (a) (Figure 7-5b). The compression force $C/2$ is the vertical component of the strut that determines the limiting stress in the bent cap.

(c) The angle the strut makes with the plane of the bridge deck (θ_z in Figure 7-5c) is limited to be between 35-55°. This angle is determined from the bridge geometry. The height of the strut, h, can be equated to the depth of the bent cap, d, less the deck thickness, t_{deck}.

$$h = d - t_{deck} \tag{7-5}$$

From Figure 7-5d, the length of the strut, l, in the plane of the bridge deck is derived from:

$$l = \sqrt{\left(\frac{G_{c/c}}{2}\right)^2 + \left(\frac{1}{3}D_c\right)^2} \tag{7-6}$$

where $G_{c/c}$ is equal to the center to center spacing of the interior girders. The horizontal distance in the longitudinal bridge direction is approximated to be 1/3 of the column diameter (D_c). The angle of the strut is determined from:

$$\theta_z = \tan^{-1}\left(\frac{h}{l}\right) \tag{7-7}$$

If this angle is greater than 55° or less than 35°, the section depth or girder spacing are modified.

(d) Obtain the axial force in the strut from the vertical compression force

$$F_{strut} = \left(\frac{C}{2(\sin\theta)}\right) \tag{7-8}$$

(e) Determine the area over which the force in Step (d) acts. The thickness of the compression field, t, is taken to correspond to the depth of the compression block of the column approximated to be $1/3D_c$ in Step (c). The width of the compression field is equal to the depth of the bent cap, d, multiplied by the sin of the strut angle:

$$w = d \sin \theta \tag{7-9}$$

(f) The stress in the compression field is equal strut force, F_{strut}, divided by the cross-sectional area over which it acts

$$\sigma = \frac{F_{strut}}{w \cdot \frac{1}{3} D_c} \leq 0.5 f_c^{'} \tag{7-10}$$

Resolving the stress term into a function of the superstructure demand moment, M_T, by recalling that $C=(3M_T/2D_c)$, Equation (1-10) can be rewritten as:

$$\sigma = \frac{3F_{strut}}{w \cdot D_c} = \frac{3C}{2wD_c \sin\theta} = \frac{9M_T}{4wD_c^2 \sin\theta} \leq 0.5 f_c^{'} \tag{7-11}$$

Torsion-Shear Friction Moment Capacity (M_{sf}).

Use the torsion shear friction model from Priestley et al. (19), to determine the maximum bent cap torsional shear friction capacity, M_{sf}. The torsion-shear friction moment capacity of the section, M_{sf}, should be greater than or equal to the bent cap torsional moment demand, $M_T/2$.

$$M_{sf} \geq \frac{M_T}{2} \tag{7-12}$$

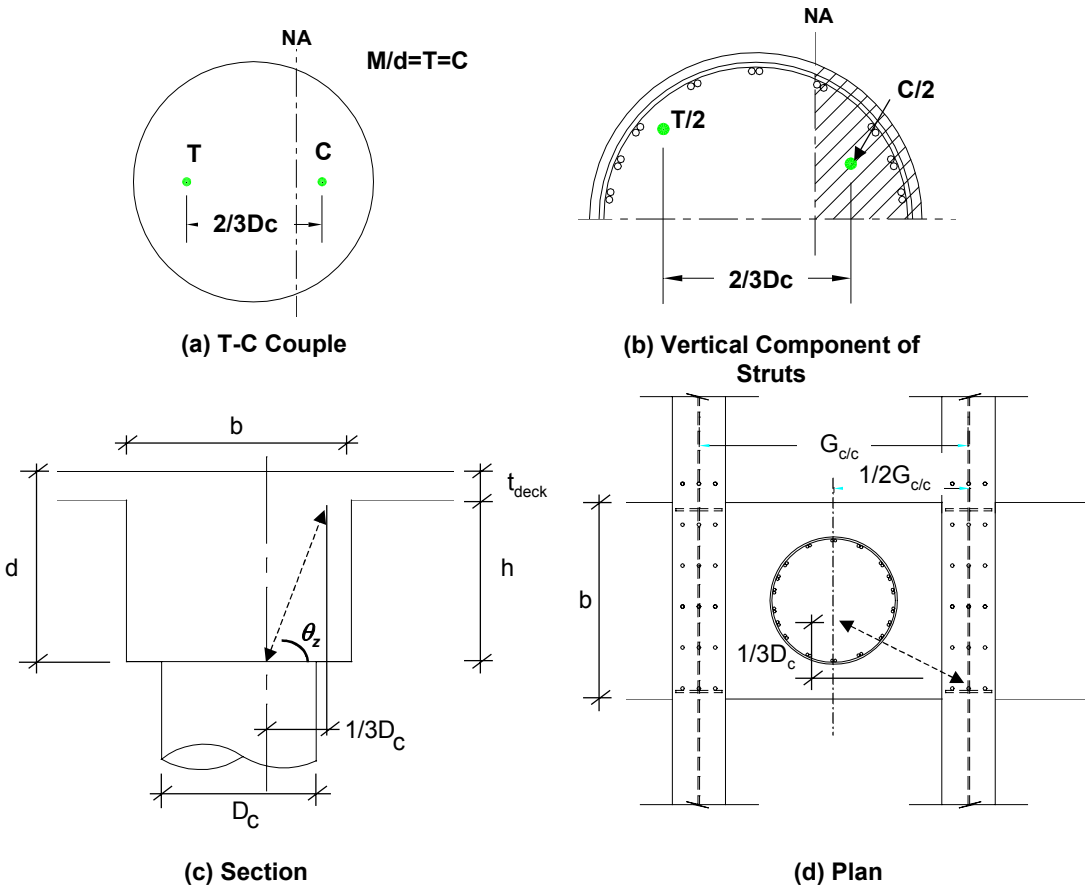

Figure 7-5 Check of Bent Cap Stress

7.3 BENT CAP DESIGN SPECIFICATIONS

From the research program, specific topics arose that warrant addressing. This section presents specifications particular to integral steel superstructure bridges continuous through concrete bent caps. Where the recommended specifications presented here conflict with specifications from AASHTO (15) or Caltrans Bridge Design Specifications (14), AASHTO or Caltrans BDS controls.

7.3.1 Joint Shear Reinforcement

Because the compression field needs to be well confined to be effective, the joint shear reinforcement needs to exist over the entire interior strut length. The joint region is defined in Section 2.6.2. and detailed in Figure 2.14 as two times the column diameter. If the center-to-center spacing of the interior girders is greater than $2D_c$, the joint region detailing should be extended to span the two interior girder (Figure 7-6).

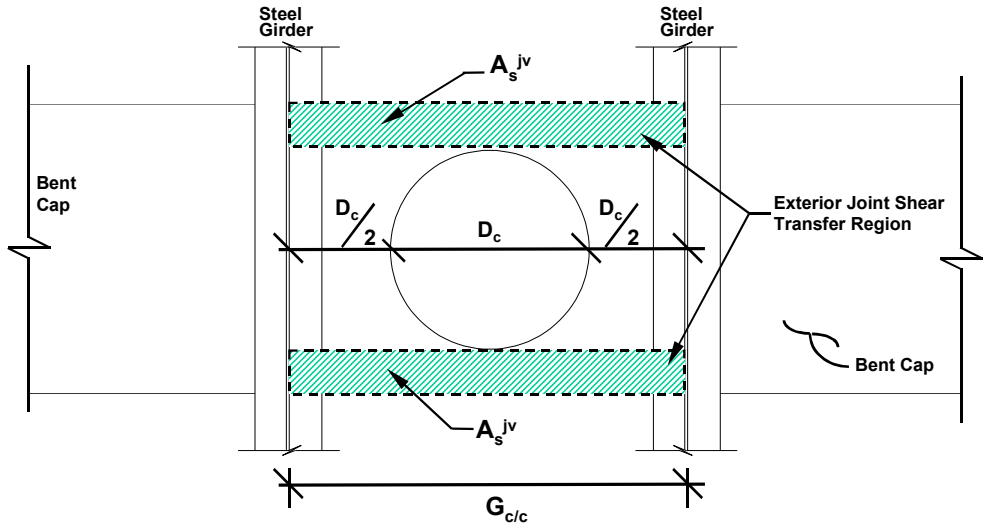

Figure 7-6 Limits of Joint Reinforcement

7.3.2 Post-Tensioning Stress Levels

Concrete stresses due to post-tensioning should not exceed those specified by the existing codes. Using the ACI (49), the maximum compressive stress in the concrete due to post-tensioning should not exceed $0.45f'_c$ and the tensile stress in the section should not exceed $6\sqrt{f'_c}$.

7.3.3 Continuous Reinforcement

The main flexural reinforcement of the bent cap shall be continuous over the entire bent cap span. For conventionally reinforced, single column bent caps, the main flexural reinforcement will pass over the steel girders. Construction reinforcement will be continuous through precut holes in the girder web. For post-tensioned, single column bents, the post-tensioning will be continuous through precut holes in the girder web.

7.3.4 Holes in Girder Webs

Holes in girder webs to allow for flexural reinforcement shall be drilled. Until fatigue experiments are conducted, drilled will produce better fatigue strength of the girders (as opposed to punching) (40).

7.3.5 Stiffener Design

Design of shear stiffeners along the length of the girder follows existing design procedures. The full height bearing stiffeners should be located at the bent cap face with a minimum concrete cover as dictated in Caltrans Bridge Design Specifications (14). The stiffener thickness is determined by limiting the stress in the stiffener to yield stress when it is subjected to the vertical component obtained in Step (b) above.

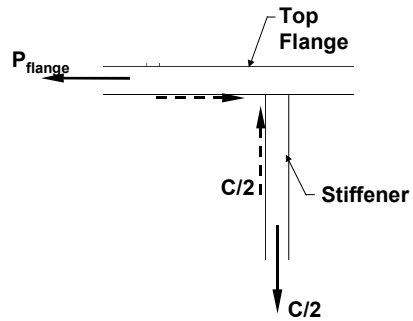

Stiffener Area:

$$A = \left(\frac{C}{2\sigma_s} \right)$$

$$t_f = \left(\frac{C}{\sigma_s \, b_f} \right)$$

Figure 7-7 Stiffener Thickness

7.3.6 Shear Studs

Shear studs required in the composite superstructure design should be continued through the bent cap. Shear studs on the bottom are at the same spacing as those on the top but are shorter to meet minimum concrete cover requirements.

7.4 CONSIDERATIONS FOR DESIGN OF ALTERNATIVE BENT CONFIGURATIONS

This research investigated in detail only single column bents. In practice, site characteristics are not always compatible to bridges with only a single column bent. This section provides a brief look at alternative concrete bent cap configurations but is by no means comprehensive.

Two bridge bents and their torsional moment diagrams are shown in Figure 7-8. Figure 7-8a depicts a concrete bent cap integral with steel box girders. The total torsional moment is equally distributed to the two box girders, therefore, the box girders need to be designed for the total torsional moment. A more important consideration is the strut reaction at the girders. With steel plate girders, the strut reacts at the web-flange-stiffener intersection. This intersection provides a well confined region, with restraints in the

transverse, vertical and longitudinal bridge directions. With steel box girders, only a reaction in the transverse bridge direction is provided. Therefore, detailing considerations need to be made in the longitudinal and vertical bridge axes.

The multi-column bridge bent shown in Figure 7-8b transfers the total column moment to one girder on each side. Because there are two columns, the design moment from the column is half that of a single column bent. However the entire moment is transferred to the bent resulting in similar bent design moments. In the single column bridge bent, reactions due to symmetry about the bridge column were used. The multi-column bent has knee joints rather than the tee joints of a single column bridge. Therefore the force transfer can't rely on the reactions developed due to bridge symmetry.

A single column bent should not be constructed with a girder directly over the column in a seismic region. This forces the single girder to transfer the entire moment through the superstructure. This unbalanced distribution of force demand results in an uneconomical bridge design.

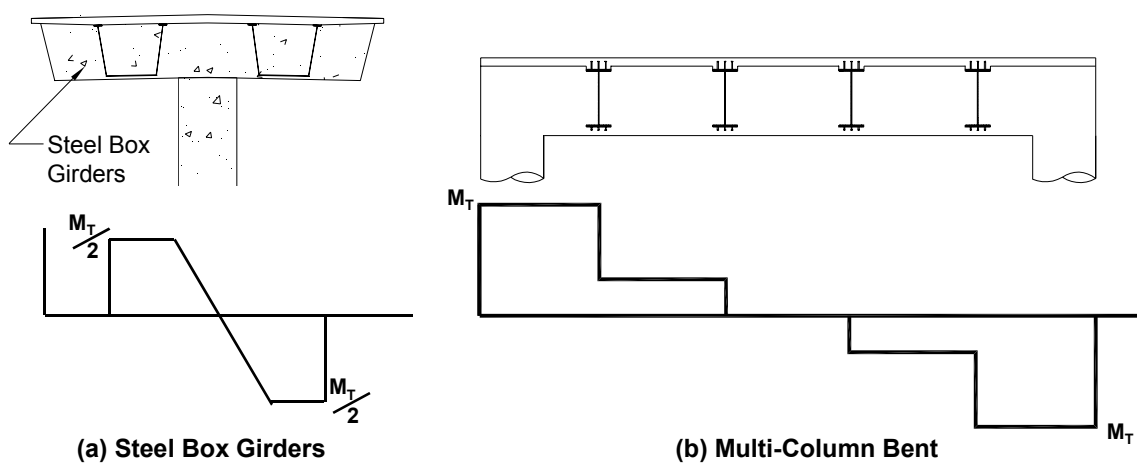

Figure 7-8 Alternative Bent Configurations

7.5 CONSTRUCTION AND MAINTENANCE CONSIDERATIONS

As introduced in Chapter 1, steel superstructure bridges integrated with concrete substructures via concrete bent caps have been constructed in nonseismic regions. Correspondence with engineers in transportation departments maintaining the bridges as

well as interviews with designers of the bridges yielded useful information into real world application and performance of integral bridges. In the integral bridge constructed in Cincinnati, Ohio, the portion of girder to be cast in the concrete was primer coated (Figure 7-9). Because post-tensioning is required to be continuous through the bent cap, the rods/strands were threaded through holes in the girder web (Figure 7-10). In construction, it was found that rods were easier to thread through the girder web rather than strands (51).

Figure 7-9 Close-up of Bridge 17, Fort Washington Way, Cincinnati, Ohio (courtesy Parsons Brinkerhoff, Ohio (50))

Figure 7-10 Construction of Bridge 17, Fort Washington Way, Cincinnati, Ohio (courtesy Parsons Brinkerhoff, Ohio (50))

7.6 SUMMARY

This chapter used results from the system tests to calibrate the truss model. Section 7.2 presented the recommended design procedure for the superstructure of an integral bridge. The superstructure demand is equal to the column moment overstrength extrapolated to the superstructure centerline, M_T. This moment demand is equally distributed to the bent cap either side of the column resulting in a bent cap design torsional moment of $M_T/2$. With this bent cap design moment, three requirements of bent cap torsional strength must be satisfied:

(a) Cracking: $T_{cr} \geq 0.6\dfrac{M_T}{2}$

(b) Limiting the compression stress in concrete at the bent cap torsional design moment to half the concrete compressive strength, $\sigma_c = \dfrac{9M_T}{4wD_c^2 \sin\theta} \leq 0.5 f_c^{'}$

(c) Ensuring the shear friction capacity is equal to or exceeds the bent cap design moment, $M_{sf} \geq \frac{M_T}{2}$.

Section 7.3 presented design specifications. Section 7.4 applied design rationale presented in Section 7.2 to bent cap configuration variations. The chapter concluded with a brief summary of lessons learned from engineers with experience constructing such details in nonseismic regions.

Chapter 8

Conclusions and Recommendations

8.1 OVERVIEW

This chapter reviews the objectives, results, and conclusions from the Caltrans research program conducted at the University of California in San Diego on the behavior of integral bridge connections when subjected to a longitudinal seismic event. Section 8.2 summarizes the conclusions drawn from the experimental and analytical work on the connections and the consequent recommendations. Recommendations for future work conclude the chapter in Section 8.3.

8.2 SUMMARY

This research established behavior profiles of four concrete bent cap designs that integrate a steel superstructure to a concrete substructure. The bent caps were designed to remain essentially elastic at a level corresponding to the maximum column overstrength moment when subjected to a longitudinal seismic event. From the experimental and analytical work on the component tests, the following conclusions are made:

- In the experiments, stiffeners increased the maximum torsional moment capacity of the bent caps by approximately 20% in comparison to the unstiffened bents. The pre-cracking finite element model showed shear stresses in bents with stiffeners being more evenly distributed around the bent cap perimeter. The effect of this as demonstrated in the strut and tie model is that the compression strut is reacted at the girder not only at the web/flange intersection but also at the web/stiffener intersection. This serves to the lower the compression strut and reduce the strut stress for a given load, thereby increasing the total load carrying of the strut, and hence, section.
- A post-tensioned bent gave the most desirable performance in the elastic range due to its minimal cracking in comparison with the conventionally reinforced bent cap.

- The failure mechanism of all tests was in the form of a shear friction failure.

The component tests served to develop and validate design models and assumptions for the effectiveness of variable parameters in the transfer of the torsional moment through the bent cap.

Applying these design models to the system tests. The system test showed all superstructure components to be in the elastic range while the column developed a complete inelastic failure mechanism.

8.3 DESIGN RECOMMENDATIONS

The experimental and analytical work presented in this thesis showed that the concept of capacity design used for reinforced concrete bridges in seismic regions can also be applied to a steel plate girder superstructure bridge integrally connected to a single column concrete substructure with a concrete bent cap.

The force transfer between an integral steel plate girder and a concrete bent cap depends on the concept of compression fields and tension ties. These fields and ties are most effective with when connected to well-confined nodes. Therefore, the recommended design detail consisted of stiffeners on the girder to provide a transverse reaction to the bent cap dilation as well as prevent buckling of the steel flanges. Additionally, providing bent cap post-tensioning decreases the level of damage in the bent cap.

Design limits were developed for an integral bridge with a post-tensioned bent cap and stiffeners on the girder web. The limits required a check of the bent cap stress and limiting that stress to half of the concrete compressive strength. The shear friction capacity of the section is determined and limited to half the torsional moment demand.

8.4 RECOMMENDATIONS FOR FUTURE WORK

As with any research, many peripheral analyses are investigated along the path to a specific solution. The concepts investigated in this research reached beyond the integration of steel and concrete and into the behavior of concrete in torsion, specifically deep beams. A parameter study on beams in torsion varying the beam span with a specific intent of establishing depth to span ratios for the occurrence of torsion shear friction failure and pure torsion failure. A skew-bending type of failure may exist

between the two extremes of friction and spiral failure. A parameter study would provide information on failure mechanisms and torsional moment capacity differences caused by depth to span ratios.

An experimental program subjecting the detail presented in this report to fatigue loading would provide beneficial information for the lifetime performance of the bridge. Once a fatigue test has been performed on the test specimen, the specimen's performance under a longitudinal seismic event should be assessed.

APPENDIX A SUPPORTING DATA FOR DESIGN OF PROTOTYPE BENT CAP

A.1 Prototype Curve from Collins and Mitchell Procedure

A.1.1 Cracking

Cracking torque: $T_{cr} = \frac{A_c^2}{p_c} 4\sqrt{f_c^{'}} \sqrt{1 + \frac{f_{pc}}{4\sqrt{f_c^{'}}}}$ in psi

$T_{cr} = 3{,}600 \text{ k - ft}$

Tube Thickness: $t = \frac{3}{4}\frac{A_c}{p_c} = 16.5 \text{ in.}$

Area enclosed by shear flow path: $A_o = (w - t)(d - t) = 5{,}128 \text{ in.}^2$

Perimeter enclosed by shear flow path: $p_o = 2(w - t + d - t) = 288 \text{ in.}$

Cracking Twist: $\psi = \frac{Tp_o}{4A_o^2 tG} = 3.98 \times 10^{-6}\ rad/in.$

A.1.2 Post – Cracking

Area enclosed by center line of stirrup:

$$A_{oh} = \left(w - 2\left(\text{cov} + {}^{d_b}\!/_2\right)\right)\left(d - 2\left(\text{cov} + {}^{d_b}\!/_2\right)\right) = 6{,}444 \text{ in.}^2$$

Perimeter enclosed by center line of stirrup:

$$p_{oh} = 2\left(w - 4\left(\text{cov} + {}^{d_b}\!/_2\right) + d\right) = 323 \text{ in.}^2$$

Crack angle is estimated $\theta = 45^\circ$ as is area enclosed by shear path, now modified due to spalling. Initial estimate taken as $A_o = 0.8A_{oh} = 5{,}155 \text{ in.}^2$ Assuming the stirrups yield first, the ultimate torsion is calculated as:

$$T = \frac{A_t f}{s}\frac{2A_o}{\tan\theta} = 11{,}247 \text{ k - ft}$$

The effective wall thickness of a concrete section in torsion can be thought of as similar to the compression block depth of a concrete section in flexure. The equation for the effective wall thickness is:

$$a_o = \frac{A_{oh}}{p_h}\left[1 - \sqrt{1 - \frac{Tp_h}{\alpha_1 f_c^{'} A_{oh}^2}\left(\tan\theta + \cot\theta\right)}\right] = 9.96 \text{ in.}$$

With the effective wall thickness calculated, the actual area and perimeter of the section enclosed by the shear path can be calculated.

$$A_o = A_{oh} - \frac{a_o}{2} p_h = 4{,}837 \text{ in.}^2$$

$$p_o = p_h - 4a_o = 283 \text{ in.}$$

The estimated A_o was used in the torsional capacity calculation therefore the calculated area is compared with the assumed area and the preceding calculations are repeated until convergence is reached. The final values are

$$A_o = 4{,}953.35 \text{ in.}^2$$
$$p_o = 285.10 \text{ in.}$$
$$T = 10{,}770 \text{ k - ft}$$

Once convergence is reached on the section dimensions, the total strain in the longitudinal reinforcement is calculated from:

$$N_v = \frac{Tp_o \cot\theta}{2A_o} = 3{,}735 \text{ kip}$$

$$\varepsilon_x = \frac{N_v - A_p E_p \Delta\varepsilon_p}{A_l E_s + A_p E_p} = 1.4E-3 = 1{,}423\mu\varepsilon$$

The terms with 'p' subscripts are indicative of properties of the prestressing strands. Next, the concrete compression is determined.

$$f_2 = \frac{Tp_h}{A_{oh}^2}\left(\tan\theta + \cot\theta\right) = 2.01 \text{ ksi}$$

The principal tensile strain is determined from

$$\varepsilon_1 = \varepsilon_x + \frac{\varepsilon_x - \varepsilon_2}{\tan^2\theta} = 5{,}846\ \mu\varepsilon$$

where ε_2 is the principal compression strain which varies across the wall thickness. It is taken as a maximum at the surface and is –0.003. The limiting compressive stress is then calculated as:

$$f_{2\max} = \frac{f_c^{'}}{0.8 + 170\varepsilon_1} = 2.23 \text{ ksi}$$

Since the concrete compressive stress has not reached the maximum, the whole procedure is repeated with a new assumption of the cracking angle. The final values are:

$$A_o = 4{,}853.1 \text{ in.}^2$$
$$p_o = 283 \text{ in.}$$
$$T = 11{,}158 \text{ k - ft}$$
$$f_2 = 2.08ksi \le 2.07ksi = f_{2\max}$$

At failure, the concrete compression strain is taken as –0.0015 resulting in stirrups strains at failure of $\varepsilon_t = \varepsilon_1 - \varepsilon_x + \varepsilon_2 = 3{,}325\ \mu\varepsilon$ which confirms that the stirrups are yielding at failure. The shear strain at failure is

$$\gamma_{xy} = 2(\varepsilon_x - \varepsilon_2)\cot\theta = 6{,}180\ \mu\varepsilon$$

which yields a twist of :

$$\psi = \frac{\theta}{L} = \frac{\gamma p_o}{2A_o} = 1.8E-4 \text{ rad/in.}$$

A.2 Prototype Curve from Hsu Procedure

A.2.1 Cracking

Cracking torque:

$$T_{np} = 6(x^2 + 10)y\sqrt[3]{f_c'} = 5{,}006 \text{ k - ft}$$
$$T_{cr} = (1 + 4\rho_t)T_{np} = 5{,}083 \text{ k - ft}$$

Cracking Twist:

$$G_c = E_c/2(1+\upsilon) = 1{,}502ksi$$
$$C = \beta x^3 y = 8{,}367{,}007in.^3$$
$$\psi = \frac{T_{cr}}{G_c C} = 4.85\times10^{-6}\ rad/in.$$

A.2.2 Post - Cracking

Hsu assumes a maximum strain at the concrete surface for multiple concrete strains, creating a nonlinear curve. Only the values for one assumed strain will be presented here and all other points of the curve are calculated with the same procedure, assuming different strains.

Starting with a maximum strain at the concrete surface of 0.0005, the tube thickness, cracking angle and softening coefficient are all initially assumed. The tube thickness t_d is assumed as 15.5 inches. The angle of cracking α is 55° and the empirical coefficient λ is 2.2 resulting in a softening coefficient (1/λ) of 0.45. With the assumed values, an initial stress for the compression block of the concrete strut is calculated from:

$$\sigma_d = k_1 \frac{1}{\lambda} f_c^{'} = 1.0 ksi$$

Where the coefficient k_1 is tabulated in Hsu's book. The area and perimeter enclosed by shear flow path are calculated using the assumed tube thickness

$$A_o = (w - t_d)(d - t_d) = 5{,}2 \text{ in.}^2$$

$$p_o = 2(w - t_d + d - t_d) = 292 \text{ in.}$$

The torsional capacity is calculated from

$$T = 2 A_o t_d \sigma_{\mathrm{d}} \sin\alpha \cos\alpha = 6{,}534 \text{ k - ft}$$

The actual tube thickness is calculated from

$$\tau_n = \frac{T p_c}{A_c^2}$$

$$t_d = \frac{A_c}{p_c}\left(0.082 + 3.405 \frac{\tau_n}{f_c^{'}}\right)\frac{1}{\sin 2\alpha} = 15.5 \text{ in.} = \text{assumed } \mathrm{t_d}$$

The cracking angle and softening coefficient are calculated

$$\cos\alpha = \sqrt{\frac{A_l f_l}{p_o \sigma_d t_d}} \Rightarrow \alpha = 55°$$

$$\lambda = \sqrt{\frac{\varepsilon_l + \varepsilon_t + \varepsilon_{ds}}{(\varepsilon_{ds}/2)} - 0.3} = 2.2$$

$$\frac{1}{\lambda} = 0.45$$

After multiple iterations, the calculated values of t_d, α, and λ are close to the assumed values. Therefore, the twist at this torque (strain) is calculated from:

$$\psi = \frac{\varepsilon_{ds}}{2 t_d \sin\alpha \cos\alpha} = 3.42 \times 10^{-5}\ rad/in.$$

APPENDIX B CONSTRUCTION DETAILS

B.1 Component Tests One and Two

Figure B. 1 Component Test Setup Specimens CR-NS and CR-S

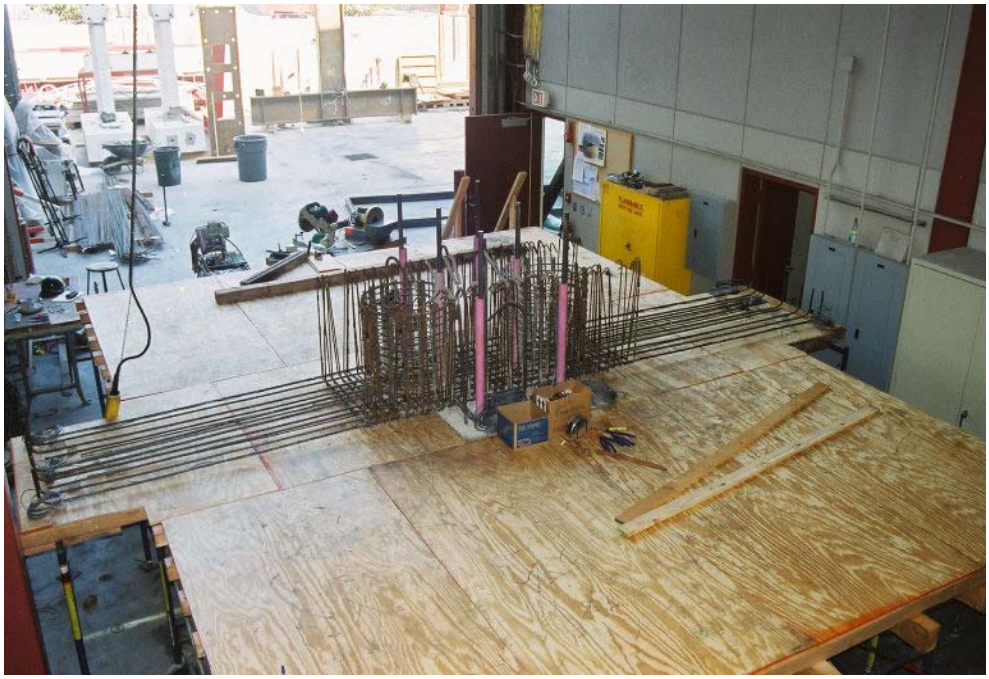

Figure B. 2 Bent Cap before Girder Placement

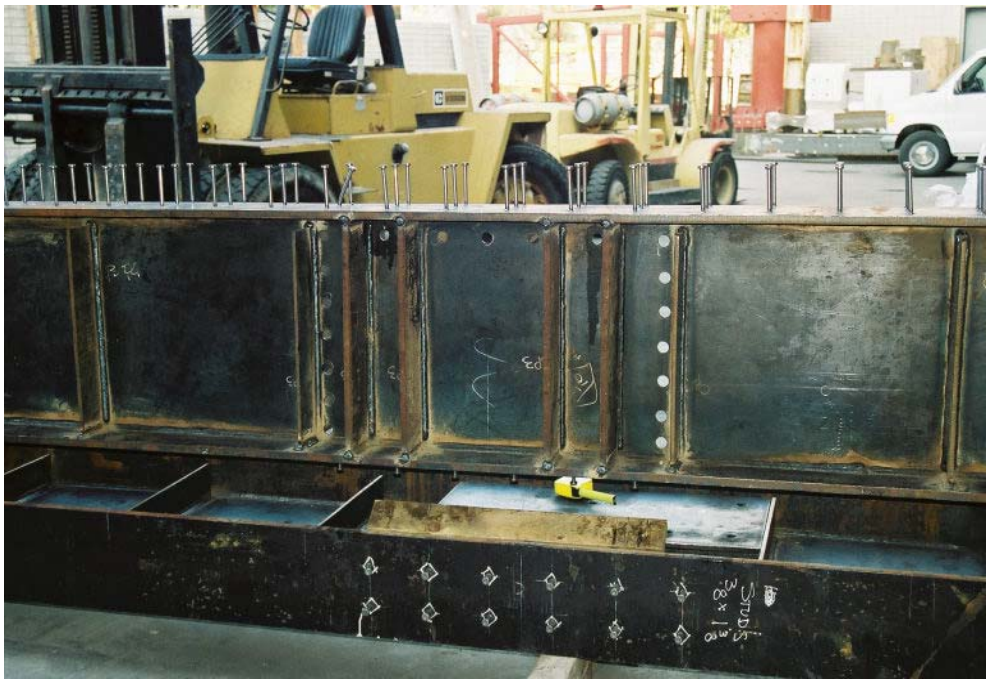

Figure B. 3 Steel Girders

Figure B. 4 Bent Cap Stirrups

Figure B. 5 Bent Cap Reinforcement Through Girder Web

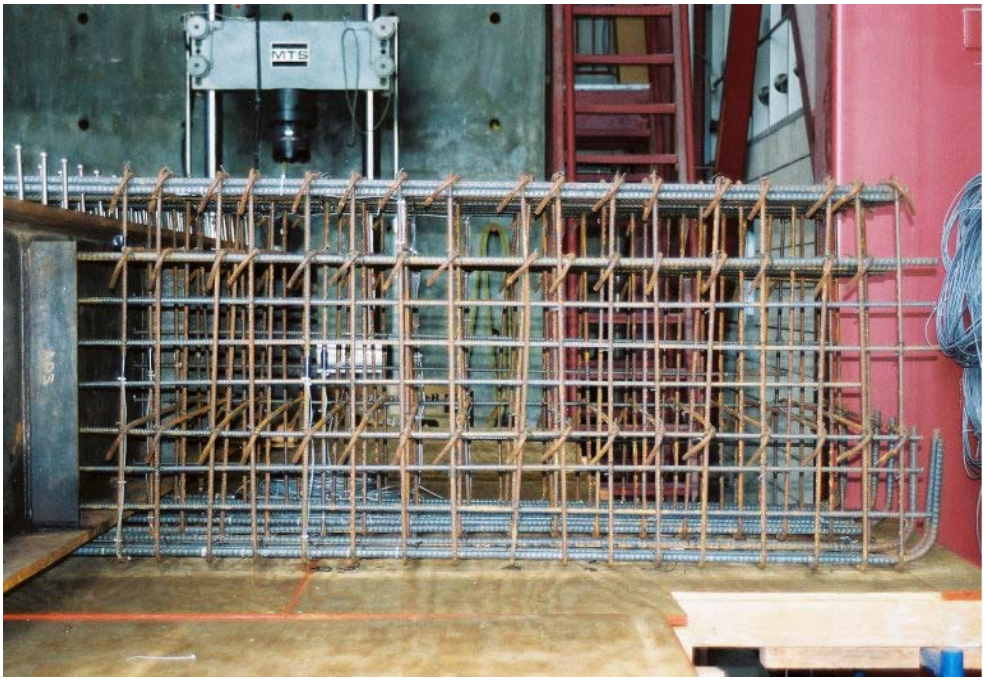

Figure B. 6 Bent Cap Reinforcement

Figure B. 7 Bent Cap Cast

Figure B. 8 Deck Steel

B.2 Component Tests Three and Four

Figure B. 9 Post-Tensioning Ducts

Figure B. 10 Post-Tensioning Anchoring in Support Block

B.3 System Test

Figure B. 11 Girders in Place

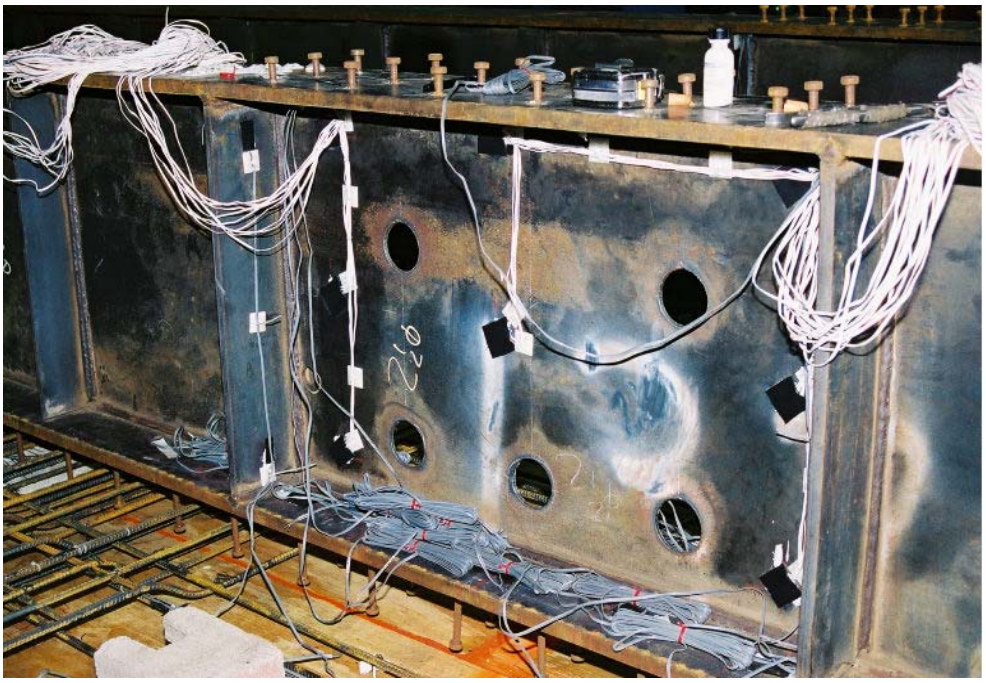

Figure B. 12 Girder in Bent Cap Region

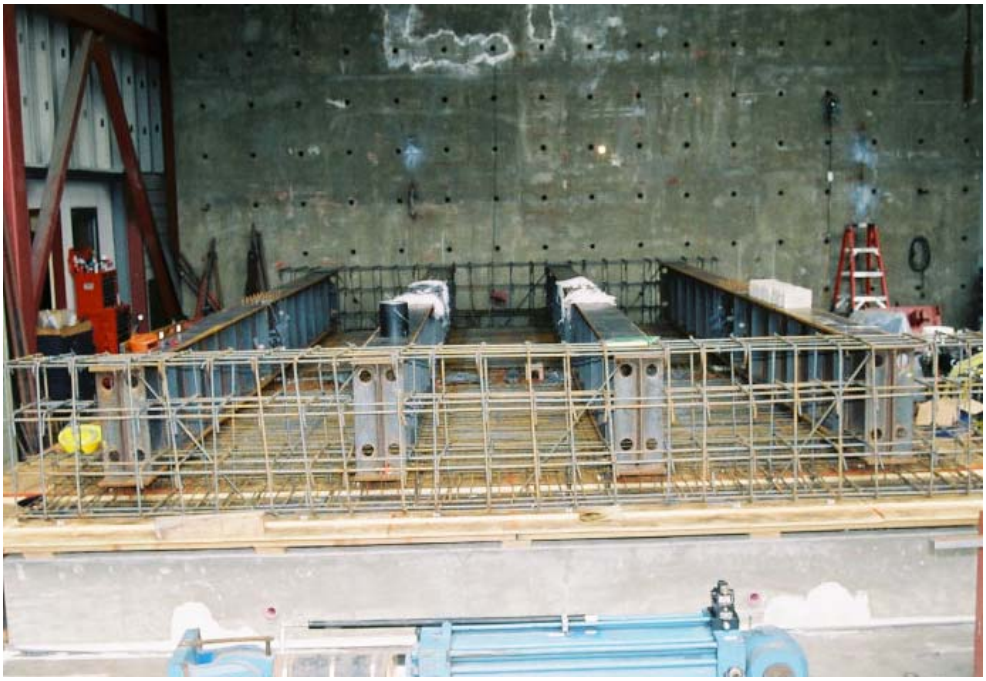

Figure B. 13 End Stubs Tied

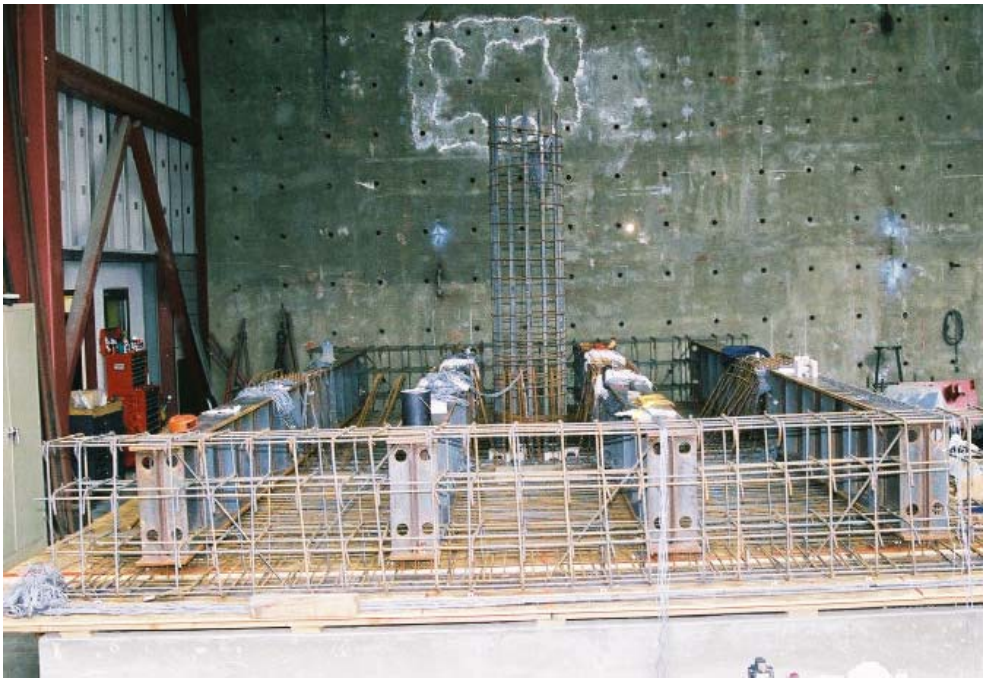

Figure B. 14 Column Cage in Place

Figure B. 16 End Stub Reinforcement

Figure B. 15 Column Cage

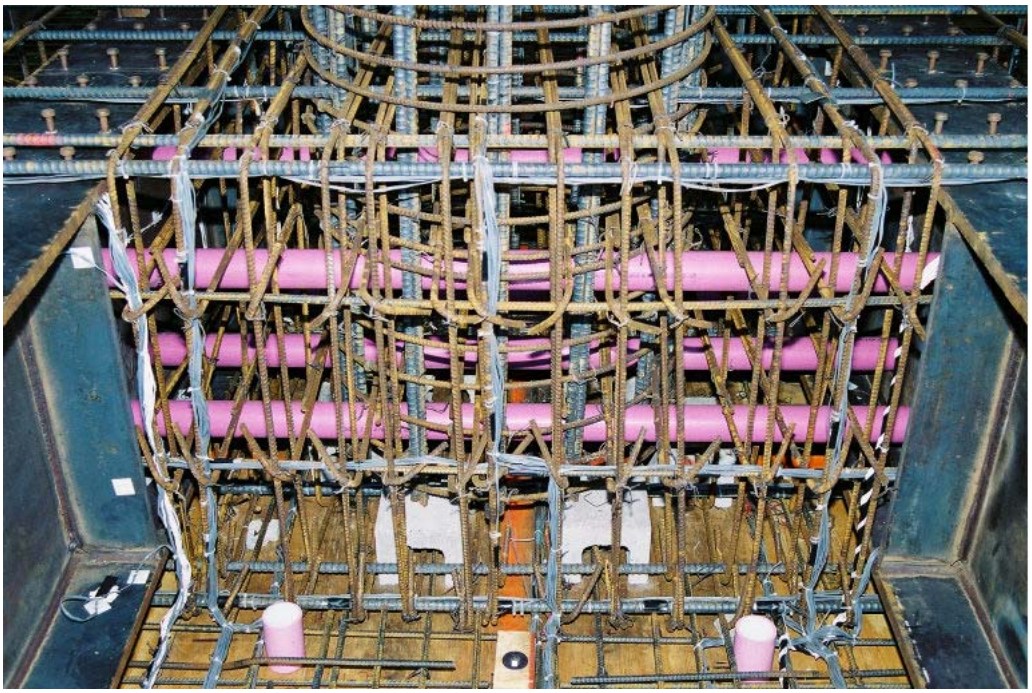

Figure B. 17 Stirrups and J-Hooks in Joint Region

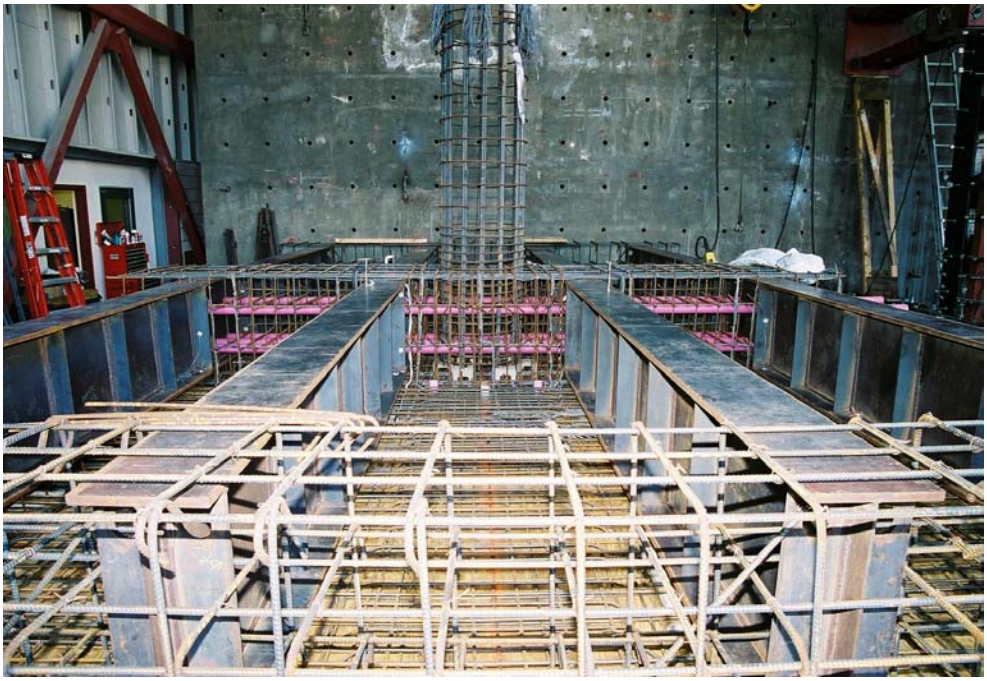

Figure B. 18 Reinforcement Complete

Figure B. 19 Deck Concrete and Joint Reinforcement

Figure B. 20 Girder at Deck Concrete

Figure B. 21 Deck Haunch Construction

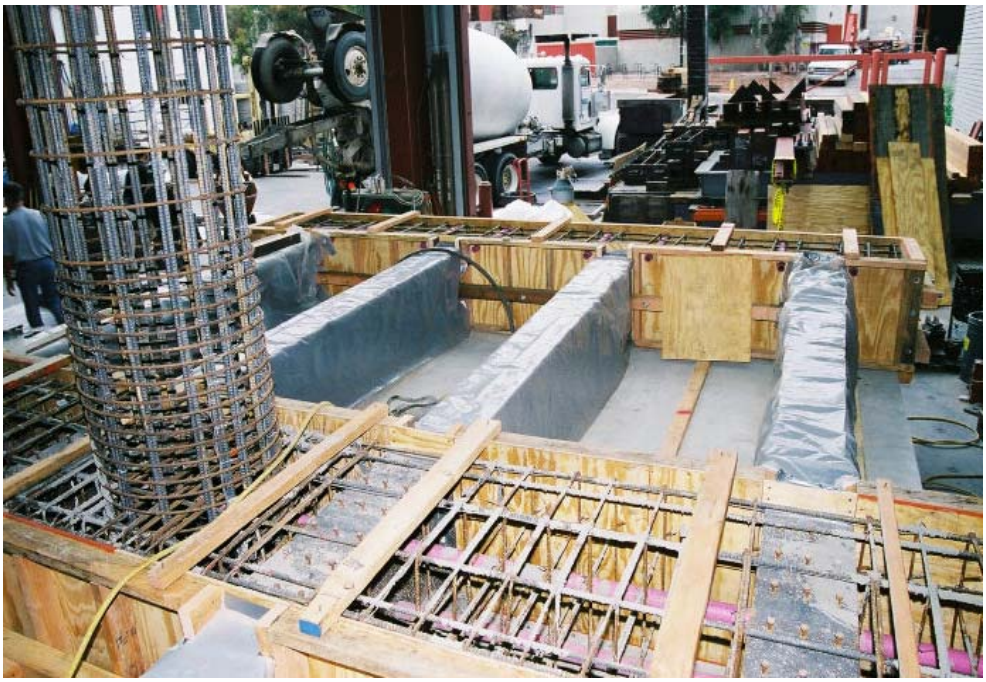

Figure B. 22 Formwork for Bent Cap and End Stubs

Figure B. 23 Column and Load Stub Formwork

Figure B. 24 Roller at Ends

Figure B. 25 Load Frame Reaction

Figure B. 27 Load Cell Reaction

Figure B. 26 Axial Load Configuration

Figure B. 28 Jack at Reaction Frame

Figure B. 29 Actuator Connected

REFERENCES

1. Burgueño, Rigoberto, Freider Seible, Vistasp Karbhari, *Design of an Advanced Composite Alternate for the Kings Stormwater Channel Bridge-Design and Analysis,* Structural Systems Research Project No. 99/06, University of California, San Diego, La Jolla, California, 1999.

2. *Caltrans, Division of Maintenance, Structure Maintenance And Investigations*, Retrieved November 2001, from http://www.dot.ca.gov/hq/structur/strmaint/

3. Wasserman, Edward P., *Integral Post-Tensioned Concrete Bent Caps*, Modern Steel Construction, Vol. 37, No. 8, July 1997, p 14.

4. Ohio Department of Transportation, *Transcript: Ohio Department of Transportation Newsletter*, June 1999.

5. *Fort Washington Way, Pier 3 Bridge 17*, Cincinnati, Ohio, Ohio Department of Transportation. Provided by Parsons Brinkerhoff Ohio, July 2001.

6. *Fort Washington Way, Pier 4 Bridge 20*, Cincinnati, Ohio, Ohio Department of Transportation. Provided by Parsons Brinkerhoff Ohio, May 1998.

7. *Sahara Avenue Interchange IR15-CL 40.55*, Louis Berger and Associates, Nevada Department of Transportation. Provided by Parsons Brinkerhoff Ohio, May 1998.

8. *I-15/Tropicana Interchange, Piers 1 and 2*, Sverdrup Corporation, Nevada Department of Transportation. Provided by Parsons Brinkerhoff Ohio, May 1998.

9. Holombo, G. J., M.J.N. Priestley, F. Seible, *Longitudinal Seismic Response of Precast Spliced-Girder Bridges*, Structural Systems Research Project Report No. 98/05, Division of Structural Engineering, Department of Applied Mechanics and Engineering Sciences, University of California, San Diego, April 1998.

10. Holombo, G. J., M.J.N. Priestley, F. Seible, *Continuity Of Precast Prestressed Spliced-Girder Bridges Under Seismic Loads*, PCI Journal, Vol. 45, No. 2, March 2000, Precast/Prestressed Concrete Institute, Chicago, IL, p 40-63.

11. Burroughs, Dan, Kenneth Price, *High Performance Steel Bridge Concepts,* Modern Steel Construction, Vol. 39, No. 14, 1999.

12. Burroughs, Dan, James Lockwood, Kenneth Price, *Innnovative Prestressed Steel Composite Short- to Medium-Span Bridges,* Transportation Research Record 1594, 1999.

13. Sritharan, Sri, Robert E. Abendroth, Lowell F. Greimann, Wadgy G. Wassef, and Justin Vander Werff, *Seismic Performance of a Concrete Column/Steel Cap/Steel Girder Integral Bridge System,* "Proceedings of the Third National Seismic Conference and Workshop on Bridges and Highways", Portland, Oregon, April 28 – May 1, 2002.

14. California Department of Transportation, *Bridge Design Specifications ATC-32.*

15. AASHTO, *Standard Specifications for Highway Bridges*, American Association of State Highway Officials, 16th Edition, Washington, DC, 1996.

16. California Department of Transportation, *Bridge Design Aids Manual*, December 1995.

17. SEQMC – Moment Curvature Analysis Package for Symmetric Sections, Demonstration Version 1.00.06, SEQAD, Provided by SC Solutions.

18. Class Notes, AMES 242, *Bridge Design,* Professor Nigel Priestley, University of California, San Diego, Department of Applied Mechanics and Engineering Sciences, La Jolla, California, May 12, 1998.

19. Priestley, M.J.N., F. Seible, and M. Calvi, *Seismic Design and Retrofit of Bridges*, John Wiley and Sons, New York, New York, 1996.

20. California Department of Transportation, *Caltrans Seismic Design Criteria*, May 1999.

21. American Institute of Steel Construction, *Load and Resistance Factor Design, Volume I*, American Institute of Steel Construction, Inc., 1995.

22. American Society for Testing and Materials, ASTM A709.

23. American Welding Society, AWS D1.5-95.

24. California Department of Transportation, *Bridge Design Details*, 1993.

25. California Department of Transportation, *Bridge Design Practice*, December 1994.

26. Hsu, T.T.C., *Torsion of Reinforced Concrete*, Van Nostrand Reinhold Company, New York, New York, 1984.

27. Collins, Michael P., Denis Mitchell, *Prestressed Concrete Structures*, Response Publications, Canada, 1997.

28. Saint-Venant, B. de, Mémoire sur la torsion des prismes (lu à l'Académie le 13 juin 1853). *Mémoires des savants étrangers*, Mémoires présentés par divers savants à l'Académie des Sciences, de l'Institut Imperial de France et imprimé par son ordre, V. 14, Imprimerie Impériale, Paris, 1856, pp. 233-560.

29. Bredt, R., "Kritische Bemerkungen zur Drehungselastizitat," *Zeitschrift des Vereiines Deutscher Ingenieure*, Band 40, No. 28, July 11, 1896, pp. 785-790; July 18, 1896, pp.813-817.

30. Ritter, W., *Die Bauweise Hennebique*, Schweizerishe Bauzeitung, Zurich, February, 1899.

31. Mörsch, E., *Der Eisenbetonbau, seine Anwendung und Theorie*, First Edition, Wayss and Freytag, A.G., Im Selbstverlag der Firma, Neustadt a. d. Haardt, May 1902, 118 pp.; *Det Eisenbetonbau, seine Theorie und Anwendung*, Second Edition, Verlag von Konrad Wittmer Stuttgart, 1906, 252 pp., Third Edition, translated into English by E.P. Goodrich, McGraw-Hill Book Co., New York, 1909, 368 pp.

32. Vecchio, F.J., and Collins, M.P., *The Response of Reinforced Concrete to In-Plane Shear and Normal Stresses*, Publication No. 82-03, Department of Civil Engineering, University of Toronto, March 1982.

33. Vecchio, F.J., and Collins, M.P., *Modified Compression Field Theory for Reinforced Concrete Elements Subjected to Shear*, ACI Journal, Vol. 83, No. 2, March-April 1986, pp. 219-231.

34. Rausch, E., *Design of Reinforced Concrete in Torsion*, (Berechnung des Eisenbetons gegen Verdrehung), Technische Hochschule, Berlin, 1929, 53 pp. (in German). Second Edition published in 1938. *Drillung (Tosion), Schub and Scherenin Stahlbetonbau*, Deutcher Ingenieur-Verlag GmbH, Dusseldorf, 1953, 168 pp.

35. Holombo, Jay, *Seismic Design of Precast Girder Bridges,* Department of Applied Mechanics and Engineering Sciences, University of California, San Diego, La Jolla, California, 1999.

36. Sritharan, Sivalingam, *Analysis of Concrete Bridge Joints Subjected to Seismic Actions,* Department of Applied Mechanics and Engineering Sciences, University of California, San Diego, La Jolla, California, 1998.

37. Ingham, Jason, *Seismic Performance of Bridge Knee Joints,* Department of Applied Mechanics and Engineering Sciences, University of California, San Diego, La Jolla, California, 1995.

38. Hsu, T.T.C., *Shear Flow Zone in Torsion of Reinforced Concrete*, Journal of Structural Engineering, ASCE, Vol. 116, No. 11, November, 1990.

39. Priestley, M.J.N., F. Seible, D.L. Anderson, *Proof Test of a Retrofit Concept for the San Francisco Double-Deck Viaducts,* Structural Systems Research Project Report No. 92/03, Department of Applied Mechanics and Engineering Sciences, University of California, San Diego, April 1992.

40. Salmon, C. G., John E. Johnson, *Steel Structures Design and Behavior,* HarperCollins College Publishers, New York, New York, 1996.

41. MacGregor, James G., *Reinforced Concrete: Mechanics and Design 2nd Edition,* Prentice Hall, Upper Saddle River, New Jersey, 1992.

42. Kanno, Ryoichi, Gregory G. Deierlein, Richard N White, *Strength, Deformation, and Seismic Resistance of Joints Between Steel Beams and Reinforced Concrete Columns*, Structural Engineering Report 93-06, School of Civil and Environmental Engineering, Cornell University, Ithaca, New York, 1993.

43. Kanno, Ryoichi, Gregory Deierlein, *Seismic Behavior of Composite (RCS) Beam-Column Joint Subassemblies*, Composite Construction, Volume III, 1996.

44. Sakaguchi, Noboru, Hiroho Tominaga, Yoshinori Murai, *Strength and Ductility of Steel Beam-RC Column Joint*, Proceedings of Ninth World Conference on Earthquake Engineering, Vol. IV, Tokyo-Kyoto, Japan, August 2-9, 1988, pp. 713-718.

45. Park, R., W.L. Gamble, *Reinforced Concrete Slabs*, John Wiley and Sons, New York, New York, 1980.

46. Micro-Measurements, *Precision Strain Gages*, Catalog 500, June 2000, p. 5.

47. Dowell, Robert, Rigoberto Burgueno, Frieder Seible, M. J. Nigel Priestley, Antonio Mari, *The Terminal Separation Replacement Structure Prooftest and Retrofit Test,* Structural Systems Research Project Report No. 94/14, Division of Structural Engineering, Department of Applied Mechanics and Engineering Sciences, University of California, San Diego, October 1994.

48. Schafer, Kurt, Joerg Schlaich, *Strut-and-Tie Models for the Design and Detailing of Structural Concrete,* Seminar Notes, ENCI 623, Calgary, September 1998.

49. American Concrete Institute, *Building Code Requirements for Reinforced Concrete,* American Concrete Institute, Detroit, Michigan, 1992.

50. Martin, Thomas O., Parsons Brinkerhoff, Cincinnati, Ohio, Personal Communication, July 10-11, 2001.

51. Taylor, David, Wilbur Smith Associates, Columbia, South Carolina, Personal Communication, June 20, 2002.